



Supramolecular approaches to mediate chemical reactivity

Edited by
Carmine Gaeta, Pablo Ballester
and Qi-Qiang Wang

Imprint

Beilstein Journal of Organic Chemistry

www.bjoc.org

ISSN 1860-5397

Email: journals-support@beilstein-institut.de

The *Beilstein Journal of Organic Chemistry* is published by the Beilstein-Institut zur Förderung der Chemischen Wissenschaften.

Beilstein-Institut zur Förderung der Chemischen Wissenschaften
Trakehner Straße 7–9
60487 Frankfurt am Main
Germany
www.beilstein-institut.de

The copyright to this document as a whole, which is published in the *Beilstein Journal of Organic Chemistry*, is held by the Beilstein-Institut zur Förderung der Chemischen Wissenschaften. The copyright to the individual articles in this document is held by the respective authors, subject to a Creative Commons Attribution license.



Supramolecular approaches to mediate chemical reactivity

Pablo Ballester^{*1,2}, Qi-Qiang Wang^{*3,4} and Carmine Gaeta^{*5}

Editorial

Open Access

Address:

¹Institute of Chemical Research of Catalonia (ICIQ), Avda. Països Catalans 16, 43007 Tarragona, Spain, ²Catalan Institution for Research and Advanced Studies (ICREA), Passeig Lluís Companys 23, 08010 Barcelona, Spain, ³Beijing National Laboratory for Molecular Sciences, CAS Key Laboratory of Molecular Recognition and Function, Institute of Chemistry, Chinese Academy of Sciences, Beijing 100190, China, ⁴University of Chinese Academy of Sciences, Beijing 100049, China and ⁵Dipartimento di Chimica e Biologia "A. Zambelli", Università di Salerno, I-84084 Fisciano, Salerno, Italy

Email:

Pablo Ballester^{*} - pballester@iciq.es; Qi-Qiang Wang^{*} - qiqiangw@iccas.ac.cn; Carmine Gaeta^{*} - cgaeta@unisa.it

^{*} Corresponding author

Beilstein J. Org. Chem. **2022**, *18*, 1463–1465.

<https://doi.org/10.3762/bjoc.18.152>

Received: 26 September 2022

Accepted: 30 September 2022

Published: 14 October 2022

This article is part of the thematic issue "Supramolecular approaches to mediate chemical reactivity".

Guest Editors: C. Gaeta, P. Ballester and Q.-Q. Wang

© 2022 Ballester et al.; licensee Beilstein-Institut.

License and terms: see end of document.

Nature continuously inspires scientists to design novel prototypes of artificial systems with more and more advanced functions and properties [1,2]. In this regard, one of the greatest innovations was the discovery that small molecules can catalyze/mediate chemical reactions by a biomimetic approach [3,4]. Very recently, many efforts have been devoted to study supramolecular catalysis processes [5–14] in which macrocyclic hosts, self-assembled capsules and metallo-cages were employed as catalysts or nanocontainers.

The primary characteristic of supramolecular catalysis is that the general modes of activation based on intermolecular interactions can operate on substrates in a selective way, and in confined environment, like the active site of natural enzymes [5–14]. As a result, molecular recognition of the substrate(s) and potentially the transition state is essential in supramolecular catalysis.

Supramolecular catalysis finds inspiration in natural enzymes, which show catalytic features such as substrates and products selectivity, efficiency, geometric control, and acceleration of

chemical reactivity [1]. If reactants are confined in the restricted space provided by an enzyme binding pocket, the increase in local concentration, due to the proximity effect, the stabilization of intermediates and transition states cause the acceleration of the reaction. Thus, learning from natural enzymes, novel supramolecular catalysts were designed that showed substrate selectivity, turnover, regioselectivity, and stereoselectivity [5–14].

Supramolecular architectures with an internal cavity are potential candidates to work as supramolecular catalysts [5–14]. The first supramolecular catalysts were based on covalent hosts, typically cyclodextrin macrocycles [1], which had an interior hydrophobic cavity decorated with catalytically useful functional groups. Recently, increased emphasis has been placed on catalysis that takes use of noncovalent hosts, including self-assembled capsules [5,6,8,9]. The capsules feature sizeable internal hydrophobic cavities that can accommodate large substrates and even allow bimolecular reactions to take place. In addition, they may ensure catalytic turnover. Transition states and reaction intermediates may also be stabilized in the cavities

of the capsules by means of intermolecular interactions. The most intriguing aspect of catalysis in confined spaces [5–14] is that the reactions can take place through unusual mechanisms. This is mainly due to the conformational control of the substrates, steric constrictions, stabilization of species, and solvent exclusion phenomena occurring in the molecular containers isolated spaces [6]. Consequently, the classical rules of organic reactivity are often violated [6,11].

Taking into account the above considerations, we organized this thematic issue focused on showcasing innovative research regarding supramolecular catalysis using macrocyclic and acyclic hosts, as well as other molecular architectures such as self-assembled capsules and metallocages.

In their contribution, Secchi and Cera [15] reported the synthesis of diphosphine gold(I) calix[6]arene complexes whose geometry, in low-polarity solvents, is controlled by the 1,2,3-alternate conformation of the calix[6]arene skeleton. These catalysts can tune the selectivity of the catalytic cycloisomerization of 1,6-enynes in response to the relative orientation of the coordinated gold(I) atom with respect to the macrocycle.

One of the major challenges in organic synthetic chemistry is the control of reaction selectivity (site, chemo, stereo etc.). Site-reaction selectivity is always essential when multiple potential reactive sites are present in the substrate. Poor site-selectivity would result in complex and sometimes even unachievable separation and purification procedures. Rui Wang and Yang Yu [16] reported an interesting review in which they summarized various site-selective reactions mediated by molecular containers. They focused their attention on reactions that give different product distributions when performed inside the containers compared to the bulk solution.

As mentioned above, activation of substrates, stabilization of intermediates and transition states through intermolecular interactions was established as one of the fundamental factors of supramolecular catalysis, and among these hydrogen bonding interactions play a pivotal role in catalysis. More recently, halogen bonding interactions have been used as a novel tool to catalyze a wide variety of processes. Other nonclassical interactions, including anion-, chalcogen-, and pnictogen bonding, have also been exploited for the design of novel supramolecular catalysts.

In their contribution Wang and co-workers [17] reported an interesting example of chalcogen bonding catalysis approach for the synthesis of calix[4]pyrrole macrocycles. The Se···O=C chalcogen bonding interactions between a selenide-based catalyst and the carbonyl-substrate catalyzed the macrocyclization

with pyrrole. Interestingly, only 5 mol % of catalyst loadings were necessary in order to promote the condensation processes, and calix[4]pyrrole derivatives were obtained in moderate to high yields. Mild reaction conditions were employed, thus highlighting the potential of this type of nonclassical interactions in catalyzing chemical transformations.

Among the examples of self-assembled catalytic capsules, the hexameric resorcinarene system was particularly investigated.

In their contribution, Alessandro Scarso and co-workers [18] showed that the hexameric capsule can catalyze the cyclization of (*S*)-citronellal forming isopulegol. In this study it was exploited the ability of the resorcinarene capsule to work as a Brønsted acid catalyst, and its aptitude to stabilize cationic intermediates and transition states inside the cavity.

Velmurugan, Hu and co-workers [19] reported an efficient photocatalytic supramolecular system based on a self-assembled nanosystem. The self-assembled system was obtained in an aqueous medium by inclusion of ammonium benzoyl-L-alaninate (G) in a tetraphenylethylene-embedded pillar[5]arene (m-TPEWP5). The resulting worm-like supramolecular nanostructures, displayed aggregation-induced emission (AIE) due to the restricted phenyl-ring rotation of m-TPEWP5 component. Inspired by natural photosynthesis and following an energy transfer process, the supramolecular nanorod assembly was employed as a nanoreactor for a photocatalytic dehalogenation reaction, i.e., debromination of 2-bromo-1-phenylethanone derivatives, with high yields and short reaction times in an aqueous solution.

In the last decades, macrocyclic hosts have been widely used as supramolecular catalysts [7]. In this work, Qi-Qiang Wang [20] and co-workers reported tetraaminobisthiourea chiral macrocycles as catalysts in decarboxylative Mannich reactions. Low macrocycle loading was used to catalyze the decarboxylative addition of malonic acid half thioesters to isatin-derived ketimines with excellent yields and good enantioselectivity. It was reported that effective activation and stereocontrol of the reaction depends on the conformational rigidity of the macrocyclic framework and a synergy between the thiourea and tertiary amine sites.

Recently, many efforts were focused on the synthesis and applications of mechanically interlocked molecules (MIMs), such as catenanes and rotaxanes. MIMs show interesting structural and topological features and offer conceptually new possibilities as catalysts. In their minireview, Krajnc and Niemeyer [21] highlighted the use of the axially chiral 1,1'-binaphthyl-2,2'-diol (BINOL) unit as a stereogenic element in MIMs. The authors

comment on the synthesis and properties of such BINOL-based chiral MIMs, together with their use in further diastereoselective modifications, their application in asymmetric catalysis, and stereoselective chemosensing.

In their minireview, Prodip Howlader and Michael Schmittel [22] highlighted the recent results in the field of the supramolecular catalysis on the use of discrete heteroleptic metallo-supramolecular complexes as catalysts. The idea of breaking/reducing symmetry has inspired many researchers to study heteroleptic metallo-complexes made up of various ligands. The authors emphasized the advantages of heteroleptic over homoleptic cages and they showed examples of nanomechanical motion influencing catalytic activity. They also discuss the regulation of the catalytic activity of heteroleptic systems by an external stimulus.

We are very grateful to all colleagues who contributed to this issue and to the Editorial Team of the Beilstein-Institut for their kind support. We are convinced that this thematic issue will stimulate new insights in the field of supramolecular catalysis.

Carmine Gaeta, Pablo Ballester, Qi-Qiang Wang

Salerno, Tarragona, Beijing, September 2022

ORCID® IDs

Pablo Ballester - <https://orcid.org/0000-0001-8377-6610>
 Qi-Qiang Wang - <https://orcid.org/0000-0001-5988-1293>
 Carmine Gaeta - <https://orcid.org/0000-0002-2160-8977>

References

1. Breslow, R. *Science* **1982**, *218*, 532–537. doi:10.1126/science.7123255
2. Arnold, F. H. *Angew. Chem., Int. Ed.* **2019**, *58*, 14420–14426. doi:10.1002/anie.201907729
3. MacMillan, D. W. C. *Nature* **2008**, *455*, 304–308. doi:10.1038/nature07367
4. List, B. *Chem. Rev.* **2007**, *107*, 5413–5415. doi:10.1021/cr078412e
5. Raynal, M.; Ballester, P.; Vidal-Ferran, A.; van Leeuwen, P. W. N. M. *Chem. Soc. Rev.* **2014**, *43*, 1660–1733. doi:10.1039/c3cs60027k
6. Gaeta, C.; La Manna, P.; De Rosa, M.; Soriente, A.; Talotta, C.; Neri, P. *ChemCatChem* **2021**, *13*, 1638–1658. doi:10.1002/cctc.202001570
7. Wang, Q.-Q. In *Supramolecular Catalysis Using Organic Macrocycles*; Liu, Y.; Chen, Y.; Zhang, H.-Y., Eds.; Handbook of Macroyclic Supramolecular Assembly; Springer: Singapore, 2019. doi:10.1007/978-981-13-1744-6_36-1
8. Catti, L.; Zhang, Q.; Tiefenbacher, K. *Chem. – Eur. J.* **2016**, *22*, 9060–9066. doi:10.1002/chem.201600726
9. Borsato, G.; Rebek, J., Jr.; Scarso, A. Capsules and Cavitands: Synthetic Catalysts of Nanometric Dimension. In *From Selective Nanocatalysts and Nanoscience*; Zecchina, A.; Bordiga, S.; Groppo, E. E., Eds.; Wiley-VCH: Weinheim, Germany, 2011; pp 105–168. doi:10.1002/9783527635689.ch4
10. Purse, B. W.; Rebek, J., Jr. *Proc. Natl. Acad. Sci. U. S. A.* **2005**, *102*, 10777–10782. doi:10.1073/pnas.0501731102
11. Toste, F. D. *Acc. Chem. Res.* **2018**, *51*, 2980–2981. doi:10.1021/acs.accounts.8b00601
12. Yoshizawa, M.; Klosterman, J. K.; Fujita, M. *Angew. Chem., Int. Ed.* **2009**, *48*, 3418–3438. doi:10.1002/anie.200805340
13. Roberts, D. A.; Pilgrim, B. S.; Nitschke, J. R. *Chem. Soc. Rev.* **2018**, *47*, 626–644. doi:10.1039/c6cs00907g
14. Brown, C. J.; Toste, F. D.; Bergman, R. G.; Raymond, K. N. *Chem. Rev.* **2015**, *115*, 3012–3035. doi:10.1021/cr4001226
15. Giovanardi, G.; Secchi, A.; Arduini, A.; Cera, G. *Beilstein J. Org. Chem.* **2022**, *18*, 190–196. doi:10.3762/bjoc.18.21
16. Wang, R.; Yu, Y. *Beilstein J. Org. Chem.* **2022**, *18*, 309–324. doi:10.3762/bjoc.18.35
17. Tong, Q.; Zhao, Z.; Wang, Y. *Beilstein J. Org. Chem.* **2022**, *18*, 325–330. doi:10.3762/bjoc.18.36
18. Lorenzetto, T.; Fabris, F.; Scarso, A. *Beilstein J. Org. Chem.* **2022**, *18*, 337–349. doi:10.3762/bjoc.18.38
19. Bai, Z.; Velmurugan, K.; Tian, X.; Zuo, M.; Wang, K.; Hu, X.-Y. *Beilstein J. Org. Chem.* **2022**, *18*, 429–437. doi:10.3762/bjoc.18.45
20. Guo, H.; Ao, Y.-F.; Wang, D.-X.; Wang, Q.-Q. *Beilstein J. Org. Chem.* **2022**, *18*, 486–496. doi:10.3762/bjoc.18.51
21. Krajnc, M.; Niemeyer, J. *Beilstein J. Org. Chem.* **2022**, *18*, 508–523. doi:10.3762/bjoc.18.53
22. Howlader, P.; Schmittel, M. *Beilstein J. Org. Chem.* **2022**, *18*, 597–630. doi:10.3762/bjoc.18.62

License and Terms

This is an open access article licensed under the terms of the Beilstein-Institut Open Access License Agreement (<https://www.beilstein-journals.org/bjoc/terms>), which is identical to the Creative Commons Attribution 4.0 International License

(<https://creativecommons.org/licenses/by/4.0/>). The reuse of material under this license requires that the author(s), source and license are credited. Third-party material in this article could be subject to other licenses (typically indicated in the credit line), and in this case, users are required to obtain permission from the license holder to reuse the material.

The definitive version of this article is the electronic one which can be found at:

<https://doi.org/10.3762/bjoc.18.152>



Diametric calix[6]arene-based phosphine gold(I) cavitands

Gabriele Giovanardi, Andrea Secchi*, Arturo Arduini and Gianpiero Cera*

Letter

Open Access

Address:

Dipartimento di Scienze Chimiche, della Vita e della Sostenibilità Ambientale, Università di Parma, Parco Area delle Scienze 17/A, 43124 Parma, Italy

Email:

Andrea Secchi* - andrea.secchi@unipr.it; Gianpiero Cera* - gianpiero.cera@unipr.it

* Corresponding author

Keywords:

1,2,3-alternate conformation; calix[6]arenes; gold(I) catalysis; phosphines

Beilstein J. Org. Chem. 2022, 18, 190–196.

<https://doi.org/10.3762/bjoc.18.21>

Received: 23 December 2021

Accepted: 02 February 2022

Published: 10 February 2022

This article is part of the thematic issue "Supramolecular approaches to mediate chemical reactivity".

Guest Editor: C. Gaeta

© 2022 Giovanardi et al.; licensee Beilstein-Institut.

License and terms: see end of document.

Abstract

We report the synthesis and characterization, in low polarity solvents, of a novel class of diametric phosphine gold(I) cavitands characterized by a *1,2,3-alternate* geometry. Preliminary catalytic studies were performed on a model cycloisomerization of 1,6-enynes as a function of the relative orientation of the bonded gold(I) nuclei with respect to the macrocyclic cavity.

Introduction

One of the latest challenges in supramolecular chemistry is the design and development of novel macrocyclic-based entities able to influence the catalytic activities of the metal center [1-3]. In this context, phosphines represent the most exploited class of ligands in homogeneous catalysis [4]. Noteworthy, reason of their wide applicability is the possibility of controlling the steric and electronic properties by proper functionalizations, hence tuning the catalytic properties of the bonded metal. This crucial aspect prompted their application in supramolecular chemistry as well. Thus, a recent evolution of their chemistry concerns the development of novel architectures in which P(III) compounds are incorporated in cavity-shaped macrocycles [5-8]. In this scenario, calix[4]- [9-13] and resorcin[4]arene [14-17] are the most exploited cavitands due to their inherent limited flexibility and already proved their ability to control the catalytic activity of late-transition metals and particularly gold(I) catalysts [18-25]. This occurs via strong steric

interactions, often outside the macrocycle (Figure 1a) [11], that affect the first coordination sphere of the metal or by creating a spatial confinement around the metal that is thus directed towards the inner cavity (Figure 1b) [26,27]. Contrarily, calix[6]arene macrocycles are less exploited in catalysis [28]. The larger macrocycle size, its conformational adaptability, and the possibility to selectively functionalize the macrocycle offered several opportunities to design synthetic receptors and prototypes of nanodevices, instead [29]. In this context, we recently devised a new family of triphosphine calix[6]arene gold(I) complexes (Figure 1c) [30]. These cavitands are able to form (pseudo)rotaxane species, by threading viologen-based guests, with a conformational control operated by the sulfonamido hydrogen-bonding donor domain [31,32]. Furthermore, their catalytic activity was demonstrated in promoting gold(I)-catalyzed cycloisomerization of 1,6-enynes, with ample scope and high regioselectivity. However, preliminary studies sug-

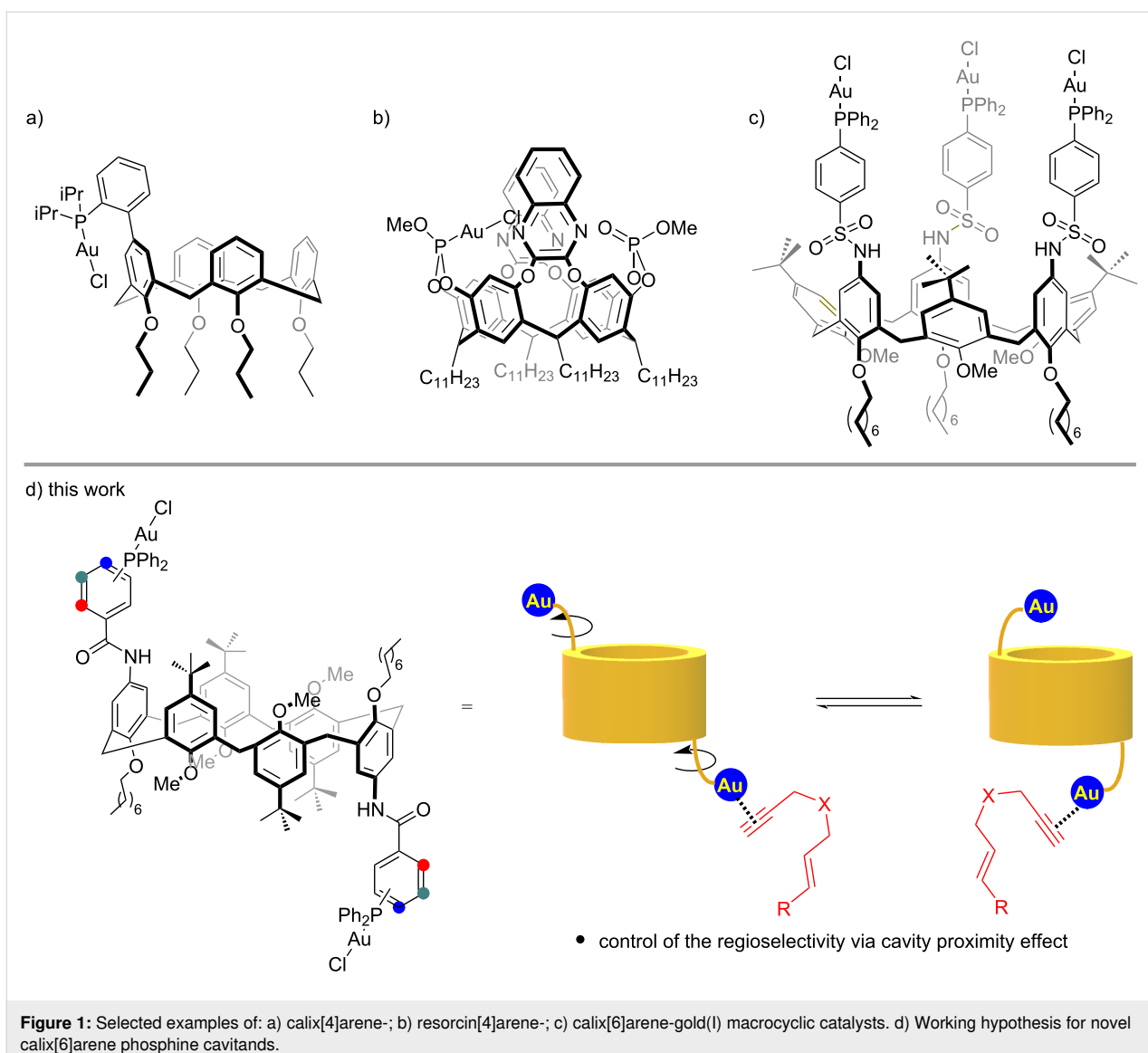


Figure 1: Selected examples of: a) calix[4]arene-; b) resorcin[4]arene-; c) calix[6]arene-gold(I) macrocyclic catalysts. d) Working hypothesis for novel calix[6]arene phosphine cavitands.

gested that the catalytic event occurs outside the macrocyclic cavity. In order to get more insights on the role of the cavity to dictate the position of the metal centers, we reasoned on the possibility to design a novel generation of diametric phosphine gold(I) cavitands exploiting a calix[6]arene scaffold characterized by a *1,2,3-alternate* conformation. As working hypothesis, this geometry would segregate two catalytically active gold(I) nuclei to the opposite sides of the macrocycle, offering them the possibility to approach the cavity, thus exerting any control over the catalytic manifold (Figure 1d).

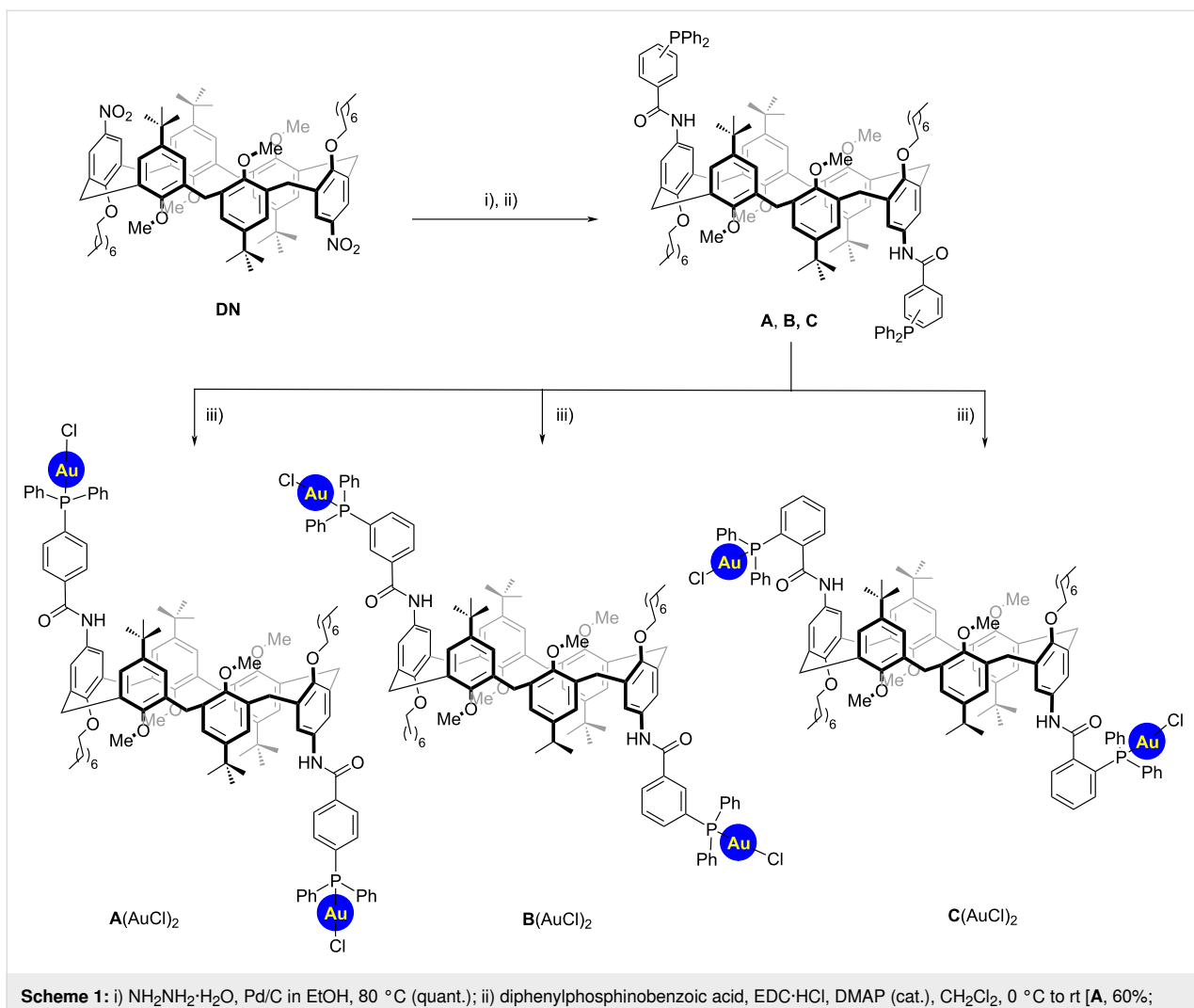
Results and Discussion

Synthesis and characterization

The synthesis of novel macrocyclic calix[6]arene ligands was first attempted starting from the known dioctyloxydinitro derivative **DN** (Scheme 1) [33]. Reduction of the nitro groups with

hydrazine, in the presence of catalytic amounts of Pd/C (10 mol %) led to the corresponding diamino intermediate. This latter could be subsequently reacted with the desired phosphino benzoic acid derivative through a user-friendly amide coupling in the presence of EDC-HCl and catalytic amounts of DMAP in CH_2Cl_2 . Under these conditions, the corresponding diphosphine intermediates **A** (*para*), **B** (*meta*), and **C** (*ortho*) were isolated in moderate yields. Finally, gold(I) catalysts could be obtained via conventional protocols using $(\text{Me}_2\text{S})\text{AuCl}$. Notably, the organometallic macrocycles **A**, **B**, **C** ($(\text{AuCl})_2$) could be isolated via column chromatography separation.

Gold(I) catalysts were subsequently fully characterized by NMR analysis and high-resolution mass spectrometry. The conformation of the catalysts, in low polarity solvents, is dominated by the *1,2,3-alternate* conformation assumed by the **DN**



intermediate, as previously demonstrated in our recent contributions [33,34]. Hence, the most notable features of ^1H NMR for **A(AuCl)₂** are represented by a pattern for the methylene bridging protons in a 1:1:1 integration ratio (Figure 2). These include: i) two doublets at 4.2 and 3.6 ppm with a geminal coupling of $^2J = 14.2$ Hz for the a/a' couple and ii) a singlet at 3.92 ppm for the b/b' couple, typical of an *anti*-orientation [35]. This situation suggests a single inversion point which confers to the macrocycle a high symmetrical geometry. Finally, a single broad peak for the four methoxy groups (\$) appears at 2.96 ppm. In analogy with parental diureido and dithioureido calix[6]arenes, we were able to observe the presence of a second minor *cone* conformer, in a \approx 4:1 ratio, highlighted by the presence of a second, single resonance for the methoxy groups (\$*) at 3.11 ppm. An analogous situation was observed for **B(AuCl)₂** and **C(AuCl)₂** as well. However, here the singlets for the b/b' couple overlap with the signals of the octyloxy chains (£) at 3.91 and 3.87 ppm, respectively.

The presence of these two major conformers, in slow exchange on the NMR timescale, was finally confirmed by variable temperature NMR analysis performed for **A(AuCl)₂** using tetrachloroethane-*d*₂ as the solvent (Figure 3).

Catalytic studies

To probe the role of the cavity and the influence of the position of the gold(I) nuclei implanted on the calix[6]arene scaffold, we carried out the synthesis of three monomeric gold catalyst analogues **A'**, **B'**, **C'**(AuCl). The synthesis of these compounds was performed using the previously optimized protocol, starting from a 4-(octyloxy)aniline intermediate (Scheme 2).

Subsequently, due to the general interest in controlling the reactivity of gold(I)-catalyzed transformations by means of supramolecular macrocycles, we choose a cycloisomerization of 1,6-enynes as a model reaction [36]. Substrate **1a** was reacted in the presence of monomeric gold(I) catalyst **A'**(AuCl) (2 mol %),

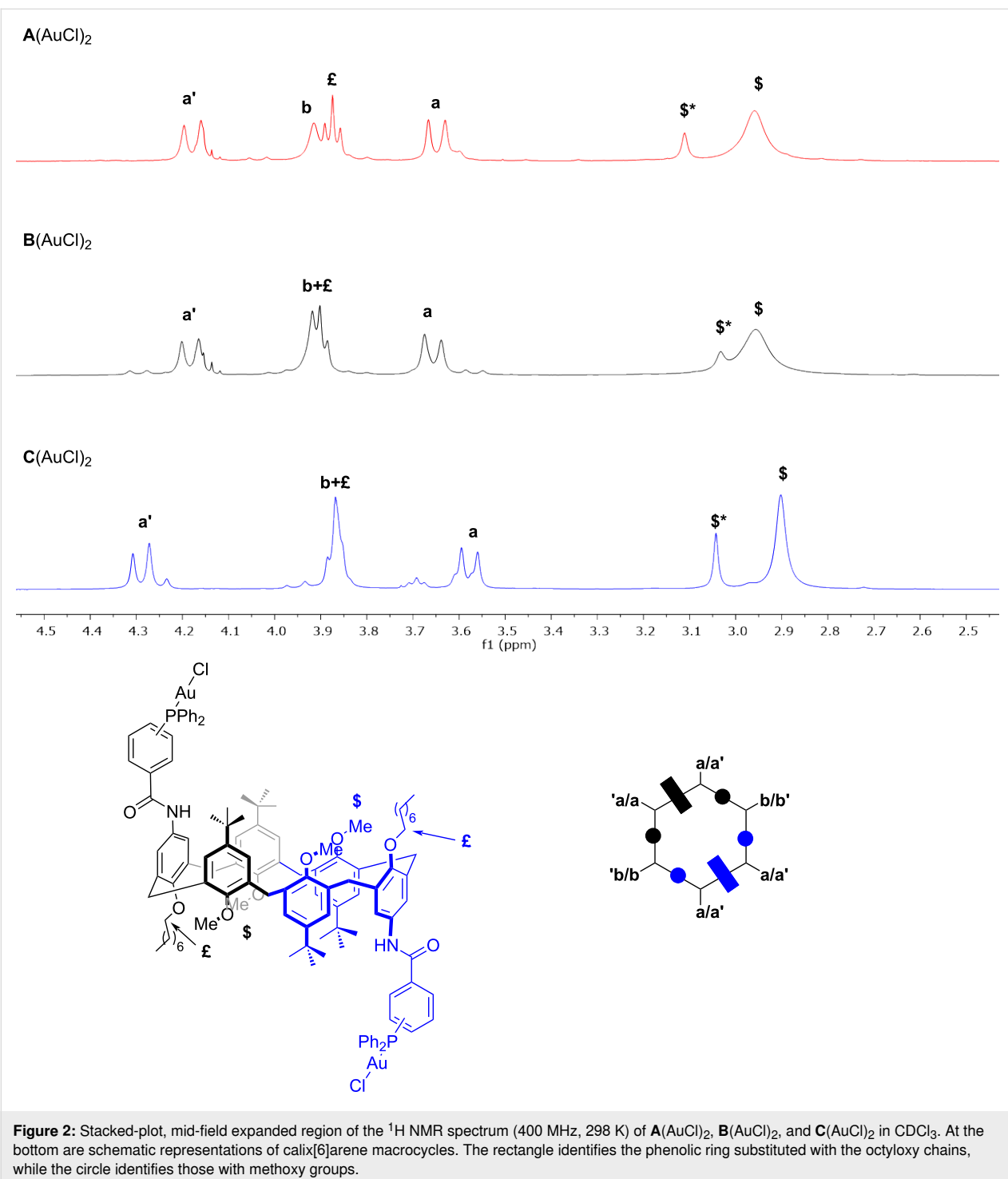


Figure 2: Stacked-plot, mid-field expanded region of the ^1H NMR spectrum (400 MHz, 298 K) of **A**(AuCl) $_2$, **B**(AuCl) $_2$, and **C**(AuCl) $_2$ in CDCl_3 . At the bottom are schematic representations of calix[6]arene macrocycles. The rectangle identifies the phenolic ring substituted with the octyloxy chains, while the circle identifies those with methoxy groups.

using AgSbF_6 as the chloride scavenger [37]. After 4 h, NMR analysis of the crude reaction mixture revealed high conversion of the starting material with the formation of the 6-*endo*-*dig* re-arranged diene **2a** and the parental regioisomer **2b** in a 1:1 ratio. Noteworthy, this latter is formed by an initial 5-*exo*-*dig* cyclization step (entry 1, Table 1) [38,39]. This result was compared with the one obtained using the macrocyclic analogue **A**(AuCl) $_2$

(1 mol %). Hence, we did not observe a significant variation in the product distribution (entry 2, Table 1).

Analogously, the reactivity in the presence of *meta*-substituted catalysts **B'**(AuCl) and **B**(AuCl) $_2$ was investigated. Also in this case, the reactivity and selectivity of the parental catalysts were comparable (entries 3 and 4, Table 1). Taken together, these

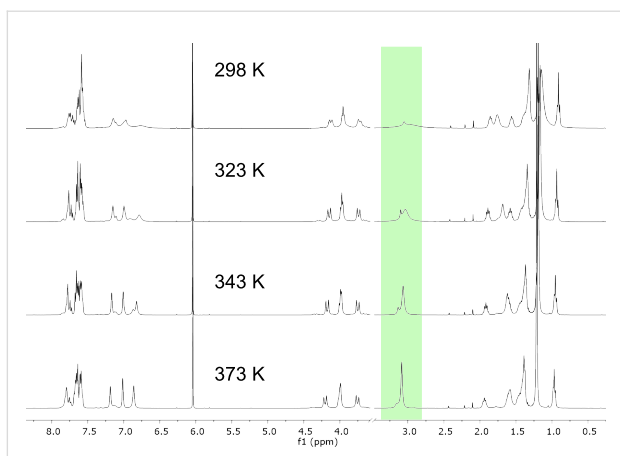
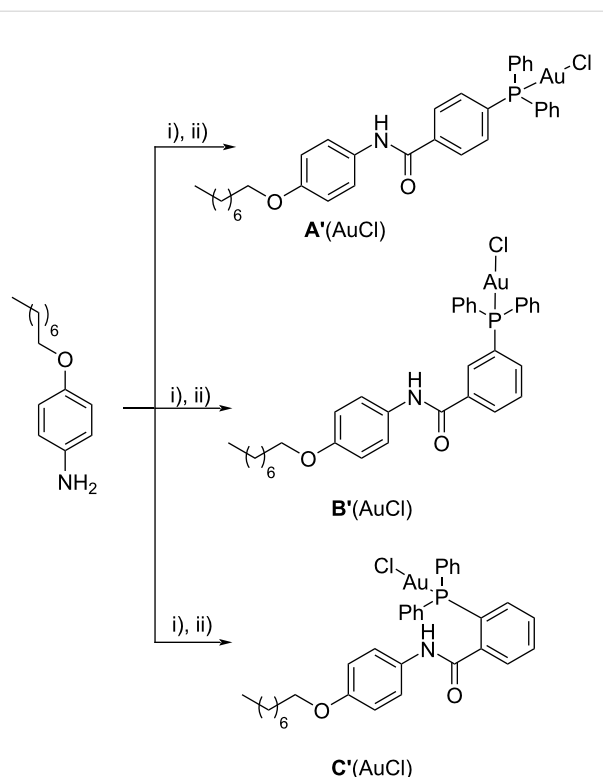


Figure 3: Stacked plot ^1H NMR (tetrachloroethane- d_2) of $\mathbf{A}(\text{AuCl})_2$ at variable temperature.

outcomes suggest that the role of the macrocycle for catalysts **A/B**(AuCl)₂ is not determining in changing the product distribution and that the catalytically active gold(I) nuclei are too far to be influenced by the cavity or by the macrocycle itself.

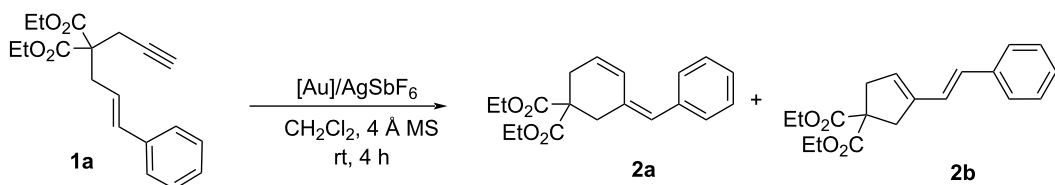
Finally, the catalytic reaction was attempted using $\mathbf{C}'(\text{AuCl})$. We thus observed a selectivity towards product **2a** (1.5:1) which might be caused by the different orientation of the phosphine ligand implanted on the aromatic ring (entry 5, Table 1). Interestingly, this effect was substantially improved with the use of the calix[6]arene-based complex $\mathbf{C}(\text{AuCl})_2$ (entry 6, Table 1). Overall, the *ortho*-substituted macrocycle $\mathbf{C}(\text{AuCl})_2$ displayed an enhanced selectivity, with respect to the parental macrocycles **A/B**(AuCl)₂, that arise from the proximity of the two gold(I) nuclei to the calix[6]arene scaffold. Although just



Scheme 2: Synthesis of the monomeric gold catalyst analogues **A'**, **B'**, **C'**(AuCl). Conditions: i) diphenylphosphinobenzoic acid, EDC·HCl, DMAP (cat.), CH_2Cl_2 , 0 °C to rt (**A'**, 71%; **B'**, 76%; **C'**, 69%); ii) (Me_2S) AuCl in DCM, 0 °C to rt (**A'**(AuCl), 94%; **B'**(AuCl), 92%; **C'**(AuCl), 96%).

preliminary, these results indicate that the conformational properties of this class of macrocycles can influence the selectivity in gold(I)-catalyzed cycloisomerization of 1,6-enynes.

Table 1: Ligand effect in gold(I)-catalyzed cycloisomerization of **1a**.



Entry ^a	[Au]	conv. [%]	2a/2b
1	A' (AuCl) (2 mol %)	89	1.0:1.0
2	A (AuCl) ₂ (1 mol %)	88	1.1:1.0
3	B' (AuCl) (2 mol %)	86	1.2:1.0
4	B (AuCl) ₂ (1 mol %)	91	1.1:1.0
5	C' (AuCl) (2 mol %)	86	1.5:1.0
6	C (AuCl) ₂ (1 mol %)	89	1.8:1.0

^aReaction conditions: **1a** (0.2 mmol), AgSbF_6 (2.0 mol %), CH_2Cl_2 (0.1 M), 4 h.

Conclusion

We reported the synthesis of a novel family of diametric diphosphine gold(I) complexes whose geometry in low-polarity solvents is controlled by the *1,2,3-alternate* conformation of the calix[6]arene precursor. These catalysts are able to tune the selectivity of catalytic cycloisomerization of 1,6-enynes as a function of the relative orientation of the bonded gold(I) nuclei with respect to the macrocycle. Further studies are currently under progress to outline the role of the macrocycle and to verify if a possible re-orientation of the gold(I) nuclei towards the center of the aromatic cavity can play any role in dictating the selectivity of the catalytic transformation.

Experimental

General procedure for catalysis: In a 10 mL two-necked round-bottomed flask containing **A**(AuCl)₂ (1.0 mol %, 4.4 mg) or **A'**(AuCl) (2.0 mol %, 3.0 mg), dry CH₂Cl₂ (2.0 mL) was added under nitrogen atmosphere. Subsequently, a tip of spatula (micro spatula, Heyman type 16 cm) of AgSbF₆ (\approx 2.0 mol %, \approx 2 mg) was added along with 20 mg of 4 Å molecular sieves. The flask was covered with an aluminum foil and the mixture stirred for 5 minutes. Subsequently, **1a** (0.2 mmol, 63.0 mg) was added and the reaction mixture was stirred for 4 hours. After completion, the mixture was diluted with 20 mL of CH₂Cl₂, filtered through a pad of celite, and transferred in a 100 mL flask where it was concentrated under reduced atmosphere. Conversions and selectivities were determined by ¹H NMR analysis (data confirmed by performing the reaction twice). ¹H NMR (**2a**) (400 MHz, CDCl₃) δ 7.48–7.19 (m, 5H), 6.63 (dtd, *J* = 10.1, 2.1, 1.0 Hz, 1H), 6.37 (s, 1H), 5.90 (dtd, *J* = 10.1, 4.0, 1.6 Hz, 1H), 4.30–4.21 (m, 4H), 2.98 (d, *J* = 1.6 Hz, 2H), 2.78 (ddd, *J* = 4.0, 2.1, 0.9 Hz, 2H), 1.32–1.24 (m, 6H). ¹H NMR (**2b**) (400 MHz, CDCl₃) δ 7.48–7.20 (m, 5H), 6.93 (d, *J* = 16.2 Hz, 1H), 6.48 (d, *J* = 16.2 Hz, 1H), 5.73 (ddd, *J* = 2.7, 1.9, 0.9 Hz, 1H), 4.23–4.14 (m, 4H), 3.28 (dd, *J* = 1.9, 0.9 Hz, 2H), 3.18 (dd, *J* = 1.9, 0.9 Hz, 2H), 1.32–1.21 (m, 6H).

Supporting Information

Supporting Information File 1

Experimental procedures, characterization data of compounds and copies of NMR spectra.
[<https://www.beilstein-journals.org/bjoc/content/supplementary/1860-5397-18-21-S1.pdf>]

Acknowledgements

The authors thank Centro Interdipartimentale di Misure of the University of Parma for NMR measurements.

Funding

This work was supported by the Italian MIUR (PRIN 20173L7W8 K). This work was carried out within the COMP-HUB Initiative, funded by the "Departments of Excellence" program of the Italian Ministry of Education, University and Research (MIUR, 2018–2020).

ORCID® IDs

Andrea Secchi - <https://orcid.org/0000-0003-4045-961X>
Gianpiero Cera - <https://orcid.org/0000-0002-2702-282X>

References

1. Kaya, Z.; Bentouhami, E.; Pelzer, K.; Arnsbach, D. *Coord. Chem. Rev.* **2021**, *445*, 214066. doi:10.1016/j.ccr.2021.214066
2. Olivo, G.; Capocasa, G.; Del Giudice, D.; Lanzalunga, O.; Di Stefano, S. *Chem. Soc. Rev.* **2021**, *50*, 7681–7724. doi:10.1039/d1cs00175b
3. Gramage-Doria, R.; Arnsbach, D.; Matt, D. *Coord. Chem. Rev.* **2013**, *257*, 776–816. doi:10.1016/j.ccr.2012.10.006
4. Kamer, P. C. J.; van Leeuwen, P. W. N. M., Eds. *Phosphorus(III) Ligands in Homogeneous Catalysis: Design and Synthesis*; John Wiley & Sons: Chichester, UK, 2012. doi:10.1002/9781118299715
5. Orton, G. R. F.; Pilgrim, B. S.; Champness, N. R. *Chem. Soc. Rev.* **2021**, *50*, 4411–4431. doi:10.1039/d0cs01556c
6. Shet, H.; Parmar, U.; Bhilare, S.; Kapdi, A. R. *Org. Chem. Front.* **2021**, *8*, 1599–1656. doi:10.1039/d0qo01194k
7. Matt, D.; Harrowfield, J. *ChemCatChem* **2021**, *13*, 153–168. doi:10.1002/cctc.202001242
8. Sémeril, D.; Matt, D. *Coord. Chem. Rev.* **2014**, *279*, 58–95. doi:10.1016/j.ccr.2014.06.019
9. Schöttle, C.; Guan, E.; Okrut, A.; Grosso-Giordano, N. A.; Palermo, A.; Solovyov, A.; Gates, B. C.; Katz, A. J. *Am. Chem. Soc.* **2019**, *141*, 4010–4015. doi:10.1021/jacs.8b13013
10. Karpus, A.; Yesipenko, O.; Boiko, V.; Poli, R.; Daran, J.-C.; Voitenko, Z.; Kalchenko, V.; Manoury, E. *Eur. J. Org. Chem.* **2016**, 3386–3394. doi:10.1002/ejoc.201600208
11. Elaieb, F.; Hedhli, A.; Sémeril, D.; Matt, D. *Eur. J. Org. Chem.* **2016**, 1867–1873. doi:10.1002/ejoc.201600055
12. Monnereau, L.; Sémeril, D.; Matt, D.; Toupet, L. *Adv. Synth. Catal.* **2009**, *351*, 1629–1636. doi:10.1002/adsc.200900074
13. Sémeril, D.; Matt, D.; Toupet, L. *Chem. – Eur. J.* **2008**, *14*, 7144–7155. doi:10.1002/chem.200800747
14. Chavagnan, T.; Sémeril, D.; Matt, D.; Toupet, L. *Eur. J. Org. Chem.* **2017**, 313–323. doi:10.1002/ejoc.201601278
15. Chavagnan, T.; Sémeril, D.; Matt, D.; Harrowfield, J.; Toupet, L. *Chem. – Eur. J.* **2015**, *21*, 6678–6681. doi:10.1002/chem.201500177
16. El Moll, H.; Sémeril, D.; Matt, D.; Toupet, L. *Adv. Synth. Catal.* **2010**, *352*, 901–908. doi:10.1002/adsc.200900767
17. El Moll, H.; Sémeril, D.; Matt, D.; Youinou, M.-T.; Toupet, L. *Org. Biomol. Chem.* **2009**, *7*, 495–501. doi:10.1039/b813373e
18. Martín-Torres, I.; Ogalla, G.; Yang, J.-M.; Rinaldi, A.; Echavarren, A. M. *Angew. Chem., Int. Ed.* **2021**, *60*, 9339–9344. doi:10.1002/anie.202017035
19. Rusali, L. E.; Schramm, M. P. *Tetrahedron Lett.* **2020**, *61*, 152333. doi:10.1016/j.tetlet.2020.152333

20. Inoue, M.; Kamiguchi, S.; Ugawa, K.; Hkiri, S.; Bouffard, J.; Sémeril, D.; Iwasawa, T. *Eur. J. Org. Chem.* **2019**, 6261–6268. doi:10.1002/ejoc.201901058
21. Ho, T. D.; Schramm, M. P. *Eur. J. Org. Chem.* **2019**, 5678–5684. doi:10.1002/ejoc.201900829
22. Inoue, M.; Ugawa, K.; Maruyama, T.; Iwasawa, T. *Eur. J. Org. Chem.* **2018**, 5304–5311. doi:10.1002/ejoc.201800948
23. Endo, N.; Inoue, M.; Iwasawa, T. *Eur. J. Org. Chem.* **2018**, 1136–1140. doi:10.1002/ejoc.201701613
24. Schramm, M. P.; Kanaura, M.; Ito, K.; Ide, M.; Iwasawa, T. *Eur. J. Org. Chem.* **2016**, 813–820. doi:10.1002/ejoc.201501426
25. Endo, N.; Kanaura, M.; Schramm, M. P.; Iwasawa, T. *Eur. J. Org. Chem.* **2016**, 2514–2521. doi:10.1002/ejoc.201600362
26. Mitschke, B.; Turberg, M.; List, B. *Chem* **2020**, *6*, 2515–2532. doi:10.1016/j.chempr.2020.09.007
27. Mouarrawis, V.; Plessius, R.; van der Vlugt, J. I.; Reek, J. N. H. *Front. Chem. (Lausanne, Switz.)* **2018**, *6*, 623. doi:10.3389/fchem.2018.00623
28. Homden, D. M.; Redshaw, C. *Chem. Rev.* **2008**, *108*, 5086–5130. doi:10.1021/cr8002196
29. Cera, G.; Arduini, A.; Secchi, A.; Credi, A.; Silvi, S. *Chem. Rec.* **2021**, *21*, 1161–1181. doi:10.1002/tcr.202100012
30. Cera, G.; Giovannardi, G.; Secchi, A.; Arduini, A. *Chem. – Eur. J.* **2021**, *27*, 10261–10266. doi:10.1002/chem.202101323
31. Cera, G.; Cester Bonati, F.; Bazzoni, M.; Secchi, A.; Arduini, A. *Org. Biomol. Chem.* **2021**, *19*, 1546–1554. doi:10.1039/d0ob02393k
32. Cera, G.; Bazzoni, M.; Arduini, A.; Secchi, A. *Org. Lett.* **2020**, *22*, 3702–3705. doi:10.1021/acs.orglett.0c01191
33. Bazzoni, M.; Zanichelli, V.; Casimiro, L.; Massera, C.; Credi, A.; Secchi, A.; Silvi, S.; Arduini, A. *Eur. J. Org. Chem.* **2019**, 3513–3524. doi:10.1002/ejoc.201900211
34. Cera, G.; Bazzoni, M.; Andreoni, L.; Cester Bonati, F.; Massera, C.; Silvi, S.; Credi, A.; Secchi, A.; Arduini, A. *Eur. J. Org. Chem.* **2021**, 5788–5798. doi:10.1002/ejoc.202101080
35. van Duynhoven, J. P. M.; Janssen, R. G.; Verboom, W.; Franken, S. M.; Casnati, A.; Pochini, A.; Ungaro, R.; de Mendoza, J.; Nieto, P. M. *J. Am. Chem. Soc.* **1994**, *116*, 5814–5822. doi:10.1021/ja00092a036
36. Nieto-Oberhuber, C.; Paz Muñoz, M.; López, S.; Jiménez-Núñez, E.; Nevado, C.; Herrero-Gómez, E.; Raducan, M.; Echavarren, A. M. *Chem. – Eur. J.* **2006**, *12*, 1677–1693. doi:10.1002/chem.200501088
37. A model reaction performed with AgSbF_6 (2 mol %) as the catalyst, in the absence of any gold(I) complex, did not lead to any conversion of starting material **1a**.
38. Fürstner, A.; Morency, L. *Angew. Chem., Int. Ed.* **2008**, *47*, 5030–5033. doi:10.1002/anie.200800934
39. Jiménez-Núñez, E.; Echavarren, A. M. *Chem. Rev.* **2008**, *108*, 3326–3350. doi:10.1021/cr0684319

License and Terms

This is an open access article licensed under the terms of the Beilstein-Institut Open Access License Agreement (<https://www.beilstein-journals.org/bjoc/terms>), which is identical to the Creative Commons Attribution 4.0 International License

(<https://creativecommons.org/licenses/by/4.0>). The reuse of material under this license requires that the author(s), source and license are credited. Third-party material in this article could be subject to other licenses (typically indicated in the credit line), and in this case, users are required to obtain permission from the license holder to reuse the material.

The definitive version of this article is the electronic one which can be found at:

<https://doi.org/10.3762/bjoc.18.21>



Site-selective reactions mediated by molecular containers

Rui Wang and Yang Yu*

Review

Open Access

Address:
Center for Supramolecular Chemistry & Catalysis and Department of Chemistry, College of Science, Shanghai University, 99 Shang-Da Road, Shanghai 200444, China

Email:
Yang Yu* - yangyu2017@shu.edu

* Corresponding author

Keywords:
confinement; microenvironment; molecular containers; noncovalent protective group; site-selectivity

Beilstein J. Org. Chem. **2022**, *18*, 309–324.
<https://doi.org/10.3762/bjoc.18.35>

Received: 31 January 2022
Accepted: 04 March 2022
Published: 14 March 2022

This article is part of the thematic issue "Supramolecular approaches to mediate chemical reactivity".

Guest Editor: C. Gaeta

© 2022 Wang and Yu; licensee Beilstein-Institut.
License and terms: see end of document.

Abstract

In this review, we summarize various site-selective reactions mediated by molecular containers. The emphasis is on those reactions that give different product distributions on the potential reactive sites inside the containers than they do outside, free in solution. Specific cases include site-selective cycloaddition and addition of arenes, reduction of epoxides, α,β -unsaturated aldehydes, azides, halides and alkenes, oxidation of remote C–H bonds and alkenes, and substitution reactions involving ring-opening cyclization of epoxides, nucleophilic substitution of allylic chlorides, and hydrolysis reactions. The product selectivity is interpreted as the consequence of the space shape and environment inside the container. The containers include supramolecular structures self-assembled through metal/ligand interactions or hydrogen bonding and open-ended covalent structures such as cyclodextrins and cavitands. Challenges and prospects for the future are also provided.

Introduction

To run reactions with discriminate control over product selectivity represents one of the huge challenges in organic synthetic chemistry [1], among which, site-selectivity is always crucial to a reaction when there is more than one potential reactive site in a certain substrate, because poor site-selectivity would result in complicated and sometimes even unachievable separation and purification procedures. Hence, in order to drive reactions economically and efficiently, organic chemists have made great efforts to increase site-selectivity, with the best result of site-specificity [2–4]. However, it is rather difficult to do so, differentiating one certain reactive site from the similar others,

because the difference between their transition-state free energies, that would modulate isomeric product ratio, is always small. The selectivity of a reaction depends on its mechanism, and the inherent feature of the substrate should be enhanced or overturned to obtain one certain isomer, with the consideration of electronic, steric, and stereoelectronic factors [5,6]. As a representative strategy, directing groups are introduced to the substrates covalently to achieve site-selective C–H bond activation, which prospered greatly in the past decades [7–9]. Template regulation is also introduced to locate reactive centers in a noncovalent way through hydrogen bonding [10–12]. Even

though chemists have developed different kinds of methods to achieve site-selectivity of various reactions, new methodologies that blend with other research fields are still needed.

After decades of rapid development, supramolecular chemistry has won two times for Nobel Prizes and already became one of the most important fields in modern chemistry [13–15]. It is based on a wide range of noncovalent interactions between molecules [16–18] and has been applied to a variety of research areas including molecular recognition, molecular devices, nanotechnology, catalysis, etc. [13–18]. By mimicking the recognition and catalysis behavior of enzymes with designed and synthesized molecular containers such as cyclodextrins, cucurbiturils, calixarenes, and resorcinarenes, chemists try to tackle problems of traditional synthetic chemistry, including increase in reactivity, induction of selectivity, and even emergence of new reaction pathways [19–24]. To simulate the aqueous environment of enzyme-catalyzed physiological transformations, researchers seek to design and synthesize supramolecular hosts in a water-soluble way. The ionic and polyol forms of them would provide good water solubility, and, on the other hand, these kinds of water-soluble moieties could also be introduced into the structures of other hosts to help them gain some extent of water solubility. In aqueous solution, the molecular containers provide hydrophobic pockets capable of binding a wide range of organic compounds. Within the molecular container, guest molecules can be encapsulated with a certain orientation and conformation through various noncovalent interactions. In this mode, the molecular container can act as reaction template and give rise to selective products. For example, the molecular container can be used as anchoring template, which fix the substrate with a certain stable conformation, exposing one specific reactive site to the catalyst and producing site-selective product [25,26]. Moreover, molecular containers have more and more been applied to modulate site-selectivity of different types of reactions and this research field has drawn much attention in the past years [27–30]. It is believed that there is still more to explore and develop in this area, so we summarize representative research works about molecular-container-confined organic reactions with site-selectivity, that is, selective reactions that take place at one specific potential reactive site out of the similar others, in this review. In the following part, the literature reports will be mainly divided according to the reaction types, namely cycloaddition/addition, reduction, oxidation, and substitution.

Review

Cycloaddition/addition

Cycloaddition reactions have long been applied to molecular container-mediated enzyme-mimicking transformations [27,31–33], and the Fujita group has done pioneering research works in

this direction [27,34]. In 2006, the authors reported unique Diels–Alder reactions of anthracene and phthalimide guests with unusual and controllable site-selectivity mediated by organopalladium-coordinated hosts in water (Figure 1) [34]. The water-solubility of the coordinated host traced from its ionic form, and the aqueous reaction conformed with the concept of green chemistry. In previous reports of supramolecular host-mediated Diels–Alder reactions of anthracenes, 9,10-adducts bridging the center rings of the anthracene frameworks were generally yielded [35–37], which resulted from the high localization of π -electron density at that sites [38]. Besides, these reactions required near-stoichiometric quantities of hosts because of the product inhibition effect, which arose from the entropic disadvantage of the need for binding two reactant molecules [39–43]. In this particular report, when the octahedral cage host **A** was used, the Diels–Alder reaction of 9-hydroxymethylanthracene (**1**) and *N*-cyclohexylphthalimide (**2**) went smoothly at 80 °C for 5 hours with near quantitative yield (Figure 1b). Only the *syn*-isomer of the 1,4-adduct **3** was detected after the reaction, which was determined by X-ray crystallographic analysis of **A**•**3**. It was also shown that the product was tightly accommodated in the cavity of **A** through π – π stacking interactions between the naphthalene ring of **3** and a triazine ligand of **A** from the X-ray crystallographic analysis. In the control experiment, without host **A**, only 44% yield of the conventional 9,10-adduct **4** was produced without any 1,4-adduct product (Figure 1c). This kind of unusual site-selectivity originated from the fixed orientation of the guest substrates confined to the cage host **A** before the reaction. Force-field calculations showed that the guest substrates **1** and **2** were parallel to each other with the double bond of **2** in close contact with the 1,4-position of **1**. On the other hand, the double bond of **2** hardly interacted with the 9,10-position of **1**, because of the steric effect induced by the cage host **A**. This methodology was also compatible with several other anthracene substrates with different substituents at the 9-position. But when the sterically less demanding *N*-propylphthalimide was used, only the 9,10-adduct was formed, which indicated that the steric bulkiness of the *N*-substituent in the dienophile also affected the 1,4-site-selectivity. It is very intriguing that when a different kind of square-pyramidal bowl host **B** was employed, the site-selectivity turned back to the 1,9-position, and with catalytic turnover (Figure 1d). Only 10 mol % of **B** promoted the Diels–Alder reaction of **1** and *N*-phenylphthalimide (**5**) almost quantitatively affording the 9,10-adduct **6** at room temperature for 5 hours. Control experiments proved the promoting effect of the hydrophobic pocket of **B**. The origin of the catalytic behavior of the bowl host **B** can be explained by two main aspects. Firstly, the bowl host **B** possesses an open cavity that facilitates rapid binding and dissociation of the guests. Secondly and more importantly, before the reaction, the anthracene moiety stacks

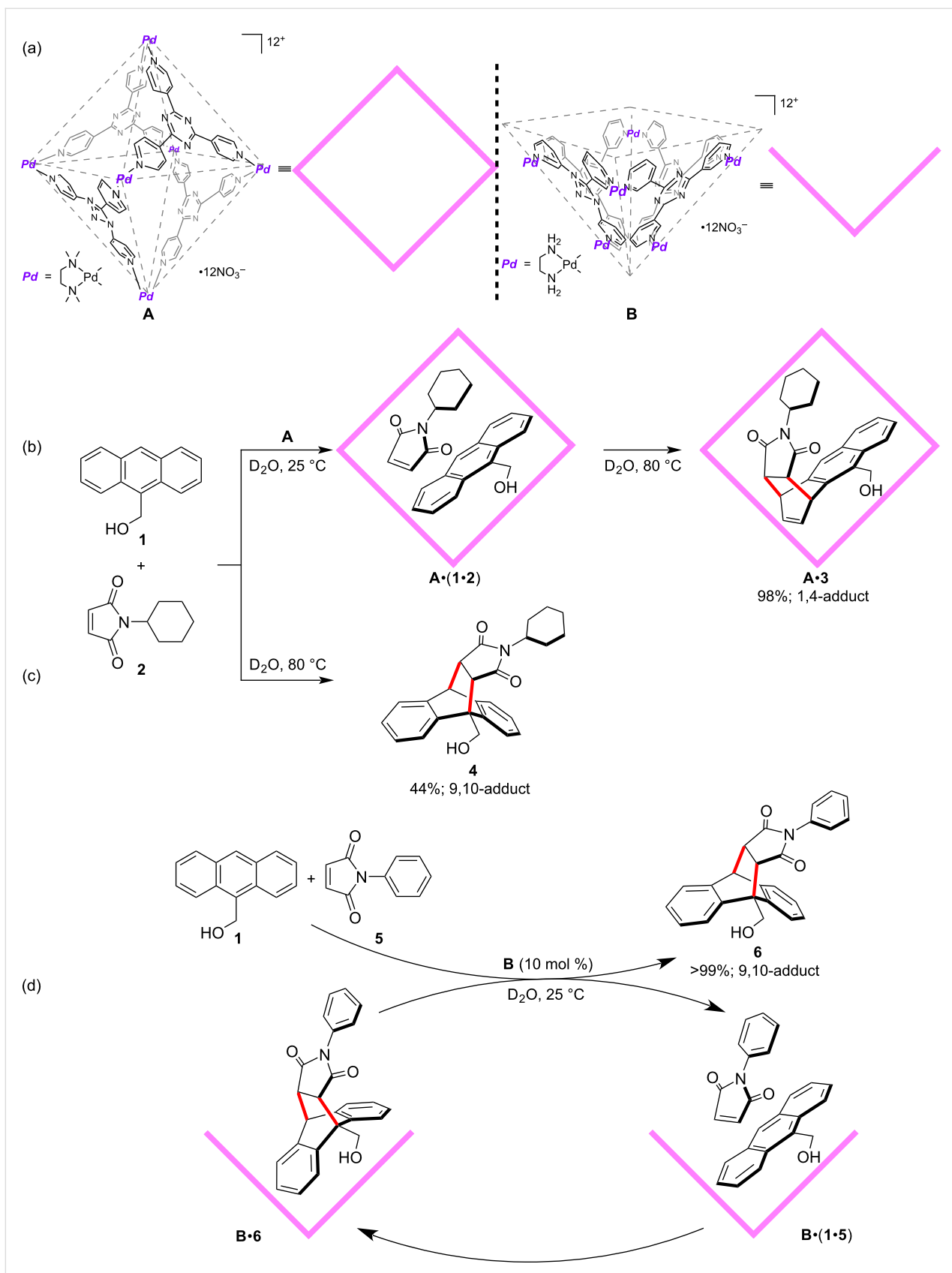


Figure 1: Site-selective Diels–Alder reaction of anthracene and phthalimide mediated by aqueous organopalladium-coordinated hosts **A** and **B**.

onto the planar triazine of **B** through π – π stacking and possible charge-transfer interaction between each other, which stabilizes the complex. However, after the reaction, the framework of the product is bent at the 9,10-position, which undermines the host–guest stacking interaction. The complex of **B** and the product is hence destabilized, resulting in the replacement by incoming reactants. This beautiful pioneering work showed elegant examples of how the designed and synthetic molecular containers could mediate and even control the site-selectivity of organic reactions.

Naphthalene is usually hard to undergo Diels–Alder reactions [44–46], even though the quantum-mechanical and thermochemical calculations suggest that the reaction is exothermic, which indicates the entropic cost is significant [47]. In 2010, the same group reported another interesting site-selective Diels–Alder and [2 + 2]-photoaddition reactions between **2** and 2,3-substituted naphthalene **7** mediated by cage host **A** mentioned above (Figure 2) [48]. Given the reduction of the entropic cost resulting from the effective concentration and preorganization of the guest reactants confined to the molecular containers, the authors designed to investigate the Diels–Alder reaction between **2** and naphthalene **7**. As expected, the reactants were encapsulated within the cage host **A** successfully at room temperature and formed a ternary complex **A**•(**7**•**2**), and after being heated at 100 °C for 8 hours, the site-selective product **8** was obtained with moderate yield. No other side reactions were observed, and the moderate yield resulted from the partial

sublimation of the reactants. The reaction proceeded site-selectively at the unsubstituted ring of the 2,3-substituted naphthalene, and produced stereoselectively the *syn* isomer **8**, which was determined and confirmed by multiple characterization methods including NMR, mass, and X-ray crystallographic analysis. The reaction did not take place without the cage host **A**. Alkyl substituents at the C2 and C3 position of naphthalene were crucial to this reaction. Control experiments upon the substituent effect indicated that it was the steric, not the electronic factor, that ruled the reactivity and selectivity. The electron-donating alkyl groups should have facilitated reaction at the substituted ring, in contrast, the reaction occurred at the unsubstituted ring. This unusual site-selectivity can be explained by the preorganization of the reactants within the cage host **A**. In the confined space of the cavity, the orientation of the substrates was fixed presumably with the unsubstituted ring of naphthalene subject to the double bond of **2**. This work showed the remarkable function of molecular containers to override natural reactivity and produce unusual site-selective products. Intriguingly, upon irradiation, a site- and stereoselective [2 + 2]-photoaddition between **2** and **7** took place smoothly, giving rise to the *syn* isomer of the 5,6-adduct **9**. In a following work, the authors reported similar site-selective Diels–Alder reactions between **2** and inert aromatics including aceanthrylene and 1*H*-cyclopenta[*I*]phenanthrene [49].

Generally, it is difficult to achieve site- and stereoselective control over radical reactions. The radical species are very reac-

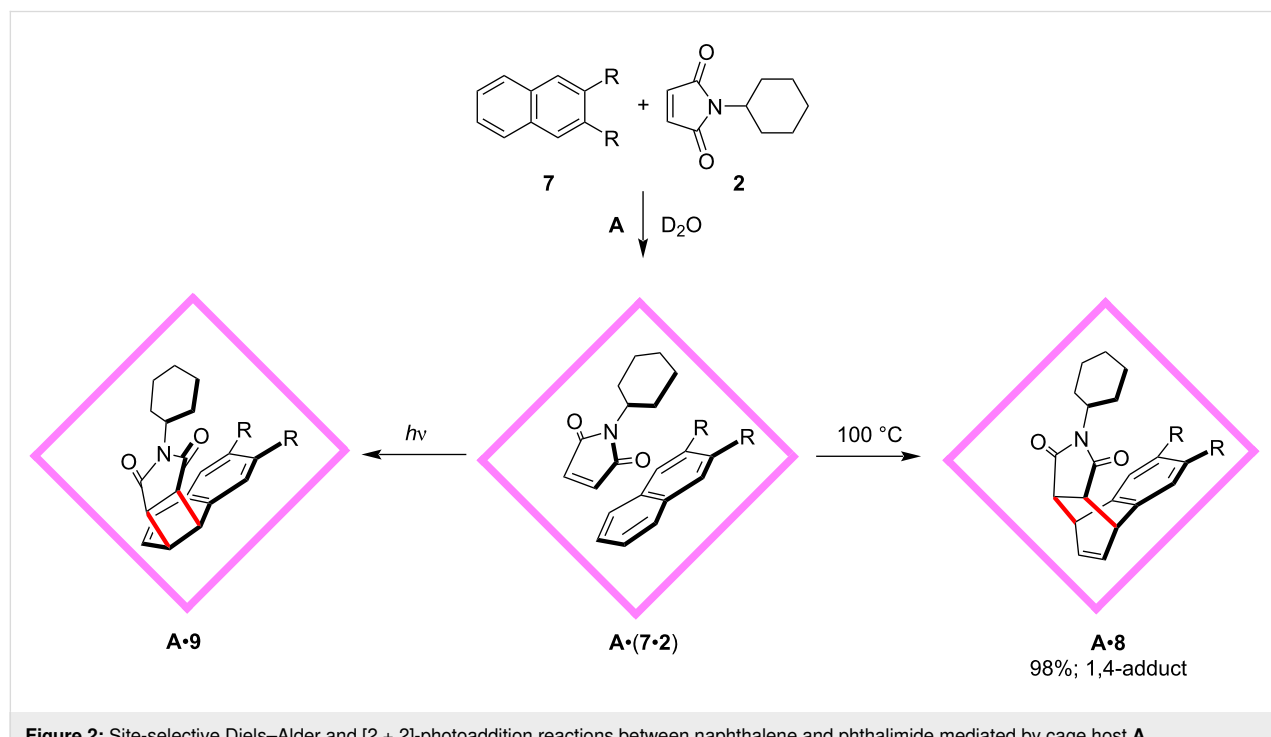


Figure 2: Site-selective Diels–Alder and [2 + 2]-photoaddition reactions between naphthalene and phthalimide mediated by cage host **A**.

tive and a complex mixture of different products will form through various pathways [50–53]. By applying the cage host **A**, the authors realized a highly site-selective radical addition reaction of *o*-quinone **10** and substituted toluene **11**, giving rise to the unusual 1,4-adduct **15** (Figure 3) [54]. Specifically, upon irradiation, biradical species **12** was generated and immediately abstracted a hydrogen atom from the methyl group of **11**. Site-selective radical coupling at the oxygen atom between **13** and **14** produced the 1,4-adduct **15**. The unusual site-selectivity of this reaction was also traced from the restricted geometry and fixed orientation of the guests inside the cage **A**. One of the carbonyl groups of **10** was in close proximity to the methyl group of **11**, which was determined by X-ray crystallography. The possible *C*-coupled 1,2-adduct and other coupling products were not detected. However, in the absence of host **A**, a mixture was formed without the *O*-coupled 1,4-adduct **15**. This indicated that the molecular container **A** favored the *O*-coupling pathway while suppressed others. This work showed the powerful site-selective control ability of molecular containers, which was normally only observed in natural enzymes.

Reduction

Except for controlled cycloadditions, the site-selective reduction is also difficult to achieve. It mainly depends on the oxidative difference between the potential reactive sites and the careful picking of reductive reagents. Once the oxidative prop-

erties of these sites are similar to each other, it is rather hard to just reduce only one site in the presence of the others. Protecting groups are widely used to prevent reaction of one or more functional groups and let others to react [55–57]. Generally, protecting groups are covalently connected to the targeted groups, which requires prefunctionalization and deprotection synthetic procedures. Based on the logical concept of protecting groups, noncovalent interactions can be considered, because they can be built up *in situ* and are weak enough to let the substrate dissociate from the “protecting template” easily, omitting the complicated prefunctionalization and deprotection processes. Moreover, functional groups that are not suitable for being functionalized with protecting groups can also be incorporated into the noncovalent protective systems. Actually, the molecular container has been applied to work as a noncovalent protective module. In this mode, the molecular container selectively binds with and shields a certain part of the guest molecule and leaves the remaining part exposed to the reaction medium. This methodology was firstly applied to the site-selective reduction reaction mediated by a cyclodextrin host. In 1991, the Takahashi group reported the cyclodextrin-mediated site-selective ring-opening reductive reaction of epoxide **16** by sodium borohydride in aqueous solution (Figure 4b) [58]. The sugar-based hosts show good water solubility and can be used for driving organic reactions in water. In this case, the cyclodextrin host and the epoxide guest formed a 2:1 complex, and the

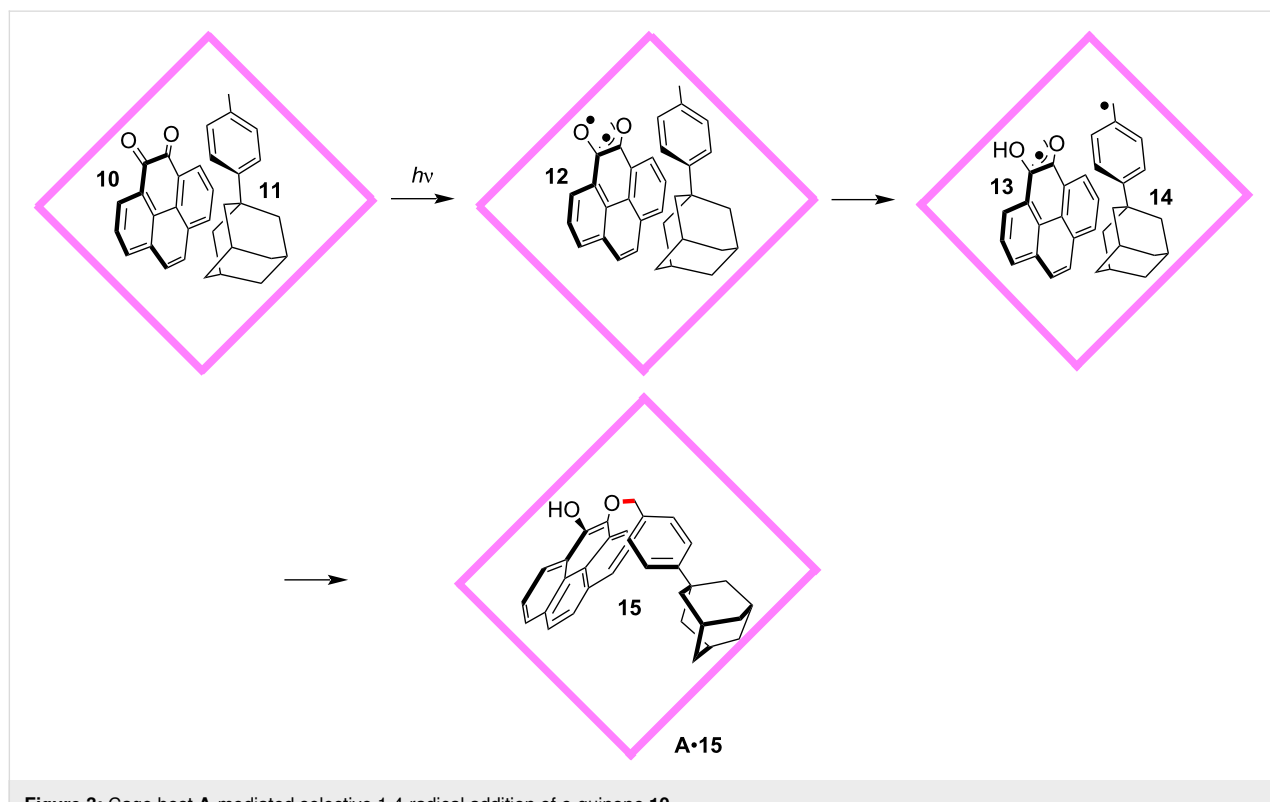


Figure 3: Cage host **A**-mediated selective 1,4-radical addition of *o*-quinone **10**.

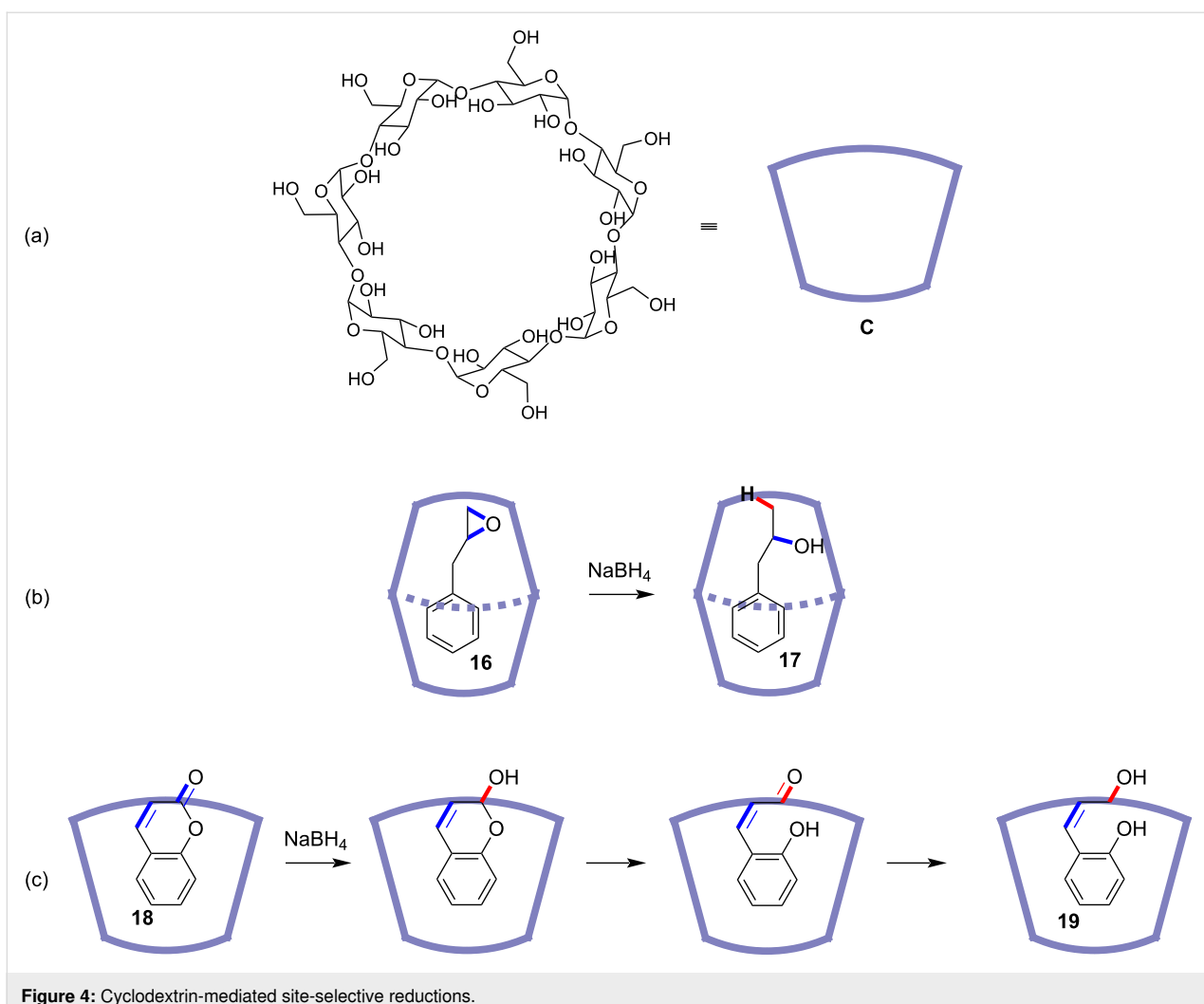


Figure 4: Cyclodextrin-mediated site-selective reductions.

internal reactive site of the epoxide was protected by the cyclodextrin host. Therefore, only the terminal site was attacked by the incoming hydride leading to epoxide-ring opening and formation of 1-phenyl-2-propanol (**17**). Utilizing the similar molecular container as the noncovalent protective group, the Pitchumani and Srinivasan group also reported that the reduction of coumarin (**18**) by sodium borohydride could be site-selectively induced in the presence of β -cyclodextrin **C** (Figure 4c) [59]. The reduction site-selectively occurred at the carbonyl not the alkenyl site, producing the final 1,2-reduction product *cis*-*O*-hydroxycinnamyl alcohol **19**. As a comparison, in the absence of the β -cyclodextrin host, both the 1,2- and 1,4-reduction products were observed. X-ray crystallography determined the host–guest complex of the coumarin and β -cyclodextrin, which could be regarded as a protective group by shielding the internal alkenyl site.

In 2016, the Rebek group achieved the site-selective reduction of an α,ω -diazide compound by trimethylphosphine (PMe_3) in

aqueous solution with a cavitand host as the protecting group for one of the azide sites (Figure 5) [60]. The host in here was a water-soluble deep cavitand **D** with methylated urea groups on the rim, which had already been used to mediate other organic reactions [61]. The feet of the host were transformed to pyridinium cationic moieties to make it soluble in water, and in other examples, similar cavitand hosts were also modified with imidazolium cationic or carboxylic anionic feet [29]. Before the reaction, NMR analysis of the host–guest complex indicated that the bound guest was in yo-yo motions time-averaged between unsymmetrical J-shaped conformations and symmetrical U-shaped ones. Treatment of the complex solution with three equivalents of PMe_3 resulted in the reduction of one of the azide groups. At this stage, the monoamine guest showed a fixed unsymmetrical J-shaped conformation with the amine end exposed and the azide end deeply protected inside the cavitand. The addition of another 3 equivalents of PMe_3 to the post-reaction mixture after 24 hours still did not induce further reduction of the residual azide group. However, control experiments gave

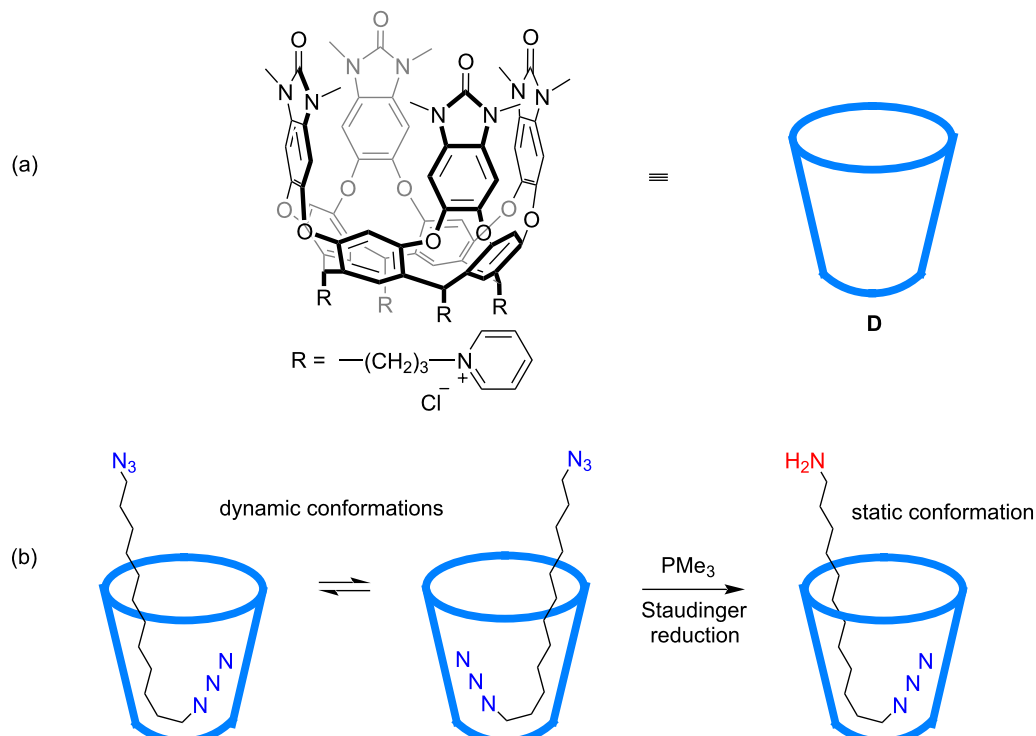


Figure 5: Selective reduction of an α,ω -diazide compound mediated by water-soluble cavitand **D**.

just the diamine products. This work opened the protective ability of water-soluble cavitands and inspired many other following examples of various site-selective mono-transformations.

Another site-selective radical monoreduction of dihalides mediated by water-soluble cavitand hosts **E** and **F** was reported later (Figure 6) [62]. Ph_3SnH was used as radical initiator and reduction reagent, and alkyl dihalide **20** could be site-selectively monoreduced to the corresponding alkyl halide **21** as major product, together with minor alkane product that arose from the reaction outside the cavitand (Figure 6b). Experiments also indicated that the binding of the guests with the hosts must show high affinities ($K_A > 1.2 \times 10^3 \text{ M}^{-1}$) to make sure the reactions occur under confinement in the host. When using a rigidified host **F**, the secondary alkyl dibromide **22** was transformed to the monoreduced product **23** with high site-selectivity, which benefited from the high K_A value ($\approx 1.5 \times 10^5 \text{ M}^{-1}$) (Figure 6c). This work represented the first example of supramolecular containers applied for a radical reaction involving external radical initiators with dynamic hosts. Later, this group reported another highly site-selective radical monoreduction of dihalides by trialkylsilanes (R_3SiH) using the similar strategy [63].

A very intriguing site-selective catalytic hydrogenation reaction mediated by a supramolecular catalyst was reported by Raymond, Bergman and Toste in 2019 (Figure 7) [64]. In this example, the supramolecular catalyst was prepared in situ by mixing a rhodium complex with the $\text{Ga}_4\text{L}_6^{12-}$ cage host **G**, which had a relatively larger size with pyrene-walled ligands (Figure 7a). The normally used analogous smaller-sized host was assembled with naphthalene-walled ligands, which had been used widely in mediating various reactions, including dehydration reaction [65], aza-Darzens reaction [66], and reductive amination [67], etc. [28]. The anionic cage host demonstrated a relatively high affinity towards cationic guests through cation– π interactions, which was crucial for the catalysis of many of the organic reactions. And similarly, the ionic form of the host made it water-soluble and reactions could be conducted in water. In this particular example, the polyenol substrate **24**, derived from linolenic acid, was monohydrogenated at the terminal, sterically accessible site inside the supramolecular supported catalyst to **25** with 74% yield at room temperature for 20 hours (Figure 7b). A control experiment showed that this kind of site-selectivity could not be achieved with just the rhodium catalyst, by which in contrast, the fully hydrogenated product was obtained. Other series of intermolecular comparative experiments also showed the selectivity of the hydroge-

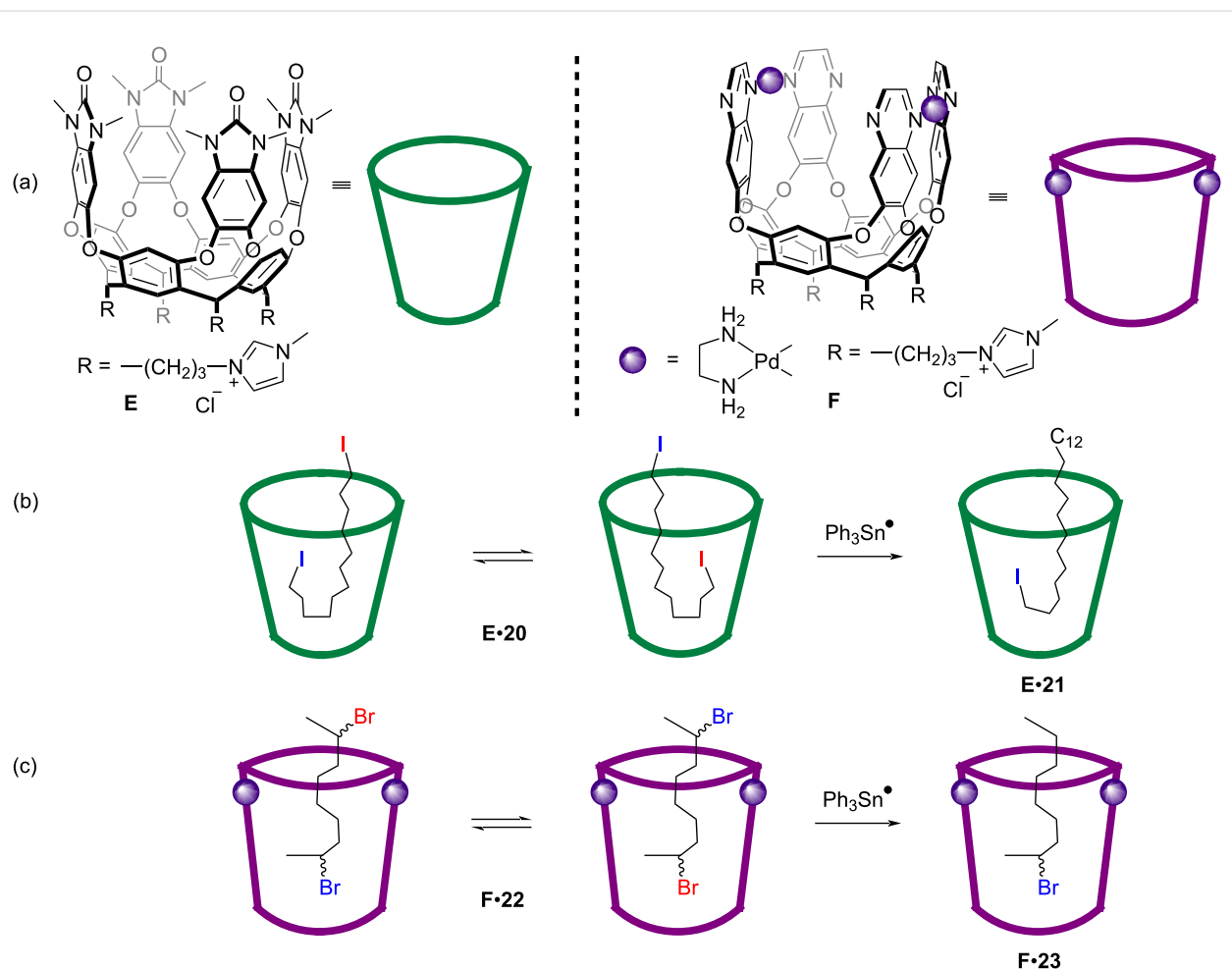


Figure 6: Selective radical reduction of α,ω -dihalides mediated by water-soluble cavitands **E** and **F**.

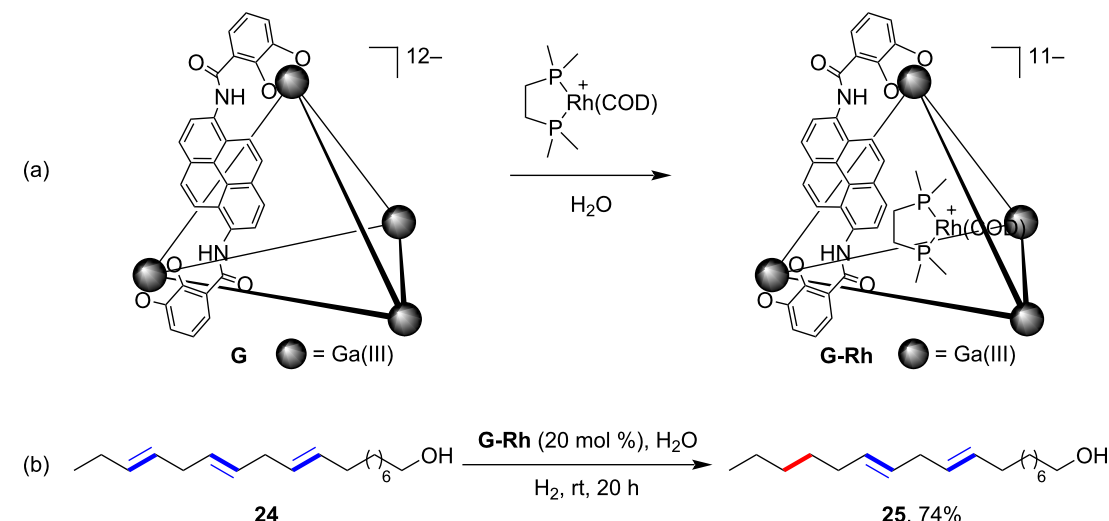


Figure 7: Site-selective hydrogenation of polyenols mediated by supramolecular encapsulated rhodium catalyst.

tion for the sterically accessible alkene over other sites and even in the presence of inherently more reactive alkynes and allylic alcohols. Both the microenvironment of the supramolecular catalyst and the steric profile of the substrate were responsible for the site-selectivity of hydrogenation. This beautiful work of a supramolecular-mediated catalytic site-selective reaction exhibited the powerful role of molecular containers to achieve precise transformation of complex molecules.

Oxidation

C–H bonds are ubiquitously distributed in nearly all of the organic compounds, which makes them predominant candidates for the modification of complex molecules. Without pre-activation, direct functionalization of C–H bonds brings reaction economy and effectiveness. However, owing to the rife-ness of the reactivity-similar C–H bonds, it is hard to achieve discriminate control over the product site-selectivity. In nature, the site-selective oxidation of C–H bonds is facilitated by enzymes with the donor molecules orienting precisely fixed towards the active site of the enzyme through multiple noncovalent interactions [68,69]. Inspired by the magical ability of the enzyme's receptor site to act on the substrate with fixed orientation, the Breslow group has done a lot of leading works [25,26] utilizing cyclodextrin as the anchoring template. For example, cyclodextrin would fix the steroid substrate with a certain set of orientation, which exposes one certain C–H bond to the metalloporphyrin catalytic moiety and produces site-selective oxidized product. As shown in Figure 8, in this methodology, the steroid substrate **26** was first modified at the hydroxy groups through esterification with a designed acid moiety possessing a *p*-*tert*-butylphenyl group and transformed to the corresponding model substrate **27**. The catalyst **H** used here was a manganese(III)-bounded porphyrin module carrying four β -cyclodextrin units at the end. Once the two parts were mixed in the reaction system, the two *p*-*tert*-butylphenyl groups of the substrate **27** were recognized by the β -cyclodextrin and anchored through the host–guest binding. At this stage, the steroid core exposed the 6-position C–H bond to the metalloporphyrin unit catalytic center and gave rise to the site-selective 6-hydroxy derivative, which was then hydrolyzed to the final site-selective product **28**. The series of work showed that the powerful molecular container could be used as the anchoring group in the template catalysis. Subsequent reports by other groups illustrated that apart from molecular containers, other designed moieties could also be used to anchor the substrate through hydrogen-bonding interactions [10–12].

In 2019, the Fujita group reported the site-selective oxidations of linear diterpenoids with the help of cage host **A** (Figure 9) [70]. The linear diterpenoid substrates have four C–C double bonds with a trisubstituted terminal one. Functionalization of

these structures would result in mixtures of products derived from each potential alkene group without site-selectivity. The cage host **A** was proved to recognize organic molecules in water and pre-organize them with certain confined conformations. In this case, the linear diterpenoid substrate **29** possessed a folded U-shaped conformation within the cavity, with the terminal trisubstituted olefin exposed to the solution while the other three internal ones were protected by the cage host. The structure of the host–guest complex was determined by NMR and X-ray crystallographic analysis. Accordingly, the terminal trisubstituted olefin moiety was site-selectively transformed to the corresponding nitratobrominated compound **30** (Figure 9a) or epoxide **31** (Figure 9b) by NBS or *m*-CPBA, respectively. The uncommon nitratobrominated product was speculated to form through the attack of NO_3^- ions, whose concentration was high around the cationic cage host, on the bromonium intermediate. Control experiments indicated the crucial noncovalent protective role of the molecular container to induce site-selectivity.

Contemporaneously, the Rebek group illustrated another interesting site-selective monoepoxidation of α,ω -dienes mediated by the water-soluble cavitand host **E** (Figure 10) [71]. The α,ω -dienes were determined to adopt a yo-yo motion between two J-shaped conformations or the rapid tumbling of a coiled conformation. For longer guests, it is more like the former type, and for shorter guests, the latter is more likely. In both cases, the two terminal olefins rapidly exchanged positions between the top and the bottom of the cavitand. Treatment of the complex solution of **E**•**32** with NBS produced the monobromohydrin intermediate **33**, which converted to the final site-selective monoepoxide product **34** with the addition of base solution. Control experiments demonstrated the crucial role of the cavitand host to achieve site-selectivity. In this mediation mode, after the monofunctionalization, the more hydrophilic alcohol terminal was exposed to the aqueous solution and the more hydrophobic olefin terminal was buried deep in the cavitand hence protected from the further functionalization. This methodology could be expanded generally to the systems of converting symmetrical hydrophobic guests to unsymmetrical, amphiphilic ones.

Substitution

In 2008, the Rebek group reported a very intriguing site-selective ring-opening reaction of epoxides mediated by cavitand host **I**, which possessed an inwardly directed carboxylic acid module (Figure 11) [72]. The ring-opening of substituted epoxides results in regiosomeric products, for example, the cyclization ring-opening of epoxide **35** could produce 5- or 6-membered products **36** and **37** via a 5-*exo* or 6-*endo* mode, respectively (Figure 11a). The cavitand host **I** used here was a deep

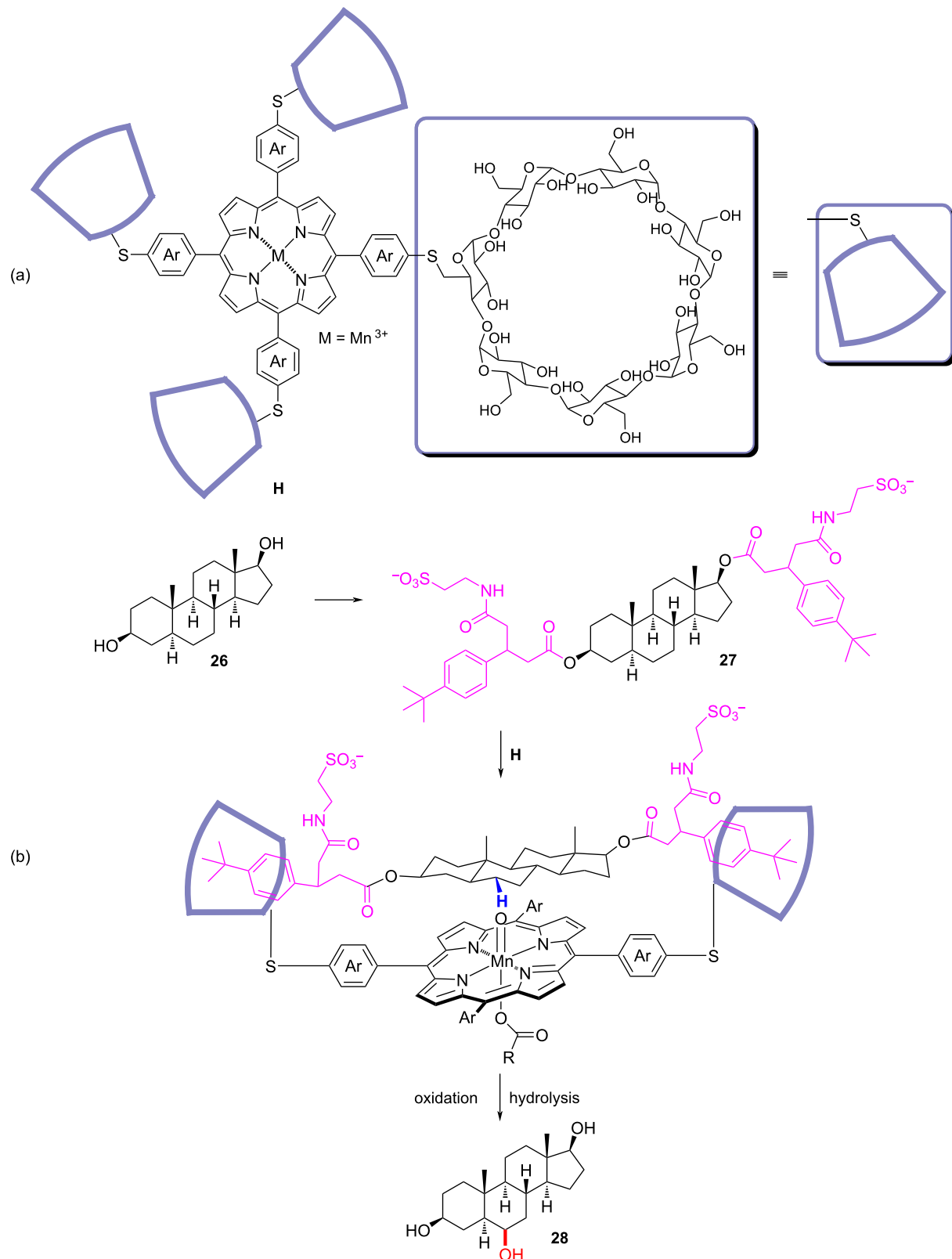
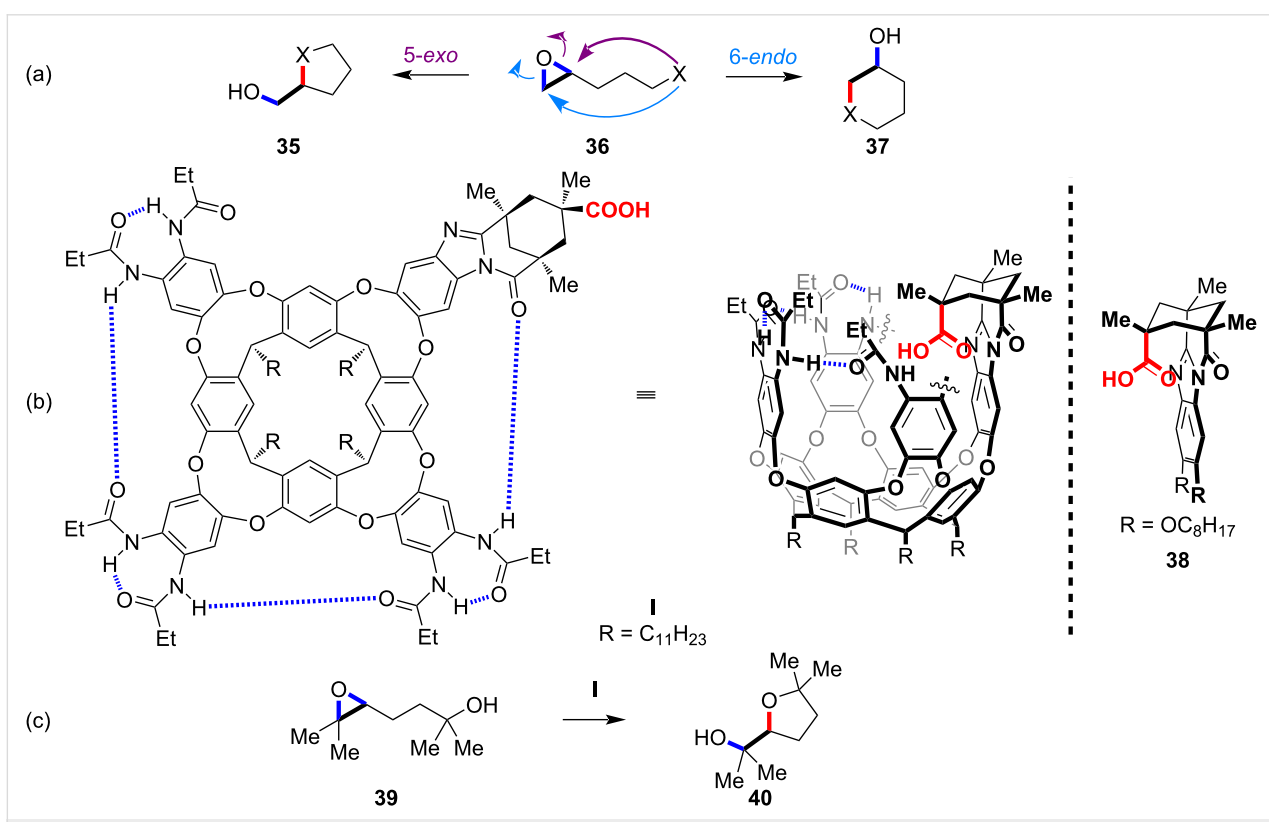
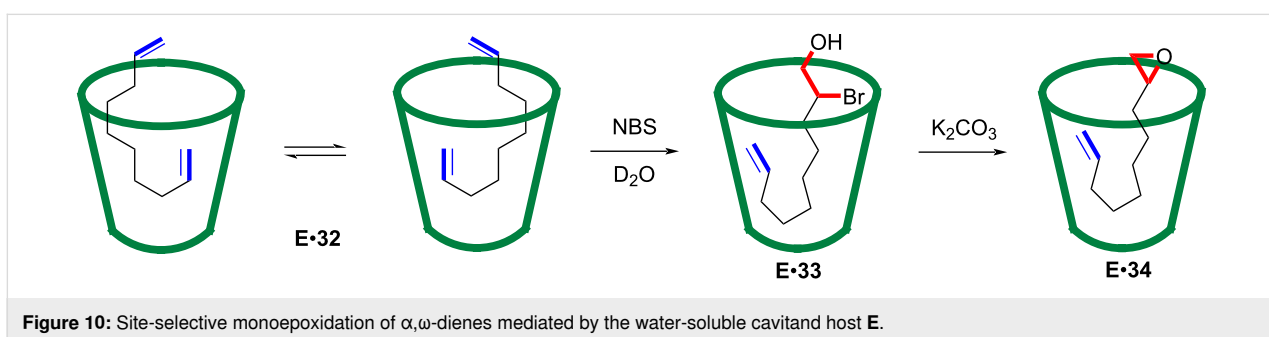
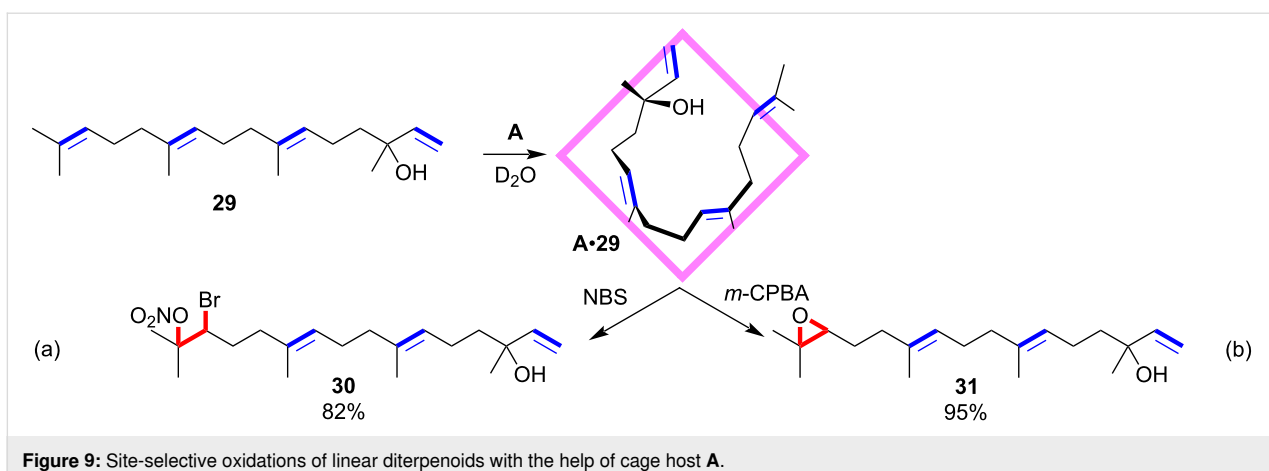


Figure 8: Site-selective oxidation of steroids using cyclodextrin as the anchoring template.



open-ended receptor functionalized with a Kemp's triacid derivative, which presented the recognized guest molecule with an inwardly directed carboxylic acid group. The hydrogen bonds provided by a cyclic array of secondary amides around the rim stabilized the vase-like conformation of the complex (Figure 11b). Adding the epoxyalcohol **39** to the solution of **I** formed 5-membered ring product **40** exclusively (Figure 11c). However, a control experiment using the model acid **38** afforded a mixture of 5- and 6-membered products. The introduced acid module facilitated the ring-opening reaction, and the CH- π interactions between the aromatic walls of the host and the alkyl backbone of the substrate induced the coiling conformation, giving rise to a compressed 5-membered-ring transition state. Later, the authors offered a detailed discussion regarding the mechanism of this reaction [73]. This example of using a synthetic receptor to achieve site-selective reaction fully

showed how a molecular container could mimic the catalysis behavior of the active sites of enzymes.

In 2012, the Fujita group reported a site-selective nucleophilic substitution reaction of allylic chlorides mediated by cage host **J** (Figure 12) [74]. Usually, this reaction occurs both at the α and γ positions of the allylic chloride, and factors like steric and electronic effects of the nucleophile and substrate and the polarity of the solvent would influence the product ratio [75]. Here, as illustrated above, the authors introduced the cage host **J** as the noncovalent protecting group of the internal reactive sites, which directed the incoming nucleophile (D_2O) to attack at the terminal site and presented terminal-induced product ratio (from 1.3:1 to 3.8:1) (Figure 12b). In this supramolecular system, two guest molecules of **41** were encapsulated per cage to form the **J** \bullet (**41**)₂ complex. Substrate screening showed the

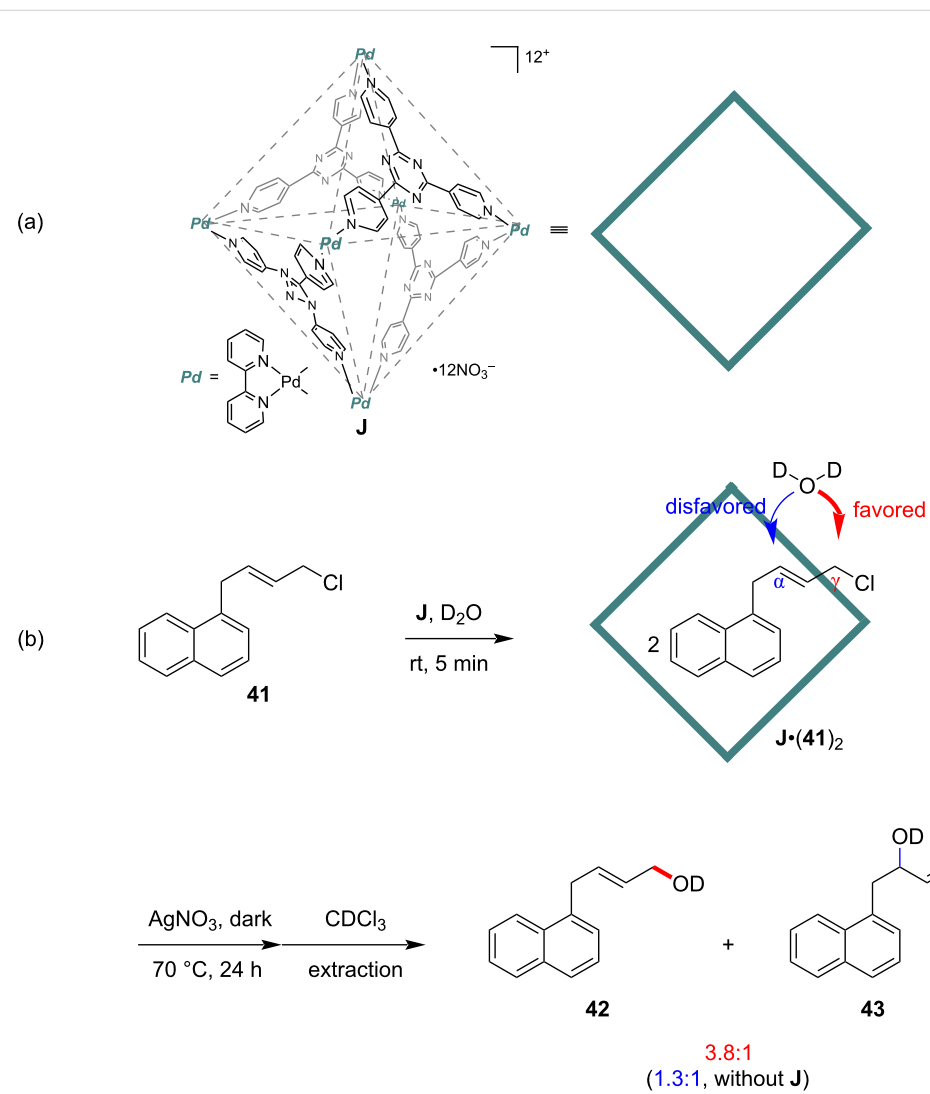


Figure 12: Site-selective nucleophilic substitution reaction of allylic chlorides mediated by cage host J.

induction effect of the reaction to terminal site-selectivity compared to the reaction in the absence of cage **J**. Even though the induced terminal site-selectivity in this work was not significant, it set an early example of how the molecular container could be beautifully used as a noncovalent protective group for substitution.

The Rebek group later reported a series of site-selective monohydrolyses of α,ω -difunctional compounds using deep water-soluble cavitands **D** and **E** (Figure 13) [76–78]. As shown in Figure 13a [76], α,ω -diester **44** showed rapidly exchanging and folded J-shape conformations, which exposed each ester group in turn to the aqueous solution. Addition of base would result in the hydrolysis of one ester group to the corresponding carboxylic acid. Product distributions indicated a two- to four-fold relative decrease in the hydrolysis rate constant of the second ester caused by the confined space in the cavitand,

which enhanced the selectivity of the monoester product **45**. Similarly, the monohydrolysis of α,ω -diisocyanate **46** was achieved using the water-soluble cavitand **D** (Figure 13b) [77]. The residual isocyanate group was buried deep in the cavity of **D** and protected from further hydrolysis. The monoamine product **47** further underwent intramolecular cyclization facilitated by the confinement of the cavitand and produced cyclized urea product **48**. In a following work (Figure 13c) [78], the binding dibromide **49** showed rapid tumbling conformation in the cavity of the cavitand host **E** on the NMR timescale. DMSO was introduced as a co-solvent to promote the S_N2 -type reaction, and the dibromide **49** was smoothly hydrolyzed site-selectively to the monohydroxy product **50**, which was fixed in an unsymmetrical manner in the cavitand. The bromide terminal was hence protected deep within the cavity of the cavitand host **E** from further hydrolysis, despite the addition of 10 equivalents DMSO after 2 days or even after one month. The experiment without

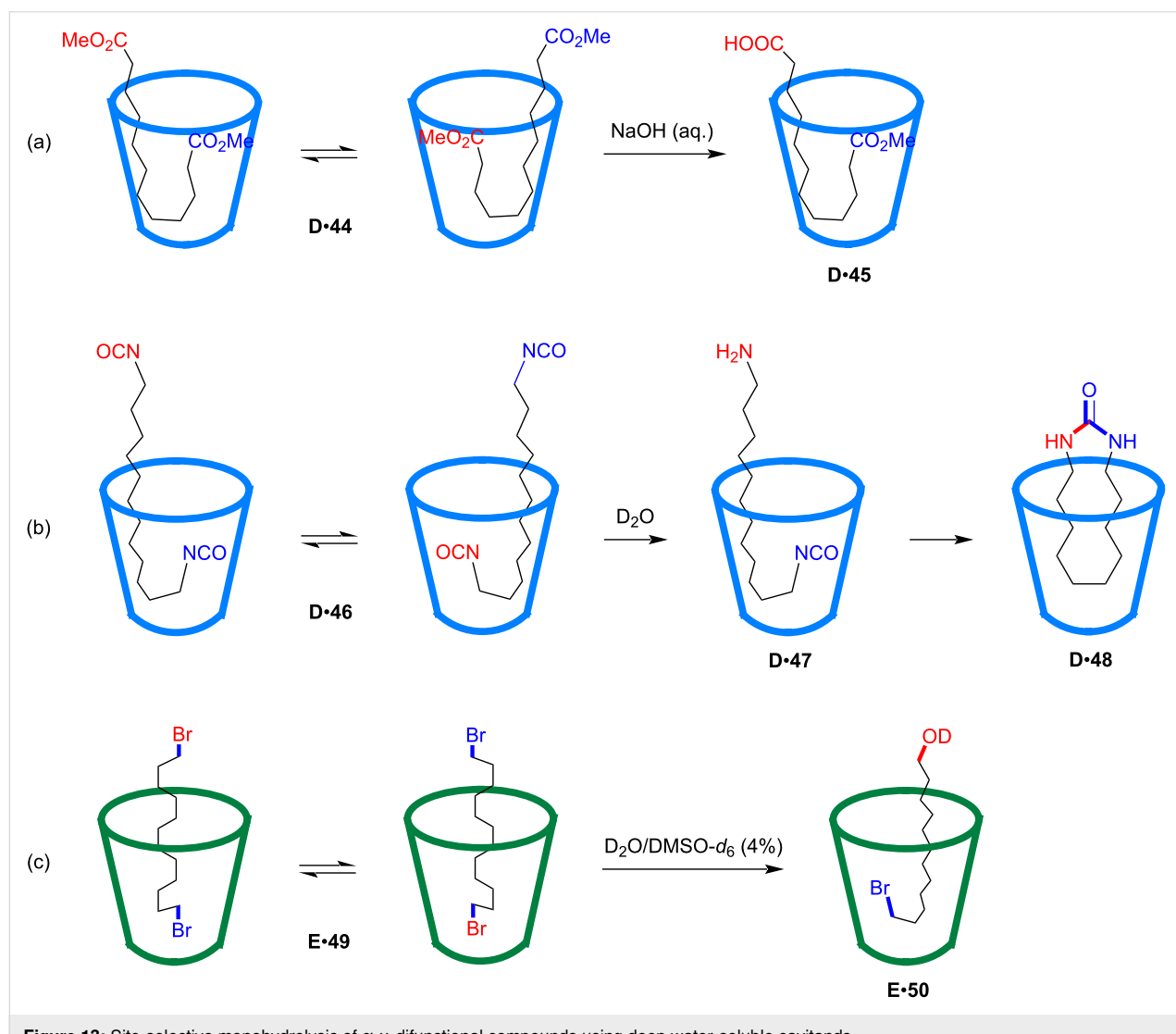


Figure 13: Site-selective monohydrolysis of α,ω -difunctional compounds using deep water-soluble cavitands.

the cavitand host produced a mixture of different products, and the dibromide was fully converted to the dihydroxy product after prolonging the reaction time or increasing DMSO concentration, without the detection of any monohydrolyzed product. This work further demonstrated the striking ability of the water-soluble cavitand to mediate site-selective reactions.

Conclusion

To summarize, we have reviewed various site-selective reactions mediated by molecular containers, which have drawn much attention in the past years and shown broad prospects in the future. The supramolecular cavity and its constrained microenvironment resemble the active site of natural enzymes, where the guest substrate is encapsulated and positioned with a specific fixed orientation and conformation through various noncovalent interactions, giving rise to discriminate control over product selectivity. In some cases, the molecular container is considered as a noncovalent protective group that prevents potential reactive sites from reacting with external reagents; in other cases, the molecular container acts as the anchoring template and fixes the substrate with a certain conformation, exposing one reactive site to the catalyst center and producing site-selective products. Even though molecular containers have been proved to be powerful tools in inducing reaction selectivity, there are still some restrictions that should be considered. For example, the substrate scopes of these methodologies are generally limited; sometimes, a near quantitative amount of the supramolecular host is required and the synthesis of macromolecular hosts is sometimes complicated. Future research should focus on those limitations as well as developing diverse catalysis systems that would induce controllable site-selectivity.

Funding

This work was supported by the National Natural Science Foundation of China (Grant No. 21801164, 22071144 and 22101169) and Shanghai University (No. 13-G210-20-201). Y.Y. thanks the Program for Professor of Special Appointment (Dongfang Scholarship) of the Shanghai Education Committee.

ORCID® IDs

Yang Yu - <https://orcid.org/0000-0001-5698-3534>

References

1. Ward, R. S. *Selectivity in Organic Synthesis*; John Wiley & Sons: Hoboken, NJ, USA, 1999.
2. Hickman, A. J.; Sanford, M. S. *ACS Catal.* **2011**, *1*, 170–174. doi:10.1021/cs1001543
3. Neufeldt, S. R.; Sanford, M. S. *Acc. Chem. Res.* **2012**, *45*, 936–946. doi:10.1021/ar300014f
4. Davis, H. J.; Phipps, R. J. *Chem. Sci.* **2017**, *8*, 864–877. doi:10.1039/c6sc04157d
5. Chao, T.-M.; Baker, J.; Hehre, W. J.; Kahn, S. D. *Pure Appl. Chem.* **1991**, *63*, 283–288. doi:10.1351/pac199163020283
6. Balcells, D.; Clot, E.; Eisenstein, O.; Nova, A.; Perrin, L. *Acc. Chem. Res.* **2016**, *49*, 1070–1078. doi:10.1021/acs.accounts.6b00099
7. Rousseau, G.; Breit, B. *Angew. Chem., Int. Ed.* **2011**, *50*, 2450–2494. doi:10.1002/anie.201006139
8. Zhang, F.-L.; Hong, K.; Li, T.-J.; Park, H.; Yu, J.-Q. *Science* **2016**, *351*, 252–256. doi:10.1126/science.aad7893
9. Rej, S.; Ano, Y.; Chatani, N. *Chem. Rev.* **2020**, *120*, 1788–1887. doi:10.1021/acs.chemrev.9b00495
10. Das, S.; Incarvito, C. D.; Crabtree, R. H.; Brudvig, G. W. *Science* **2006**, *312*, 1941–1943. doi:10.1126/science.1127899
11. Frost, J. R.; Huber, S. M.; Breitenlechner, S.; Bannwarth, C.; Bach, T. *Angew. Chem., Int. Ed.* **2015**, *54*, 691–695. doi:10.1002/anie.201409224
12. Olivo, G.; Farinelli, G.; Barbieri, A.; Lanzalunga, O.; Di Stefano, S.; Costas, M. *Angew. Chem., Int. Ed.* **2017**, *56*, 16347–16351. doi:10.1002/anie.201709280
13. Ariga, K.; Kunitake, T. *Supramolecular Chemistry: Fundamentals and Applications*; Springer: Heidelberg, Germany, 2006. doi:10.1007/b137036
14. Kolesnichenko, I. V.; Anslyn, E. V. *Chem. Soc. Rev.* **2017**, *46*, 2385–2390. doi:10.1039/c7cs00078b
15. Housecroft, C. E. *Chemistry* **2021**, *3*, 509–510. doi:10.3390/chemistry3020035
16. Lehn, J.-M. *Science* **1993**, *260*, 1762–1763. doi:10.1126/science.8511582
17. Lehn, J.-M. *Supramolecular Chemistry: Concepts and Perspectives*; Wiley-VCH: Weinheim, Germany, 1995. doi:10.1002/3527607439
18. Holliday, B. J.; Mirkin, C. A. *Angew. Chem., Int. Ed.* **2001**, *40*, 2022–2043. doi:10.1002/1521-3773(20010601)40:11<2022::aid-anie2022>3.0.co;2-d
19. Vriezema, D. M.; Comellas Aragonès, M.; Elemans, J. A. A. W.; Cornelissen, J. J. L. M.; Rowan, A. E.; Nolte, R. J. M. *Chem. Rev.* **2005**, *105*, 1445–1490. doi:10.1021/cr0300688
20. van Leeuwen, P. W. N. M. *Supramolecular Catalysis*; Wiley-VCH: Weinheim, Germany, 2008. doi:10.1002/9783527621781
21. Koblenz, T. S.; Wassenaar, J.; Reek, J. N. H. *Chem. Soc. Rev.* **2008**, *37*, 247–262. doi:10.1039/b614961h
22. Hooley, R. J.; Rebek, J., Jr. *Chem. Biol.* **2009**, *16*, 255–264. doi:10.1016/j.chembiol.2008.09.015
23. Zhang, Q.; Catti, L.; Tiefenbacher, K. *Acc. Chem. Res.* **2018**, *51*, 2107–2114. doi:10.1021/acs.accounts.8b00320
24. Olivo, G.; Capocasa, G.; Del Giudice, D.; Lanzalunga, O.; Di Stefano, S. *Chem. Soc. Rev.* **2021**, *50*, 7681–7724. doi:10.1039/d1cs00175b
25. Breslow, R.; Huang, Y.; Zhang, X.; Yang, J. *Proc. Natl. Acad. Sci. U. S. A.* **1997**, *94*, 11156–11158. doi:10.1073/pnas.94.21.11156
26. Breslow, R.; Zhang, X.; Huang, Y. *J. Am. Chem. Soc.* **1997**, *119*, 4535–4536. doi:10.1021/ja9704951
27. Murase, T.; Fujita, M. *Chem. Rec.* **2010**, *10*, 342–347. doi:10.1002/tcr.201000027
28. Hong, C. M.; Bergman, R. G.; Raymond, K. N.; Toste, F. D. *Acc. Chem. Res.* **2018**, *51*, 2447–2455. doi:10.1021/acs.accounts.8b00328
29. Yu, Y.; Rebek, J., Jr. *Acc. Chem. Res.* **2018**, *51*, 3031–3040. doi:10.1021/acs.accounts.8b00269

30. Morimoto, M.; Bierschenk, S. M.; Xia, K. T.; Bergman, R. G.; Raymond, K. N.; Toste, F. D. *Nat. Catal.* **2020**, *3*, 969–984. doi:10.1038/s41929-020-00528-3
31. Floresta, G.; Talotta, C.; Gaeta, C.; De Rosa, M.; Chiacchio, U.; Neri, P.; Rescifina, A. *J. Org. Chem.* **2017**, *82*, 4631–4639. doi:10.1021/acs.joc.7b00227
32. La Manna, P.; De Rosa, M.; Talotta, C.; Gaeta, C.; Soriente, A.; Floresta, G.; Rescifina, A.; Neri, P. *Org. Chem. Front.* **2018**, *5*, 827–837. doi:10.1039/c7qo00942a
33. Gentile, D.; Floresta, G.; Patamia, V.; Nicosia, A.; Mineo, P. G.; Rescifina, A. *Org. Biomol. Chem.* **2020**, *18*, 1194–1203. doi:10.1039/c9ob02352f
34. Yoshizawa, M.; Tamura, M.; Fujita, M. *Science* **2006**, *312*, 251–254. doi:10.1126/science.1124985
35. Breslow, R. *Acc. Chem. Res.* **1991**, *24*, 159–164. doi:10.1021/ar00006a001
36. Fringuelli, F.; Taticchi, A. *The Diels-Alder Reaction: Selected Practical Methods*; John Wiley & Sons: Chichester, UK, 2002. doi:10.1002/0470845813
37. Stuhlmann, F.; Jäschke, A. *J. Am. Chem. Soc.* **2002**, *124*, 3238–3244. doi:10.1021/ja0167405
38. Cheng, M.-F.; Li, W.-K. *Chem. Phys. Lett.* **2003**, *368*, 630–638. doi:10.1016/s0009-2614(02)01955-3
39. Kang, J.; Rebek, J., Jr. *Nature* **1997**, *385*, 50–52. doi:10.1038/385050a0
40. Marty, M.; Clyde-Watson, Z.; Twyman, L. J.; Nakash, M.; Sanders, J. K. M. *Chem. Commun.* **1998**, 2265–2266. doi:10.1039/a806070c
41. Kang, J.; Santamaría, J.; Hilmersson, G.; Rebek, J., Jr. *J. Am. Chem. Soc.* **1998**, *120*, 7389–7390. doi:10.1021/ja980927n
42. Chen, J.; Rebek, J., Jr. *Org. Lett.* **2002**, *4*, 327–329. doi:10.1021/o10168115
43. Kusukawa, T.; Nakai, T.; Okano, T.; Fujita, M. *Chem. Lett.* **2003**, *32*, 284–285. doi:10.1246/cl.2003.284
44. Kloetzel, M. C.; Dayton, R. P.; Herzog, H. L. *J. Am. Chem. Soc.* **1950**, *72*, 273–277. doi:10.1021/ja01157a073
45. Oku, A.; Ohnishi, Y.; Mashio, F. *J. Org. Chem.* **1972**, *37*, 4264–4269. doi:10.1021/jo00799a009
46. He, Y.; Junk, C. P.; Lemal, D. M. *Org. Lett.* **2003**, *5*, 2135–2136. doi:10.1021/o10300524
47. Kiselev, V. D.; Kashaeva, E. A.; Potapova, L. N.; Iskhakova, G. G. *Russ. Chem. Bull.* **2004**, *53*, 51–54. doi:10.1023/b:rucb.0000024828.37329.10
48. Murase, T.; Horiuchi, S.; Fujita, M. *J. Am. Chem. Soc.* **2010**, *132*, 2866–2867. doi:10.1021/ja9107275
49. Horiuchi, S.; Nishioka, Y.; Murase, T.; Fujita, M. *Chem. Commun.* **2010**, *46*, 3460–3462. doi:10.1039/c003191g
50. Nonhebel, D. C.; Walton, J. C. *Free-radical Chemistry*; Cambridge University Press: Cambridge, UK, 1974.
51. Parsons, A. F. *An Introduction to Free Radical Chemistry*; Blackwell Science: Oxford, UK, 2000.
52. Perkins, M. J. *Radical Chemistry: The Fundamentals*; Oxford University Press: Oxford, UK, 2000.
53. Togo, H. *Advanced Free Radical Reactions for Organic Synthesis*; Elsevier: Amsterdam, Netherlands, 2004. doi:10.1016/b978-0-08-044374-4.x5000-2
54. Yamaguchi, T.; Fujita, M. *Angew. Chem., Int. Ed.* **2008**, *47*, 2067–2069. doi:10.1002/anie.200705139
55. Schelhaas, M.; Waldmann, H. *Angew. Chem., Int. Ed. Engl.* **1996**, *35*, 2056–2083. doi:10.1002/anie.199620561
56. Isidro-Llobet, A.; Álvarez, M.; Albericio, F. *Chem. Rev.* **2009**, *109*, 2455–2504. doi:10.1021/cr800323s
57. Klán, P.; Šolomek, T.; Bochet, C. G.; Blanc, A.; Givens, R.; Rubina, M.; Popik, V.; Kostík, A.; Wirz, J. *Chem. Rev.* **2013**, *113*, 119–191. doi:10.1021/cr300177k
58. Hu, Y.; Uno, M.; Harada, A.; Takahashi, S. *Bull. Chem. Soc. Jpn.* **1991**, *64*, 1884–1888. doi:10.1246/bcsj.64.1884
59. Pitchumani, K.; Velusamy, P.; Srinivasan, C. *Tetrahedron* **1994**, *50*, 12979–12988. doi:10.1016/s0040-4020(01)81217-5
60. Masseroni, D.; Mosca, S.; Mower, M. P.; Blackmond, D. G.; Rebek, J., Jr. *Angew. Chem., Int. Ed.* **2016**, *55*, 8290–8293. doi:10.1002/anie.201602355
61. Mosca, S.; Yu, Y.; Gavette, J. V.; Zhang, K.-D.; Rebek, J., Jr. *J. Am. Chem. Soc.* **2015**, *137*, 14582–14585. doi:10.1021/jacs.5b10028
62. Petroselli, M.; Angamuthu, V.; Rahman, F.-U.; Zhao, X.; Yu, Y.; Rebek, J., Jr. *J. Am. Chem. Soc.* **2020**, *142*, 2396–2403. doi:10.1021/jacs.9b11595
63. Petroselli, M.; Rebek, J., Jr.; Yu, Y. *Chem. – Eur. J.* **2021**, *27*, 3284–3287. doi:10.1002/chem.202004953
64. Bender, T. A.; Bergman, R. G.; Raymond, K. N.; Toste, F. D. *J. Am. Chem. Soc.* **2019**, *141*, 11806–11810. doi:10.1021/jacs.9b05604
65. Patamia, V.; Floresta, G.; Pistarà, V.; Rescifina, A. *Int. J. Mol. Sci.* **2022**, *23*, 236. doi:10.3390/ijms23010236
66. Bierschenk, S. M.; Bergman, R. G.; Raymond, K. N.; Toste, F. D. *J. Am. Chem. Soc.* **2020**, *142*, 733–737. doi:10.1021/jacs.9b13177
67. Morimoto, M.; Cao, W.; Bergman, R. G.; Raymond, K. N.; Toste, F. D. *J. Am. Chem. Soc.* **2021**, *143*, 2108–2114. doi:10.1021/jacs.0c12479
68. Bredt, D. S.; Hwang, P. M.; Glatt, C. E.; Lowenstein, C.; Reed, R. R.; Snyder, S. H. *Nature* **1991**, *351*, 714–718. doi:10.1038/351714a0
69. Mega, J. L.; Close, S. L.; Wivott, S. D.; Shen, L.; Hockett, R. D.; Brandt, J. T.; Walker, J. R.; Antman, E. M.; Macias, W.; Braunwald, E.; Sabatine, M. S. *N. Engl. J. Med.* **2009**, *360*, 354–362. doi:10.1056/nejmoa0809171
70. Takezawa, H.; Kanda, T.; Nanjo, H.; Fujita, M. *J. Am. Chem. Soc.* **2019**, *141*, 5112–5115. doi:10.1021/jacs.9b00131
71. Angamuthu, V.; Rahman, F.-U.; Petroselli, M.; Li, Y.; Yu, Y.; Rebek, J., Jr. *Org. Chem. Front.* **2019**, *6*, 3220–3223. doi:10.1039/c9qo00849g
72. Shenoy, S. R.; Pinacho Crisóstomo, F. R.; Iwasawa, T.; Rebek, J., Jr. *J. Am. Chem. Soc.* **2008**, *130*, 5658–5659. doi:10.1021/ja801107r
73. Pinacho Crisóstomo, F. R.; Lledó, A.; Shenoy, S. R.; Iwasawa, T.; Rebek, J., Jr. *J. Am. Chem. Soc.* **2009**, *131*, 7402–7410. doi:10.1021/ja900766b
74. Kohyama, Y.; Murase, T.; Fujita, M. *Chem. Commun.* **2012**, *48*, 7811–7813. doi:10.1039/c2cc33660j
75. DeWolfe, R. H.; Young, W. G. *Chem. Rev.* **1956**, *56*, 753–901. doi:10.1021/cr50010a002
76. Shi, Q.; Mower, M. P.; Blackmond, D. G.; Rebek, J., Jr. *Proc. Natl. Acad. Sci. U. S. A.* **2016**, *113*, 9199–9203. doi:10.1073/pnas.1610006113
77. Wu, N.-W.; Rebek, J., Jr. *J. Am. Chem. Soc.* **2016**, *138*, 7512–7515. doi:10.1021/jacs.6b04278
78. Angamuthu, V.; Petroselli, M.; Rahman, F.-U.; Yu, Y.; Rebek, J., Jr. *Org. Biomol. Chem.* **2019**, *17*, 5279–5282. doi:10.1039/c9ob01018a

License and Terms

This is an open access article licensed under the terms of the Beilstein-Institut Open Access License Agreement (<https://www.beilstein-journals.org/bjoc/terms>), which is identical to the Creative Commons Attribution 4.0 International License (<https://creativecommons.org/licenses/by/4.0>). The reuse of material under this license requires that the author(s), source and license are credited. Third-party material in this article could be subject to other licenses (typically indicated in the credit line), and in this case, users are required to obtain permission from the license holder to reuse the material.

The definitive version of this article is the electronic one which can be found at:

<https://doi.org/10.3762/bjoc.18.35>



A Se···O bonding catalysis approach to the synthesis of calix[4]pyrroles

Qingzhe Tong[†], Zhiguo Zhao[†] and Yao Wang^{*}

Letter

Open Access

Address:

School of Chemistry and Chemical Engineering, Key Laboratory of the Colloid and Interface Chemistry, Shandong University, Jinan 250100, China

Beilstein J. Org. Chem. **2022**, *18*, 325–330.

<https://doi.org/10.3762/bjoc.18.36>

Email:

Yao Wang^{*} - yaowang@sdu.edu.cn

Received: 29 January 2022

Accepted: 09 March 2022

Published: 18 March 2022

^{*} Corresponding author [†] Equal contributors

This article is part of the thematic issue "Supramolecular approaches to mediate chemical reactivity".

Keywords:

calix[4]pyrrole; chalcogen bonding; ketones; Se···O bonding interactions; supramolecular catalysis

Guest Editor: C. Gaeta

© 2022 Tong et al.; licensee Beilstein-Institut.

License and terms: see end of document.

Abstract

Described herein is a chalcogen bonding catalysis approach to the synthesis of calix[4]pyrrole derivatives. The Se···O bonding interactions between selenide catalysts and ketones gave rise to the catalytic activity in the condensation reactions between pyrrole and ketones, leading to the generation of calix[4]pyrrole derivatives in moderate to high yields. This chalcogen bonding catalysis approach was efficient since only 5 mol % catalyst loading was used to promote the consecutive condensation processes while the reactions could be carried out at room temperature, thus highlighting the potential of this type of nonclassical interactions in catalyzing relative complex transformations.

Introduction

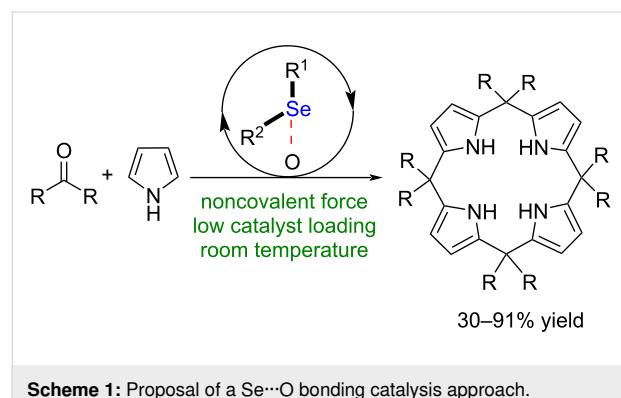
Noncovalent catalysis has been established as one of the fundamental concepts in organic synthesis that enables achieving numerous chemical transformations [1]. Among these noncovalent forces, hydrogen bonding interactions play a central role in noncovalent catalysis [2] while halogen bonding interactions have lately been exploited as a new tool to catalyze a diverse array of reactions [3–5]. In addition, nonclassical interactions such as anion–π [6–11] as well as chalcogen [12–17] and pnictogen [18–23] bonds were established as emerging driving forces for the development of organic reactions. Very recently, catalysis with carbon bonding interactions was realized and this type of catalysis mode was capable of facilitating a range of

typical reactions [24], thus providing a new platform for organic synthesis.

The phenomenon of chalcogen bonding was initially observed in the crystal structures of small organic molecules as well as proteins [25]. The application of this type of bonding interactions has achieved significant advances in the research fields of crystal engineering [26], medicinal chemistry [27], anion recognition [28–32] and transport [33–35]. In addition, intramolecular chalcogen bonding interactions have been suggested to stabilize reactive intermediates in a range of isothiourea-catalyzed transformations, which play a key factor to modulate the selec-

tivity of these reactions [36–40]. In addition, few examples demonstrated that disubstituted chalcogens could be used as effective catalysts through intermolecular chalcogen bonding interactions [41–49]. Despite these significant advances, catalysis with chalcogen bonding interactions is still in its infancy and the development of new types of reactions is highly desirable.

Calix[4]pyrrole derivatives have been widely used as transition metal ligands and functional materials [50–53]. Thus far, several synthetic methods to access these compounds have been reported [54,55]. The classical approaches to synthesis of calix[4]pyrrole derivatives mainly involved a stepwise synthesis and Lewis acid as well as Brønsted acid catalysis [54,55]. Notably, a noncovalent catalysis approach to accessing calix[4]pyrrole derivatives remains underdeveloped. To provide a new strategy to synthesize calix[4]pyrrole derivatives, herein, we describe a Se···O bonding catalysis approach to accessing this type of compounds (Scheme 1).



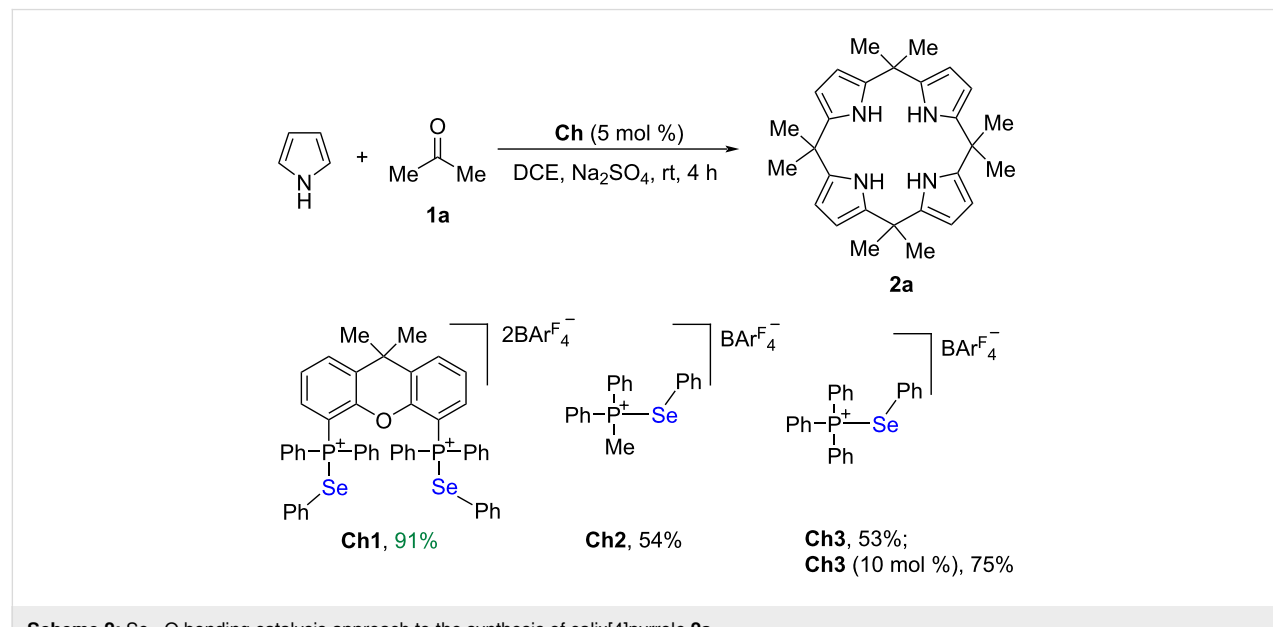
Results and Discussion

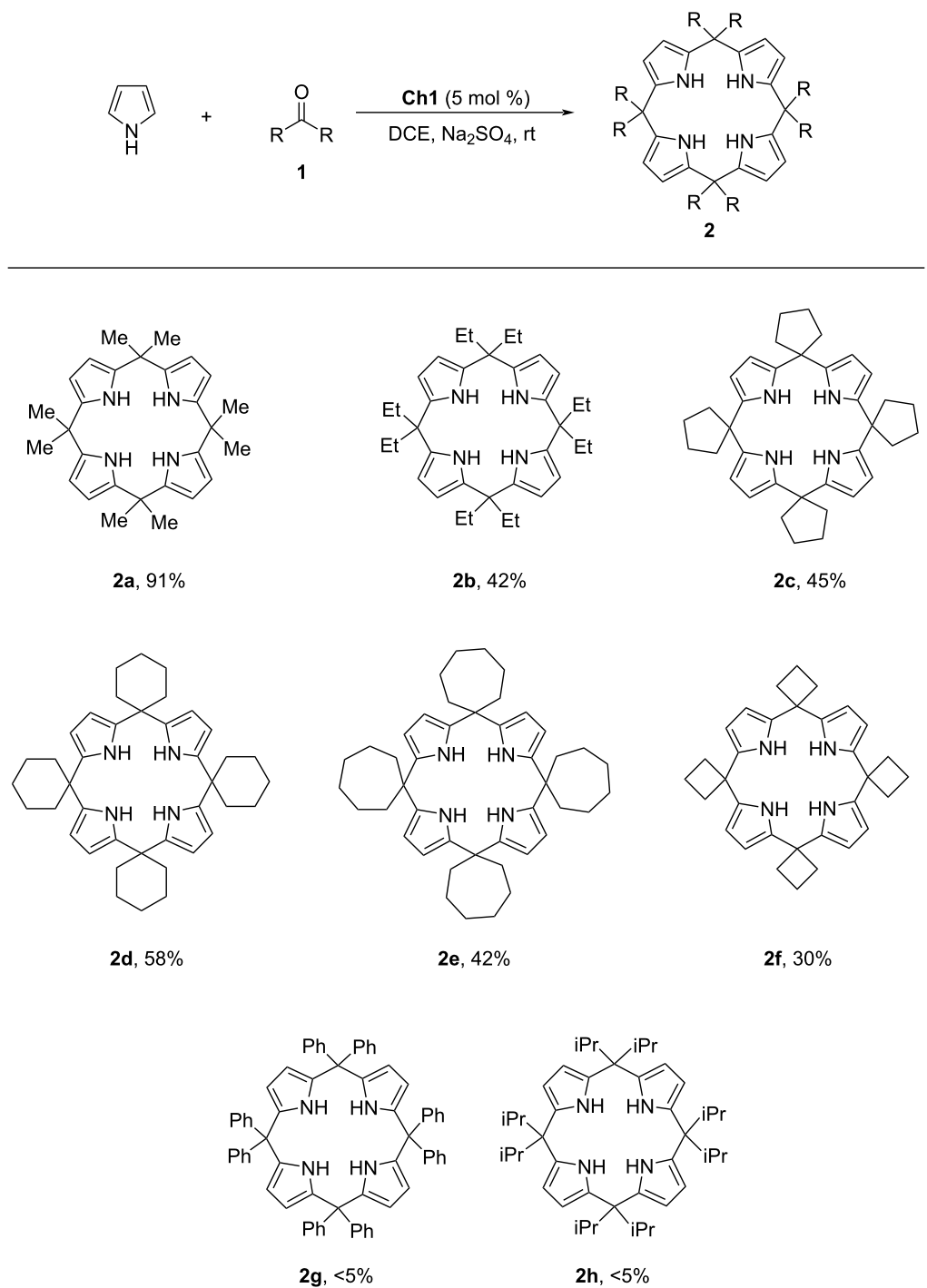
Evaluation of catalysts

We developed a class of phosphonium selenide catalysts which showed catalytic activity in assembly reactions [41], Michael addition reactions [41], Rauhut–Currier reactions [42], cyanosilylation reactions [43], and cycloaddition of vinylindoles through chalcogen–π bonding catalysis [44]. Our previous works demonstrated that Se···O bonding interactions between phosphonium selenides and carbonyls can significantly activate carbonyl groups [41–43], thus providing a new opportunity to develop carbonyl chemistry. To expand the catalysis capability of chalcogen bonding interactions, we envisioned that consecutive condensations between ketones and pyrrole might take place to give calix[4]pyrrole derivatives under catalysis of a selenide catalyst. In the absence of a catalyst, no reaction took place. Indeed, even in presence of 5 mol % representative catalyst **Ch1** [44], the condensation reaction between acetone and pyrrole worked efficiently at room temperature. We note that this reaction did not stop at a bis(pyrrole)methane stage, but consecutive condensations between four molecules of acetone and four molecules of pyrrole took place to give calix[4]pyrrole **2a** in 91% yield after 4 h (Scheme 2). Further investigations revealed that the monodentate catalysts were less active and only a moderate yield was obtained regardless of whether **Ch2** or **Ch3** was used. In the presence of 10 mol % catalyst **Ch3**, 75% yield of **2a** was obtained.

Reaction scope

Inspired by the good result obtained with catalyst **Ch1**, the scope of ketones was investigated (Scheme 3). Both linear and cyclic aliphatic ketones could be used to synthesize



**Scheme 3:** Reaction scope.

calix[4]pyrrole derivatives under catalysis of 5 mol % **Ch1** at room temperature. It was found that this chalcogen bonding catalysis approach was susceptible to the variation of the steric environment of ketones. Upon changing acetone to pentan-3-one, the chemical yield decreased significantly and product **2b** was obtained in 42% yield. Using cyclopentanone as a reactant,

product **2c** was obtained in 45% yield. Moreover, cyclohexanone and cycloheptanone could also be used as effective reactants, and products **2d** and **2e** were obtained in 58% and 42% yield, respectively. Further investigation revealed that cyclobutanone was reactive in this transformation to give product **2f**, albeit with 30% yield. However, benzophenone and 2,4-

dimethylpentan-3-one with high steric hindrance failed to give desirable products **2g** and **2h**. Further investigation on using an asymmetric ketone such as pentan-2-one as a reactant showed that the reaction gave an inseparable mixture of diastereomers. Meanwhile, upon using benzaldehyde as a reactant, the reaction system was complex and there was no major product.

Proposed activation mode

The chalcogen bonding interactions between catalysts **Ch1**, **Ch2** and acetone were examined by ^{13}C NMR experiments in CD_2Cl_2 . The interaction between bidentate catalyst **Ch1** or monodentate catalyst **Ch2** and acetone could result in a variation of the ^{13}C signal of the carbonyl group. Analysis of a 1:1 mixture of **Ch1** and acetone in CD_2Cl_2 indicated a 1.07 ppm downfield shift of the ^{13}C signal of the carbonyl group, while a 0.28 ppm downfield shift of the ^{13}C signal of the carbonyl group was observed upon analysis of a 2:1 mixture of **Ch2** and acetone (Scheme 4). Therefore, in line with the catalytic results as depicted in Scheme 2, both monodentate and bidentate catalysts could activate ketones. Accordingly, either a single activation or a double activation mode could be an effective driving force to promote this transformation, albeit with distinct catalytic activity.

Conclusion

In summary, we developed a Se...O bonding catalysis approach to the synthesis of calix[4]pyrroles. In the presence of 5 mol % selenide catalyst, calix[4]pyrrole products were obtained in moderate to good yields at room temperature. The experimental results showed that both bidentate and monodentate catalysts were catalytically active in the condensation reactions between pyrrole and ketones. In addition, both cyclic and linear aliphatic ketones were effective reactants in this transformation. This work provides a new strategy to access calix[4]pyrrole derivatives and makes an important complementation to the research topic of chalcogen bonding catalysis.

Full experimental procedures and compound characterization.
[<https://www.beilstein-journals.org/bjoc/content/supplementary/1860-5397-18-36-S1.pdf>]

Supporting Information

Supporting Information File 1

Technical support from Shandong University structural constituent and physical property research facilities is acknowledged.

Acknowledgements

We gratefully acknowledge the National Natural Science Foundation of China (22022105, 21971147), the Natural Science Foundation of Shandong Province (ZR2019JQ08, ZR2020ZD35).

Funding

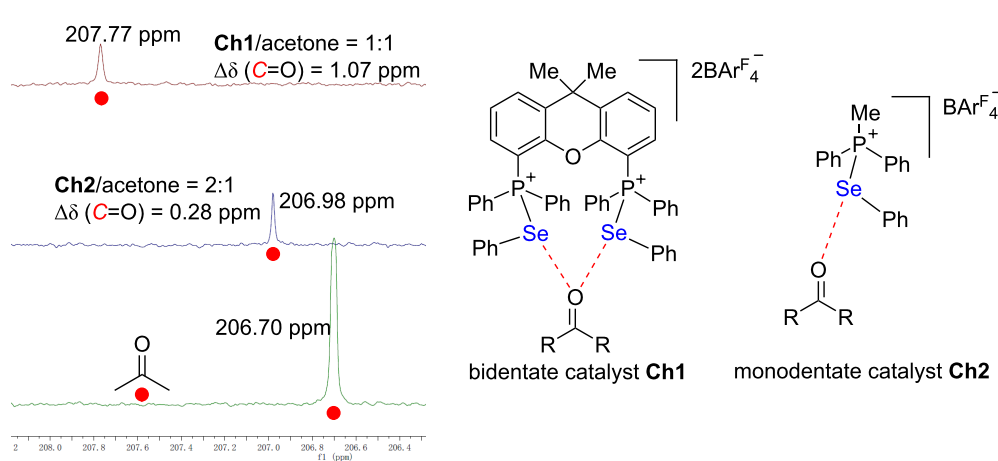
We gratefully acknowledge the National Natural Science Foundation of China (22022105, 21971147), the Natural Science Foundation of Shandong Province (ZR2019JQ08, ZR2020ZD35).

ORCID® IDs

Yao Wang - <https://orcid.org/0000-0002-8071-3267>

References

1. van Leeuwen, P. W. N. M.; Raynal, M., Eds. *Supramolecular Catalysis: New Directions and Developments*; Wiley-VCH: Weinheim, Germany, 2022. doi:10.1002/9783527832033
2. Doyle, A. G.; Jacobsen, E. N. *Chem. Rev.* **2007**, *107*, 5713–5743. doi:10.1021/cr068373r
3. Alkorta, I.; Elguero, J.; Frontera, A. *Crystals* **2020**, *10*, 180. doi:10.3390/cryst10030180



Scheme 4: Proposed activation mode.

4. Bulfield, D.; Huber, S. M. *Chem. – Eur. J.* **2016**, *22*, 14434–14450. doi:10.1002/chem.201601844
5. Sutar, R. L.; Huber, S. M. *ACS Catal.* **2019**, *9*, 9622–9639. doi:10.1021/acscatal.9b02894
6. Zhao, Y.; Domoto, Y.; Orentas, E.; Beuchat, C.; Emery, D.; Mareda, J.; Sakai, N.; Matile, S. *Angew. Chem., Int. Ed.* **2013**, *52*, 9940–9943. doi:10.1002/anie.201305356
7. Zhao, Y.; Beuchat, C.; Domoto, Y.; Gajewy, J.; Wilson, A.; Mareda, J.; Sakai, N.; Matile, S. *J. Am. Chem. Soc.* **2014**, *136*, 2101–2111. doi:10.1021/ja412290r
8. Zhao, Y.; Cottelle, Y.; Liu, L.; López-Andarias, J.; Bornhof, A.-B.; Akamatsu, M.; Sakai, N.; Matile, S. *Acc. Chem. Res.* **2018**, *51*, 2255–2263. doi:10.1021/acs.accounts.8b00223
9. Paraja, M.; Matile, S. *Angew. Chem., Int. Ed.* **2020**, *59*, 6273–6277. doi:10.1002/anie.202000579
10. Luo, N.; Ao, Y.-F.; Wang, D.-X.; Wang, Q.-Q. *Angew. Chem., Int. Ed.* **2021**, *60*, 20650–20655. doi:10.1002/anie.202106509
11. Luo, N.; Ao, Y.-F.; Wang, D.-X.; Wang, Q.-Q. *Chem. – Eur. J.* **2022**, *28*, e202103303. doi:10.1002/chem.202103303
12. Aakeroy, C. B.; Bryce, D. L.; Desiraju, G. R.; Frontera, A.; Legon, A. C.; Nicotra, F.; Rissanen, K.; Scheiner, S.; Terraneo, G.; Metrangolo, P.; Resnati, G. *Pure Appl. Chem.* **2019**, *91*, 1889–1892. doi:10.1515/pac-2018-0713
13. Yan, W.; Zheng, M.; Xu, C.; Chen, F.-E. *Green Synth. Catal.* **2021**, *2*, 329–336. doi:10.1016/j.gresc.2021.08.002
14. Vogel, L.; Wonner, P.; Huber, S. M. *Angew. Chem., Int. Ed.* **2019**, *58*, 1880–1891. doi:10.1002/anie.201809432
15. Breugst, M.; Koenig, J. J. *Eur. J. Org. Chem.* **2020**, 5473–5487. doi:10.1002/ejoc.202000660
16. Bamberger, J.; Ostler, F.; Mancheño, O. G. *ChemCatChem* **2019**, *11*, 5198–5211. doi:10.1002/cctc.201901215
17. Frontera, A.; Bauza, A. *Int. J. Mol. Sci.* **2021**, *22*, 12550. doi:10.3390/ijms222212550
18. Benz, S.; Poblador-Bahamonde, A. I.; Low-Ders, N.; Matile, S. *Angew. Chem., Int. Ed.* **2018**, *57*, 5408–5412. doi:10.1002/anie.201801452
19. Yang, M.; Tofan, D.; Chen, C.-H.; Jack, K. M.; Gabbaï, F. P. *Angew. Chem., Int. Ed.* **2018**, *57*, 13868–13872. doi:10.1002/anie.201808551
20. Gini, A.; Paraja, M.; Galmés, B.; Besnard, C.; Poblador-Bahamonde, A. I.; Sakai, N.; Frontera, A.; Matile, S. *Chem. Sci.* **2020**, *11*, 7086–7091. doi:10.1039/d0sc02551h
21. Yang, M.; Hirai, M.; Gabbaï, F. P. *Dalton Trans.* **2019**, *48*, 6685–6689. doi:10.1039/c9dt01357a
22. Paraja, M.; Gini, A.; Sakai, N.; Matile, S. *Chem. – Eur. J.* **2020**, *26*, 15471–15476. doi:10.1002/chem.202003426
23. Zhang, J.; Wei, J.; Ding, W.-Y.; Li, S.; Xiang, S.-H.; Tan, B. *J. Am. Chem. Soc.* **2021**, *143*, 6382–6387. doi:10.1021/jacs.1c02808
24. Wang, W.; Li, X.; Zhou, P.-P.; Wang, Y. *Angew. Chem., Int. Ed.* **2021**, *60*, 22717–22721. doi:10.1002/anie.202108973
25. Rosenfield, R. E., Jr.; Parthasarathy, R.; Dunitz, J. D. *J. Am. Chem. Soc.* **1977**, *99*, 4860–4862. doi:10.1021/ja00456a072
26. Fourmigué, M.; Dhaka, A. *Coord. Chem. Rev.* **2020**, *403*, 213084. doi:10.1016/j.ccr.2019.213084
27. Beno, B. R.; Yeung, K.-S.; Barthberger, M. D.; Pennington, L. D.; Meanwell, N. A. *J. Med. Chem.* **2015**, *58*, 4383–4438. doi:10.1021/jm501853m
28. Zhao, H.; Gabbaï, F. P. *Nat. Chem.* **2010**, *2*, 984–990. doi:10.1038/nchem.838
29. Garrett, G. E.; Gibson, G. L.; Straus, R. N.; Seferos, D. S.; Taylor, M. S. *J. Am. Chem. Soc.* **2015**, *137*, 4126–4133. doi:10.1021/ja512183e
30. Garrett, G. E.; Carrera, E. I.; Seferos, D. S.; Taylor, M. S. *Chem. Commun.* **2016**, *52*, 9881–9884. doi:10.1039/c6cc04818h
31. Lim, J. Y. C.; Marques, I.; Thompson, A. L.; Christensen, K. E.; Félix, V.; Beer, P. D. *J. Am. Chem. Soc.* **2017**, *139*, 3122–3133. doi:10.1021/jacs.6b12745
32. Borissov, A.; Marques, I.; Lim, J. Y. C.; Félix, V.; Smith, M. D.; Beer, P. D. *J. Am. Chem. Soc.* **2019**, *141*, 4119–4129. doi:10.1021/jacs.9b00148
33. Benz, S.; Macchione, M.; Verolet, Q.; Mareda, J.; Sakai, N.; Matile, S. *J. Am. Chem. Soc.* **2016**, *138*, 9093–9096. doi:10.1021/jacs.6b05779
34. Macchione, M.; Tsemperouli, M.; Goujon, A.; Mallia, A. R.; Sakai, N.; Sugihara, K.; Matile, S. *Helv. Chim. Acta* **2018**, *101*, e1800014. doi:10.1002/hlca.201800014
35. Lee, L. M.; Tsemperouli, M.; Poblador-Bahamonde, A. I.; Benz, S.; Sakai, N.; Sugihara, K.; Matile, S. *J. Am. Chem. Soc.* **2019**, *141*, 810–814. doi:10.1021/jacs.8b12554
36. Birman, V. B.; Li, X.; Han, Z. *Org. Lett.* **2007**, *9*, 37–40. doi:10.1021/oj0623419
37. Leverett, C. A.; Purohit, V. C.; Romo, D. *Angew. Chem., Int. Ed.* **2010**, *49*, 9479–9483. doi:10.1002/anie.201004671
38. Robinson, E. R. T.; Fallan, C.; Simal, C.; Slawin, A. M. Z.; Smith, A. D. *Chem. Sci.* **2013**, *4*, 2193–2200. doi:10.1039/c3sc50199j
39. Robinson, E. R. T.; Walden, D. M.; Fallan, C.; Greenhalgh, M. D.; Cheong, P. H.-Y.; Smith, A. D. *Chem. Sci.* **2016**, *7*, 6919–6927. doi:10.1039/c6sc00940a
40. Young, C. M.; Elmi, A.; Pascoe, D. J.; Morris, R. K.; McLaughlin, C.; Woods, A. M.; Frost, A. B.; de la Houpliere, A.; Ling, K. B.; Smith, T. K.; Slawin, A. M. Z.; Willoughby, P. H.; Cockcroft, S. L.; Smith, A. D. *Angew. Chem., Int. Ed.* **2020**, *59*, 3705–3710. doi:10.1002/anie.201914421
41. Wang, W.; Zhu, H.; Liu, S.; Zhao, Z.; Zhang, L.; Hao, J.; Wang, Y. *J. Am. Chem. Soc.* **2019**, *141*, 9175–9179. doi:10.1021/jacs.9b03806
42. Wang, W.; Zhu, H.; Feng, L.; Yu, Q.; Hao, J.; Zhu, R.; Wang, Y. *J. Am. Chem. Soc.* **2020**, *142*, 3117–3124. doi:10.1021/jacs.9b12610
43. Bao, L.; Kong, X.; Wang, Y. *Asian J. Org. Chem.* **2020**, *9*, 757–760. doi:10.1002/ajoc.202000127
44. Kong, X.; Zhou, P.-P.; Wang, Y. *Angew. Chem., Int. Ed.* **2021**, *60*, 9395–9400. doi:10.1002/anie.202101140
45. Benz, S.; López-Andarias, J.; Mareda, J.; Sakai, N.; Matile, S. *Angew. Chem., Int. Ed.* **2017**, *56*, 812–815. doi:10.1002/anie.201611019
46. Benz, S.; Mareda, J.; Besnard, C.; Sakai, N.; Matile, S. *Chem. Sci.* **2017**, *8*, 8164–8169. doi:10.1039/c7sc03866f
47. Wonner, P.; Vogel, L.; Dürer, M.; Gomes, L.; Kniep, F.; Mallick, B.; Werz, D. B.; Huber, S. M. *Angew. Chem., Int. Ed.* **2017**, *56*, 12009–12012. doi:10.1002/anie.201704816
48. Wonner, P.; Dreger, A.; Vogel, L.; Engelage, E.; Huber, S. M. *Angew. Chem., Int. Ed.* **2019**, *58*, 16923–16927. doi:10.1002/anie.201910639
49. Wonner, P.; Steinke, T.; Vogel, L.; Huber, S. M. *Chem. – Eur. J.* **2020**, *26*, 1258–1262. doi:10.1002/chem.201905057
50. Kim, D. S.; Sessler, J. L. *Chem. Soc. Rev.* **2015**, *44*, 532–546. doi:10.1039/c4cs00157e
51. Ding, Y.; Tang, Y.; Zhu, W.; Xie, Y. *Chem. Soc. Rev.* **2015**, *44*, 1101–1112. doi:10.1039/c4cs00436a
52. Tanaka, T.; Osuka, A. *Chem. Soc. Rev.* **2015**, *44*, 943–969. doi:10.1039/c3cs60443h

53. Saha, I.; Lee, J. T.; Lee, C.-H. *Eur. J. Org. Chem.* **2015**, 3859–3885.

doi:10.1002/ejoc.201403701

54. Lindsey, J. S. *Acc. Chem. Res.* **2010**, *43*, 300–311.

doi:10.1021/ar900212t

55. Rather, I. A.; Ali, R. *Green Chem.* **2021**, *23*, 5849–5855.

doi:10.1039/d1gc01515j

License and Terms

This is an open access article licensed under the terms of the Beilstein-Institut Open Access License Agreement (<https://www.beilstein-journals.org/bjoc/terms>), which is identical to the Creative Commons Attribution 4.0 International License

(<https://creativecommons.org/licenses/by/4.0>). The reuse of material under this license requires that the author(s), source and license are credited. Third-party material in this article could be subject to other licenses (typically indicated in the credit line), and in this case, users are required to obtain permission from the license holder to reuse the material.

The definitive version of this article is the electronic one which can be found at:

<https://doi.org/10.3762/bjoc.18.36>



A resorcin[4]arene hexameric capsule as a supramolecular catalyst in elimination and isomerization reactions

Tommaso Lorenzetto, Fabrizio Fabris and Alessandro Scarsò*

Letter

Open Access

Address:

Dipartimento di Scienze Molecolari e Nanosistemi, Università Ca' Foscari di Venezia, via Torino 155, 30172, Mestre-Venezia, Italy

Email:

Alessandro Scarsò* - alesca@unve.it

* Corresponding author

Keywords:

cationic intermediates; encapsulation; organocatalysis; resorcin[4]arene hexamer; supramolecular catalysis

Beilstein J. Org. Chem. **2022**, *18*, 337–349.

<https://doi.org/10.3762/bjoc.18.38>

Received: 04 February 2022

Accepted: 16 March 2022

Published: 28 March 2022

This article is part of the thematic issue "Supramolecular approaches to mediate chemical reactivity".

Guest Editor: C. Gaeta

© 2022 Lorenzetto et al.; licensee Beilstein-Institut.

License and terms: see end of document.

Abstract

The hexameric resorcin[4]arene capsule as a self-assembled organocatalyst promotes a series of reactions like the carbonyl–ene cyclization of (*S*)-citronellal preferentially to isopulegol, the water elimination from 1,1-diphenylethanol, the isomerization of α -pinene and β -pinene preferentially to limonene and minor amounts of camphene. The role of the supramolecular catalyst consists in promoting the protonation of the substrates leading to the formation of cationic intermediates that are stabilized within the cavity with consequent peculiar features in terms of acceleration and product selectivity. In all cases the catalytic activity displayed by the hexameric capsule is remarkable if compared to many other strong Brønsted or Lewis acids.

Introduction

In enzymatic catalysis, the substrate is selected matching the size, shape and specific functional groups present in the active site of the enzyme. Once bound, substrate activation is carried out by specific amino acid side chains that adorn the inner surface of the cavity by means of a combination of covalent and/or weak intermolecular interactions leading to the stabilization of intermediate species and transition states of the reaction with impressive accelerations, substrate, and product selectivities. The development of artificial catalytic systems able to activate substrates and to stabilize intermediate species through weak

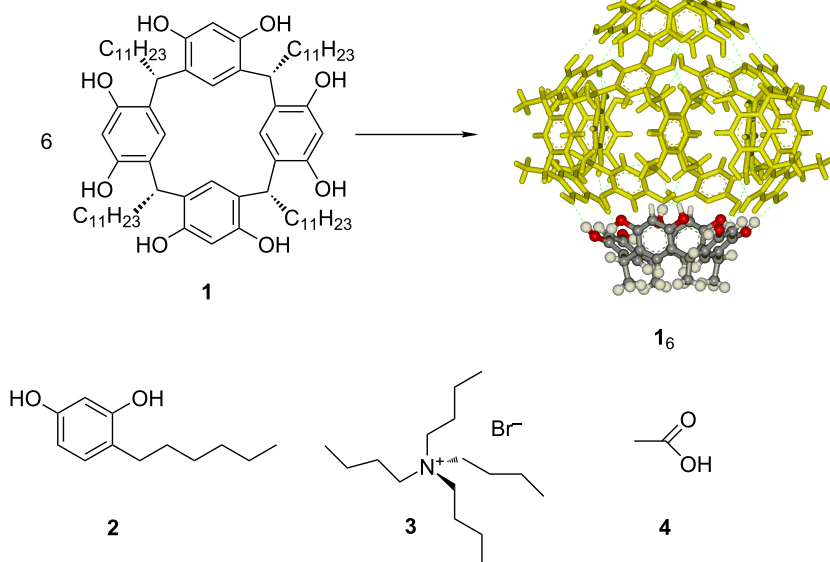
noncovalent interactions is the scope of supramolecular catalysis [1–4]. Several examples of supramolecular catalysts [5–7] have been introduced in the recent years [3,8] where the catalytic host is designed to bind substrates, accelerate reactions, and steer product [9–12] and substrate [13,14] selectivities thanks to confinement effects [15–17]. Many host structures endowed with catalytic features are full covalent units (e.g., cyclodextrins, cucurbiturils, pillararenes and other derivatives) whose synthesis can be sometimes time consuming. Alternatively, supramolecular catalysts can be obtained through self-assem-

bling units [18,19], metal-ligand components [20] or hydrogen bonding units. In the latter case, a key role is played by the resorcin[4]arene **1** as a one-step multigram synthesis product, that spontaneously self-assembles in wet apolar solvents like chloroform or benzene forming a hexameric structure [21] thanks to the formation of a seam of sixty hydrogen bonds between six units of **1** and eight water molecules (Scheme 1). A very recent publication investigated different possible assemblies that are present in solution as function of the water content [22]. The pseudo-spherical host structure is highly dynamic, with a large cavity of about 1375 \AA^3 that is accessible [23] for cationic guests [24] thanks to extended cation- π interactions [25] as well as other electron poor molecules [26,27]. After our seminal work on the use of **1**₆ as a nanoreactor to bind an Au(I) catalyst and to impart unique product [28] as well as substrate [29] selectivity, the capsule attracted the attention of several other research groups bringing this self-assembled nanocontainer to the forefront in the field of supramolecular catalysts. The specific field of research has been recently reviewed [19,30–33] to underline the potentialities of this simple and efficient organocatalyst. Recent promoted reactions by the resorcin[4]arene capsule include the intramolecular ether cyclization [34], the synthesis of bis(heteroaryl)methanes [35], the imine formation [36], the Michael addition reactions of *N*-methylpyrrole on methyl vinyl ketone [37], the synthesis of sesquiterpene natural product derivatives [38,39] and the carbonyl olefin metathesis leading to 2,5-dihydropyrroles [40].

Herein we present our investigation on the ability of the hexameric capsule **1**₆ to act as a supramolecular self-assembled organocatalyst for a series of unimolecular reactions involving the formation of cationic intermediate species [41] like water elimination from an alcohol to provide the corresponding alkene, the isomerization of β -pinene and α -pinene and the cyclization of (*S*)-citronellal to secondary alcohols. The key point to interpret the action of the capsule in all these reactions is the combination of its weak Brønsted acidity [42] that, by protonation of the substrate, leads to the formation of cationic species [43] and the stabilization of the latter through cation- π interactions [44] within the electron-rich aromatic cavity of the capsule, thus providing acceleration of the reaction and specific product selectivities.

Results and Discussion

We decided to explore the application of the resorcin[4]arene capsule **1**₆ to new classes of unimolecular reactions which are known to occur through the formation of cationic intermediate species, that can be expected to be efficiently stabilized within the electron-rich cavity of the capsule. Aiming at ascertaining the real role played by the self-assembled capsule, the solvent chloroform-*d* was previously passed on basic alumina in order to avoid traces of HCl, that recently demonstrated to combine catalytic effects with the nano-environment provided by the capsule [45]. Moreover, all reactions were also tested i) using 4-*n*-hexylresorcinol (**2**) as a molecular unit able to provide the



Scheme 1: Resorcin[4]arene **1** forming the corresponding hexameric capsule **1**₆ and the species used for control experiments like 4-*n*-hexylresorcinol (**2**) to mimic the H-bonding properties of the capsule, tetrabutylammonium bromide (**3**) to act as a competitive guest for the cavity and acetic acid (**4**) to mimic just the Brønsted acidity of the capsule.

same hydrogen bonding properties of the resorcin[4]arene but lacking the formation of the cavity ii) in the presence of the capsule with an excess of tetrabutylammonium bromide (**3**) as a competitive guest for the capsule, to demonstrate the importance of the presence of an accessible cavity, and iii) acetic acid (**4**) in order to mimic only the Brønsted acidity of the capsule without providing the stabilization properties related to the presence of electron-rich aromatic surfaces.

In a recent publication, Reek [22] further investigated the self-assembly properties of **1** as function of the content of water in chloroform-*d* demonstrating that the symmetrical hexameric capsule **1**₆·(H₂O)₈ comprising 8 water molecules (capsule A) is present only with water content lower than 50 mM, while in the presence of increasing amounts of water a second capsule B is also present comprising overall 15 water molecules, 6–7 of which spontaneously incorporated into a single edge of the cubic suprastructure leading to increased Brønsted acidity. Therefore, we performed extra control experiments for each investigated reaction also only with the more symmetrical and less acidic capsule A to underline the effect of the water content on the catalytic activity.

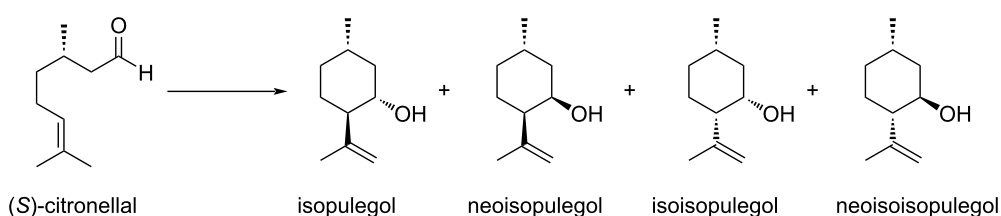
(*S*)-Citronellal isomerization to cyclic secondary alcohols

(*S*)-Citronellal is an enantiopure monoterpenoid, isolated from oils distilled from citronella plants, which is very effective as a repellent and antifungal. In the presence of Brønsted or Lewis acids (*S*)-citronellal undergoes an intramolecular carbonyl–ene cyclization reaction forming two new stereogenic centers, which turns out into four possible diastereoisomeric secondary alcohols (Scheme 2).

The reaction of (*S*)-citronellal in the presence of 10 mol % of **1** at 60 °C was monitored by ¹H NMR observing the rapid disappearance of the triplet signal at 9.78 ppm relative to the aldehyde hydrogen atom and consequent increase of the signals at 4.9 ppm relative to the vinylic hydrogen atoms of the isopulegol obtained in higher amount with respect to neoisopulegol (Figure 1 and Table 1, entry 1). In order to achieve

larger substrate conversion, the reaction was repeated for 72 h at 60 °C observing almost complete substrate conversion and high isopulegol to neoisopulegol ratio (Table 1, entry 2). The reaction with **1**₆ occupied by **3** as a competitive guest led to a marked decrease of catalytic activity, and negligible conversion was observed using 4-*n*-hexylresorcinol (**2**) as a molecule with similar H-bonding properties compared to **1** (Figure 1D and E; Table 1, entries 3 and 4). The reaction promoted by acetic acid (**4**) as purely Brønsted acid led to comparable conversion of the substrate with respect to the use of **1**₆, albeit with much similar product distribution between isopulegol and neoisopulegol, even extending the reaction time up to 72 h at 60 °C (Table 1, entries 5 and 6). The reaction with the symmetrical capsule A (**1**₆·8H₂O) characterized by lower intrinsic acidity [22] led to lower conversion with respect to the same reaction in the presence of high water content (Figure 1G; Table 1, entry 7). Overall for this reaction the capsule acts primarily as a Brønsted acid and the presence of the accessible cavity of the capsule steers product distribution.

It is worth to note that the preferred product isopulegol is an important intermediate product in the industrial production of menthol by the Takasago and BASF processes [46,47]. Many catalytic methods for the cyclization of citronellal have been developed mostly based on transition metals, both as heterogeneous and homogeneous catalysts frequently under much harsher experimental conditions [48–50]. The same cyclization of citronellal was reported also by Raymond and collaborators in water using a tetrahedral polyanionic metal-ligand capsule as supramolecular catalyst, observing lower catalytic activity and product distribution favoring isopulegol but also with large amounts of neoisopulegol and neoisoisopulegol (52%, 32% and 11%, respectively) [51]. More favorable selectivity towards isopulegol was obtained by the same group with a larger tetrahedral capsule using pyrene in place of naphthalene units observing isopulegol, neoisopulegol and neoisoisopulegol with 71%, 24% and 4% selectivity [52]. The comparison between the metal-ligand tetrahedral capsules and the H-bonded **1**₆ shows a common trend of selectivity towards isopulegol with increasing the volume of the cavity.



Scheme 2: Carbonyl–ene intramolecular cyclization of (*S*)-citronellal to the corresponding diastereoisomeric cyclic secondary alcohols.

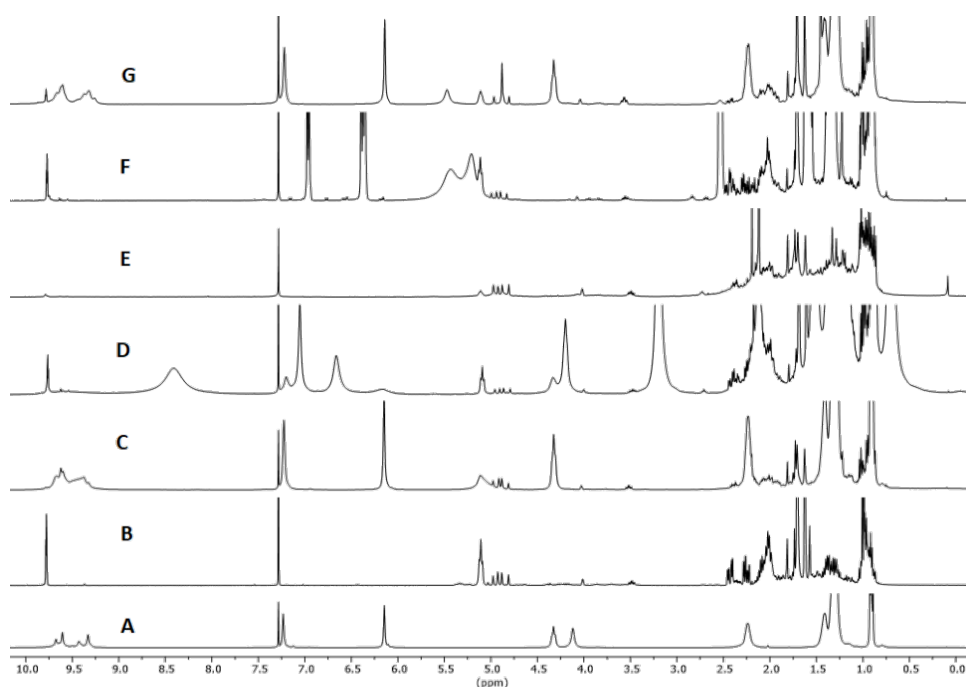


Figure 1: ^1H NMR spectra in water-saturated CDCl_3 except for G. A: **[16]** (7.5 mM); B: citronellal; C: citronellal (75 mM), **[16]** (7.5 mM); D: citronellal (75 mM), **[16]** (7.5 mM), Bu_4NBr (**3**, 78 mM); E: citronellal (75 mM), acetic acid (29 mM); F: citronellal (75 mM), *n*-hexylresorcinol (**2**, 30 mM); G: citronellal (75 mM), **[16·8H₂O]** (7.5 mM). Spectra recorded after 24 h at 60 °C, while A and B were recorded right after sample preparation.

Table 1: Conversion and selectivity for the carbonyl–ene isomerization of (*S*)-citronellal at 60 °C for 24 h.

#	Catalyst	Conv. (%)	Isopulegol (%)	Neoisopulegol (%)
1	16 ^a	49	32	15
2	16 ^{a,b}	95	73	22
3	16 + 3	0	0	0
4	2	6	3	3
5	AcOH (4) ^a	49	21	26
6	AcOH (4) ^{a,b}	60	28	32
7	capsule A (16·8H₂O) ^a	33	23	8

^a3% of other diastereoisomeric secondary alcohols; ^b60 °C for 72 h.



As a further investigation concerning other possible isomerization reactions involving protonation of the substrate, and formation of possible cationic intermediate species, we tested the menthone isomerization to isomenthone [53] without observing any product formation with 10 mol % of capsule after 24 h at 60 °C. Similarly, the carvone isomerization [54] involving protonation of the exocyclic double bond of the substrate followed by two hydride shifts and aromatization to carvacrol did not

proceed at all with 10 mol % of capsule after 24 h at 60 °C. Carvone isomerization was achieved at 60 °C for 24 h only combining the use of 10 mol % of capsule and 10 mol % of HBF_4 . Nevertheless, the reaction under identical conditions, but in the presence of 10 equiv of **3** as competitive guest, led only to a minimal inhibition of the reaction, thus excluding a fundamental role of the cavity under such experimental conditions for carvone isomerization.

Dehydration of 1,1-diphenylethanol to 1,1-diphenylethylene

The dehydration reaction of 1,1-diphenylethanol to 1,1-diphenylethylene occurs with protonation at the oxygen atom of the reagent with subsequent water elimination leading to a stable tertiary, bis-benzyl carbocation that evolves forming the corresponding alkene by proton elimination (Scheme 3). The reaction was carried out at 60 °C with 10 mol % of **1₆** (Table 2, entry 1), monitoring the formation of the products by ¹H NMR and GC–MS (see Supporting Information File 1).

Table 2: Dehydration of 1,1-diphenylethanol to 1,1-diphenylethylene 3 h and 20 h at 60 °C.

#	Catalyst	Yield (%), 3 h	Yield (%), 20 h
1	1₆	87	100
2	1₆ + 3	0	3
3	2	0	2
4	AcOH (4)	0	1
5	capsule A (1₆ ·8H ₂ O)	44	100

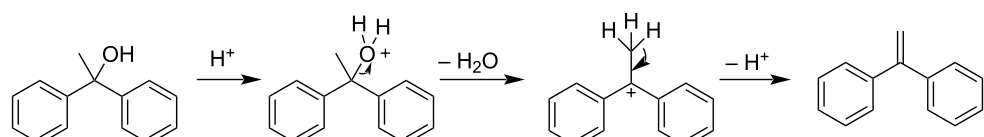
From the ¹H NMR spectra it was possible to follow the consumption of the substrate characterized by a singlet at 2.00 ppm attributed to the methyl hydrogens and the appearance of the characteristic singlet signal of the vinyl hydrogens at 5.5 ppm for the product (Figure 2), with quantitative yield after 20 h at 60 °C in the presence of 10 mol % of the capsule. The same reaction carried out with the capsule **1₆** and in the presence of **3** as competitive guest led to complete inhibition of the formation of the corresponding alkene (Figure 2D, Table 2, entry 2). This provides evidence of the importance of an accessible cavity for the activation of the reaction after alcohol protonation. It is known that **1₆** behaves as a weakly acidic assembly with *pK_a* of about 5.5 [42], while the resorcinol moiety presents a *pK_a* of 9.15. This enhanced acidity is likely to promote the protonation of the substrate. The reaction was repeated with **2** as a hydrogen bonding unit and with acetic acid (**4**) as a comparable Brønsted acid observing in both cases that the formation of 1,1-diphenylethylene was negligible (Figure 2E and F, Table 2, entries 3 and 4). Further control experiments with the capsule A (**1₆**·8H₂O) with water content lower than 50 mM showed after 3 h much lower product forma-

tion with respect to the same reaction with higher water content (Figure 2G and Table 2, entry 5), in agreement with the lower acidity of capsule A [22] that leads to lower formation of the intermediate carbocation species. It has also to be considered that water elimination during the progress of the reaction changes the ratio between capsules A and B thus accelerating product formation. The intrinsic stability of the carbocation formed by water elimination from the corresponding alcohol is crucial to observe activation of the reaction by the capsule. In fact, the reaction with the capsule under identical experimental conditions using 1-phenylethanol as substrate did not provide any evidence of formation of the corresponding alkene product even after 20 h at 60 °C. Secondary aliphatic alcohols can be efficiently dehydrated by the capsule only in combination with HCl, leading to an acceleration of two orders of magnitude with respect to the same reaction in the absence of the supramolecular catalyst [55]. The group of Tiefenbacher reported about the reactivity of tertiary alcohols bearing a trisubstituted alkene in the side chain [56] for which the reaction catalyzed by the same capsule led to the protonation of the alkene unit with an intramolecular nucleophilic attack by the alcohol moiety forming a final cyclic ether product. In the latter case the tertiary alcohol could not easily eliminate water and protonation occurred preferentially on the alkene moiety.

It is worth to note that the present dehydration reaction of 1,1-diphenylethanol with **1₆** occurs under mild experimental conditions with respect to recent examples in the literature operating with strong Brønsted and Lewis acids like sulfuric acid [57], *p*-toluenesulfonic acid [58,59] or with scandium tris(trifluoromethanesulfonate) [60]. These results clearly speak for the combined effect provided by the capsule consisting in sufficient Brønsted acidity and concomitant stabilization of the cationic intermediate within the electron-rich cavity leading to the promotion of the elimination reaction.

β-Pinene isomerization

β-Pinene is a bicyclic monoterpene bearing an exocyclic C=C double bond that can be recovered in large quantities from the production processes of cellulose from the wood of conifers. β-Pinene is in equilibrium with the more stable endocyclic alkene α-pinene by protonation. From the common cationic



Scheme 3: Dehydration reaction of 1,1-diphenylethanol to 1,1-diphenylethylene.

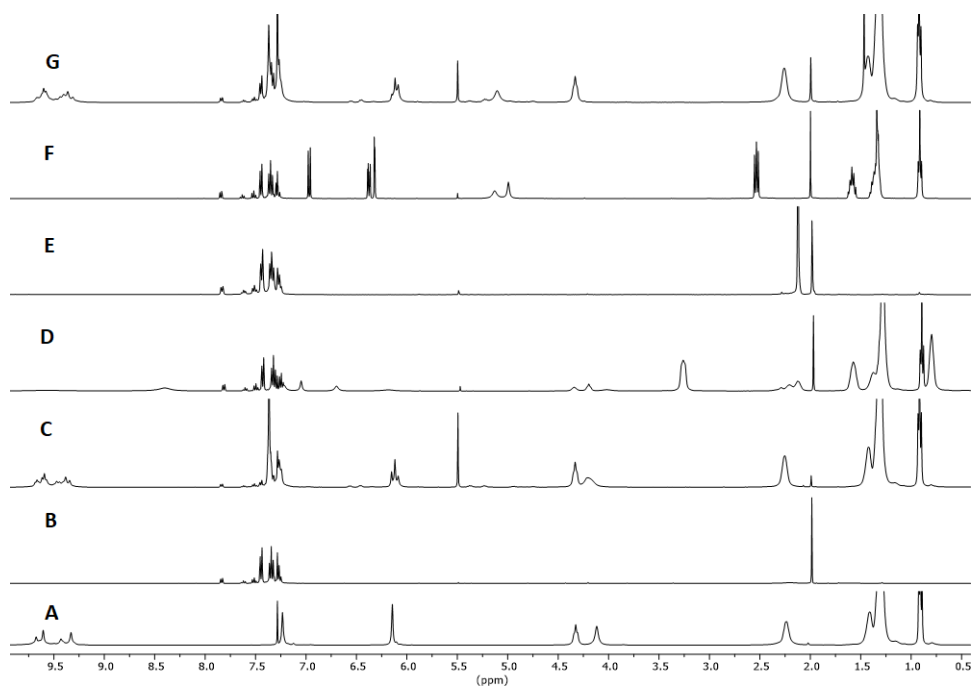
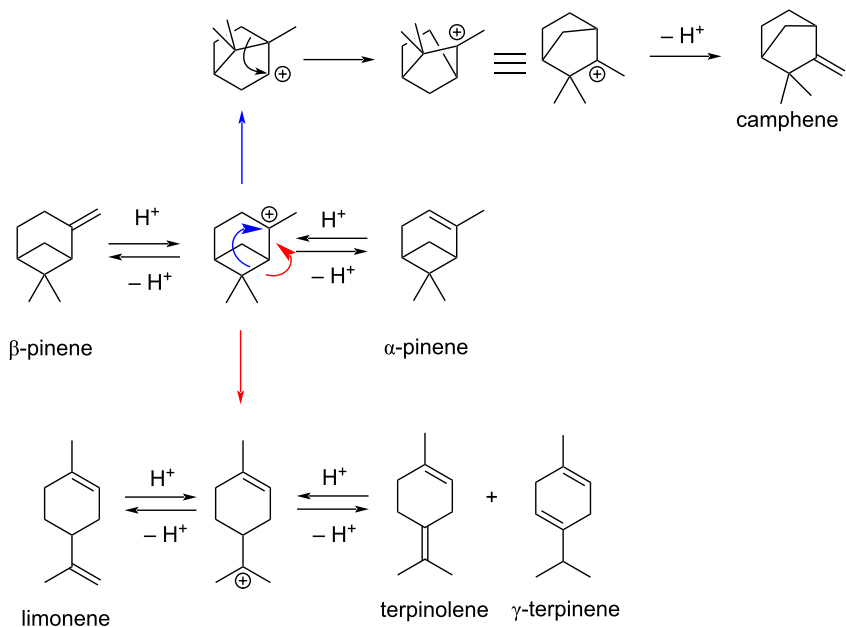


Figure 2: ^1H NMR spectra in water-saturated CDCl_3 except for G. A: $[\mathbf{1}_6]$ (7.5 mM); B: 1,1-diphenylethanol; C: 1,1-diphenylethanol (75 mM), $[\mathbf{1}_6]$ (7.5 mM); D: 1,1-diphenylethanol (75 mM), $[\mathbf{1}_6]$ (7.5 mM), Bu_4NBr (3, 78 mM); E: 1,1-diphenylethanol (75 mM), acetic acid (29 mM); F: 1,1-diphenylethanol (75 mM), *n*-hexylresorcinol (2, 30 mM); G: 1,1-diphenylethanol (75 mM), $[\mathbf{1}_6\cdot 8\text{H}_2\text{O}]$ (7.5 mM). Spectra recorded after 3 h at 60 °C, while A and B were recorded right after sample preparation.

intermediate species, many rearrangement products can be obtained, some of which derived by the ring opening of the tensioned 4-membered ring (Scheme 4).

α -Pinene possesses a more stable endocyclic double bond and therefore tends to react less rapidly than β -pinene. The reaction of α -pinene was monitored following the disappearing of the



Scheme 4: Possible isomerization products from β -pinene and α -pinene.

resonance of the vinylic hydrogen atom at 5.23 ppm. Concomitant formation of a new resonance at 5.43 attributed to limonene and at 4.52 for camphene was observed. In the presence of 10 mol % of **1₆** substrate conversion after 24 h at 60 °C corresponded to 75%, leading to double amounts of limonene with respect to camphene (Figure 3C and Table 3 entries 1 and 2). All the control experiments with the cavity of the capsule occupied by the competitive guest **3**, or with **2** or acetic acid as catalysts led to no product formation under identical experimental conditions (Figure 3D, E and F, Table 3, entries 3–5).

The reaction carried out with capsule A (**1₆·8H₂O**) obtained with low water content led to diminished catalytic activity with similar product distribution compared to the reaction containing both capsules (Figure 3G, Table 3, entries 6 and 7). As suggested in the literature [22], the higher Brønsted acidity of the capsule B present under high water content could also in this

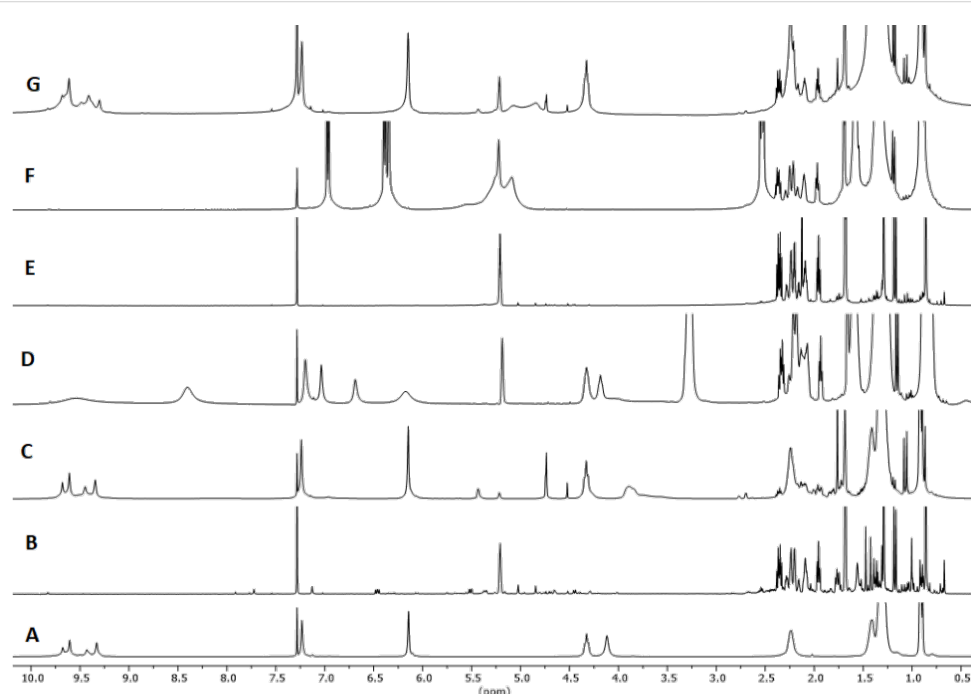
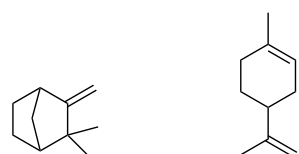


Figure 3: ^1H NMR spectra in water-saturated CDCl_3 except for G. A: $[\mathbf{1}_6]$ (7.5 mM); B: α -pinene; C: α -pinene (75 mM), $[\mathbf{1}_6]$ (7.5 mM); D: α -pinene (75 mM), $[\mathbf{1}_6]$ (7.5 mM), Bu_4NBr (**3**, 78 mM); E: α -pinene (75 mM), acetic acid (29 mM); F: α -pinene (75 mM), *n*-hexylresorcinol (**2**, 30 mM); G: α -pinene (75 mM), $[\mathbf{1}_6\cdot 8\text{H}_2\text{O}]$ (7.5 mM). Spectra recorded after 24 h at 60 °C, while A and B were recorded right after sample preparation.

Table 3: Product distribution for the isomerization reaction of α -pinene at 60 °C.

#	Catalyst	Time	Conv. (%)	Camphene (%)	Limonene (%)
1	1₆	3 h	5	3	2
2	1₆	24 h	75 ^a	24	50
3	1₆ + 3	24 h	0	–	–
4	2	24 h	0	–	–
5	AcOH (4)	24 h	0	–	–
6	capsule A (1₆·8H₂O)	3 h	3	2	1
7	capsule A (1₆·8H₂O)	24 h	15	5	10

^a1% of other monocyclic isomerization products.



case be responsible for the larger formation of the cationic intermediate further stabilized within the capsule with consequent enhanced catalytic activity.

β -Pinene is characterized by a more reactive, exocyclic double bond and this led to higher conversions compared to α -pinene (Table 4 and Figure 4). By ^1H NMR it was observed the de-

crease in intensity of the signal at 4.60 ppm characteristic for the vinylic H atoms of β -pinene and the appearance of different signals related to the formation of limonene as major product, camphene, α -pinene and other monocyclic isomerization products like terpinolene, α - and γ -terpinene, in traces (Table 4, entries 1, 2 and 3). Quantitative conversion was observed with 10 mol % of **1₆** after 24 h at 60 °C, while the reaction with **1₆** in

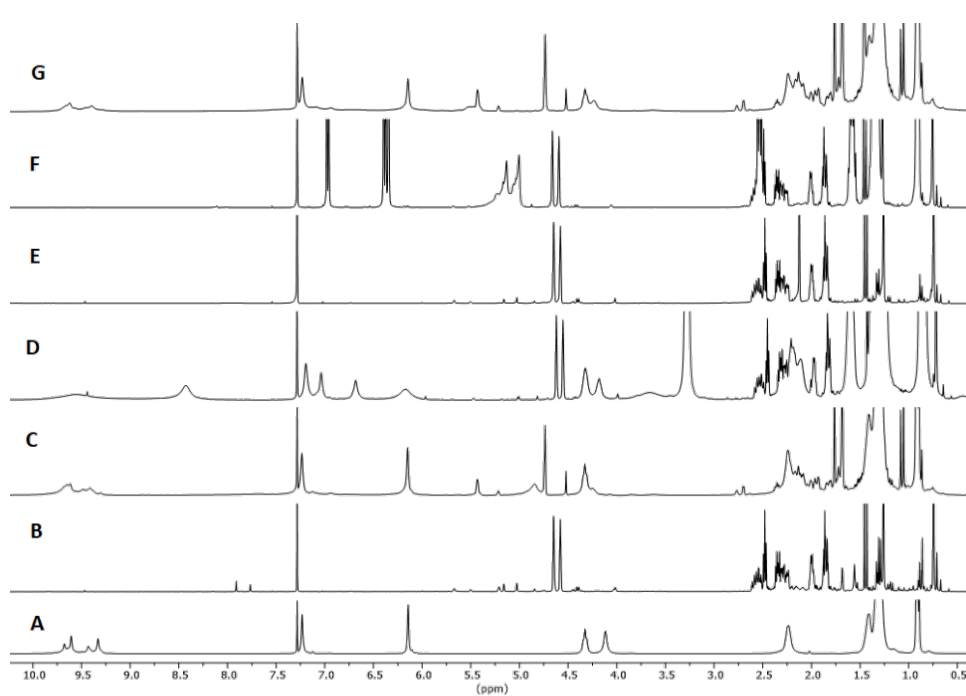


Figure 4: ^1H NMR spectra in water-saturated CDCl_3 except for G. A: $[\mathbf{1}_6]$ (7.5 mM); B: β -pinene; C: β -pinene (75 mM), $[\mathbf{1}_6]$ (7.5 mM); D: β -pinene (75 mM), $[\mathbf{1}_6]$ (7.5 mM), Bu_4NBr (**3**, 78 mM); E: β -pinene (75 mM), acetic acid (29 mM); F: β -pinene (75 mM), *n*-hexylresorcinol (**2**, 30 mM); G: β -pinene (75 mM), $[\mathbf{1}_6\cdot 8\text{H}_2\text{O}]$ (7.5 mM). Spectra recorded after 24 h at 60 °C, while A and B were recorded right after sample preparation.

Table 4: Product distribution for the isomerization reaction of β -pinene at 60 °C.

#	Catalyst	Time	Conv. (%)	α -Pinene (%)	Camphene (%)	Limonene (%)
1	1₆	1.5 h	14	2	4	8
2	1₆	3 h	30	4	9	17
3	1₆	24 h	100 ^a	10	26	62
4	1₆ + 3	24 h	0	–	–	–
5	2	24 h	0	–	–	–
6	AcOH (4)	24 h	0	–	–	–
7	capsule A ($[\mathbf{1}_6\cdot 8\text{H}_2\text{O}]$)	1.5 h	35	5	10	20
8	capsule A ($[\mathbf{1}_6\cdot 8\text{H}_2\text{O}]$)	3 h	62	8	18	36
9	capsule A ($[\mathbf{1}_6\cdot 8\text{H}_2\text{O}]$)	24 h	100 ^a	1	30	67

^a2% of other monocyclic isomerization products.

the presence of 10 equiv of the competitive ammonium guest **3** led to a drastic reduction of the catalytic activity (Table 4, entries 3 and 4). No conversion was detected in the presence of 4-*n*-hexylresorcinol (**2**), and the same was observed for the reaction in the presence of acetic acid (**4**, Table 4, entries 5 and 6, respectively). The reaction with capsule A (**1₆·8H₂O**) [22] showed a higher conversion to products at 1.5 and 3 h reaction compared to capsule **1₆** (see Supporting Information File 1), with almost identical product yields after 24 h. The faster activity of capsule A (**1₆·8H₂O**) with respect to **1₆** observed with β -pinene is opposite to what observed for α -pinene, and clearly cannot be related to the specific acidities of the two capsules A and B.

Due to the complete conversion observed at 60 °C, we also tested the isomerization of β -pinene at room temperature (Figure 5 and Table 5) confirming that substrate conversion was higher when using the symmetrical capsule A (**1₆·8H₂O**) under low water content conditions [22], with respect to capsule **1₆** as mixture of A and B (Figure 5A and E). A possible explanation could be related to the fact that β -pinene is a higher energy isomer with respect to α -pinene and because of this it does not benefit from the higher acidity of capsule B compared to capsule A. Both capsules provide sufficient protonation to β -pinene leading to the carbocationic intermediate species which is likely to be stabilized more effectively by the more symmetric and tighter capsule A (**1₆·8H₂O**), which is held on by

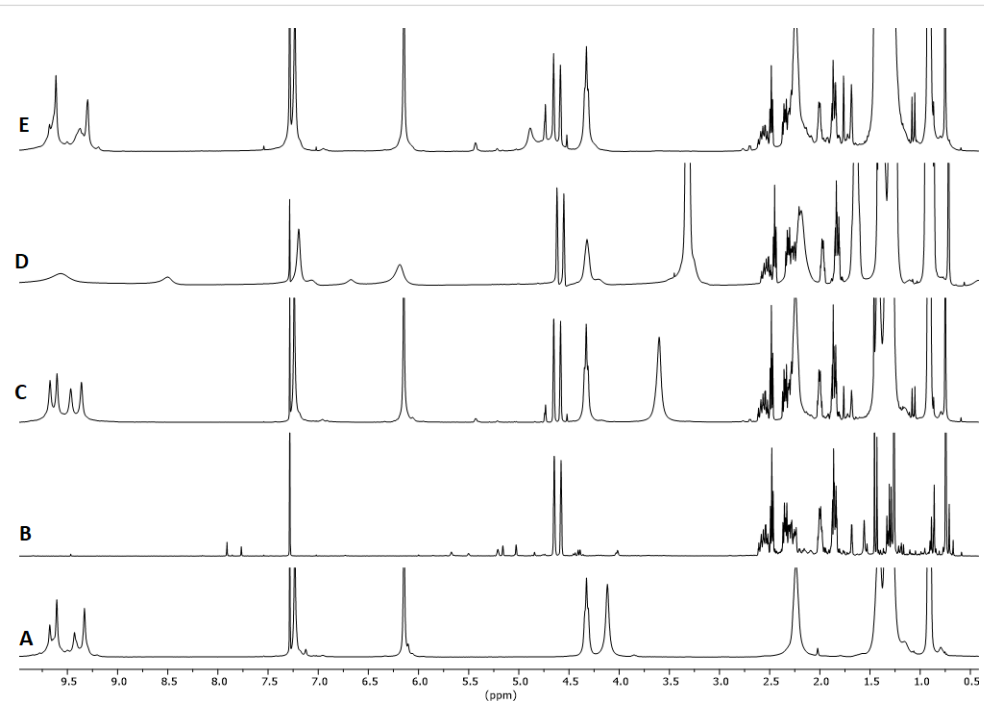
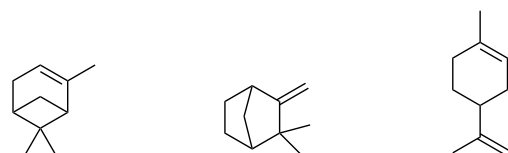


Figure 5: ^1H NMR spectra in water-saturated CDCl_3 , except for E. A: $[\mathbf{1}_6]$ (7.5 mM); B: β -pinene; C: β -pinene (75 mM), $[\mathbf{1}_6]$ (7.5 mM); D: β -pinene (75 mM), $[\mathbf{1}_6]$ (7.5 mM), Bu_4NBr (**3**, 78 mM); E: β -pinene (75 mM), $[\mathbf{1}_6\cdot 8\text{H}_2\text{O}]$ (7.5 mM). Spectra recorded after 64 h at room temperature, while A and B were recorded right after sample preparation.

Table 5: Product distribution for the isomerization reaction of β -pinene at rt for 64 h.

#	Catalyst	Conv. (%)	α -Pinene (%)	Camphene (%)	Limonene (%)
1	1₆	8	1	3	4
2	1₆ + 3	0	—	—	—
3	capsule A (1₆·8H₂O)	20	3	6	11



the minimum amount of water to form the network of hydrogen bonds with hydroxy moieties. Indeed, the capsule B, is looser because of the presence of extra water molecules that can arguably interact with their hydrogens with the lone pairs of the hydroxy moieties of the aromatic units thus diminishing the electron density of the cavity, which results less stabilizing for the carbocationic intermediate.

All these experiments demonstrated that the reaction was promoted by **1₆**. The Brønsted acidity of the capsule led to the formation of the intermediate carbocationic species that was stabilized within the cavity of the hexamer and converted to limonene as major product. We also tried to intercept the carbocationic intermediate using good nucleophiles in equimolar amounts such as *N*-methylindole or 2-mercaptoethanol but in all cases the reactions conducted in the presence of such nucleophiles proceeded forming only the isomerization products.

It is worth to notice that the conversion observed with the capsule was comparable to that what was frequently observed with typical heterogeneous Lewis or Brønsted catalysts under harsher experimental conditions with *T* higher than 100 °C in the gas phase [61]. More importantly, the product distribution observed is rather unusual if compared to many other heterogeneous catalytic systems known in the literature for leading to higher selectivity for camphene [62–66], and less likely to comparable amounts of camphene and limonene [67,68]. The preferential formation of limonene, which compared to camphene is a much more valuable product, has been less frequently observed, for instance in the case of heteropolyacids on SBA-15 [69]. The use of the capsule **1₆** represents a competitive catalytic system especially considering the milder experimental conditions, the lack of strong Brønsted or Lewis acids and the simple supramolecular catalytic approach.

Conclusion

In conclusion, we described a series of examples of supramolecular catalysis where the hexameric capsule **1₆** acts mimicking enzymes by combination of the activation of substrates by protonation, stabilization of cationic intermediate species with consequent acceleration of its conversion and selective product formation thanks to weak intermolecular interactions between the cationic intermediates and the internal surface of the capsule. Specifically, the capsule efficiently promoted the carbonyl–ene cyclization of (*S*)-citronellal forming isopulegol as the main product, the elimination of water from 1,1-diphenylethanol forming 1,1-diphenylethylene, the isomerization of α -pinene and β -pinene forming preferentially limonene with respect to camphene. For these unimolecular reactions the

use of the capsule represents a competitive catalytic system with respect to several literature methods especially considering the mild experimental conditions and absence of strong Brønsted or Lewis acids. A series of control experiments supported in all cases the evidence that the reaction is not just promoted by the acidity of **1₆** or its H-bonding properties, but that a combination of weak Brønsted acidity together with the presence of an accessible electron-rich cavity that favors the stabilization of the cationic intermediates is crucial for the supramolecular catalytic activity observed. In the reactions studied, the capsule plays a crucial role in steering product selectivity, thus further stimulating the investigation of new reactions.

Experimental

Instrumentation and operating conditions

The ¹H NMR spectra were acquired at 298 K with a Bruker AVANCE 300 spectrometer operating at 300.15 MHz and with a Bruker 400 spectrometer operating at 400.15 MHz. The chemical shift values (δ) in ppm refer to SiMe₄ (TMS) as standard. For GC–MS analysis a GC Trace GC 2000 apparatus was used equipped with an HP5-MS column (30 m, ID 0.25 mm, 0.5 μ m film), the carrier gas used was He coupled to a quadrupole MS Thermo Finnigan Trace MS (full scan, EI at 70 eV).

All the chemicals are commercially available and were used as received by the seller without further purification. The water-saturated chloroform-*d* was prepared by adding, at room temperature, a few drops of bi-distilled water to a 100 mL bottle chloroform-*d* previously passed on basic alumina in agreement with recent literature results to avoid interference by HCl [45]. Resorcin[4]arene **1** was synthesized and purified according to the procedure reported in the literature [49,70,71].

Experiments with substrates and capsule

1 (0.027 mmol, 6 equiv with respect to the hexameric capsule, 45 mM, 10 mol % of capsule with respect to substrate) was dissolved in an NMR tube containing 0.6 mL of water-saturated chloroform-*d* previously passed on basic alumina. Subsequently, the substrate (75 mM) was introduced, and the tube was maintained at 60 °C. The progress of the reaction was monitored by ¹H NMR and GC–MS by periodic sampling of the solution. Product assignments in the ¹H NMR spectra were carried out in accordance with literature data: for citronellal isomerization products [72–75], for 1,1-diphenylethene [76], for pinenes isomerization products [77,78].

Control experiments with 4-*n*-hexylresorcinol (**2**)

4-*n*-Hexylresorcinol (**2**, 0.108 mmol, 30 mM, 24 equiv with respect to the capsule) was dissolved in an NMR tube contain-

ing 0.6 mL of water-saturated chloroform-*d* previously passed on basic alumina. Subsequently, the substrate was introduced (75 mM), and the tube was heated at 60 °C. The progress of the reaction was monitored by ¹H NMR and GC–MS by periodic sampling of the solution.

Control experiments with capsule and competitive ammonium guests **3**

In an NMR tube containing 0.6 mL of water-saturated chloroform-*d* previously passed on basic alumina, **1** (0.027 mmol, 6 equiv with respect to the capsule, 45 mM) was dissolved. Tetrabutylammonium bromide (**3**, 10 equiv with respect to the capsule, 75 mM) was added and the tube heated until clear. Subsequently, the substrate was added (75 mM), and the tube maintained at 60 °C. The progress of the reaction was monitored by ¹H NMR and GC–MS by periodic sampling of the solution.

Control experiments with acetic acid (**4**)

The substrate (75 mM) was introduced into an NMR tube with 0.6 mL of water-saturated chloroform-*d* previously passed on basic alumina. Subsequently, acetic acid (**4**, 30 mM, 4 equiv with respect to the capsule) was added. The tube was heated at 60 °C. The progress of the reaction was monitored by ¹H NMR and GC–MS by periodic sampling of the solution.

Control experiments with low water content and hexameric capsule **A** (**1₆·8H₂O**)

Compound **1** (500 mg) was triturated with cyclohexane (10 mL) and the latter was removed under vacuum with gentle heating in order to remove the azeotropic mixture of water/cyclohexane. The treatment with cyclohexane was repeated two more times. The solid product was left under high vacuum for 20 h to remove traces of cyclohexane. A mother solution of **1** (0.27 mmol, 6 equiv with respect to the hexameric capsule, 45 mM) was prepared with 6 mL of chloroform-*d* previously passed on basic alumina which provide sufficiently dry solvent. To favor dissolution the mixture was heated gently and sonicated. This provided a solution of the hexameric capsule **A** (**1₆·8H₂O**) with water content <50 mM in agreement with a recent publication by Reek [22].

Supporting Information

Supporting Information File 1

Details on experimental procedures and ¹H NMR spectra for the catalytic tests.

[<https://www.beilstein-journals.org/bjoc/content/supplementary/1860-5397-18-38-S1.pdf>]

Acknowledgements

The authors acknowledge Dr. Laura Sperni, Dr. Giuseppe Borsato and Dr. Matteo Bertoldini for GC–MS analyses. AS is grateful to the DSMN colleagues who co-financed the 400 MHz NMR.

Funding

This research was funded by the CARIPARO project SELECT.

ORCID® IDs

Tommaso Lorenzetto - <https://orcid.org/0000-0002-7975-861X>

Fabrizio Fabris - <https://orcid.org/0000-0001-9209-1680>

Alessandro Scarso - <https://orcid.org/0000-0001-6114-9181>

Preprint

A non-peer-reviewed version of this article has been previously published as a preprint: <https://doi.org/10.3762/bxiv.2022.6.v1>

References

1. van Leeuwen, P. W. N. M. *Supramolecular Catalysis*; Wiley-VCH: Weinheim, Germany, 2008.
2. Dalgarno, S. J.; Power, N. P.; Atwood, J. L. *Coord. Chem. Rev.* **2008**, *252*, 825–841. doi:10.1016/j.ccr.2007.10.010
3. Vriezema, D. M.; Comellas Aragónès, M.; Elemans, J. A. A. W.; Cornelissen, J. J. L. M.; Rowan, A. E.; Nolte, R. J. M. *Chem. Rev.* **2005**, *105*, 1445–1490. doi:10.1021/cr0300688
4. Olivo, G.; Capocasa, G.; Del Giudice, D.; Lanzalunga, O.; Di Stefano, S. *Chem. Soc. Rev.* **2021**, *50*, 7681–7724. doi:10.1039/d1cs00175b
5. Wang, K.; Jordan, J. H.; Hu, X.-Y.; Wang, L. *Angew. Chem., Int. Ed.* **2020**, *59*, 13712–13721. doi:10.1002/anie.202000045
6. Leclercq, L.; Douyère, G.; Nardello-Rataj, V. *Catalysts* **2019**, *9*, 163. doi:10.3390/catal9020163
7. Morimoto, M.; Bierschenk, S. M.; Xia, K. T.; Bergman, R. G.; Raymond, K. N.; Toste, F. D. *Nat. Catal.* **2020**, *3*, 969–984. doi:10.1038/s41929-020-00528-3
8. Wei, H.; Wang, E. *Chem. Soc. Rev.* **2013**, *42*, 6060–6093. doi:10.1039/c3cs35486e
9. Raynal, M.; Ballester, P.; Vidal-Ferran, A.; van Leeuwen, P. W. N. M. *Chem. Soc. Rev.* **2014**, *43*, 1660–1733. doi:10.1039/c3cs60027k
10. Raynal, M.; Ballester, P.; Vidal-Ferran, A.; van Leeuwen, P. W. N. M. *Chem. Soc. Rev.* **2014**, *43*, 1734–1787. doi:10.1039/c3cs60037h
11. Dydio, P.; Reek, J. N. H. *Chem. Sci.* **2014**, *5*, 2135–2145. doi:10.1039/c3sc53505c
12. Leenders, S. H. A. M.; Gramage-Doria, R.; de Bruin, B.; Reek, J. N. H. *Chem. Soc. Rev.* **2015**, *44*, 433–448. doi:10.1039/c4cs00192c
13. Lindbäck, E.; Dawaigher, S.; Wärnmark, K. *Chem. – Eur. J.* **2014**, *20*, 13432–13481. doi:10.1002/chem.201402548
14. Otte, M. *ACS Catal.* **2016**, *6*, 6491–6510. doi:10.1021/acscatal.6b01776
15. Mouarrawi, V.; Plessius, R.; van der Vlugt, J. I.; Reek, J. N. H. *Front. Chem. (Lausanne, Switz.)* **2018**, *6*, 623. doi:10.3389/fchem.2018.00623
16. Poli, R. *Effects of Nanoconfinement on Catalysis*; Springer: Berlin, Germany, 2017.

17. Grommet, A. B.; Feller, M.; Klajn, R. *Nat. Nanotechnol.* **2020**, *15*, 256–271. doi:10.1038/s41565-020-0652-2
18. Caulder, D. L.; Raymond, K. N. *Acc. Chem. Res.* **1999**, *32*, 975–982. doi:10.1021/ar970224v
19. Catti, L.; Zhang, Q.; Tiefenbacher, K. *Chem. – Eur. J.* **2016**, *22*, 9060–9066. doi:10.1002/chem.201600726
20. Brown, C. J.; Toste, F. D.; Bergman, R. G.; Raymond, K. N. *Chem. Rev.* **2015**, *115*, 3012–3035. doi:10.1021/cr4001226
21. MacGillivray, L. R.; Atwood, J. L. *Nature* **1997**, *389*, 469–472. doi:10.1038/38985
22. Poole, D. A., III; Mathew, S.; Reek, J. N. H. *J. Am. Chem. Soc.* **2021**, *143*, 16419–16427. doi:10.1021/jacs.1c04924
23. Avram, L.; Cohen, Y.; Rebek, J., Jr. *Chem. Commun.* **2011**, *47*, 5368–5375. doi:10.1039/c1cc10150a
24. Shvanyuk, A.; Rebek, J., Jr. *Proc. Natl. Acad. Sci. U. S. A.* **2001**, *98*, 7662–7665. doi:10.1073/pnas.141226898
25. Dougherty, D. A. *Acc. Chem. Res.* **2013**, *46*, 885–893. doi:10.1021/ar300265y
26. Bianchini, G.; La Sorella, G.; Canever, N.; Scarso, A.; Strukul, G. *Chem. Commun.* **2013**, *49*, 5322–5324. doi:10.1039/c3cc42233j
27. La Sorella, G.; Sperni, L.; Strukul, G.; Scarso, A. *ChemCatChem* **2015**, *7*, 291–296. doi:10.1002/cctc.201402631
28. Cavarzan, A.; Scarso, A.; Sgarbossa, P.; Strukul, G.; Reek, J. N. H. *J. Am. Chem. Soc.* **2011**, *133*, 2848–2851. doi:10.1021/ja111060x
29. Cavarzan, A.; Reek, J. N. H.; Trentin, F.; Scarso, A.; Strukul, G. *Catal. Sci. Technol.* **2013**, *3*, 2898–2901. doi:10.1039/c3cy00300k
30. Borsato, G.; Scarso, A. *Catalysis Within the Self-Assembled Resorcin[4]arene Hexamer*. In *Organic Nanoreactors*; Sadjadi, S., Ed.; Academic Press: Chennai, India, 2016; pp 203–234. doi:10.1016/b978-0-12-801713-5.00007-0
31. Zhang, Q.; Catti, L.; Kaila, V. R. I.; Tiefenbacher, K. *Chem. Sci.* **2017**, *8*, 1653–1657. doi:10.1039/c6sc04565k
32. Gaeta, C.; Talotta, C.; De Rosa, M.; La Manna, P.; Soriente, A.; Neri, P. *Chem. – Eur. J.* **2019**, *25*, 4899–4913. doi:10.1002/chem.201805206
33. Zhang, Q.; Catti, L.; Tiefenbacher, K. *Acc. Chem. Res.* **2018**, *51*, 2107–2114. doi:10.1021/acs.accounts.8b00320
34. Hao, X.; Li, T.-R.; Chen, H.; Gini, A.; Zhang, X.; Rosset, S.; Mazet, C.; Tiefenbacher, K.; Matile, S. *Chem. – Eur. J.* **2021**, *27*, 12215–12223. doi:10.1002/chem.202101548
35. Gambaro, S.; La Manna, P.; De Rosa, M.; Soriente, A.; Talotta, C.; Gaeta, C.; Neri, P. *Front. Chem. (Lausanne, Switz.)* **2019**, *7*, 687. doi:10.3389/fchem.2019.00687
36. Gambaro, S.; Talotta, C.; Della Sala, P.; Soriente, A.; De Rosa, M.; Gaeta, C.; Neri, P. *J. Am. Chem. Soc.* **2020**, *142*, 14914–14923. doi:10.1021/jacs.0c04705
37. La Manna, P.; De Rosa, M.; Talotta, C.; Rescifina, A.; Floresta, G.; Soriente, A.; Gaeta, C.; Neri, P. *Angew. Chem., Int. Ed.* **2020**, *59*, 811–818. doi:10.1002/anie.201909865
38. Syntirianis, L.-D.; Némethová, I.; Schmid, D.; Levi, S.; Prescimone, A.; Bissegger, F.; Major, D. T.; Tiefenbacher, K. *J. Am. Chem. Soc.* **2020**, *142*, 5894–5900. doi:10.1021/jacs.0c01464
39. Zhang, Q.; Tiefenbacher, K. *Angew. Chem., Int. Ed.* **2019**, *58*, 12688–12695. doi:10.1002/anie.201906753
40. Huck, F.; Catti, L.; Reber, G. L.; Tiefenbacher, K. *J. Org. Chem.* **2022**, *87*, 419–428. doi:10.1021/acs.joc.1c02447
41. Catti, L.; Zhang, Q.; Tiefenbacher, K. *Synthesis* **2016**, *48*, 313–328. doi:10.1055/s-0035-1560362
42. Zhang, Q.; Tiefenbacher, K. *J. Am. Chem. Soc.* **2013**, *135*, 16213–16219. doi:10.1021/ja4080375
43. Naredla, R. R.; Klumpp, D. A. *Chem. Rev.* **2013**, *113*, 6905–6948. doi:10.1021/cr4001385
44. Mahadevi, A. S.; Sastry, G. N. *Chem. Rev.* **2013**, *113*, 2100–2138. doi:10.1021/cr300222d
45. Köster, J. M.; Tiefenbacher, K. *ChemCatChem* **2018**, *10*, 2941–2944. doi:10.1002/cctc.201800326
46. Iwata, T.; Okeda, Y.; Hori, Y. *Process for producing isopulegol*. U.S. Patent US6774269B2, Aug 10, 2004.
47. Friedrich, M.; Ebel, K.; Götz, N. *Method for the production of isopulegol*. U.S. Patent US7550633B2, June 23, 2009.
48. Chen, H.; Zou, H.; Hao, Y.; Yang, H. *ChemSusChem* **2017**, *10*, 1989–1995. doi:10.1002/cssc.201700318
49. Vandichel, M.; Vermoortele, F.; Cottenie, S.; De Vos, D. E.; Waroquier, M.; Van Speybroeck, V. *J. Catal.* **2013**, *305*, 118–129. doi:10.1016/j.jcat.2013.04.017
50. Kikukawa, Y.; Yamaguchi, S.; Nakagawa, Y.; Uehara, K.; Uchida, S.; Yamaguchi, K.; Mizuno, N. *J. Am. Chem. Soc.* **2008**, *130*, 15872–15878. doi:10.1021/ja8014154
51. Hart-Cooper, W. M.; Clary, K. N.; Toste, F. D.; Bergman, R. G.; Raymond, K. N. *J. Am. Chem. Soc.* **2012**, *134*, 17873–17876. doi:10.1021/ja308254k
52. Hart-Cooper, W. M.; Zhao, C.; Triano, R. M.; Yaghoubi, P.; Ozores, H. L.; Burford, K. N.; Toste, F. D.; Bergman, R. G.; Raymond, K. N. *Chem. Sci.* **2015**, *6*, 1383–1393. doi:10.1039/c4sc02735c
53. Ginzburg, A. L.; Baca, N. A.; Hampton, P. D. *J. Chem. Educ.* **2014**, *91*, 1748–1750. doi:10.1021/ed500124f
54. Kjonaas, R. A.; Mattingly, S. P. *J. Chem. Educ.* **2005**, *82*, 1813–1814. doi:10.1021/ed082p1813
55. Zhang, W.; Cheng, G.; Haller, G. L.; Liu, Y.; Lercher, J. A. *ACS Catal.* **2020**, *10*, 13371–13376. doi:10.1021/acscatal.0c03625
56. Catti, L.; Tiefenbacher, K. *Chem. Commun.* **2015**, *51*, 892–894. doi:10.1039/c4cc02811g
57. Sumrit, P.; Chuawong, P.; Nanok, T.; Duangthongyou, T.; Hormnirun, P. *Dalton Trans.* **2016**, *45*, 9250–9266. doi:10.1039/c6dt00990e
58. Alberti, M. N.; Orfanopoulos, M. *Org. Lett.* **2009**, *11*, 1659–1662. doi:10.1021/o1900363n
59. Lirag, R. C.; Miljanić, O. Š. *Chem. Commun.* **2014**, *50*, 9401–9404. doi:10.1039/c4cc02990a
60. Zhu, X.; Hong, G.; Hu, C.; Wu, S.; Wang, L. *Eur. J. Org. Chem.* **2017**, 1547–1551. doi:10.1002/ejoc.201700221
61. Wróblewska, A.; Miądlicki, P.; Sreńcek-Nazzal, J.; Sadłowski, M.; Koren, Z. C.; Michalkiewicz, B. *Microporous Mesoporous Mater.* **2018**, *258*, 72–82. doi:10.1016/j.micromeso.2017.09.007
62. Name, L. L.; Toma, S. H.; Pereira Nogueira, H.; Avanzi, L. H.; dos Santos Pereira, S.; Peffi Ferreira, L. F.; Araki, K.; Celli, R.; Toyama, M. M. *RSC Adv.* **2021**, *11*, 14203–14212. doi:10.1039/d1ra00012h
63. Huang, G.; Zhou, S.; Liu, J.; Su, S.; Yin, D. *RSC Adv.* **2020**, *10*, 10606–10611. doi:10.1039/d0ra01093f
64. Sánchez-Velandia, J. E.; Pájaro, E.; Villa, A. L.; Martínez-O, F. *Microporous Mesoporous Mater.* **2021**, *324*, 111273. doi:10.1016/j.micromeso.2021.111273
65. Miądlicki, P.; Wróblewska, A.; Kielbasa, K.; Koren, Z. C.; Michalkiewicz, B. *Microporous Mesoporous Mater.* **2021**, *324*, 111266. doi:10.1016/j.micromeso.2021.111266
66. Gackowski, M.; Kuterasiński, Ł.; Podobiński, J.; Korzeniowska, A.; Sulikowski, B.; Datka, J. *Appl. Catal., A* **2019**, *578*, 53–62. doi:10.1016/j.apcata.2019.03.016

67. Srećsek-Nazzal, J.; Kamińska, A.; Miądlicki, P.; Wróblewska, A.; Kielbasa, K.; Wróbel, R. J.; Serafin, J.; Michalkiewicz, B. *Materials* **2021**, *14*, 7811. doi:10.3390/ma14247811
68. Sidorenko, A. Y.; Aho, A.; Ganbaatar, J.; Batsuren, D.; Utentova, D. B.; Sen'kov, G. M.; Wärnå, J.; Murzin, D. Y.; Agabekov, V. E. *Mol. Catal.* **2017**, *443*, 193–202. doi:10.1016/j.mcat.2017.10.014
69. Frattini, L.; Isaacs, M. A.; Parlett, C. M. A.; Wilson, K.; Kyriakou, G.; Lee, A. F. *Appl. Catal., B* **2017**, *200*, 10–18. doi:10.1016/j.apcatb.2016.06.064
70. Hoegberg, A. G. S. *J. Org. Chem.* **1980**, *45*, 4498–4500. doi:10.1021/jo01310a046
71. Antesberger, J.; Cave, G. W. V.; Ferrarelli, M. C.; Heaven, M. W.; Raston, C. L.; Atwood, J. L. *Chem. Commun.* **2005**, 892–894. doi:10.1039/b412251h
72. Chittiboyina, A. G.; Peddikotla, P.; Avery, M. A.; Khan, I. A. *J. Org. Chem.* **2013**, *78*, 9223–9232. doi:10.1021/jo401461x
73. Meng, D.; Ollevier, T. *Synlett* **2018**, *29*, 640–644. doi:10.1055/s-0036-1591858
74. Nomoto, Y.; Horinouchi, R.; Nishiyama, N.; Nakano, K.; Ichikawa, Y.; Kotsuki, H. *Synlett* **2017**, *28*, 265–269. doi:10.1055/s-0036-1588618
75. Liu, X.; Xia, Q.; Zhang, Y.; Chen, C.; Chen, W. *J. Org. Chem.* **2013**, *78*, 8531–8536. doi:10.1021/o401252d
76. Ajdačić, V.; Nikolić, A.; Kerner, M.; Wipf, P.; Opsenica, I. M. *Synlett* **2018**, *29*, 1781–1785. doi:10.1055/s-0037-1610433
77. Guo, S.; Zhang, W.; Liang, J.; You, C.; Geng, Z.; Wang, C.; Du, S. *Molecules* **2016**, *21*, 504. doi:10.3390/molecules21040504
78. Park, K. D.; Lee, Y. J. *Magn. Reson. Chem.* **2006**, *44*, 887–891. doi:10.1002/mrc.1871

License and Terms

This is an open access article licensed under the terms of the Beilstein-Institut Open Access License Agreement (<https://www.beilstein-journals.org/bjoc/terms>), which is identical to the Creative Commons Attribution 4.0 International License (<https://creativecommons.org/licenses/by/4.0>). The reuse of material under this license requires that the author(s), source and license are credited. Third-party material in this article could be subject to other licenses (typically indicated in the credit line), and in this case, users are required to obtain permission from the license holder to reuse the material.

The definitive version of this article is the electronic one which can be found at:

<https://doi.org/10.3762/bjoc.18.38>



Tetraphenylethylene-embedded pillar[5]arene-based orthogonal self-assembly for efficient photocatalysis in water

Zhihang Bai, Krishnasamy Velmurugan*, Xueqi Tian, Minzan Zuo, Kaiya Wang and Xiao-Yu Hu*

Full Research Paper

Open Access

Address:

College of Materials Science and Technology, Nanjing University of Aeronautics and Astronautics, Nanjing 211106, P. R. China

Email:

Krishnasamy Velmurugan* - velu117@nuaa.edu.cn; Xiao-Yu Hu* - huxy@nuaa.edu.cn

* Corresponding author

Keywords:

aggregation-induced emission; Förster resonance energy transfer; host-guest interaction; photocatalysis; supramolecular self-assembly

Beilstein J. Org. Chem. **2022**, *18*, 429–437.

<https://doi.org/10.3762/bjoc.18.45>

Received: 28 January 2022

Accepted: 04 April 2022

Published: 13 April 2022

This article is part of the thematic issue "Supramolecular approaches to mediate chemical reactivity".

Guest Editor: C. Gaeta

© 2022 Bai et al.; licensee Beilstein-Institut.

License and terms: see end of document.

Abstract

Herein, we have designed and fabricated a simple and efficient supramolecular self-assembled nanosystem based on host-guest interactions between water-soluble tetraphenylethylene-embedded pillar[5]arene (**m-TPEWP5**) and ammonium benzoyl-L-alaninate (**G**) in an aqueous medium. The obtained assembly of **m-TPEWP5** and **G** showed aggregation-induced emission (AIE) via the blocking of intramolecular phenyl-ring rotations and functioned as an ideal donor. After the loading of eosin Y (**EsY**) as acceptor on the surface of the assembly of **m-TPEWP5** and **G**, the worm-like nanostructures changed into nanorods, which facilitates a Förster resonance energy transfer (FRET) from the **m-TPEWP5** and **G** assembled donor to the **EsY** acceptor present in the nanorod assembly. The system comprising **m-TPEWP5**, **G** and **EsY** displayed moderate FRET efficiency (31%) at a 2:1 molar ratio of donor-to-acceptor. Moreover, the obtained supramolecular nanorod assembly could act as a nanoreactor mimicking natural photosynthesis and exhibited a high catalytic efficiency for the photocatalytic dehalogenation reaction of various bromoketone derivatives with good yields in short reaction time in water.

Introduction

Photosynthesis is one of the most significant processes in nature, which balances the energy level in living systems [1-3]. In particular, green plants absorb photons of light and convert them into another form of energy through photosynthesis similar to solar power factories, containing many manufacturing units called chloroplasts. Briefly, the antenna molecules capture

the light energy by using protein-pigment complexes and transfer it to the specialized reaction centers via the FRET process, where the excited state energy is transferred into useable chemical energy [4-6]. Mainly, both antenna molecules and proteins on the thylakoid membrane are combined to form a light-harvesting system through noncovalent interactions.

Inspired by photosynthesis, extensive research has been devoted to construct energy transfer systems for the better utilization of solar energy [7]. In general, an effective supramolecular donor–acceptor system was employed to construct a photocatalytic system using FRET [6,8]. To fabricate a successful FRET system, the following key points need to be considered, i) the acceptor absorption spectrum should have good overlapping with the donor emission spectrum; ii) the distance between the donor and an acceptor should be within 10 nm; iii) dipoles of the donor and acceptor molecules must be adopted constructively vicinity to each other [9]. These fundamental criteria provide a wonderful approach for the construction of supramolecular photocatalytic systems by self-assembly strategies [10,11].

Recently, FRET-based supramolecular self-assembled systems [12,13] as nanoreactors for various photocatalytic reactions have received significant attention from the supramolecular community because of their robust molecular design and tunable self-assembly, such as vesicles [14–16], micelles [17–19], nanocrystals [20], coordination-driven assemblies [9,21,22], host–guest interactions [15,23–25], etc. In the above systems, catalysts are encapsulated by supramolecular assemblies and thus provide a suitable environment to improve the efficiency of chemical reactions in water [26]. Until now, various macrocyclic host-assisted supramolecular donor–acceptor systems have been developed based on the FRET process and further utilized for different photochemical reactions [27,28]. For instance, Yi et al. [29] developed a supramolecular assembly with a two-step FRET process by the utilization of a metallacycle-tetraphenylethylene (TPE) donor and eosin Y (EsY) and sulforhodamine (SR101) as first and second acceptors, respectively. The resulting supramolecular energy transfer system was applied to the alkylation of C–H bonds via a photochemical catalytic reaction in aqueous medium. In addition, our group [30] reported the construction of a supramolecular photocatalytic system with a two-step FRET process through the supramolecular assembly of water-soluble pillar[5]arene and TPE derivatives as donor and EsY and Nile Red (NiR) as acceptors. The obtained vesicles could be utilized as a nanoreactor for photocatalyzed dehalogenation reactions in water. However, the above reported supramolecular nanosystem requires a long time to produce the dehalogenated product with high yield. Therefore, the development of a potential nanoreactor for dehalogenation reaction with high yields within shorter reaction time is vastly essential and of industrial importance.

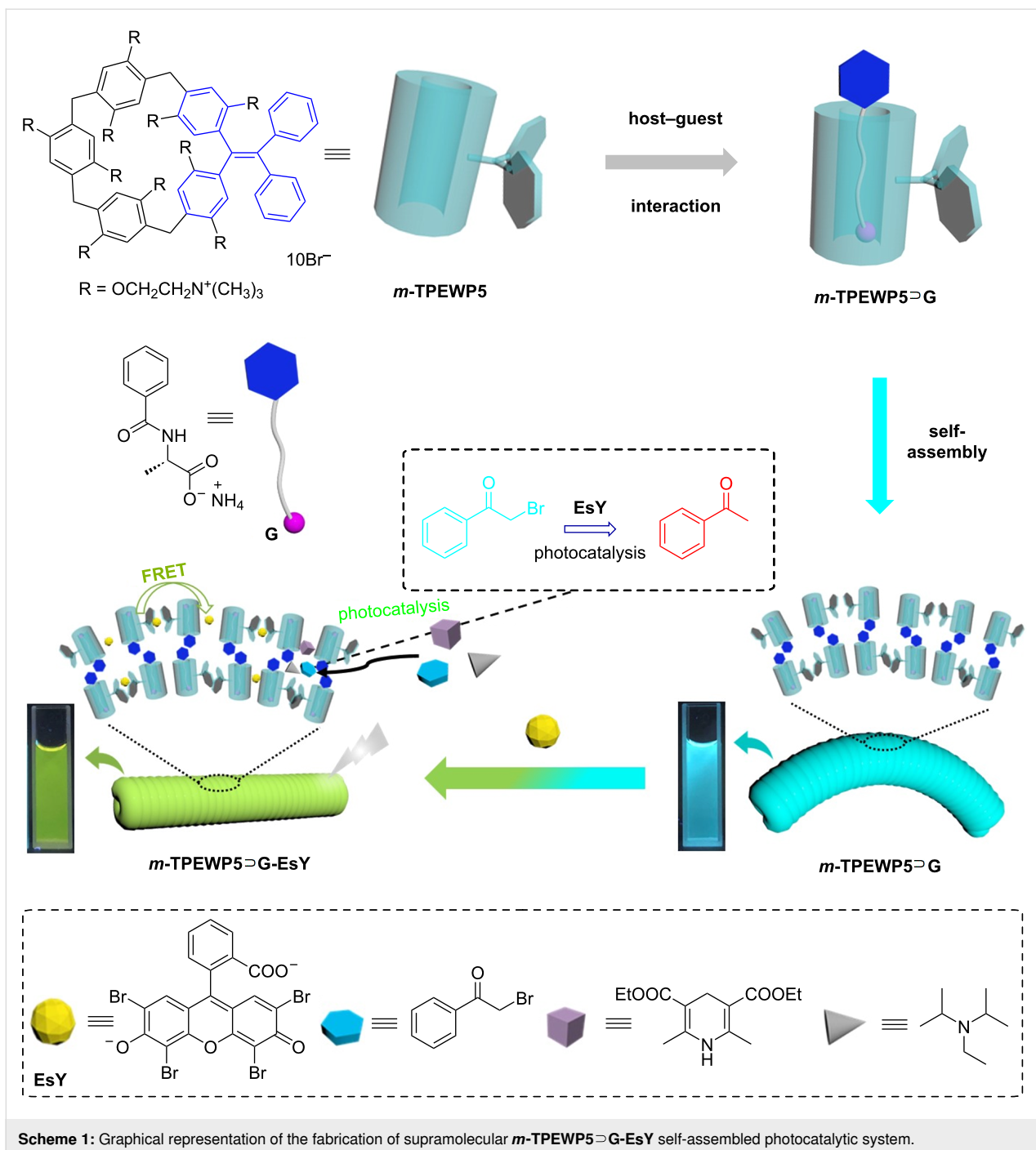
Herein, we have fabricated a supramolecular AIE-emissive photocatalytic system (**m-TPEWP5**–**G**–**EsY**) based on the host–guest interactions between *meso*-TPE embedded water-

soluble pillar[5]arene (**m-TPEWP5**) as host and the guest ammonium benzoyl-L-alaninate (**G**) forming the **m-TPEWP5**–**G** complex onto which **EsY** was loaded to achieve moderate FRET efficiency in water (Scheme 1). When the guest **G** was added to the host **m-TPEWP5** a stable host–guest complex formed, which strongly inhibited the intramolecular phenyl-ring rotations thus enhancing the AIE property. The resulting **m-TPEWP5**–**G** self-assembled worm-like nanosystem acts as an ideal donor and loading **EsY** as acceptor on the surface of the worm-like nanostructure, leads to the generation of a nanorod assembly via electrostatic interactions. The final AIE-emissive **m-TPEWP5**–**G**–**EsY** self-assembled FRET system could be employed to promote the photocatalyzed dehalogenation of various haloketone derivatives with excellent yields in water.

Results and Discussion

The **m-TPEWP5** host and ammonium benzoyl-L-alaninate (**G**) were synthesized according to our previous work [31,32] and their detailed synthetic routes and characterization data are provided in Supporting Information File 1 (Figure S1). Since **m-TPEWP5** and **G** have good solubility in water, therefore, the **m-TPEWP5**–**G** and **m-TPEWP5**–**G**–**EsY** supramolecular assemblies could be potentially fabricated in an aqueous solution. Before studying the FRET process, we firstly investigated the host–guest interactions between **m-TPEWP5** and **G** in D₂O. Upon the addition of **G** (1 equiv) to **m-TPEWP5**, the resonance peaks of **G** containing H_a and H_b protons shifted to the upfield region in the NMR scale (Figure 1). Meanwhile, the **m-TPEWP5** aromatic H₁ proton signal shifted to the downfield region, displaying that the guest molecule has a good binding affinity with the **m-TPEWP5** host to form a stable host–guest complex. In addition, 2D NOESY NMR (Figure S2 in Supporting Information File 1) was carried out to further confirm the interaction between **m-TPEWP5** and **G** (1 equiv of each) in D₂O. A strong cross-correlation peak was perceived between the **m-TPEWP5** aromatic protons and the H_c proton of **G**. The above results evidenced that the alanine pendant of the guest unit stayed in the **m-TPEWP5** cavity.

Besides, in order to confirm the host–guest interactions between **m-TPEWP5** and **G**, fluorescence titration studies were carried out in aqueous solution. As shown in Figure 2a, the free host **m-TPEWP5** showed a maximum emission at 465 nm. Upon gradually increasing the concentration of **G** (0 to 1 equiv) into **m-TPEWP5**, the fluorescence intensities were significantly increased with respect to **G** concentrations and no considerable changes were observed when further increasing the **G** concentration (1.2 equiv). The above results corroborated that the free rotation of **m-TPEWP5** rings was arrested during the com-



Scheme 1: Graphical representation of the fabrication of supramolecular **m-TPEWP5** \supset **G-EsY** self-assembled photocatalytic system.

plexation with **G**, thus further leads to the enhanced AIE effect [33,34].

To examine the binding stoichiometric ratio of the host-guest complex, Job's plot [35] method was employed by using fluorescence titration experiments. As shown in Figure S3 (see Supporting Information File 1), the maximum mole fraction was observed at 0.5 (Figure 2b), which corresponds to a 1:1 binding stoichiometric ratio between **G** and **m-TPEWP5** in the aqueous

solution. Furthermore, the association constant (K_a) [36] was calculated to be $8.62 \times 10^4 \text{ M}^{-1}$ based on the UV-vis titration experiment (Figure S4, Supporting Information File 1). This result further confirmed that the binding interaction between **m-TPEWP5** and **G** is strong enough to form a stable complex in an aqueous solution.

The morphology of the supramolecular **m-TPEWP5** \supset **G** and **m-TPEWP5** \supset **G-EsY** systems was monitored by using trans-

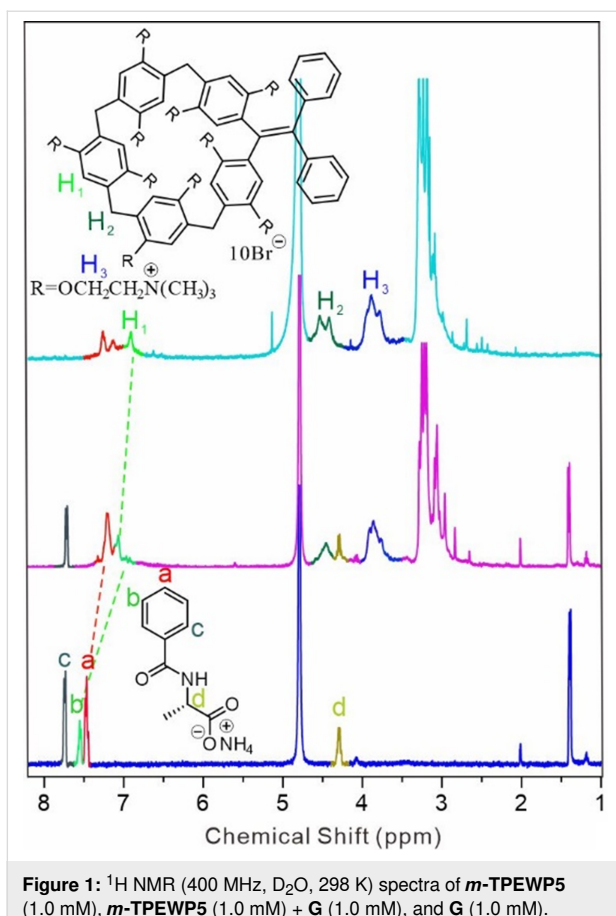


Figure 1: ^1H NMR (400 MHz, D_2O , 298 K) spectra of **m-TPEWP5** (1.0 mM), **m-TPEWP5** (1.0 mM) + **G** (1.0 mM), and **G** (1.0 mM).

mission electron microscopy (TEM). As shown in Figure 3, **m-TPEWP5** self-assembled to form a worm-like nanostructure (diameter = 748 nm). After the loading of **EsY** into

m-TPEWP5, the worm-like structure changed into a nanorod (diameter = 652 nm) assembly via electrostatic interactions. In comparison, the diameter and length of the **m-TPEWP5** assembly were slightly higher than that of **m-TPEWP5**–**G**–**EsY**, which revealed that host–guest complex aggregated to form a stable structural assembly, then a dye-loaded composite system [32].

The energy transfer efficiency of the supramolecular **m-TPEWP5**–**G**–**EsY** self-assembled composite system was examined by using **m-TPEWP5**–**G** and **EsY** as an ideal donor and acceptor, respectively. Initially, we compared the overlapping efficiencies of both donor and acceptor systems by using UV–vis and fluorescence spectroscopy. The absorption band of the **EsY** acceptor shows good overlapping with the emission band of **m-TPEWP5**–**G** donor (Figure 4a). We therefore speculated, that there may be an efficient FRET process between the donor and acceptor containing nanorod assembly. As shown in Figure 4b, upon exciting at the donor wavelength ($\lambda_{\text{ex}} = 320$ nm), the fluorescence intensity of the **m-TPEWP5**–**G** donor gradually decreased, whereas the **EsY** acceptor emission peak at 540 nm gradually increased thus indicating an efficient energy transfer is taking place. This was further supported by the observation, that upon loading of **EsY** into the **m-TPEWP5**–**G** assembly, the color of the donor solution changed from sky blue to greenish-yellow under UV light. At a 2:1 donor/acceptor molar ratio, a maximum FRET efficiency of 31% was achieved [30]. This result suggested that **m-TPEWP5**–**G**–**EsY** self-assembled nanosystem could be used as a nanoreactor for organic photocatalytic reactions in an aqueous medium. The nature of the interaction between

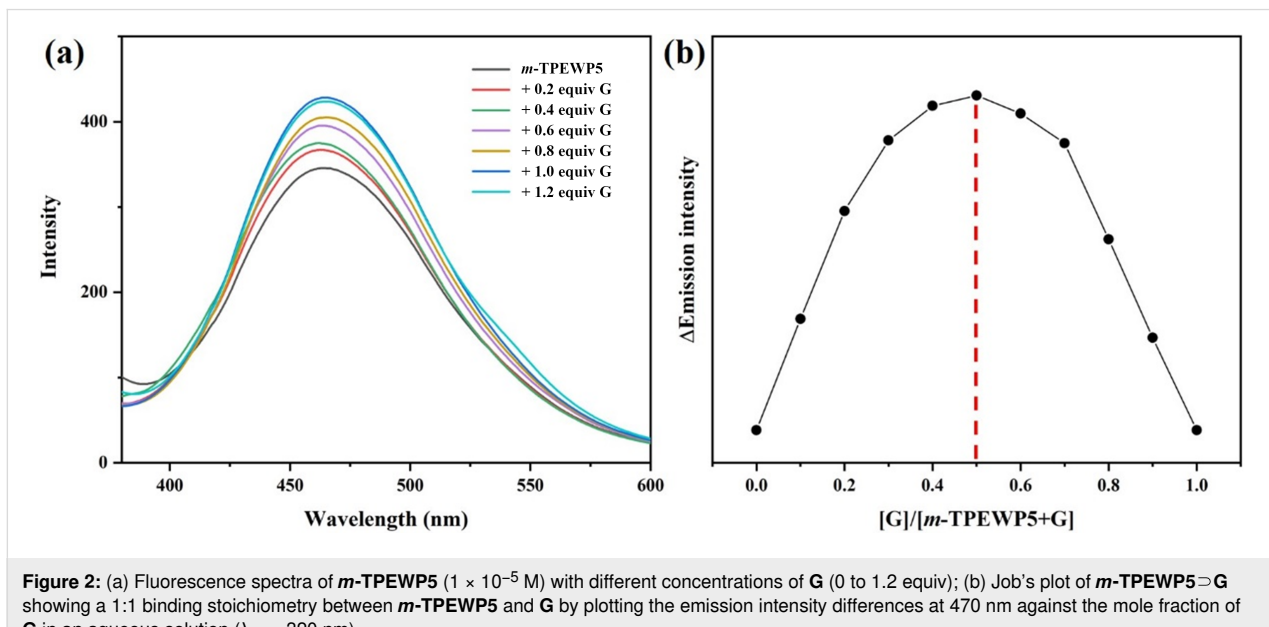


Figure 2: (a) Fluorescence spectra of **m-TPEWP5** (1×10^{-5} M) with different concentrations of **G** (0 to 1.2 equiv); (b) Job's plot of **m-TPEWP5**–**G** showing a 1:1 binding stoichiometry between **m-TPEWP5** and **G** by plotting the emission intensity differences at 470 nm against the mole fraction of **G** in an aqueous solution ($\lambda_{\text{ex}} = 320$ nm).

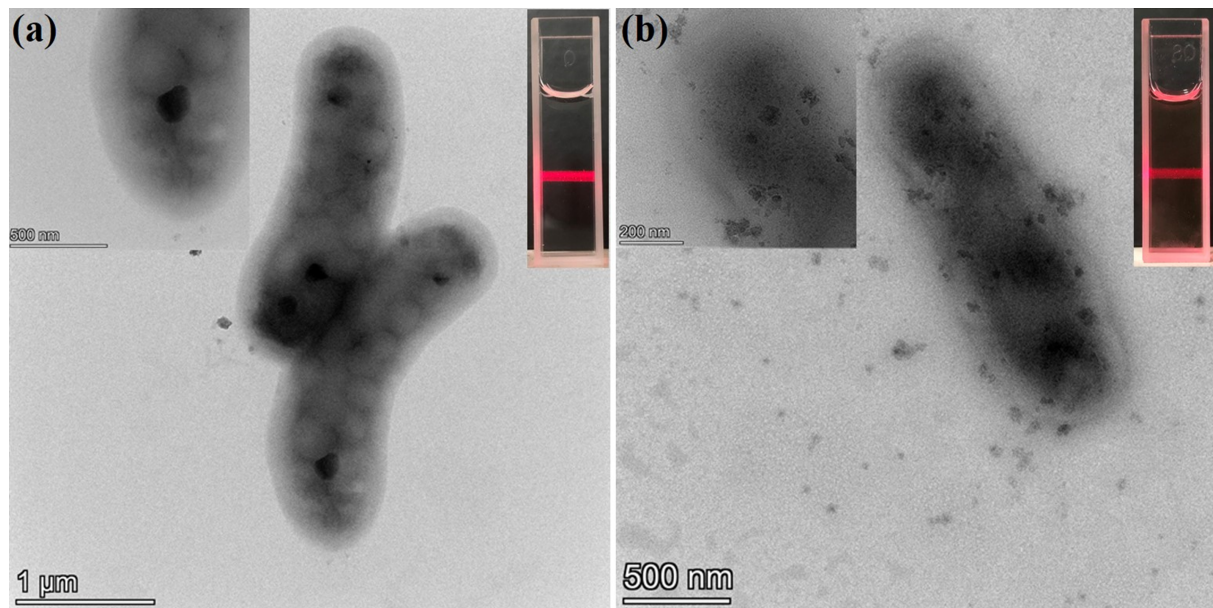


Figure 3: TEM images of (a) ***m***-TPEWP5 \supset G; (b) ***m***-TPEWP5 \supset G-EsY. $[m\text{-TPEWP5}] = 1 \times 10^{-4}$ M, $[\mathbf{G}] = 1 \times 10^{-4}$ M, $[\mathbf{EsY}] = 1 \times 10^{-4}$ M.

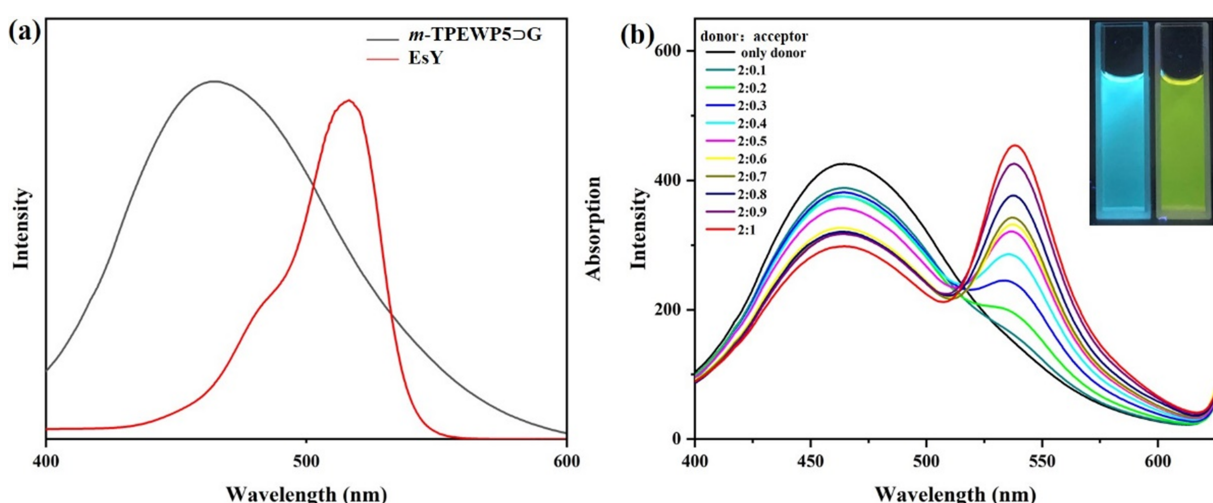


Figure 4: (a) Normalized absorption and emission spectra of the EsY acceptor and the ***m***-TPEWP5 \supset G donor assembly; (b) Fluorescence spectra of the ***m***-TPEWP5 \supset G assembly with steadily increasing the equivalents of EsY in an aqueous medium ($\lambda_{\text{ex.}} = 320$ nm). Inset: Photograph of ***m***-TPEWP5 \supset G before and after the addition of EsY under UV light.

m-TPEWP5 \supset G and EsY was evaluated by ^1H NMR titration studies in D_2O (Figure S5 in Supporting Information File 1). When 1 equiv of EsY was added into the ***m***-TPEWP5 \supset G solution, the resonance signals of EsY were shifted to upfield regions, which was caused by steric effects and electrostatic interactions between the quaternary ammonium groups containing ***m***-TPEWP5 and the negatively charged EsY. These results evidenced that the EsY molecule was adsorbed on the surface of ***m***-TPEWP5 via electrostatic interactions.

To mimic natural photosynthesis, the harvested energy of the ***m***-TPEWP5 \supset G-EsY nanoreactor system could potentially be applied to a photocatalytic dehalogenation reaction. Normally, most chromophoric dye molecules can be utilized in photoredox reactions under the irradiation of light with suitable wavelength [6]. However, in the case of the ***m***-TPEWP5 \supset G-EsY nanosystem, which contains conjugated molecules and displays harvesting antenna effects from ultraviolet to visible light wavelengths, solar light might be successfully employed to catalyze

these reactions. Here, we used white light (20 W) as a solar light simulator for the photocatalytic dehalogenation reactions. Upon light irradiation, the absorbed light energy could be transferred from the **m-TPEWP5 \supset G** donor to the **EsY** acceptor through the FRET process, whilst the **m-TPEWP5 \supset G-EsY** nanorod assembly could act as a nanoreactor providing a suitable environment for the photochemical catalytic reaction in aqueous solution under visible light irradiation.

In the presence of 0.5 mol % **m-TPEWP5 \supset G-EsY** in aqueous solution, 2-bromo-1-phenylethanone (**1a**) gave acetophenone (**2a**) as product in good yield (97%) under white light irradiation for 2 hours (Table 1 and Supporting Information File 1, Figure S6). In comparison, we added an internal standard (1,3,5-trimethoxybenzene) to the final crude reaction mixture and calculated the NMR yield of the product. From the above method, the yield of the product **2a** (97%) is almost identical with our previous results (i.e., assumption of complete conversion of the starting material) as shown in Figure S7 (Supporting Information File 1). Therefore, these results corroborated that there were almost no other byproducts in the system. For further confirmation, we have included the ^{13}C NMR spectrum of the crude product **2a** in Supporting Information File 1 (Figure S8).

Table 1: 2-Bromo-1-phenylethanone dehalogenation reaction under various reaction conditions.^a

Entry	Photocatalyst ^a	Light irradiation	Yield ^b [%]
1	none	yes	28
2	EsY	yes	38
3	m-TPEWP5\supsetG	yes	40
4	m-TPEWP5\supsetG-EsY	yes	97
5 ^c	m-TPEWP5\supsetG-EsY	no	no reaction

^aReaction conditions: Bromoacetophenone (20 mg, 0.1 mmol), Hantzsch ester (28 mg, 0.11 mmol), *N,N*-diisopropylethylamine (DIPEA, 35 μ L, 0.2 mmol), **m-TPEWP5 \supset G-EsY** in water (2.5 mL), 20 W white light, rt, N_2 , 2 h. ^bProduct yield obtained from ^1H NMR spectra; ^cUnder dark conditions (no light irradiation).

As a control experiment, the reaction was carried out in the absence of catalyst **m-TPEWP5 \supset G** with **EsY** alone (Figure S14, Supporting Information File 1), respectively, and the obtained product yield was very low under light irradiation. Notably, under dark conditions (no light irradiation), there was no product observed in the resulting solution. The above result evidenced that a light source is indispensable for the catalytic

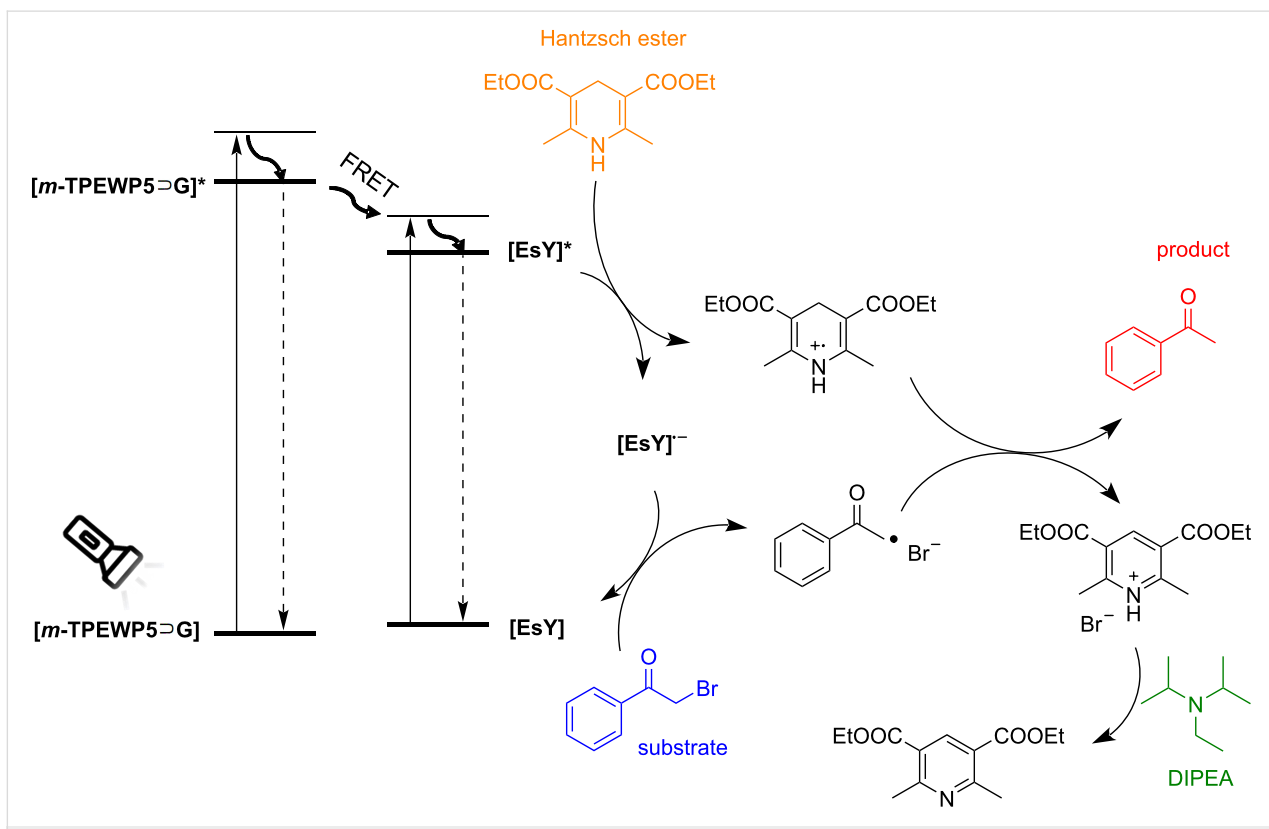
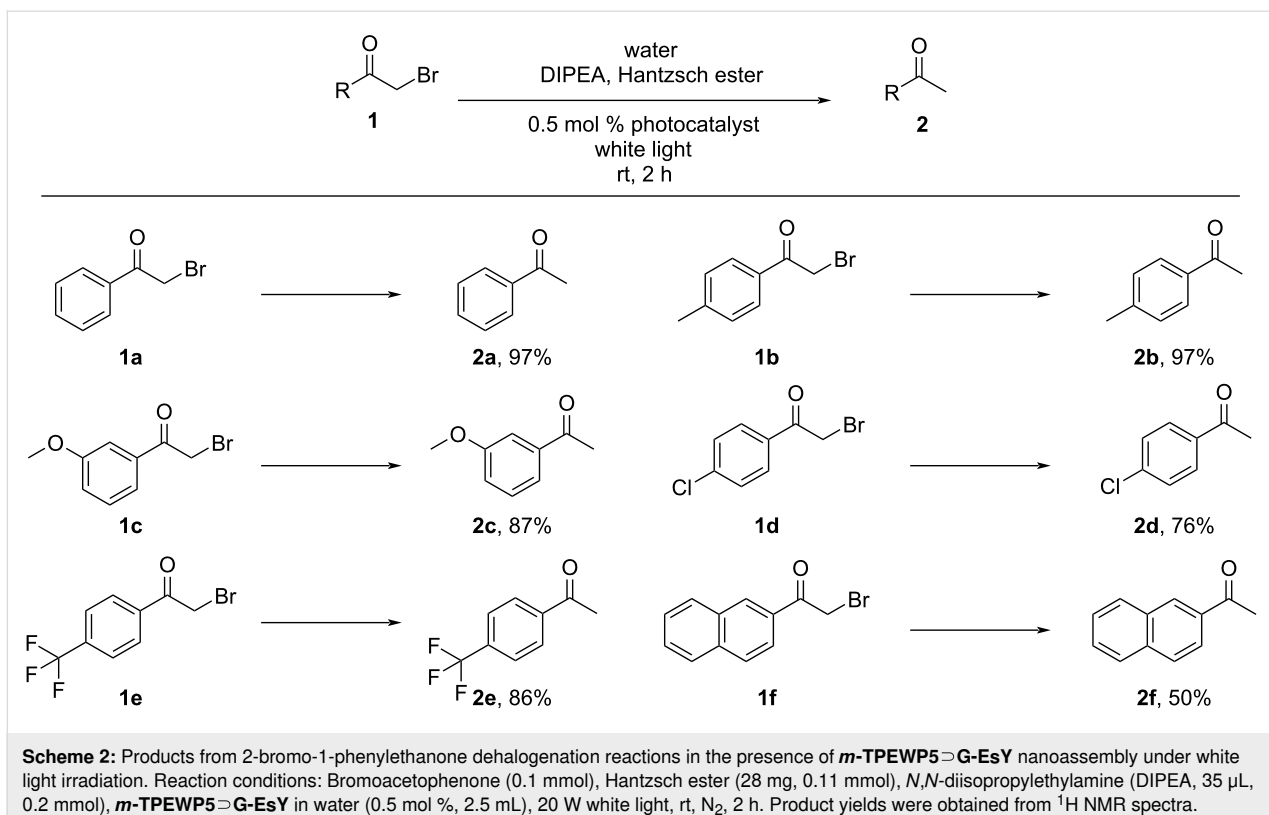
dehalogenation reaction in an aqueous environment. Overall, the **m-TPEWP5 \supset G-EsY** system showed high catalytic efficiency within a short time of light irradiation in aqueous solution, which was due to the fact that the loaded **EsY** dye molecules on the surface of the **TPEWP5 \supset G** nanorod assembly significantly decreased photobleaching during light irradiation. In addition, the AIE donor molecules allowed an ordered arrangement of the loaded negatively charged dye acceptor on the positively charged surface, which might avoid aggregation-caused quenching effects and produced better catalytic efficiency. These results revealed that the **m-TPEWP5 \supset G-EsY** nanoreactor can act as an effective photocatalytic system to harvest and transform solar energy into chemical energy in aqueous solution.

Similarly, we carried out the dehalogenation reactions by using various α -bromoacetophenone derivatives as substrates. As shown in Scheme 2, different substrates **1** containing electron-donating (**1b,c**) and electron-withdrawing substituents (**1d,e**) and 2-bromo-2-acetonaphthone (**1f**) were examined in the reaction. Most substrates afforded the corresponding products in good yields (the ^1H NMR spectra of the reaction mixtures used for calculation of yields are collected in Supporting Information File 1): good yields were observed for 4-methylacetophenone (**2b**, 97%, Figure S9), 3-methoxyacetophenone (**2c**, 87%, Figure S10), 4-chloroacetophenone (**2d**, 76%, Figure S11), and 4-(trifluoromethyl)acetophenone (**2e**, 86%, Figure S12) and a moderate yield was obtained for 2-acetonaphthone (**2j**, 50%, Figure S13) demonstrating the general applicability of **m-TPEWP5 \supset G-EsY** as an efficient photocatalyst.

To understand the process for this photocatalytic dehalogenation reaction, a possible reaction mechanism is proposed in Figure 5 [37]. Upon light irradiation, the ground state of **m-TPEWP5 \supset G** donor absorbs light energy and changes to the excited state (**TPEWP5 \supset G***) energy level. Through energy transfer from **TPEWP5 \supset G*** to ground state **EsY** the latter undergoes excitation to the excited state **EsY*** and is reduced by the Hantzsch ester to generate the radical anion **EsY $^{\bullet-}$** . Subsequently, electron transfer from **EsY $^{\bullet-}$** to the substrate α -bromoacetophenone (**1a**) gives the corresponding acetophenone radical, whilst **EsY $^{\bullet-}$** is oxidized to **EsY**. The acetophenone radical combines with a H-atom abstracted from the radical cation of the Hantzsch ester to form acetophenone (**2a**) as the final product and diethyl 2,6-dimethylpyridine-3,5-dicarboxylate after deprotonation in the presence of the base DIPEA.

Conclusion

In conclusion, we have fabricated a simple and efficient supramolecular photocatalytic system based on host–guest self-assembled **m-TPEWP5 \supset G** donor and **EsY** as acceptor.



Briefly, the **m-TPEWP5** host and **G** guest molecule were involved in the inclusion complex and further self-assembled to form worm-like supramolecular nanostructures, which displayed an AIE effect via restricted phenyl-ring rotation of **m-TPEWP5**. After that, the negative **EsY** acceptor was loaded on the positively charged surface of the **m-TPEWP5**–**G** donor assembly to form a nanorod structure, which exhibited moderate FRET efficiency at a 2:1 molar ratio of the donor/acceptor. Inspired by photosynthesis and followed by the energy transfer process, the **m-TPEWP5**–**G**–**EsY** supramolecular nanorod assembly could be employed as a nanoreactor for a photocatalytic dehalogenation reaction, i.e., debromination of 2-bromo-1-phenylethanone derivatives with high yields and short reaction time in an aqueous solution. Based on the above results, the fabricated AIE-emissive FRET system with chiral guest can be further utilized for asymmetric catalysis in water, which is currently underway in our laboratory.

Supporting Information

Supporting Information File 1

Experimental details, NMR spectra, host–guest interaction, FRET, and other materials.

[<https://www.beilstein-journals.org/bjoc/content/supplementary/1860-5397-18-45-S1.pdf>]

Funding

This work was supported by the National Natural Science Foundation of China for Sino-German Mobility Program (No. M-0411), the Natural Science Foundation of Jiangsu Province (BK20211179, BK20200432), and the Fundamental Research Funds for the Central Universities (NS2021040).

ORCID® iDs

Xiao-Yu Hu - <https://orcid.org/0000-0002-9634-315X>

References

- McDermott, G.; Prince, S. M.; Freer, A. A.; Hawthornthwaite-Lawless, A. M.; Papiz, M. Z.; Cogdell, R. J.; Isaacs, N. W. *Nature* **1995**, *374*, 517–521. doi:10.1038/374517a0
- Holt, N. E.; Zigmantas, D.; Valkunas, L.; Li, X.-P.; Niyogi, K. K.; Fleming, G. R. *Science* **2005**, *307*, 433–436. doi:10.1126/science.1105833
- Polívka, T.; Frank, H. A. *Acc. Chem. Res.* **2010**, *43*, 1125–1134. doi:10.1021/ar100030m
- Scholes, G. D.; Fleming, G. R.; Olaya-Castro, A.; van Grondelle, R. *Nat. Chem.* **2011**, *3*, 763–774. doi:10.1038/nchem.1145
- Xiao, T.; Zhong, W.; Zhou, L.; Xu, L.; Sun, X.-Q.; Elmes, R. B. P.; Hu, X.-Y.; Wang, L. *Chin. Chem. Lett.* **2019**, *30*, 31–36. doi:10.1016/j.cclet.2018.05.034
- Wang, K.; Velmurugan, K.; Li, B.; Hu, X.-Y. *Chem. Commun.* **2021**, *57*, 13641–13654. doi:10.1039/d1cc06011b
- Barber, J. *Chem. Soc. Rev.* **2009**, *38*, 185–196. doi:10.1039/b802262n
- Teunissen, A. J. P.; Pérez-Medina, C.; Meijerink, A.; Mulder, W. J. M. *Chem. Soc. Rev.* **2018**, *47*, 7027–7044. doi:10.1039/c8cs00278a
- Jia, P.-P.; Xu, L.; Hu, Y.-X.; Li, W.-J.; Wang, X.-Q.; Ling, Q.-H.; Shi, X.; Yin, G.-Q.; Li, X.; Sun, H.; Jiang, Y.; Yang, H.-B. *J. Am. Chem. Soc.* **2021**, *143*, 399–408. doi:10.1021/jacs.0c11370
- Wang, K.; Jordan, J. H.; Velmurugan, K.; Tian, X.; Zuo, M.; Hu, X.-Y.; Wang, L. *Angew. Chem., Int. Ed.* **2021**, *60*, 9205–9214. doi:10.1002/anie.202010150
- Zuo, M.; Velmurugan, K.; Wang, K.; Tian, X.; Hu, X.-Y. *Beilstein J. Org. Chem.* **2021**, *17*, 139–155. doi:10.3762/bjoc.17.15
- Pochan, D.; Scherman, O. *Chem. Rev.* **2021**, *121*, 13699–13700. doi:10.1021/acs.chemrev.1c00884
- Hartgerink, J. D.; Beniash, E.; Stupp, S. I. *Science* **2001**, *294*, 1684–1688. doi:10.1126/science.1063187
- Huang, J.; Yu, Y.; Wang, L.; Wang, X.; Gu, Z.; Zhang, S. *ACS Appl. Mater. Interfaces* **2017**, *9*, 29030–29037. doi:10.1021/acsami.7b06954
- Guo, S.; Song, Y.; He, Y.; Hu, X.-Y.; Wang, L. *Angew. Chem., Int. Ed.* **2018**, *57*, 3163–3167. doi:10.1002/anie.201800175
- Huo, M.; Ye, Q.; Che, H.; Wang, X.; Wei, Y.; Yuan, J. *Macromolecules* **2017**, *50*, 1126–1133. doi:10.1021/acs.macromol.6b02499
- Peng, H.-Q.; Chen, Y.-Z.; Zhao, Y.; Yang, Q.-Z.; Wu, L.-Z.; Tung, C.-H.; Zhang, L.-P.; Tong, Q.-X. *Angew. Chem., Int. Ed.* **2012**, *51*, 2088–2092. doi:10.1002/anie.201107723
- Chadha, G.; Yang, Q.-Z.; Zhao, Y. *Chem. Commun.* **2015**, *51*, 12939–12942. doi:10.1039/c5cc04377h
- Pallavi, P.; Sk, B.; Ahir, P.; Patra, A. *Chem. – Eur. J.* **2018**, *24*, 1151–1158. doi:10.1002/chem.201704437
- Chen, P.-Z.; Weng, Y.-X.; Niu, L.-Y.; Chen, Y.-Z.; Wu, L.-Z.; Tung, C.-H.; Yang, Q.-Z. *Angew. Chem., Int. Ed.* **2016**, *55*, 2759–2763. doi:10.1002/anie.201510503
- Ling, Q.; Cheng, T.; Tan, S.; Huang, J.; Xu, L. *Chin. Chem. Lett.* **2020**, *31*, 2884–2890. doi:10.1016/j.cclet.2020.08.020
- Li, Y.; Rajasree, S. S.; Lee, G. Y.; Yu, J.; Tang, J.-H.; Ni, R.; Li, G.; Houk, K. N.; Deria, P.; Stang, P. J. *J. Am. Chem. Soc.* **2021**, *143*, 2908–2919. doi:10.1021/jacs.0c12853
- Kim, H.-J.; Nandajan, P. C.; Gierschner, J.; Park, S. Y. *Adv. Funct. Mater.* **2018**, *28*, 1705141. doi:10.1002/adfm.201705141
- Zhang, D.; Liu, Y.; Fan, Y.; Yu, C.; Zheng, Y.; Jin, H.; Fu, L.; Zhou, Y.; Yan, D. *Adv. Funct. Mater.* **2016**, *26*, 7652–7661. doi:10.1002/adfm.201603118
- Sun, G.; Qian, W.; Jiao, J.; Han, T.; Shi, Y.; Hu, X.-Y.; Wang, L. *J. Mater. Chem. A* **2020**, *8*, 9590–9596. doi:10.1039/d0ta03169k
- Petroselli, M.; Chen, Y.-Q.; Rebek, J., Jr.; Yu, Y. *Green Synth. Catal.* **2021**, *2*, 123–130. doi:10.1016/j.gresc.2021.03.004
- Ogoshi, T.; Yamafuji, D.; Yamagishi, T.-a.; Brouwer, A. M. *Chem. Commun.* **2013**, *49*, 5468–5470. doi:10.1039/c3cc42612b
- Wang, X.-H.; Song, N.; Hou, W.; Wang, C.-Y.; Wang, Y.; Tang, J.; Yang, Y.-W. *Adv. Mater. (Weinheim, Ger.)* **2019**, *31*, 1903962. doi:10.1002/adma.201903962
- Zhang, D.; Yu, W.; Li, S.; Xia, Y.; Li, Y.; Yi, T. *J. Am. Chem. Soc.* **2021**, *143*, 1313–1317. doi:10.1021/jacs.0c12522
- Hao, M.; Sun, G.; Zuo, M.; Xu, Z.; Chen, Y.; Hu, X.-Y.; Wang, L. *Angew. Chem., Int. Ed.* **2020**, *59*, 10095–10100. doi:10.1002/anie.201912654

31. Tian, X.; Zuo, M.; Niu, P.; Velmurugan, K.; Wang, K.; Zhao, Y.; Wang, L.; Hu, X.-Y. *ACS Appl. Mater. Interfaces* **2021**, *13*, 37466–37474. doi:10.1021/acsami.1c07106
32. Velmurugan, K.; Murtaza, A.; Saeed, A.; Li, J.; Wang, K.; Zuo, M.; Liu, Q.; Hu, X.-Y. *CCS Chem.* **2022**, in press. doi:10.31635/ccschem.022.202101749
33. Luo, J.; Xie, Z.; Lam, J. W. Y.; Cheng, L.; Chen, H.; Qiu, C.; Kwok, H. S.; Zhan, X.; Liu, Y.; Zhu, D.; Tang, B. Z. *Chem. Commun.* **2001**, 1740–1741. doi:10.1039/b105159h
34. Le Guével, X.; Hötzer, B.; Jung, G.; Schneider, M. *J. Mater. Chem.* **2011**, *21*, 2974–2981. doi:10.1039/c0jm02660c
35. Velmurugan, K.; Thamilselvan, A.; Antony, R.; Kannan, V. R.; Tang, L.; Nandhakumar, R. *J. Photochem. Photobiol., A* **2017**, *333*, 130–141. doi:10.1016/j.jphotochem.2016.10.025
36. Prabakaran, G.; Velmurugan, K.; Vickram, R.; David, C. I.; Thamilselvan, A.; Prabhu, J.; Nandhakumar, R. *Spectrochim. Acta, Part A* **2021**, *246*, 119018. doi:10.1016/j.saa.2020.119018
37. Sun, G.; Zuo, M.; Qian, W.; Jiao, J.; Hu, X.-Y.; Wang, L. *Green Synth. Catal.* **2021**, *2*, 32–37. doi:10.1016/j.gresc.2021.01.003

License and Terms

This is an open access article licensed under the terms of the Beilstein-Institut Open Access License Agreement (<https://www.beilstein-journals.org/bjoc/terms>), which is identical to the Creative Commons Attribution 4.0 International License (<https://creativecommons.org/licenses/by/4.0>). The reuse of material under this license requires that the author(s), source and license are credited. Third-party material in this article could be subject to other licenses (typically indicated in the credit line), and in this case, users are required to obtain permission from the license holder to reuse the material.

The definitive version of this article is the electronic one which can be found at:

<https://doi.org/10.3762/bjoc.18.45>



Bioinspired tetraamino-bisthiourea chiral macrocycles in catalyzing decarboxylative Mannich reactions

Hao Guo^{1,2}, Yu-Fei Ao^{1,2}, De-Xian Wang^{1,2} and Qi-Qiang Wang^{*1,2}

Full Research Paper

Open Access

Address:

¹Beijing National Laboratory for Molecular Sciences, CAS Key Laboratory of Molecular Recognition and Function, Institute of Chemistry, Chinese Academy of Sciences, Beijing 100190, China and ²University of Chinese Academy of Sciences, Beijing 100049, China

Beilstein J. Org. Chem. **2022**, *18*, 486–496.

<https://doi.org/10.3762/bjoc.18.51>

Received: 17 March 2022

Accepted: 26 April 2022

Published: 02 May 2022

Email:

Qi-Qiang Wang* - qiqiangw@iccas.ac.cn

This article is part of the thematic issue "Supramolecular approaches to mediate chemical reactivity".

* Corresponding author

Associate Editor: N. Sewald

Keywords:

chiral macrocycles; cooperative asymmetric catalysis; decarboxylative Mannich reactions; supramolecular catalysis; thiourea

© 2022 Guo et al.; licensee Beilstein-Institut.

License and terms: see end of document.

Abstract

A series of tetraamino-bisthiourea chiral macrocycles containing two diarylthiourea and two chiral diamine units were synthesized by a fragment-coupling approach in high yields. Different chiral diamine units, including cyclohexanediamines and diphenylethane-diamines were readily incorporated by both homo and hetero [1 + 1] macrocyclic condensation of bisamine and bisothiocyanate fragments. With the easy synthesis, gram-scale of macrocycle products can be readily obtained. These chiral macrocycles were applied in catalyzing bioinspired decarboxylative Mannich reactions. Only 5 mol % of the optimal macrocycle catalyst efficiently catalyzed the decarboxylative addition of a broad scope of malonic acid half thioesters to isatin-derived ketimines with excellent yields and good enantioselectivity. The rigid macrocyclic framework and the cooperation between the thiourea and tertiary amine sites were found to be crucial for achieving efficient activation and stereocontrol. As shown in control experiments, catalysis with the acyclic analogues having the same structural motifs were non-selective.

Introduction

In the past decades, the development of supramolecular chemistry has enabled abundant host scaffolds and assembly tools for boosting catalytic processes, and stimulated the emergence of supramolecular catalysis [1–14]. Among which, macrocyclic compounds have attracted extensive attentions due to their enzyme-mimicking cavity and preorganized binding sites [4,6,15,16]. Various macrocyclic compounds including the priv-

ileged scaffolds like cyclodextrins [17–19], calixarenes [20–23], cucurbiturils [24,25], and cavitands [26,27] have been widely applied. While these conventional macrocycles can usually enable a confinement effect or serve as a supporting scaffold, they do not contain definite catalytic sites in their cyclic skeletons. When required, an additional catalytic functional group was commonly introduced through in-situ, noncovalent inclu-

sion/encapsulation in the cavity or by covalent, post-functionalization of the macrocyclic scaffold. The encapsulated catalytic group could occupy the space for substrate entering, or has a risk to be squeezed out of the cavity under complex catalytic conditions. On the other hand, the covalently pendant catalytic group may reside far away from the center of the cavity.

On the other hand, we envisaged by use of tailored building units already containing definite catalytic sites to directly form a macrocycle scaffold could provide a different situation. In this way the catalytic functionalities are permanently installed within the macrocyclic skeleton by forming a persistent catalytic cavity. Following this idea, we have recently constructed a series of bisthiourea macrocycles [28–30]. Thiourea groups were introduced due to their superior anion binding property and potent electrophilic activation ability [31–36]. To incorporate extra functionality, tertiary amine groups can be also embedded as Lewis base sites for realizing electrophilic/nucleophilic cooperative catalysis [37–39]. For this purpose, one kind of tetraamino-bisthiourea chiral macrocycles were synthesized [30]. When applied in catalyzing the decarboxylative addition of phenyl β -ketoacids to cyclic imines bearing sulfamate heading group, an interesting substrate-induced assembly catalysis mode was uncovered [30]. To expand more applications, herein we report a systematic synthesis of tetraamino-bisthiourea chiral macrocycles and their performance in catalyzing the decarboxylative Mannich addition of malonic acid half thioesters (MAHTs) to isatin-derived ketimines. The macrocycle-enabled hydrogen-bonding activation network and the associated confined cavity could resemble the circumstance of the catalytic triad of Polyketide synthases (PKSs) [40–42] (Figure 1). On the other hand, the organocatalytic asymmetric decarboxylative addition reactions of MAHTs to imines provide an efficient means for accessing valuable chiral β -amino esters [43–52].

Results and Discussion

Synthesis of macrocycles

The tetraamino-bisthiourea chiral macrocycles were synthesized by a stepwise strategy (Scheme 1). The easily available chiral diamines including 1,2-cyclohexanediamines and 1,2-diphenylethylenediamines were chosen as the linking components to afford Lewis base sites and also for introduction of chirality. Different alkyl substituents including methyl, *n*-propyl, isopropyl, and 3-pentyl were incorporated in order to tune the size and steric effect of the macrocyclic cavity and thus to enable diverse cavity environments. Among these macrocycles, **M1**, **M5**, **M7**, and **M8** were previously synthesized [30] and the route can be similarly followed for the synthesis of the other macrocycles. To start the synthesis, enantiopure *N,N'*-disubstituted (*S,S*)-1,2-cyclohexanediamines **1a–d** or (*S,S*)-1,2-diphenylethanediamines **1e,f** were firstly reacted with two equiv 3-nitro-5-(trifluoromethyl)benzyl bromide (**2**) in the presence of a base to afford the dinitro compounds **3a–f** in moderate to excellent yields (Scheme 1a). The diminished yield for product **3d** was probably caused by the large steric hindrance of the 3-pentyl substituent. Reduction of the nitro groups by SnCl_2 under acidic conditions gave the bisamine fragments **4a–f** in 83–98% yields. The bisamine fragments were further converted to the bisisothiocyanates **5a–f** by reaction with 1,1'-thiocarbonyldiimidazole in 66–89% yields.

Having the bisamine and bisisothiocyanate fragments in hand, macrocyclic condensations were then pursued. The homo-condensations between the homologous bisamine and bisisothiocyanate fragments were firstly tried (Scheme 1b). In the presence of an organic base, reactions between **4a–f** and **5a–f** went smoothly and afforded the desired macrocycle products **M1–M6** in 35–72% yields. It is worth noting that common dilute conditions for macrocyclization reactions was not required here. Due to the very high efficiency, gram-scale prepa-

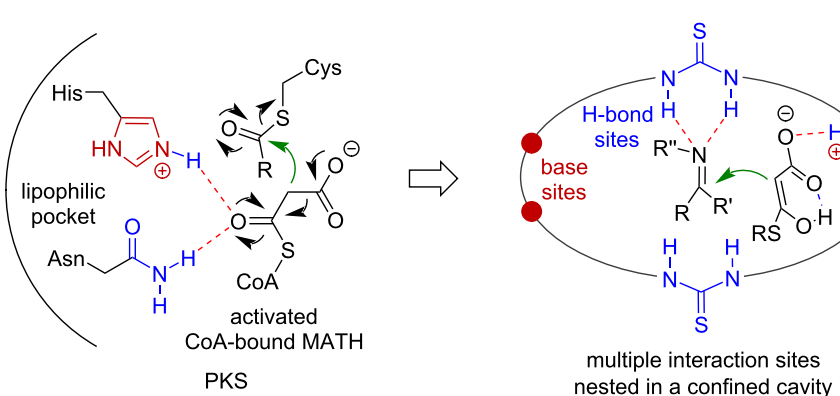
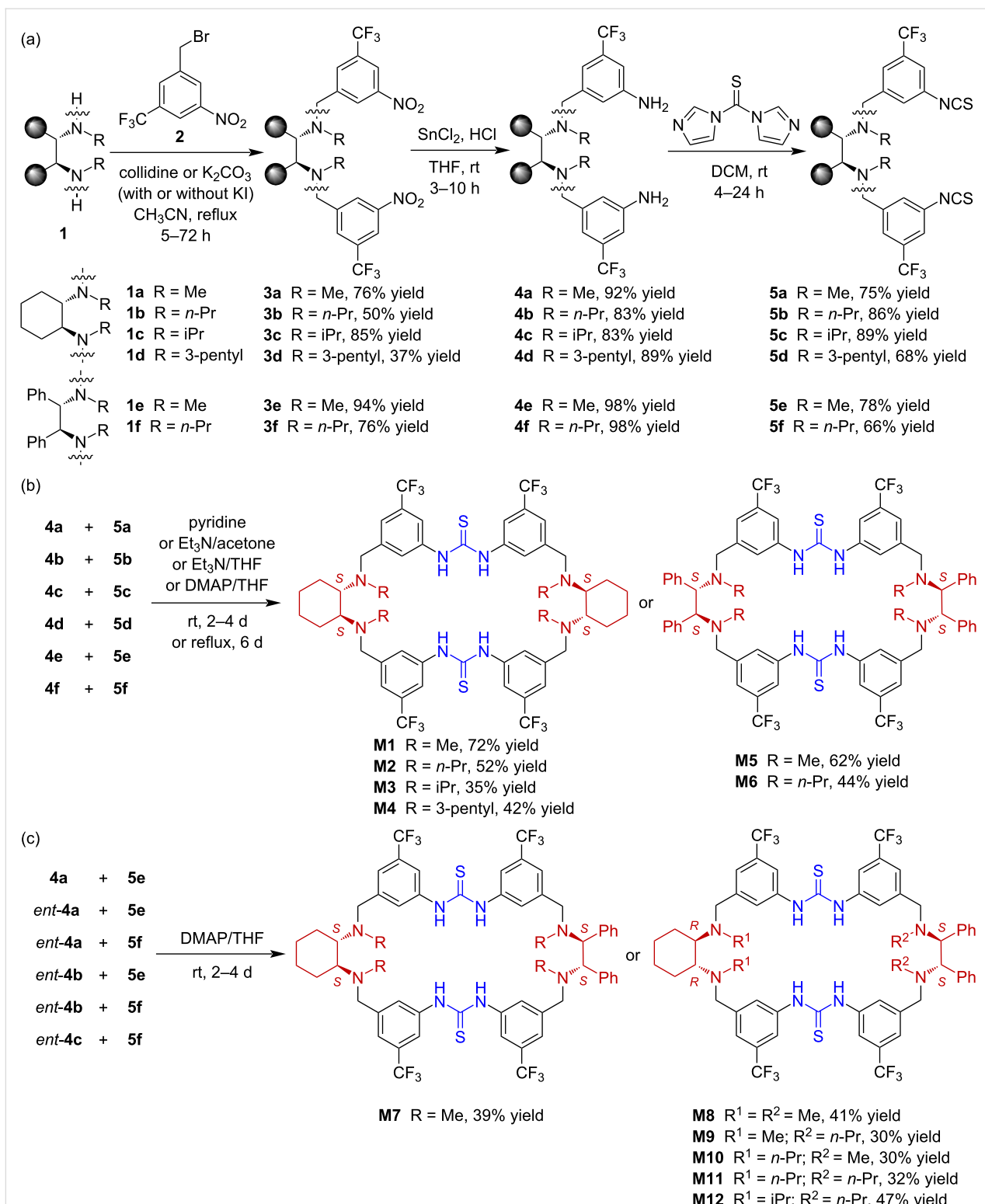


Figure 1: Design of PKS-inspired multifunctional amino-thiourea macrocycle catalysts.



Scheme 1: Synthesis of tetraamino-bisthiourea chiral macrocycles **M1–M12**. The synthesis of **M1**, **M5**, **M7**, and **M8** was previously reported [30].

ration of the chiral macrocycles was readily achieved (see Supporting Information File 1). To enrich the diversity of the macrocyclic scaffolds, hetero-condensations between different

bisamine and bisisothiocyanate fragments, including combination of different chiral configurations, were also investigated (Scheme 1c). Reactions between cyclohexanediamine-derived

bisamine fragments **4a** or the enantiomers *ent*-**4a–c** with diphenylethylenediamine-derived bisisothiocyanate fragments **5e,f** afforded the desired hetero-combination macrocycles **M7–M12** without additional difficulties. It should be noted that the incorporation of CF_3 groups on the aryl moieties was to increase the acidity of thiourea so as to provide better hydrogen-bonding complexation and activation ability.

Catalytic reaction optimization

The synthesized macrocycles were then applied as catalysts in the decarboxylative addition of malonic acid half thioesters (MAHTs) to isatin-derived ketimines [48]. The reaction between ketimine **6a** and MAHT **7a** was initially performed in THF at room temperature with just 2 mol % loading of the chiral macrocycle catalysts (Table 1). All macrocycles were evaluated, and in all cases product **8a** was obtained in moderate yields. Different diamine linking components and different substituents on the tertiary amine sites showed an important influence on the reaction stereoselectivity. The cyclohexanediamine-linking macrocycles **M1–M4** afforded the product with overall higher enantiomeric excess (ee) (Table 1, entries 1–4). Among which the isopropyl-substituted macrocycle **M3** gave the best selectivity, i.e., 42% ee. This suggested a suitable crowding cavity environment may be good for stereocontrol. The diphenylethylenediamine-linking macrocycles **M5** and **M6**, however, gave very low ees (Table 1, entries 5 and 6). The

hetero-macrocycles **M7–M12** did not afford better selectivity as well (Table 1, entries 7–12). It is interesting to note that **M9–M12** led to reversed selectivity, which may imply that the chiral cyclohexanediamine other than diphenylethylenediamine moiety governed the stereoselection process.

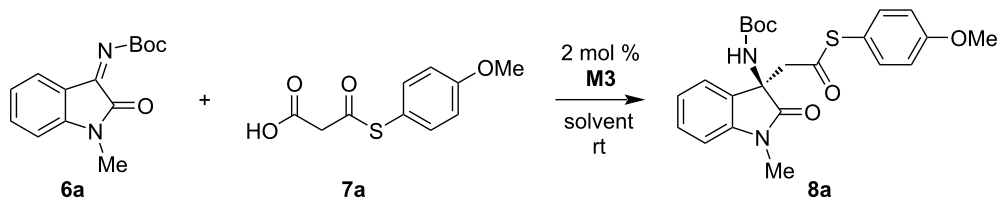
Using **M3** as the optimal catalyst, the reaction solvent was then screened (Table 2). Ethyl ether was found to give a better conversion, but with decreased selectivity (Table 2, entry 2). The reaction in 1,4-dioxane afforded the product with a moderate yield and the best selectivity so far, 62% ee (Table 2, entry 3). To our delight, among the other ether solvents screened (Table 2, entries 4–7), cyclopentyl methyl ether (CPME) gave an excellent conversion (90% yield) and only a slightly diminished selectivity (58% ee). Reactions in other more polar solvents including toluene, ethyl acetate, halohydrocarbons, and acetonitrile gave overall very good conversions, but with very low selectivity except for the reaction in ethyl acetate which afforded the product in 43% ee (Table 2, entries 8–12).

Finally, the other reaction parameters, including catalyst loading, reaction temperature, and concentration were evaluated (Table 3). With CPME as the optimal solvent, increasing the loading of catalyst **M3** from 2 mol % to 5 mol % led to an obviously more rapid conversion and furnished the product in 92% yield in 36 h (Table 3, entries 1 and 2). To our delight, the

Table 1: Evaluation of different macrocycle catalysts^a.

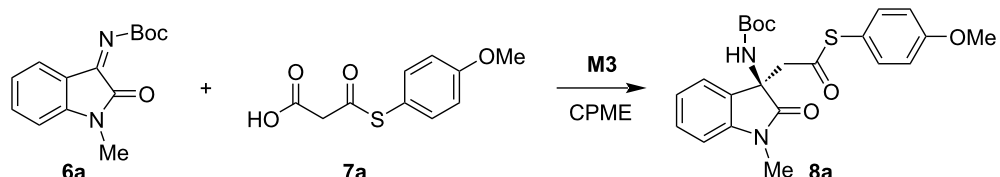
Entry	Cat.	Yield (%) ^b	ee (%) ^c	Reaction scheme:		
				6a	7a	8a
1	M1	32	9			
2	M2	43	11			
3	M3	41	42			
4	M4	49	29			
5	M5	48	4			
6	M6	51	0			
7	M7	45	13			
8	M8	39	9			
9	M9	31	-4			
10	M10	42	-12			
11	M11	31	-12			
12	M12	41	-4			

^aReaction conditions: **6a** (0.2 mmol), **7a** (0.3 mmol), 1 mL of THF; ^bisolated yields after column chromatography; ^cdetermined by HPLC analysis on a chiral stationary phase.

Table 2: Evaluation of solvents^a.

Entry	Solvent	Time (h)	Yield (%) ^b	ee (%) ^c
1	THF	96	41	42
2	Et ₂ O	96	73	34
3	1,4-dioxane	96	52	62
4	TBME	96	79	33
5	CPME	96	90	58
6	DME	96	47	49
7	EVE	96	39	9
8	toluene	36	96	2
9	EA	84	81	43
10	CH ₂ Cl ₂	36	97	0
11	CHCl ₃	36	93	1
12	CH ₃ CN	84	71	12

^aReaction conditions: **6a** (0.2 mmol), **7a** (0.3 mmol), 1 mL of solvent; ^bisolated yields after column chromatography; ^cdetermined by HPLC analysis on a chiral stationary phase. TBME: *tert*-butyl methyl ether; CPME: cyclopentyl methyl ether; DME: 1,2-dimethoxyethane; EVE: ethyl vinyl ether; EA: ethyl acetate.

Table 3: Evaluation of catalyst loading, reaction temperature, and concentration^a.

Entry	Cat. (mol %)	Temp.	Conc. [M] ^b	Time (h)	Yield (%) ^c	ee (%) ^d
1	M3 (2)	rt	0.2	96	90	58
2	M3 (5)	rt	0.2	36	92	71
3	M3 (10)	rt	0.2	24	72	72
4 ^e	M3 (5)	rt	0.2	24	82	72
5 ^f	M3 (5)	rt	0.2	48	94	60
6	M3 (5)	0 °C	0.2	120	65	63
7	M3 (5)	40 °C	0.2	12	75	64
8	M3 (5)	rt	0.4	24	92	56
9	M3 (5)	rt	0.1	44	88	72
10	M3 (5)	rt	0.05	48	54	59

^aReaction conditions: **6a** (0.2 mmol) and **7a** (0.3 mmol, 1.5 equiv) in CPME (cyclopentyl methyl ether) except otherwise noted; ^bconcentration of **6a**; ^cisolated yields after column chromatography; ^ddetermined by HPLC analysis on a chiral stationary phase; ^e1.0 equiv **7a** used; ^f2.0 equiv **7a** used.

selectivity was also increased to 71% ee. However, further increasing the macrocycle loading to 10 mol % led to a diminished yield and nearly unchanged selectivity (Table 3, entry 3). The decreased yield for the addition product was due to the

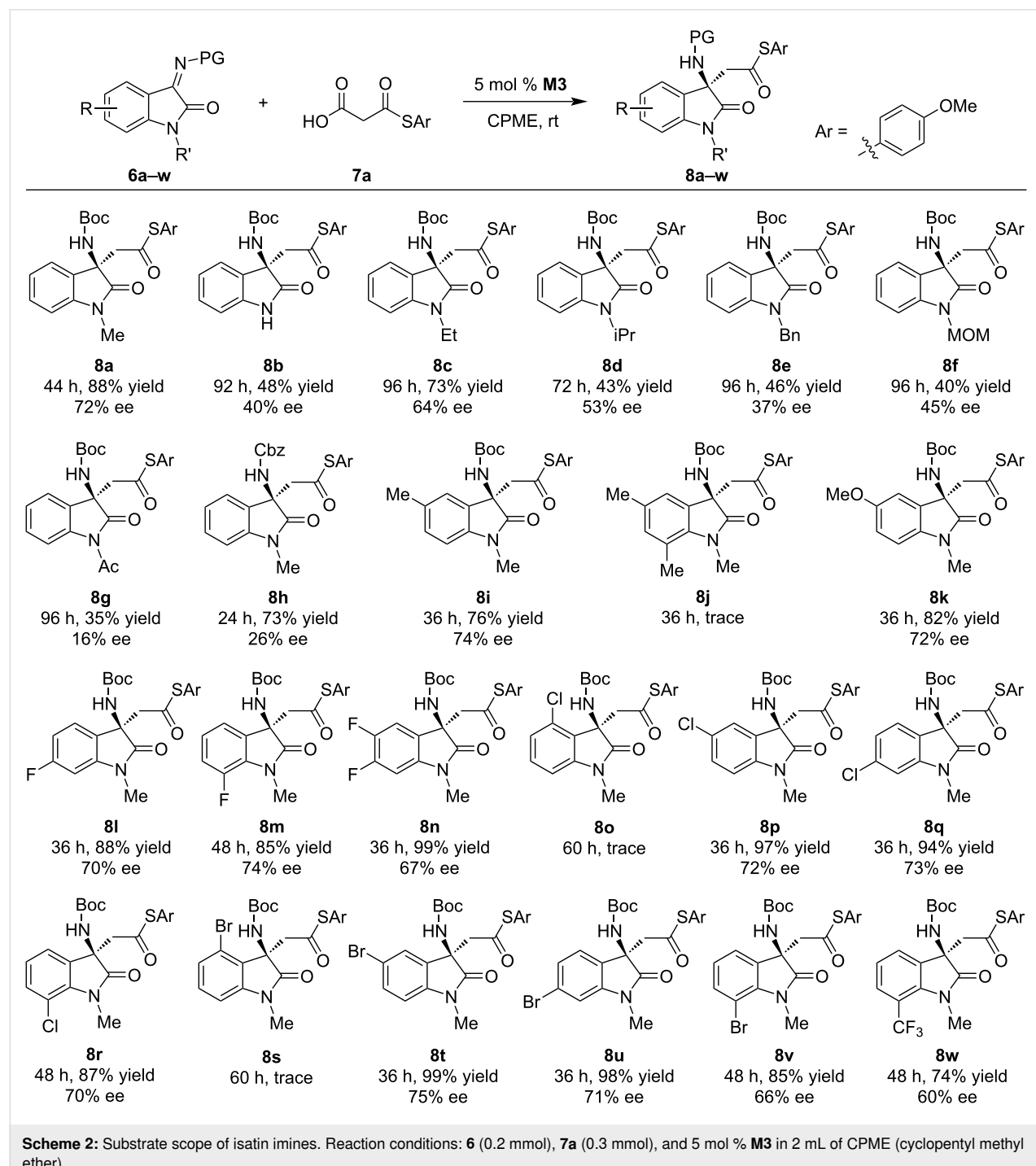
competitive decarboxylation of the sole MAHT substrate in the presence of a higher loading of the macrocycle containing tertiary amine basic sites. Decreasing the amount of MAHT substrate from 1.5 equiv to 1.0 equiv or increasing to 2.0 equiv

did not give better outcome (Table 3, entries 4 and 5). Performing the reaction at 0 °C led to a very slow conversion, while at 40 °C the reaction became much faster but gave a diminished yield due to the competitive decarboxylation side reaction (Table 3, entries 6 and 7). In both cases, the enantioselectivity did not turn out to be better. A suitable reaction concentration (0.1–0.2 M) was found to be important. A very high or low reaction concentration led to decreased stereoselectivity

probably due to the existence of catalyst aggregation or background reactions (Table 3, entries 8–10).

Substrate scope

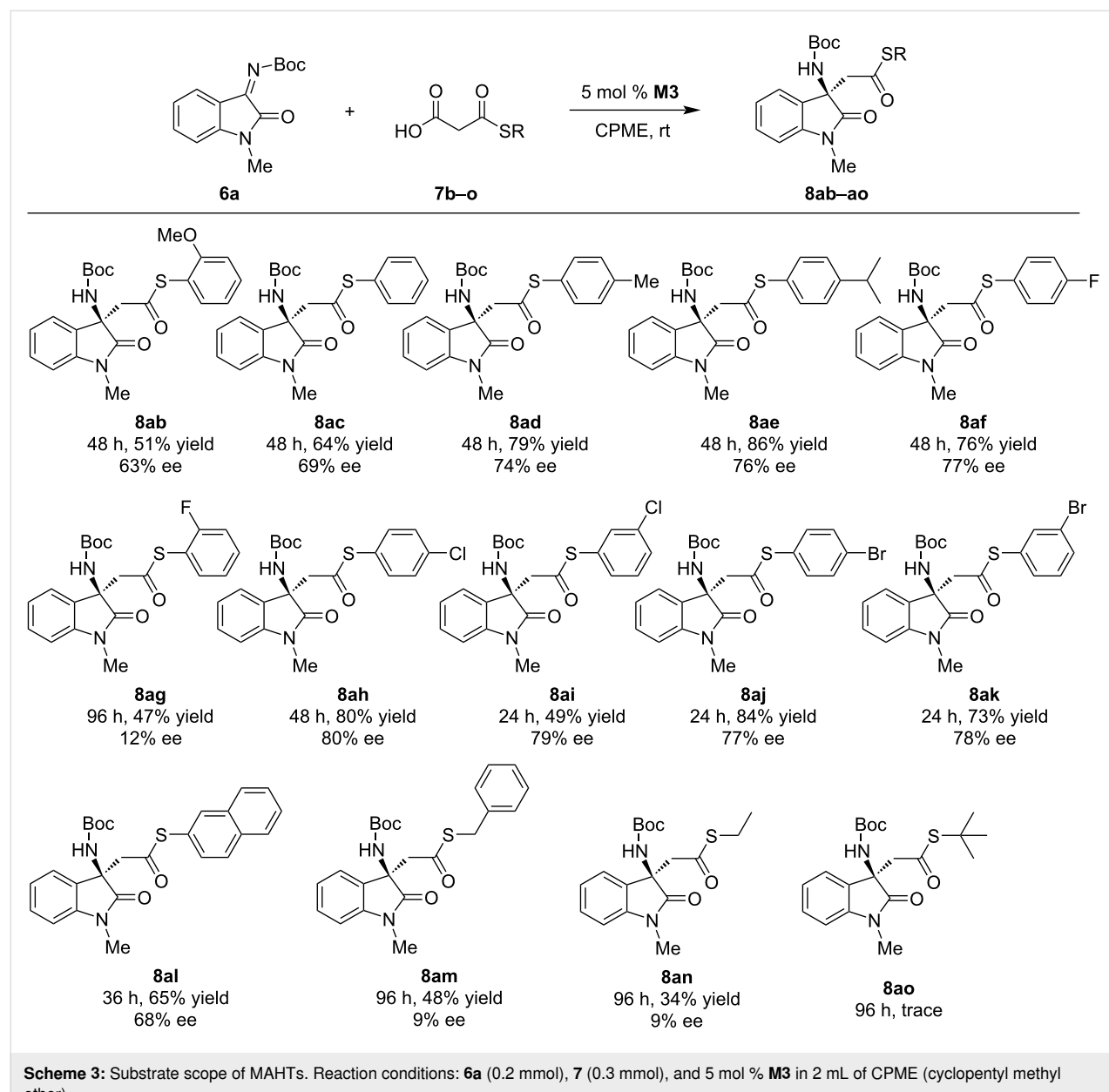
Having established the optimal reaction conditions, the substrate scope was explored. Reactions of various isatin imines **6a–w** with MAHT **7a** were firstly investigated (Scheme 2). Different *N*-substituents on isatins caused a significant effect. For



non-substituted (**6b**) or other substrates with larger substituents (**6c–g**), the corresponding products **8b–g** were obtained in only moderate yields with decreased selectivity. Replacing the Boc-protecting group on the imine site by a Cbz group led to a largely decreased selectivity (**8h**). For a series of substrates with various substituents on the 5, 6, or 7-position, including 5-methyl (**8i**), 5-methoxy (**8k**), 6- or 7-fluoro (**8l,m**), 5,6-difluoro (**8n**), 5-, 6- or 7-chloro (**8p–r**), 5-, 6-, or 7-bromo (**8t–v**), and 7-trifluoromethyl (**8w**), all reactions completed within 36–48 h and afforded the products in good to excellent yields with 60–75% ee. In contrast, the reaction was disrupted by 4-substitution, and only trace conversion was observed for the 4-chloro or 4-bromo-substituted substrate (**8o,s**). This was

probably caused by a steric effect as the 4-substituent is close to the imine reactive site and accordingly blocked it toward activation and nucleophilic attack. Interestingly, for the 5,7-dimethyl-substituted substrate, only trace conversion was observed as well (**8j**). This may be due to that the substrate was too bulky to fit within the macrocycle cavity.

For MAHT substrates, various *p*- or *m*-substituents on the S-phenyl moiety caused negligible effects, and all the products were obtained in moderate to good yields with 69–80% ee (Scheme 3). For *o*-substitution, especially for the *o*-fluorosubstituent (**8ag**), however, only a moderate yield and low selectivity (12% ee) were obtained. For the S-naphthyl sub-



Scheme 3: Substrate scope of MAHTs. Reaction conditions: **6a** (0.2 mmol), **7** (0.3 mmol), and 5 mol % **M3** in 2 mL of CPME (cyclopentyl methyl ether).

strate, the reaction went smoothly as well and afforded the product in 65% yield with 68% ee (**8al**). The reactions for S-benzyl and S-ethyl substrates became sluggish and afforded the products in 34–48% yields in 96 h with very low selectivity (**8am** and **8an**). For the S-*tert*-butyl substrate, only trace conversion was observed.

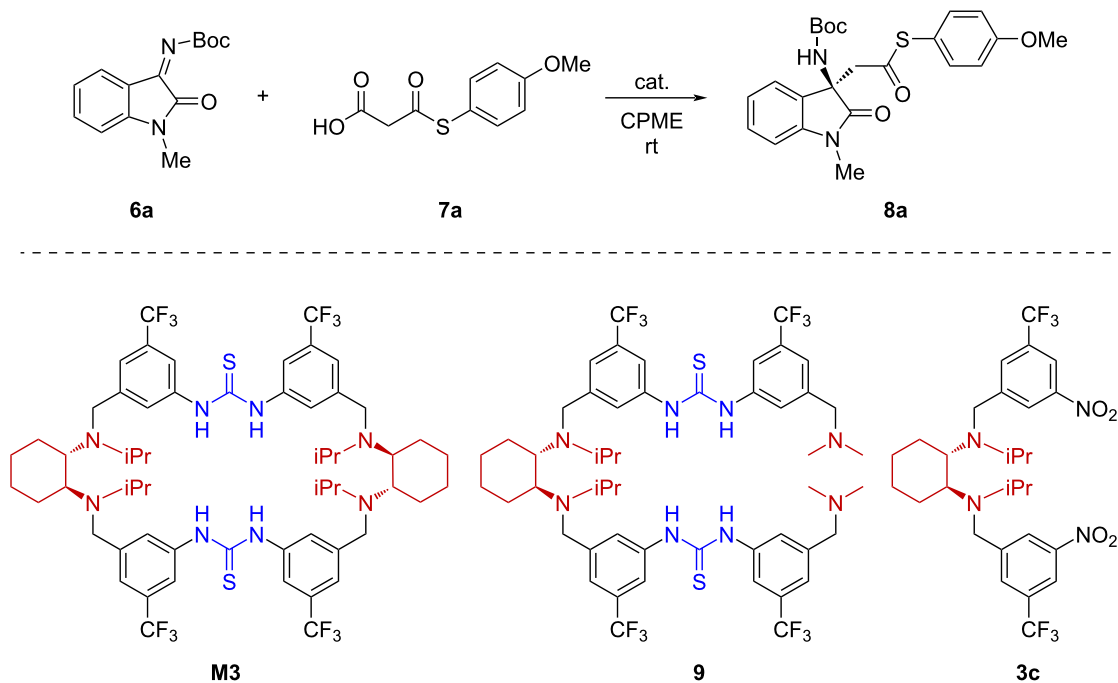
Macrocyclic effect and catalytic mechanism

The above results showed that the tetraamino-bisthiourea chiral macrocycles can efficiently catalyze the decarboxylative addition reactions with good yields and enantioselectivity. To check the role of the macrocyclic framework, two acyclic compounds (**9** and **3c**) containing the similar structural motifs as the macrocycle catalyst were applied as catalysts in the reaction (Table 4). In compound **9**, all the structural units of the macrocycle **M3**, including the two diarylthioureas and the four tertiary amine sites, were maximally maintained, except for one of the cyclohexanediamine units which was replaced by two dimethylamino groups to cut off the macrocyclic skeleton (for synthesis, see Supporting Information File 1). The compound **3c** contains

one cyclohexanediamine unit but no thiourea moieties. As shown in Table 4, macrocycle **M3** catalyzed the reaction of **6a** and **7a** to afford **8a** in 88% yield with 72% ee. Under the same conditions, compound **9** also efficiently catalyzed the reaction and promoted an excellent conversion, however, it furnished the product in nearly racemic form. This suggested that the macrocyclic framework is essential in enabling a defined chiral environment for efficient stereocontrol. On the other hand, compound **3c** led to a much slower conversion and also nearly racemic product formation, indicating that the thiourea units must have engaged in activation and being cooperative with the tertiary amine sites.

With the reaction outcomes and pronounced macrocyclic effect observed, a plausible catalytic mechanism is represented in Figure 2. The MAHT substrate is deprotonated by one of the tertiary amine sites, and the formed enolate intermediate can be stabilized by hydrogen bonding-mediated ion-pair interaction within the macrocyclic cavity. The imine substrate is activated by one or both of the two thiourea sites through hydrogen bond-

Table 4: Evaluation of macrocyclic effect^a.



Entry	Cat.	Time (h)	Yield (%) ^b	ee (%) ^c
1	M3 (5 mol %)	44	88	72
2	9 (5 mol %)	44	92	3
3	3c (10 mol %)	72	47	-2

^aReaction conditions: **6a** (0.2 mmol), **7a** (0.3 mmol), 2 mL of CPME (cyclopentyl methyl ether), room temperature; ^bisolated yields after column chromatography; ^cdetermined by HPLC analysis on a chiral stationary phase.

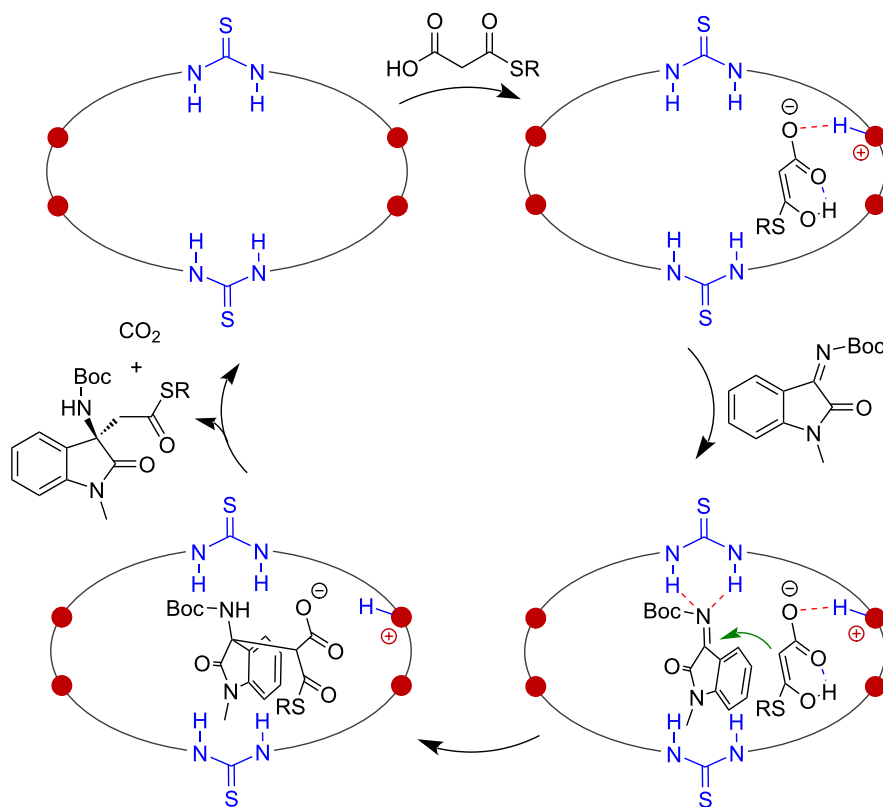


Figure 2: Proposed catalytic mechanism.

ing to accept the enolate attack. The chiral environment provided by the *(S,S)*-cyclohexanediamine part governed the face-selective attack and led to the *R*-configured product. In the last step, the decarboxylation leads to the enolate of the thioester, which is more basic than the MAHT-enolate and can thus be protonated by the ammonium fragment in the macrocycle. This leads to the neutral product, which can easily escape from the macrocyclic cavity, releasing the macrocycle catalyst to enter the next catalytic cycle. As suggested by the above control experiments, the rigid macrocyclic framework is crucial in organizing the multiple functional sites for cooperative binding and activation.

Conclusion

In conclusion, a series of multifunctional tetraamino-bisthiourea chiral macrocycles were efficiently synthesized. By using a modular fragment-coupling approach, different chiral diamine units, including the homo- and hetero-combination, can be easily incorporated. This provides a very rich structural diversity of the macrocycles and allows for fine tuning of the chiral cavity environments. With the short and high-yielding synthesis, gram-scale of macrocycle products can be readily obtained. This kind of macrocycles can efficiently catalyze the decarboxylative addition of malonic acid half thioesters to isatin-derived

ketimines, affording a series of chiral β -amino ester products in excellent yields and good enantioselectivity. In contrast, reactions catalyzed by acyclic analogues containing very similar structural units were non-selective, suggesting the essential role of the rigid macrocyclic framework in realizing efficient stereocontrol. With the easy synthesis, rich structural diversity, cooperative binding and activation sites, we believe this type of biomimetic chiral macrocycles will find more applications as catalysts in other reactions.

Supporting Information

Supporting Information File 1

Experimental procedures, characterization data, copies of ^1H and ^{13}C NMR spectra.

[<https://www.beilstein-journals.org/bjoc/content/supplementary/1860-5397-18-51-S1.pdf>]

Funding

This work was financially supported by National Key R&D Program of China (2021YFA1501600) and National Natural Science Foundation of China (22022112, 21871276).

ORCID® iDs

Yu-Fei Ao - <https://orcid.org/0000-0002-9415-2181>
 Qi-Qiang Wang - <https://orcid.org/0000-0001-5988-1293>

References

- van Leeuwen, P. W. N. M., Ed. *Supramolecular Catalysis*; Wiley-VCH: Weinheim, Germany, 2008. doi:10.1002/9783527621781
- Yoshizawa, M.; Klosterman, J. K.; Fujita, M. *Angew. Chem., Int. Ed.* **2009**, *48*, 3418–3438. doi:10.1002/anie.200805340
- Meeuwissen, J.; Reek, J. N. H. *Nat. Chem.* **2010**, *2*, 615–621. doi:10.1038/nchem.744
- Dong, Z.; Luo, Q.; Liu, J. *Chem. Soc. Rev.* **2012**, *41*, 7890–7908. doi:10.1039/c2cs35207a
- Raynal, M.; Ballester, P.; Vidal-Ferran, A.; van Leeuwen, P. W. N. M. *Chem. Soc. Rev.* **2014**, *43*, 1660–1733. doi:10.1039/c3cs60027k
- Raynal, M.; Ballester, P.; Vidal-Ferran, A.; van Leeuwen, P. W. N. M. *Chem. Soc. Rev.* **2014**, *43*, 1734–1787. doi:10.1039/c3cs60037h
- Dydio, P.; Reek, J. N. H. *Chem. Sci.* **2014**, *5*, 2135–2145. doi:10.1039/c3sc53505c
- Leenders, S. H. A. M.; Gramage-Doria, R.; de Bruin, B.; Reek, J. N. H. *Chem. Soc. Rev.* **2015**, *44*, 433–448. doi:10.1039/c4cs00192c
- Brown, C. J.; Toste, F. D.; Bergman, R. G.; Raymond, K. N. *Chem. Rev.* **2015**, *115*, 3012–3035. doi:10.1021/cr4001226
- Blanco, V.; Leigh, D. A.; Marcos, V. *Chem. Soc. Rev.* **2015**, *44*, 5341–5370. doi:10.1039/c5cs00096c
- Vaquero, M.; Rovira, L.; Vidal-Ferran, A. *Chem. Commun.* **2016**, *52*, 11038–11051. doi:10.1039/c6cc04474c
- Davis, H. J.; Phipps, R. J. *Chem. Sci.* **2017**, *8*, 864–877. doi:10.1039/c6sc04157d
- Jiang, J.; Ouyang, G.; Zhang, L.; Liu, M. *Chem. – Eur. J.* **2017**, *23*, 9439–9450. doi:10.1002/chem.201700727
- Wang, K.; Jordan, J. H.; Hu, X.-Y.; Wang, L. *Angew. Chem., Int. Ed.* **2020**, *59*, 13712–13721. doi:10.1002/anie.202000045
- Wang, Q.-Q. *Supramolecular Catalysis Using Organic Macrocycles*. In *Handbook of Macrocyclic Supramolecular Assembly*; Liu, Y.; Chen, Y.; Zhang, H.-Y., Eds.; Springer: Singapore, 2019. doi:10.1007/978-981-13-1744-6_36-1
- Kauerhof, D.; Niemeyer, J. *ChemPlusChem* **2020**, *85*, 889–899. doi:10.1002/cplu.202000152
- Breslow, R.; Dong, S. D. *Chem. Rev.* **1998**, *98*, 1997–2012. doi:10.1021/cr970011j
- Takahashi, K. *Chem. Rev.* **1998**, *98*, 2013–2034. doi:10.1021/cr9700235
- Engeldinger, E.; Arnsbach, D.; Matt, D. *Chem. Rev.* **2003**, *103*, 4147–4174. doi:10.1021/cr030670y
- Homden, D. M.; Redshaw, C. *Chem. Rev.* **2008**, *108*, 5086–5130. doi:10.1021/cr8002196
- Le Poul, N.; Le Mest, Y.; Jabin, I.; Reinaud, O. *Acc. Chem. Res.* **2015**, *48*, 2097–2106. doi:10.1021/acs.accounts.5b00152
- Salvio, R.; Cacciapaglia, R.; Casnati, A. *Calixarenes as Supramolecular Catalysts Endowed with Esterase and Phosphodiesterase Activity*. In *Calixarenes and Beyond*; Neri, P.; Sessler, J. L.; Wang, M.-X., Eds.; Springer International Publishing: Cham, Switzerland, 2016; pp 691–717. doi:10.1007/978-3-319-31867-7_26
- Yilmaz, M.; Sayin, S. *Calixarenes in Organo and Biomimetic Catalysis*. In *Calixarenes and Beyond*; Neri, P.; Sessler, J. L.; Wang, M.-X., Eds.; Springer International Publishing: Cham, Switzerland, 2016; pp 719–742. doi:10.1007/978-3-319-31867-7_27
- Pemberton, B. C.; Raghunathan, R.; Volla, S.; Sivaguru, J. *Chem. – Eur. J.* **2012**, *18*, 12178–12190. doi:10.1002/chem.201202083
- Assaf, K. I.; Nau, W. M. *Chem. Soc. Rev.* **2015**, *44*, 394–418. doi:10.1039/c4cs00273c
- Hooley, R. J.; Rebek, J., Jr. *Chem. Biol.* **2009**, *16*, 255–264. doi:10.1016/j.chembiol.2008.09.015
- Yu, Y.; Rebek, J., Jr. *Acc. Chem. Res.* **2018**, *51*, 3031–3040. doi:10.1021/acs.accounts.8b00269
- Ning, R.; Ao, Y.-F.; Wang, D.-X.; Wang, Q.-Q. *Chem. – Eur. J.* **2018**, *24*, 4268–4272. doi:10.1002/chem.201800326
- Ning, R.; Zhou, H.; Nie, S.-X.; Ao, Y.-F.; Wang, D.-X.; Wang, Q.-Q. *Angew. Chem., Int. Ed.* **2020**, *59*, 10894–10898. doi:10.1002/anie.202003673
- Guo, H.; Zhang, L.-W.; Zhou, H.; Meng, W.; Ao, Y.-F.; Wang, D.-X.; Wang, Q.-Q. *Angew. Chem., Int. Ed.* **2020**, *59*, 2623–2627. doi:10.1002/anie.201910399
- Li, A.-F.; Wang, J.-H.; Wang, F.; Jiang, Y.-B. *Chem. Soc. Rev.* **2010**, *39*, 3729–3745. doi:10.1039/b926160p
- Amendola, V.; Fabbrizzi, L.; Mosca, L. *Chem. Soc. Rev.* **2010**, *39*, 3889–3915. doi:10.1039/b822552b
- Wittkopp, A.; Schreiner, P. R. *Chem. – Eur. J.* **2003**, *9*, 407–414. doi:10.1002/chem.200390042
- Schreiner, P. R. *Chem. Soc. Rev.* **2003**, *32*, 289–296. doi:10.1039/b107298f
- Zhang, Z.; Schreiner, P. R. *Chem. Soc. Rev.* **2009**, *38*, 1187–1198. doi:10.1039/b801793j
- Park, Y.; Harper, K. C.; Kuhl, N.; Kwan, E. E.; Liu, R. Y.; Jacobsen, E. N. *Science* **2017**, *355*, 162–166. doi:10.1126/science.aa1875
- Takemoto, Y. *Org. Biomol. Chem.* **2005**, *3*, 4299–4306. doi:10.1039/b511216h
- Connon, S. J. *Chem. Commun.* **2008**, 2499–2510. doi:10.1039/b719249e
- Fang, X.; Wang, C.-J. *Chem. Commun.* **2015**, *51*, 1185–1197. doi:10.1039/c4cc07909d
- Jez, J. M.; Austin, M. B.; Ferrer, J.-L.; Bowman, M. E.; Schröder, J.; Noel, J. P. *Chem. Biol.* **2000**, *7*, 919–930. doi:10.1016/s1074-5521(00)00041-7
- Austin, M. B.; Izumikawa, M.; Bowman, M. E.; Udwary, D. W.; Ferrer, J.-L.; Moore, B. S.; Noel, J. P. *J. Biol. Chem.* **2004**, *279*, 45162–45174. doi:10.1074/jbc.m406567200
- Zhang, Y.-M.; Hurlbert, J.; White, S. W.; Rock, C. O. *J. Biol. Chem.* **2006**, *281*, 17390–17399. doi:10.1074/jbc.m513199200
- Pan, Y.; Tan, C.-H. *Synthesis* **2011**, 2044–2053. doi:10.1055/s-0030-1260607
- Wang, Z.-L. *Adv. Synth. Catal.* **2013**, *355*, 2745–2755. doi:10.1002/adsc.201300375
- Nakamura, S. *Org. Biomol. Chem.* **2014**, *12*, 394–405. doi:10.1039/c3ob42161a
- Ricci, A.; Pettersen, D.; Bernardi, L.; Fini, F.; Fochi, M.; Herrera, R. P.; Sgarzani, V. *Adv. Synth. Catal.* **2007**, *349*, 1037–1040. doi:10.1002/adsc.200600536
- Pan, Y.; Kee, C. W.; Jiang, Z.; Ma, T.; Zhao, Y.; Yang, Y.; Xue, H.; Tan, C.-H. *Chem. – Eur. J.* **2011**, *17*, 8363–8370. doi:10.1002/chem.201100687
- Hara, N.; Nakamura, S.; Sano, M.; Tamura, R.; Funahashi, Y.; Shibata, N. *Chem. – Eur. J.* **2012**, *18*, 9276–9280. doi:10.1002/chem.201200367
- Yuan, H.-N.; Li, S.; Nie, J.; Zheng, Y.; Ma, J.-A. *Chem. – Eur. J.* **2013**, *19*, 15856–15860. doi:10.1002/chem.201303307

50. Bahlinger, A.; Fritz, S. P.; Wennemers, H. *Angew. Chem., Int. Ed.* **2014**, *53*, 8779–8783. doi:10.1002/anie.201310532
51. Nakamura, S.; Sano, M.; Toda, A.; Nakane, D.; Masuda, H. *Chem. – Eur. J.* **2015**, *21*, 3929–3932. doi:10.1002/chem.201406270
52. Kaur, J.; Kumari, A.; Bhardwaj, V. K.; Chimni, S. S. *Adv. Synth. Catal.* **2017**, *359*, 1725–1734. doi:10.1002/adsc.201700011

License and Terms

This is an open access article licensed under the terms of the Beilstein-Institut Open Access License Agreement (<https://www.beilstein-journals.org/bjoc/terms>), which is identical to the Creative Commons Attribution 4.0 International License (<https://creativecommons.org/licenses/by/4.0>). The reuse of material under this license requires that the author(s), source and license are credited. Third-party material in this article could be subject to other licenses (typically indicated in the credit line), and in this case, users are required to obtain permission from the license holder to reuse the material.

The definitive version of this article is the electronic one which can be found at:

<https://doi.org/10.3762/bjoc.18.51>



BINOL as a chiral element in mechanically interlocked molecules

Matthias Krajnc and Jochen Niemeyer*

Review

Open Access

Address:

Faculty of Chemistry (Organic Chemistry) and Centre of Nanointegration Duisburg-Essen (CENIDE), University of Duisburg-Essen, Universitätsstr. 7, 45141 Essen, Germany

Email:

Jochen.Niemeyer* - jochen.niemeyer@uni-due.de

* Corresponding author

Keywords:

axial chirality; BINOL; catenanes; interlocked molecules; rotaxanes

Beilstein J. Org. Chem. **2022**, *18*, 508–523.

<https://doi.org/10.3762/bjoc.18.53>

Received: 08 March 2022

Accepted: 22 April 2022

Published: 06 May 2022

This article is part of the thematic issue "Supramolecular approaches to mediate chemical reactivity".

Guest Editor: C. Gaeta

© 2022 Krajnc and Niemeyer; licensee Beilstein-Institut.

License and terms: see end of document.

Abstract

In this minireview we present the use of the axially chiral 1,1'-binaphthyl-2,2'-diol (BINOL) unit as a stereogenic element in mechanically interlocked molecules (MIMs). We describe the synthesis and properties of such BINOL-based chiral MIMs, together with their use in further diastereoselective modifications, their application in asymmetric catalysis, and their use in stereoselective chemosensing. Given the growing importance of mechanically interlocked molecules and the key advantages of the privileged chiral BINOL backbone, we believe that this research area will continue to grow and deliver many useful applications in the future.

Introduction

In the last decades the synthesis and application of mechanically interlocked molecules (MIMs), such as catenanes and rotaxanes, has gained more and more attention [1–4]. MIMs offer conceptually new possibilities through their unique structure, with applications as molecular switches, muscles, and motors [5–11], as novel materials [12], as medically active compounds [13,14], as catalysts [15–19], as chemosensors [20–24], and many more [25]. In view of their template-based synthesis and the importance of noncovalent interactions between the subcomponents, MIMs have established them-

selves as an important subdiscipline of supramolecular chemistry.

The introduction of chirality into MIMs is of high interest in order to develop applications in which the chirality can be exploited, e.g., in enantioselective chemosensing or in asymmetric catalysis. The selection of suitable stereogenic elements is of great importance [26–28]. The most straightforward way to create a chiral rotaxane or catenane is the introduction of classical chiral elements, such molecular parts with axial chirality,

point chirality, or planar chirality into at least one of the subcomponents.

One of the most important chiral molecular frameworks in general is the 1,1'-binaphthyl-2,2'-diol unit (BINOL, see Figure 1).

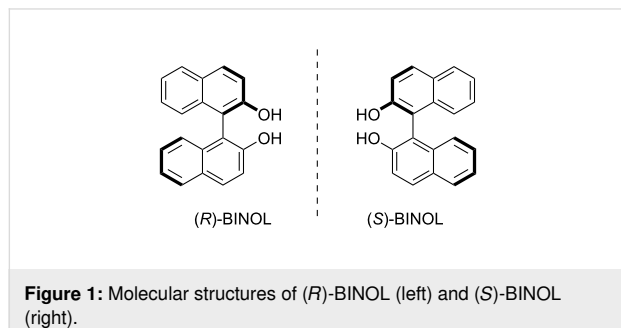


Figure 1: Molecular structures of (R)-BINOL (left) and (S)-BINOL (right).

BINOL is an axially chiral molecule with a high configurational stability and a well-established synthetic chemistry towards a large variety of substituted BINOL derivatives [29]. Another big advantage is the commercial availability of both (R)- and (S)-BINOL in enantiomerically pure forms. BINOL and its derivatives have served as a chiral backbone for numerous stereoselective applications, most importantly (but not limited to) metal- and organocatalysis [30] and stereoselective chemosensing [31,32].

By introduction of an axially chiral BINOL unit into a MIM, it is possible to combine the unique applicability of the chiral BINOL unit with the special possibilities offered by interlocked molecules. In this minireview, we will first present synthetic strategies that can be used to introduce BINOL units into MIMs, based on earlier examples from this research field (section 1). Then, an overview of more recent BINOL-containing MIMs is discussed in detail, including their syntheses and applications (section 2). This topic is divided into three subcategories, namely (mechano)intramolecular chirality transfer (section 2.1), stereoselective catalysis (section 2.2), and stereoselective sensing (section 2.3). Finally, we give a short conclusion about BINOL as a chiral element in interlocked molecules.

Review

1 Incorporating BINOL into MIMs

The introduction of axially chiral BINOL units into interlocked compounds can be achieved by different types of supramolecular template strategies that have been developed for MIM synthesis in the past decades, including passive metal templates [33,34], active metal templates [35–38], anion templates [39,40], ammonium crown ether templates [41], and templates based on π – π interactions [42].

In 2004, Sauvage and co-workers have used a Cu(I)-based passive metal template approach to synthesize a [2]catenane containing an optically pure BINOL unit in each macrocycle [43]. The template complex (S)-3 was assembled by mixing the macrocycle (S)-1 (containing both a phenanthroline ligand and a BINOL unit) with [Cu(CH₃CN)₄]PF₆ and the acyclic phenanthroline precursor 2. Then, the BINOL-based diiodide (S)-4 and Cs₂CO₃ were added successively over 18 hours. This resulted in the formation of the desired chiral homocircuit [2]catenane (S,S)-5 in 21% yield. By treating (S,S)-5 with a large excess of aqueous KCN, demetalation occurred to give the corresponding [2]catenane (S,S)-6.

Interestingly, the Cu-containing catenane (S,S)-5 shows a strong CD signal at wavelengths characteristic for the diphenylphenanthroline units (281 and 337 nm). This indicates a chiral coordination geometry around the Cu ion, most probably brought about by a non-perpendicular orientation of the phenanthrolines. Thus, the axially chiral BINOL units induce a chiral, helical geometry for the Cu complex. Accordingly, demetalation leads to an almost complete disappearance of the CD signals in this area (see Figure 2).

Saito and coworkers demonstrated that the homochiral [2]rotaxane (R)-10 can be efficiently synthesized using an active metal template approach [44,45]. The macrocyclic phenanthroline (R)-7 was treated with copper iodide to obtain the phenanthroline–Cu(I) complex (R)-8. A Glaser-type coupling with the terminal alkynes 9, followed by demetalation, proceeds smoothly in 78% yield. This furnishes the desired chiral rotaxane (R)-10, consisting of a BINOL-based macrocycle and a diyne thread. The CD spectrum of (R)-10 shows intense signals at 321 and 344 nm, which were assigned to the diyne thread located inside the chiral environment of the BINOL-based macrocycle (see Figure 3).

An example of a metal-free template approach for the synthesis of a BINOL-based [2]rotaxane was reported by Stoddart and co-workers [46]. They reacted the amine axle 11 with the axially chiral macrocycle (rac)-12 in a mixture of dichloromethane and trifluoroacetic acid in order to generate the pseudorotaxane (rac)-13. Then, an isocyanate stopper was added for the formation of the [2]rotaxane (rac)-14 in a yield of 42%. The X-ray analysis revealed the presence of the expected [N–H···O] hydrogen bonds between the secondary ammonium station and the crown-ether macrocycle, but also additional [C–H···O] hydrogen bonds involving the benzylammonium methylene groups (see Figure 4). Interestingly, the presence of the directional thread also leads to a desymmetrization of the BINOL-based macrocycle (loss of *C*₂ symmetry), as seen by ¹³C NMR spectroscopy.

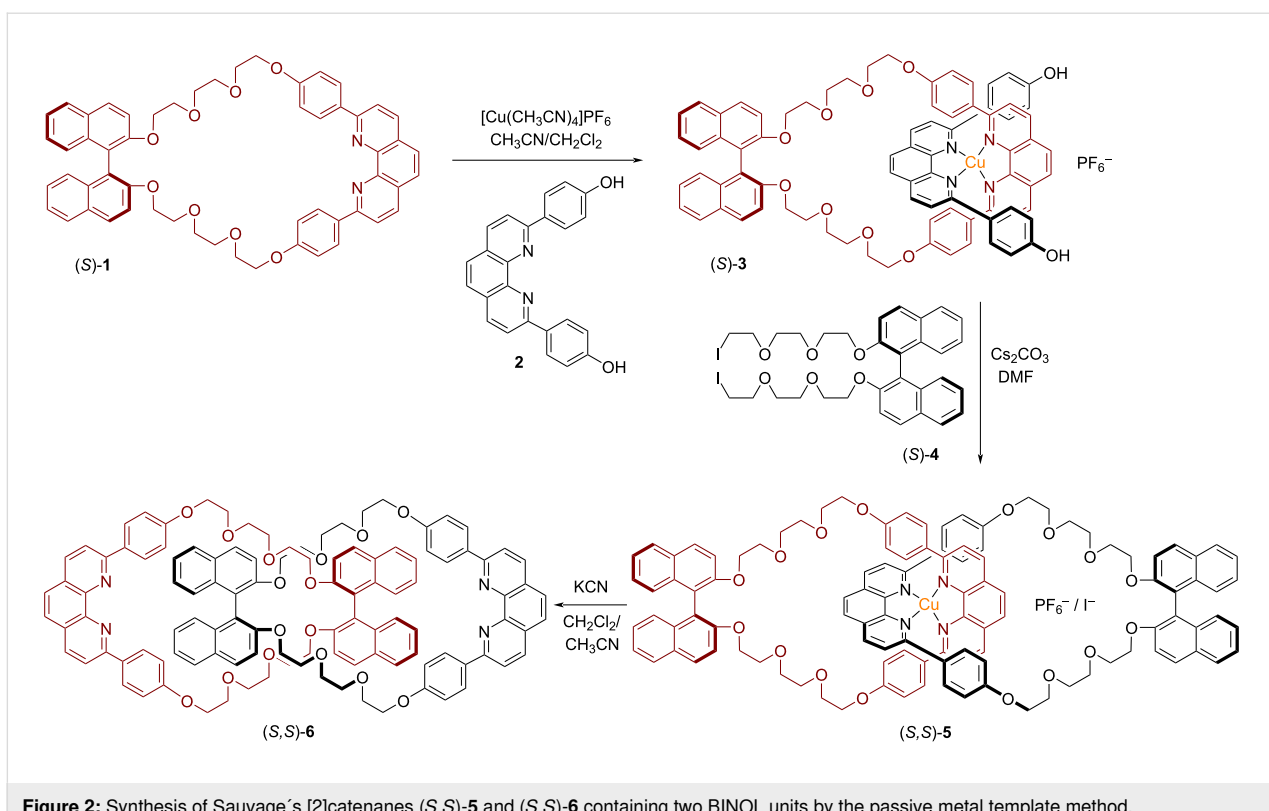


Figure 2: Synthesis of Sauvage's [2]catenanes (S,S)-5 and (S,S)-6 containing two BINOL units by the passive metal template method.

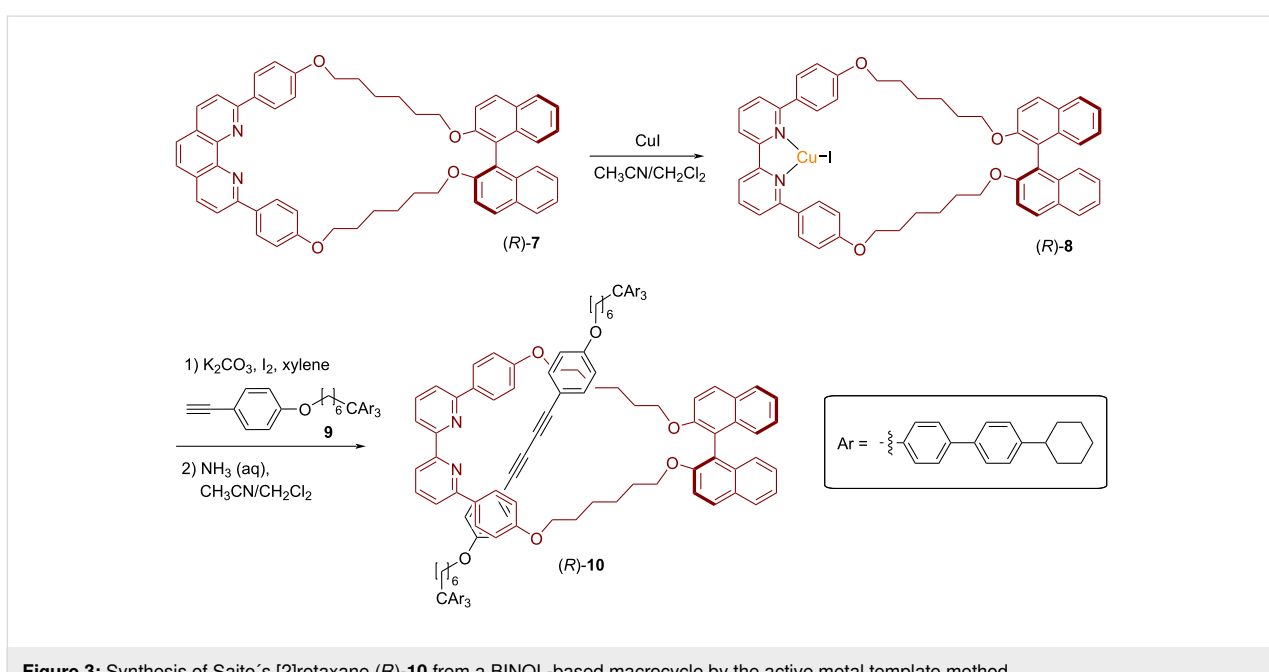


Figure 3: Synthesis of Saito's [2]rotaxane (R)-10 from a BINOL-based macrocycle by the active metal template method.

Stoddart and co-workers also used their $\pi-\pi$ -recognition approach for the synthesis of BINOL-containing cationic catenanes [47,48]. They employed BINOL-based macrocycles containing electron-rich hydroquinone or 1,5-dioxynaphthalene units (macrocycles **15/21/23**), together with suitable dicationic

bis-bipyridinium precursors (**16/19**). Self-assembly of the corresponding pseudorotaxanes by $\pi-\pi$ stacking, following by capping with dibromo-*p*-xylene **17** gave rise to a series of chiral catenanes (**18/20/22/24**). Firstly, the synthetic approach was validated by using a racemic mixture of the BINOL-based

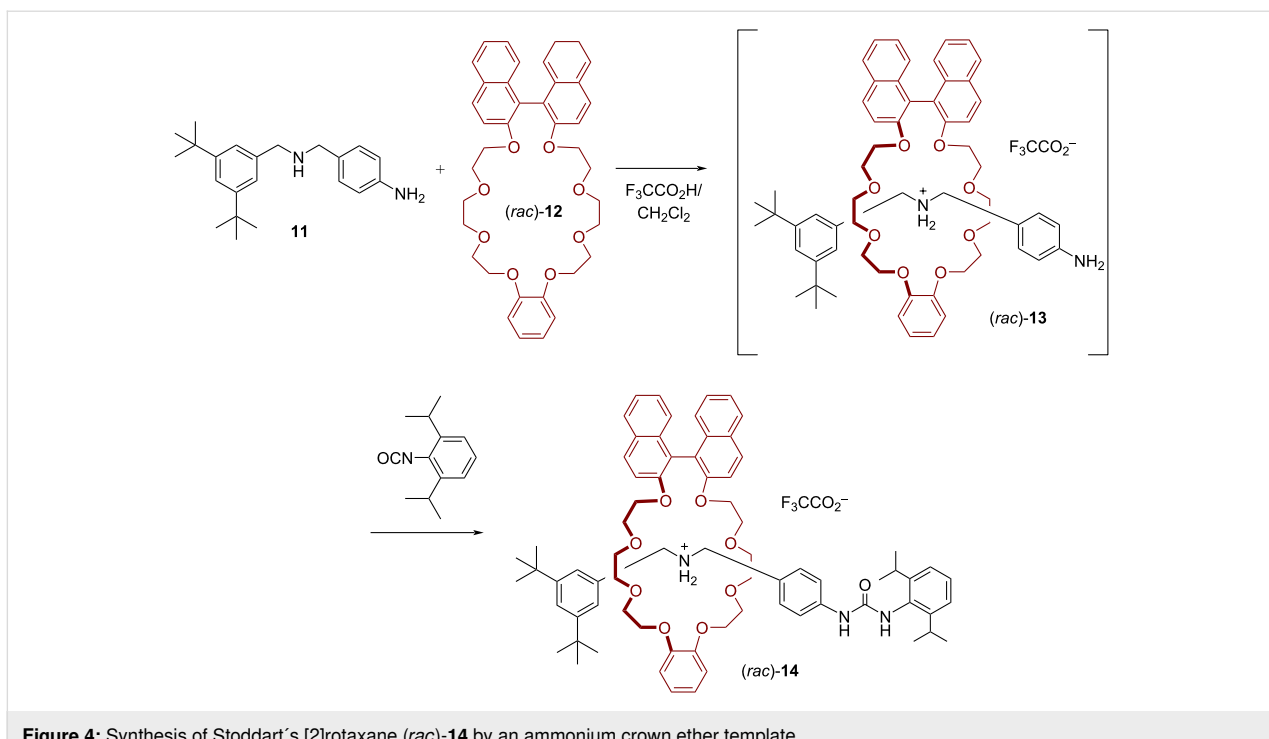


Figure 4: Synthesis of Stoddart's [2]rotaxane (rac)-14 by an ammonium crown ether template.

macrocycle (rac)-15, which was reacted with the achiral dicationic precursor **16** and dibromide **17** to give the racemic mixture of the corresponding rotaxane (rac)-18 (20% yield, see Figure 5a).

Next, the authors showed that the application of the chiral BINOL-based bisbipyridinium precursor **19** (in combination with **15** and **17**) leads to the corresponding catenane **20**, which contains two BINOL-based macrocycles (see Figure 5b). When using (rac)-15 and (R)-19, the (S,R)-diastereomer of the product is formed preferentially under kinetic control ($\text{er} = 67:33$, total yield 23%). Interestingly, employing (R)-15 together with (rac)-19 gave a significantly lower diastereoselectivity ($\text{er} = 56:44$), albeit at slightly increased yield (33%).

Similarly, the reaction of the chiral isomannide-based macrocycle (D,D)-**21** with (rac)-19 and **17** gave the desired catenane **22** in 25% yield (see Figure 5c), but only with low diastereoselectivity ($\text{er} = 58:42$ in favor of the (D,D,R)-isomer). Unfortunately, in this case the combination of (rac)-**21** with (R)-**19** was not investigated.

Variable-temperature ^1H NMR spectroscopic analysis of the [2]catenanes (**18**, **20**, and **22**) revealed various dynamic processes in solution. While circumrotation of the polyether macrocycle around the tetracationic cyclophane was either impossible (for **18** and **20**, due to the presence of the sterically demanding BINOL unit) or slow on the NMR timescale at room tempera-

ture (for **22**), the other two dynamic processes, namely circumrotation of the tetracationic cyclophane through the cavity of the polyether and a “rocking motion” of the oxygen–oxygen axis of the hydroquinone units, were fast on the NMR timescale at room temperature.

In a follow-up study, Stoddart and co-workers employed the BINOL-based macrocycle **23** which contains a 1,5-dioxynaphthalene (DNP) unit (in contrast to the hydroquinone unit in macrocycles **15/21**). Upon reaction with the achiral precursors **16** and **17**, this gives rise to the chiral catenane **24**, which was produced in enantiopure and racemic forms ((S)-**24**/(R)-**24**/(rac)-**24**, 46–51% yield) (see Figure 5d). However, in these catenanes, the BINOL unit (with its fixed chirality) is not the only stereogenic element: Firstly, the tilting of the macrocycle planes out of a 90° angle leads to a helical, co-conformational chirality (*M* and *P* isomers), similar to (S,S)-**5** (see Figure 2). Secondly, the embedding of the DNP unit in the tetracationic cyclophane leads to an element of planar chirality (R_p and S_p isomers). Thus, for each configuration of BINOL, four different diastereoisomers are possible. However, for these specific rotaxanes, the helicity is predetermined by the planar chirality (based on the underlying macrocycle–macrocycle interactions), so that only two diastereoisomers remain for a given BINOL configuration (e.g., (R)-(R_p) and (R)-(S_p) in case of (R)-BINOL). In contrast to the axial chirality of the BINOL unit, the planar chirality of the DNP unit can be inverted by dynamic processes (e.g., by a pirouetting motion of the BINOL macro-

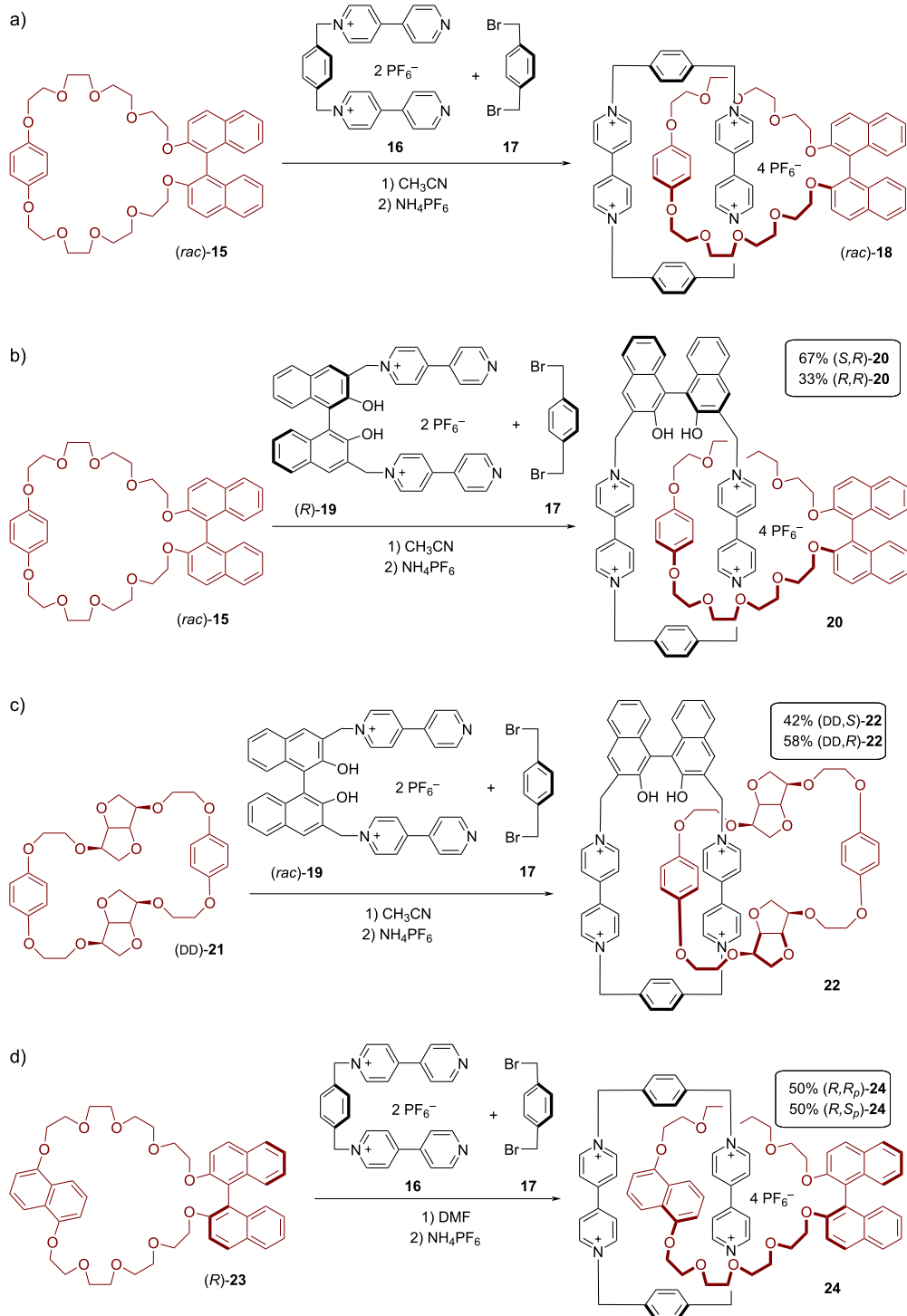


Figure 5: Synthesis of Stoddart's BINOL-containing [2]catenanes **18/20/22/24** by π - π recognition.

cycle). Indeed, both diastereomers are observed by NMR and interconvert with a barrier of 7.9 kcal/mol. No chiral induction of the axial chirality on the planar chirality is observed, so that both diastereoisomers are observed in a 1:1 ratio.

2 Applications

The development of suitable template-based synthetic approaches has opened the way for the application of the resulting chiral MIMs. Here, we will present an overview of the most

recent applications reported so far, together with the synthesis of the corresponding BINOL-based MIMs. Some selected examples of pseudorotaxanes and pseudocatenanes are not included in this review [49–51].

2.1 (Mechano)intramolecular chirality transfer

Takata and co-workers reported two examples for a chirality transfer via the mechanical bond, namely from a BINOL-based macrocycle onto the axle. First, they developed [2]rotaxane **27** [52]. Here, the methacrylate-functionalized ammonium salt **25** and the bis-BINOL macrocycle *(R,R)*-**26** give the pseudorotaxane *(R,R)*-**27** through self-assembly. Stopping of the pseudorotaxane was achieved by radical addition of a thiol-based stopper to the α,β -unsaturated carbonyl unit in 12% yield.

In this reaction, addition of the thiyl radical to the β -position first gives rise to the corresponding rotaxane radical with the unpaired electron in the α -position, followed by hydrogen abstraction from the next thiol. This generates a new stereocenter in the α -position, which takes place under the chiral environment of the BINOL-based macrocycle. However, the hydrogen abstraction takes place with little stereoselectivity, so that both diastereoisomers are formed in almost equal amounts ($er = 53:47$, see Figure 6a).

Subsequently, Takata and co-workers presented a highly diastereoselective synthesis of [2]rotaxane amine *N*-oxides via intercomponent chirality transfer (see Figure 6b) [53]. For the synthesis of the rotaxanes, complexes of hydroxy-terminated

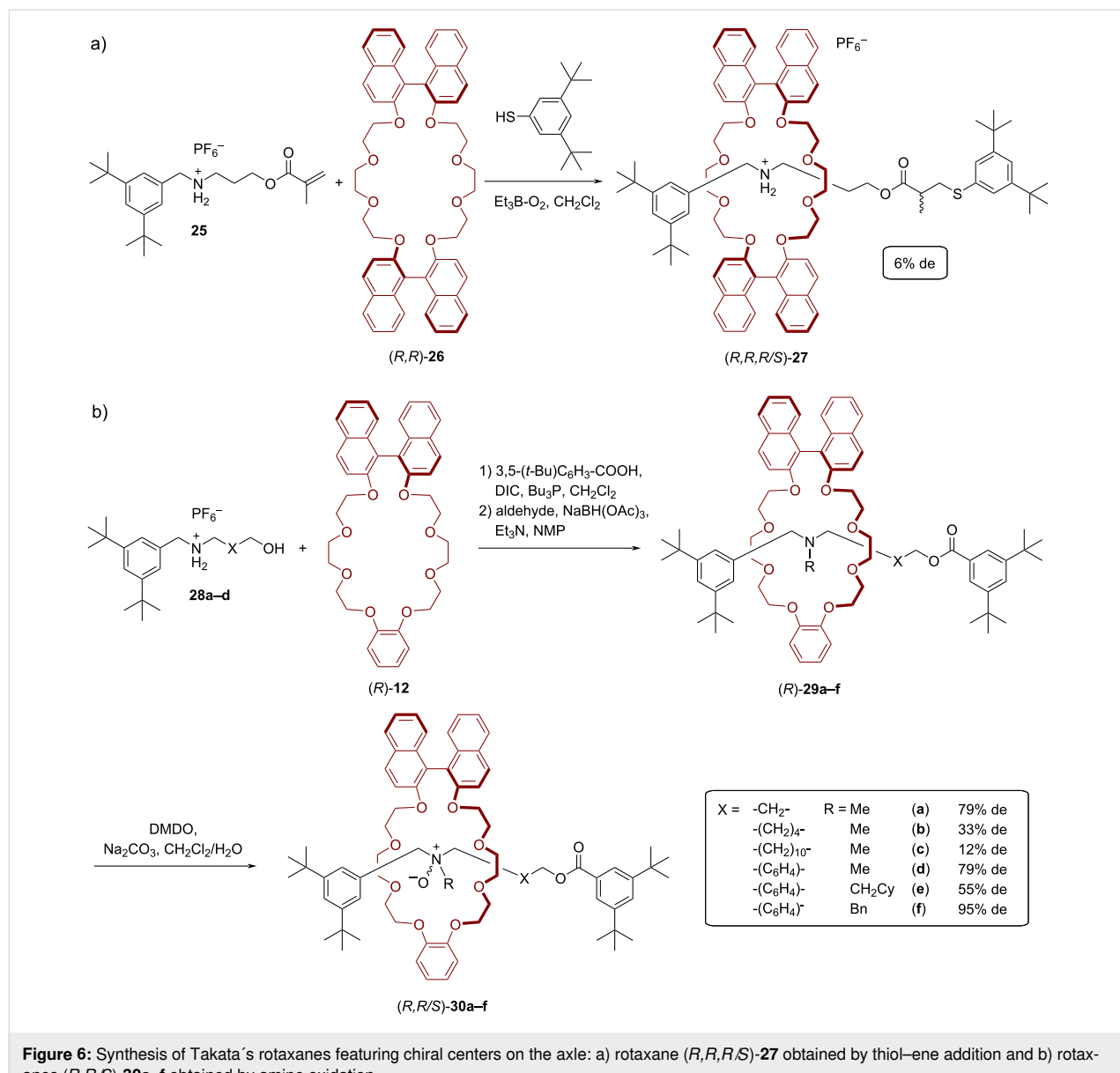


Figure 6: Synthesis of Takata's rotaxanes featuring chiral centers on the axle: a) rotaxane *(R,R,R/S)*-**27** obtained by thiol–ene addition and b) rotaxanes *(R,R/S)*-**30a–f** obtained by amine oxidation.

ammonium salts **28a–d** and BINOL-based macrocycle (*R*)-**12** were coupled with a benzoic acid-based stopper using *N,N'*-diisopropylcarbodiimide (DIC) and tributylphosphine (26–75% yield). The isolated rotaxanes were then used for subsequent reductive *N*-alkylation to obtain the *tert*-amine-type rotaxanes (*R*)-**29a–f** in yields of 67–92%. Finally, dimethyldioxirane (DMDO) was used to obtain the corresponding amine *N*-oxides (*R,R/S*)-**30a–f** in 80–99% yield. This oxidation takes place inside the chiral macrocycle, so that the resulting stereogenic nitrogen is formed in a diastereoselective fashion. Interestingly, for rotaxanes (*R,R/S*)-**30a–c**, which feature C₃/C₆/C₁₂-alkylene-linkers, the diastereoselectivity decreases with increasing linker length (79/33/12% de for C₃/C₆/C₁₂-linkers, respectively). This is in line with an expected localization of the macrocycle around the ester functionality due to weak [C–H···O] interactions from the COOCH₂ group to the macrocycle, which leads to a greater distance between the amine and the chiral macrocycle with increasing chain length. For rotaxanes (*R,R/S*)-**30d–f**, which commonly feature a *p*-xylylene-linker, but different *N*-substituents, it was found the *N*-benzyl group gives rise to the best diastereoselectivity (79/55/95% de for *N*-Me/*N*-CH₂Cy/*N*-Bn).

In 2011, Takata and co-workers reported a functionalized polyacetylene which features [2]rotaxane side chains with chiral BINOL-based macrocycles. The aim of this study was the investigation of a possible chirality transfer from the chiral rotaxane onto the helically chiral polyacetylene, with a special focus on the different possible co-conformations of the rotaxane (see Figure 7) [54].

The synthesis of the acetylene monomers **31**, containing a chiral rotaxane side-chain, was achieved by tributylphosphane-catalyzed esterification. Two different macrocycles having either one BINOL unit (**12**, used in both enantiomeric forms) or two BINOL units (**26**) were used for the construction of the rotaxane. The subsequent rhodium-catalyzed polymerization gave the corresponding polymers **32** in high yields of 89–98%. Here, the BINOL-based macrocycle is localized at the ammonium functionality of the axle, placing it away from the polymer backbone. By *N*-acylation of the ammonium group, a shuttling of the macrocycle towards the ester moiety is achieved, placing the chiral information of the macrocycle in closer proximity to the polymer backbone (polymers **33**). The influence of the chiral BINOL unit on the helicity of the polyacetylene was investigated by CD spectroscopy. Here, no chiral induction was observed for the ammonium species **32**, while the *N*-acylated polymers **33** showed clear Cotton effects in the absorption range of the polymer main chain (490 nm), demonstrating an effective chirality transfer from the macrocycle onto the polymers. Accordingly, use of the enantiomeric macrocycles (*S*)-**12** and (*R*)-**12** gives rise to polyacetylenes with an opposite helix sense. Interestingly, employing the bis-BINOL macrocycle (*R*)-**26** led to an inverted helix configuration in comparison to the mono-BINOL derivative (*R*)-**12**.

In a subsequent work, Takata and co-workers showed that such chirality transfer can also be achieved by deprotonation/reprotonation of the ammonium station, leading to formation of the different co-conformers in a reversible fashion [55].

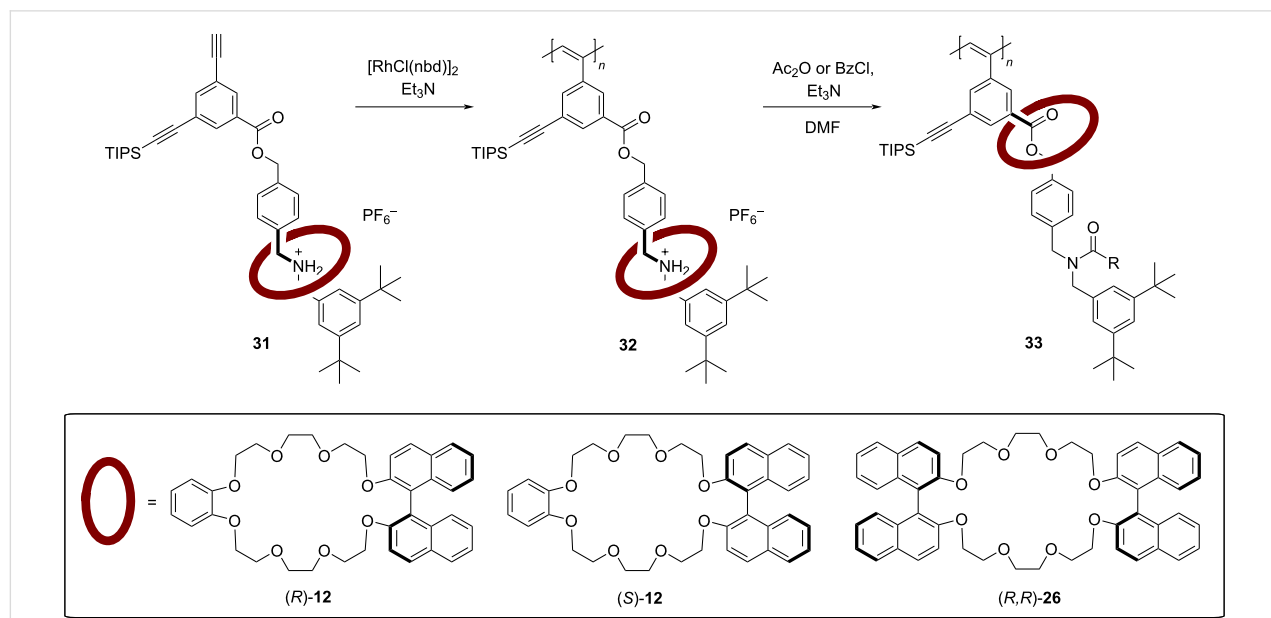


Figure 7: Takata's chiral polyacetylenes **32/33** featuring BINOL-based [2]rotaxane side chains.

2.2 Stereoselective catalysis

As described in chapter 1, the mechanical bond allows a chirality transfer from a chiral, BINOL-based macrocycle to an achiral thread. Thus, it is conceivable that placing a catalytically active group onto the thread would allow for asymmetric catalysis based on chirality transfer from a BINOL macrocycle.

In 2004, Takata and co-workers synthesized thiazolium-based chiral [2]rotaxanes as catalysts for the asymmetric benzoin condensation [56,57]. For the synthesis of the rotaxane, ammonium salts **34a/b** and the BINOL-based macrocycle **(R)-12** were interlocked via tributylphosphine-catalyzed acylative end-capping. The resulting compounds were treated with chloroacetic anhydride and then with thiazole. After anion exchange the chiral thiazolium salts **(R)-35a/b**, which differ in the chain length of the axle, were obtained in 9%/42% overall yield (see Figure 8a).

For comparison, a rotaxane containing a BINOL-based axle and an achiral macrocycle was also synthesized. This design was chosen to investigate the difference between a covalently and a mechanically linked chiral unit with regard to the chiral induction in asymmetric catalysis. By acylative end-capping, followed by introduction of the thiazole unit, rotaxane **(R)-38** was obtained in 35% overall yield (see Figure 8b).

These rotaxanes were then used as catalysts for the asymmetric benzoin condensation of benzaldehyde (**39**). The best yield (90%) could be generated at 0 °C in methanol with

10 mol % of catalyst **(R)-35a**, albeit with a low stereoselectivity (21% ee). Lowering the catalyst loading (to 5 mol % or 1 mol %) led to decreased yields (34%/14%), but slightly increased enantioselectivities (23%/32% ee). Incorporating a longer axle into the catalyst (**(R)-35b**) led to similar results (34% yield, 16% ee at 5 mol % catalyst loading). The catalyst **(R)-38**, featuring the BINOL unit on the axle, does not allow for higher stereoselectivities (19% ee), but interestingly gives the other product enantiomer as the main product (see Figure 9).

In 2016, Takata and co-workers reported a pyridine-based rotaxane catalyst for the *O*-acylative asymmetric desymmetrization of *meso*-1,2-diols [58]. The [2]rotaxane **(R)-42** was synthesized by interaction of the ammonium salt **41** with the BINOL-based macrocycle **(R)-12** and end-capping with 3,5-di-*tert*-butylbenzoic acid (see Figure 10).

In the asymmetric desymmetrization reaction of *meso*-hydrobenzoin, rotaxane **(R)-42** gave the (1*R*,2*S*)-product **45** in high yields and enantioselectivities (78/92/98% ee at +25/−40/−80 °C, respectively). In comparison, a non-interlocked mixture of model catalyst **43** and macrocycle **(R)-12** only gave 8% ee at 25 °C, demonstrating the role of the mechanical bond for the chirality transfer (see Figure 11).

In 2017, our working group showed that bifunctional catenanes can serve as highly efficient organocatalysts. The chiral homocircuit [2]catenane (*S,S*)-**47**, which features two axially chiral

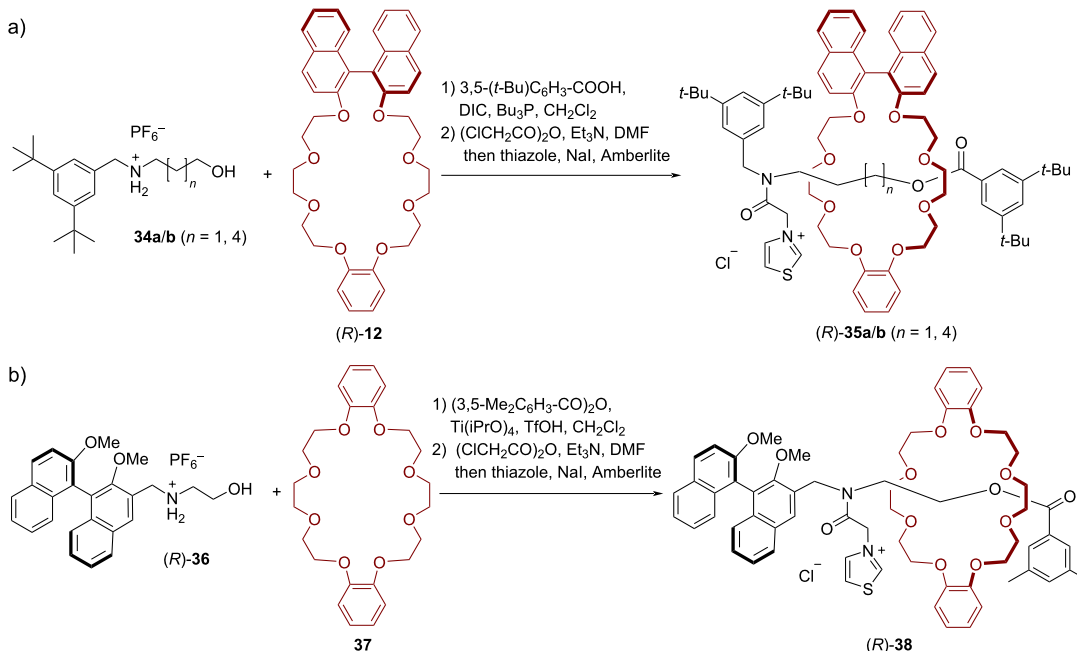
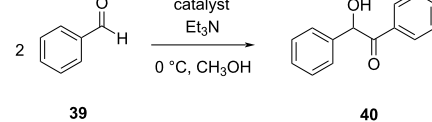
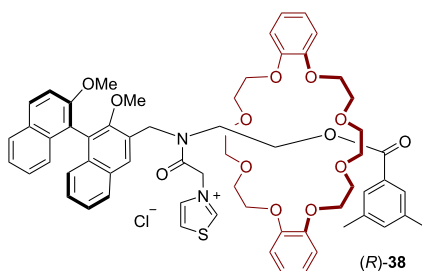
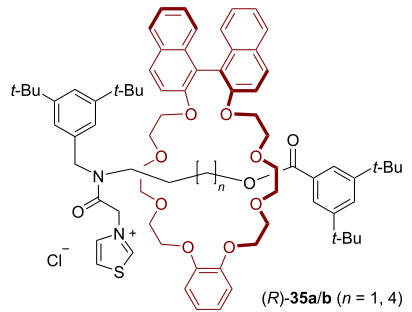


Figure 8: Synthesis of Takata's chiral thiazolium [2]rotaxanes **(R)-35a/b** and **(R)-38**.



catalyst	cat. loading	yield (%)	ee (%)
(R)-35a	10 mol %	90	21 (R)
(R)-35a	5 mol %	34	23 (R)
(R)-35a	1 mol %	14	32 (R)
(R)-35b	5 mol %	34	16 (R)
(R)-38	5 mol %	40	19 (S)

Figure 9: Results for the asymmetric benzoin condensation of benzaldehyde (39) with catalysts (R)-35a/b and (R)-38.

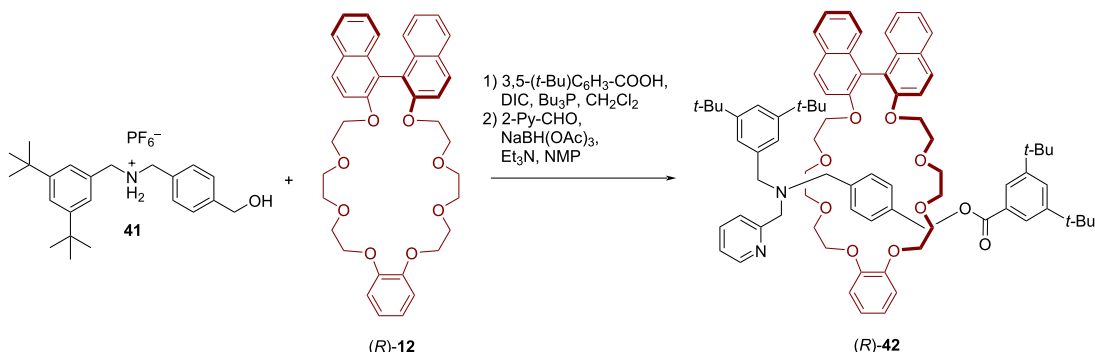


Figure 10: Synthesis of Takata's pyridine-based [2]rotaxane (R)-42.

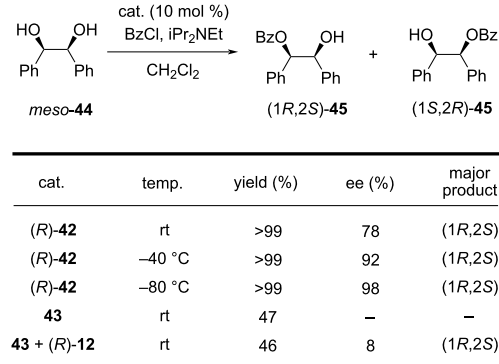
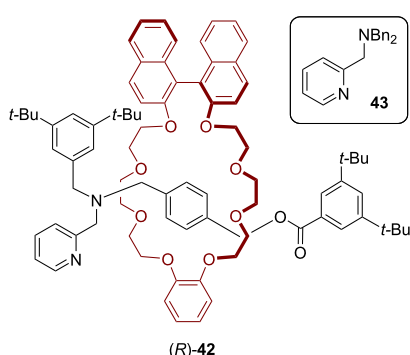


Figure 11: The asymmetric desymmetrization reaction of meso-1,2-diols with rotaxane (R)-42.

1,1'-binaphthyl phosphoric acids, was synthesized in a passive metal template approach. To this end, two equivalents of the acyclic precursor (*S*)-46 were preorganized by a Ca template and catenation was achieved by two-fold ring closing metathesis. This reaction yielded catenane (*S,S*)-47 (14% yield, see Figure 12) together with the non-interlocked macrocycle (*S,S*)-48 (22% yield, for the structure see Figure 13) [59].

The catenane catalyst allows for the asymmetric transfer hydrogenation of 2-substituted quinolines by Hantzsch esters in a highly stereoselective fashion [60]. It was found that the catenated catalyst gives superior stereoselectivities in comparison to the macrocyclic and the acyclic reference catalysts ((*S*)-48/(*S*)-49, see Figure 13) for a broad range of substrates. While the bifunctional catenane (*S,S*)-47 delivers enantioselect-

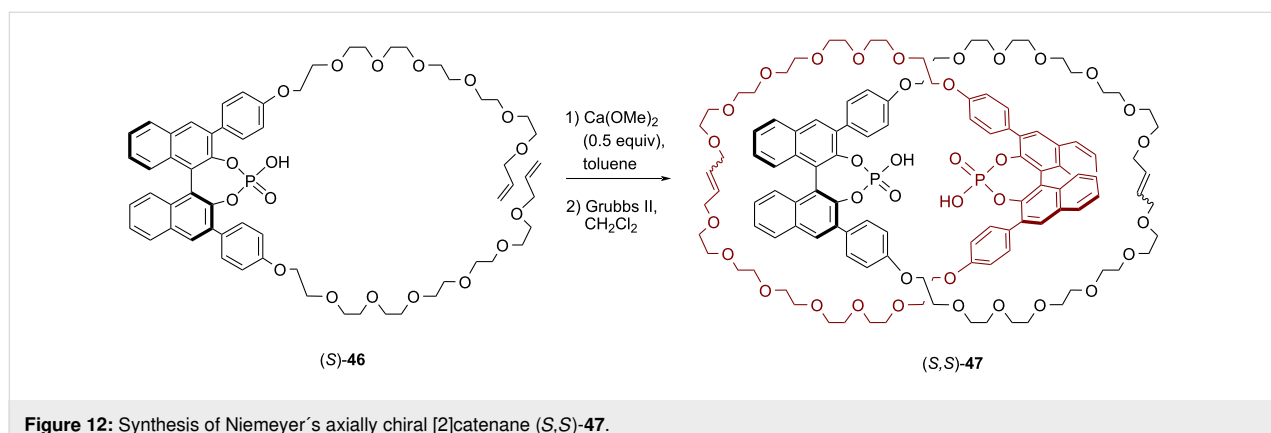


Figure 12: Synthesis of Niemeyer's axially chiral [2]catenane (*S,S*)-47.

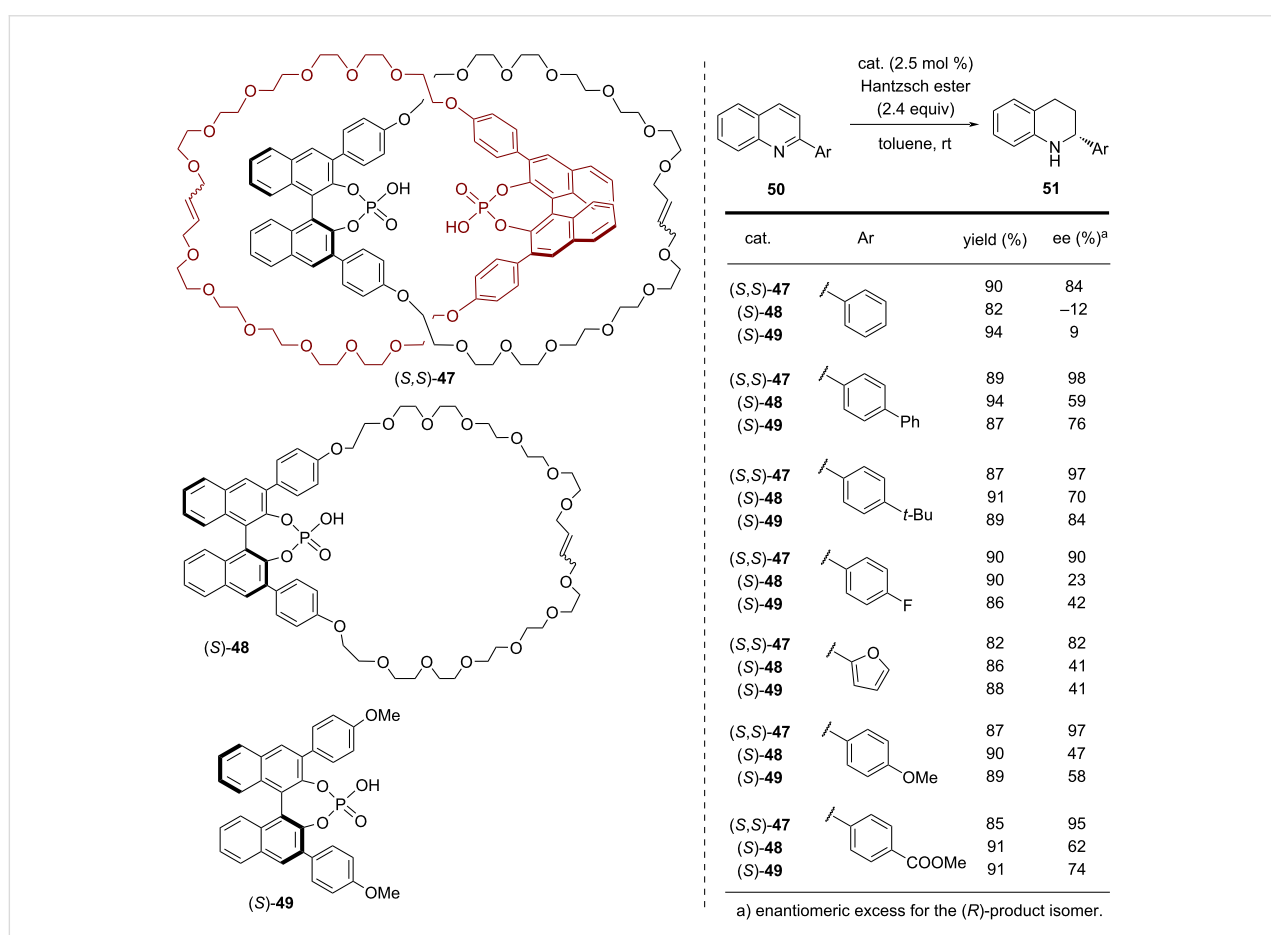


Figure 13: Results for the enantioselective transfer hydrogenation of 2-phenylquinoline with catalysts (*S,S*)-47, (*S*)-48, and (*S*)-49.

tivities between 84–98% ee, the monophosphoric acids *(S)*-**48** and *(S)*-**49** gave lower enantiomeric excesses (12–70% ee for *(S)*-**48** and 9–84% ee for *(S)*-**49**). Density functional theory (DFT) studies suggested that the excellent stereoselectivities of the catenane are a direct result of the cooperative interaction of both phosphoric acid groups, enabled by the mechanical bond. Follow-up studies showed that such acid–acid interactions are also relevant for monophosphoric acid catalysts (e.g., *(S)*-**49**), based on intermolecular interactions that are relevant especially at higher catalyst loadings [61].

Subsequently, our working group reported the synthesis and application of the BINOL-based [2]rotaxanes *(S)*-**56** and *(S)*-**57** [62]. For their synthesis, the phosphoric acid macrocycles *(S)*-**52**/*(S)*-**53** were mixed with the dialkynylated amine **54** to give the pseudorotaxanes based on ammonium–phosphate interactions. Subsequent stoppering with bulky azides **55a/b** gave rotaxanes *(S)*-**56a/b** and *(S)*-**57a/b** in yields of 28–58%. These catalysts differ in the length of the axle ($n = 0$ or 1, for **a** or **b**) and in the substitution pattern of the macrocycle ($R = H$ or iPr in the 3,5-positions of the phenylene linkers, for **56** or **57**; see Figure 14).

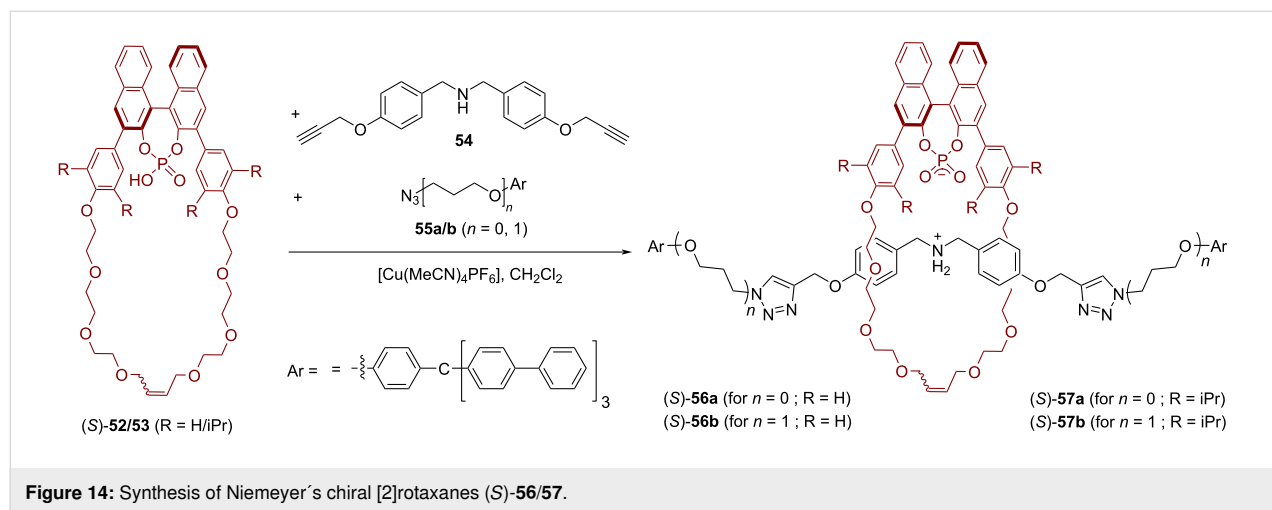
These heterobifunctional chiral catalysts were studied for the asymmetric Michael addition of malonic acid diethyl ester (**59**) to cinnamaldehydes **58**. While the zwitterionic ammonium phosphate rotaxanes were inactive, deprotonation with LiOH led to active catalysts for this reaction. In all cases, the interlocked catalysts showed faster conversion (87–92% conversion after 7 days) than the corresponding non-interlocked mixtures of macrocycle and thread (35–78% conversion) which were used as reference catalysts. With regard to enantioselectivity, it was found the less bulky rotaxanes *(S)*-**56a/b** performed even worse than the reference systems (14%/14% ee for *(S)*-**56a/b**, 23%/22% ee for the reference catalysts). However, an introduc-

tion of the bulky iPr substituents on the macrocycle led to significantly increased stereoselectivities for the rotaxanes (37%/53% ee for *(S)*-**57a/b**), while the reference catalysts gave almost racemic material (7%/9% ee). The same trend was found for the MeO/NO_2 -substituted versions of cinnamaldehyde (44%/49% ee for *(S)*-**57a/b**, 14%/16% ee for the non-interlocked mixture, see Figure 15).

DFT calculations showed that the reaction takes place by cooperative action of the Li phosphate macrocycle and the amine thread, enabled by the mechanical bond. The Li phosphate acts as a Lewis acid to activate the malonic acid diethyl ester, which is then deprotonated by the amine to generate the enolate nucleophile. After the Michael addition, the anionic intermediate is protonated by the ammonium group to liberate the product. Although this cooperative catalysis is facilitated by the mechanical bond, the racemic background reaction only has a slightly higher barrier, which is probably the reason for the low overall stereoselectivities.

2.3 Stereoselective sensing

As last part of this minireview, we will present the application of BINOL-based interlocked molecules for stereoselective chemosensing. This research field was pioneered by Beer and co-workers, with a strong focus on using rotaxanes with halogen-bond (XB) donors that act as binding sites for anionic guest molecules [23]. In 2017, Beer and co-workers reported the synthesis of the BINOL-containing chiral [2]rotaxanes **64** and their application for enantioselective anion recognition [63]. Macrocycle *(S)*-**61**, featuring two iodotriazole units, was reacted with bis-iodoalkyne **62** and azides **63a/b** in order to establish the mechanical bond in an active metal template approach (using the conformational flexibility of the iodotriazole groups for copper *N*-ligation). Subsequent *N*-methylation of the pyridine axle, followed by ion exchange, gave rise to the cationic



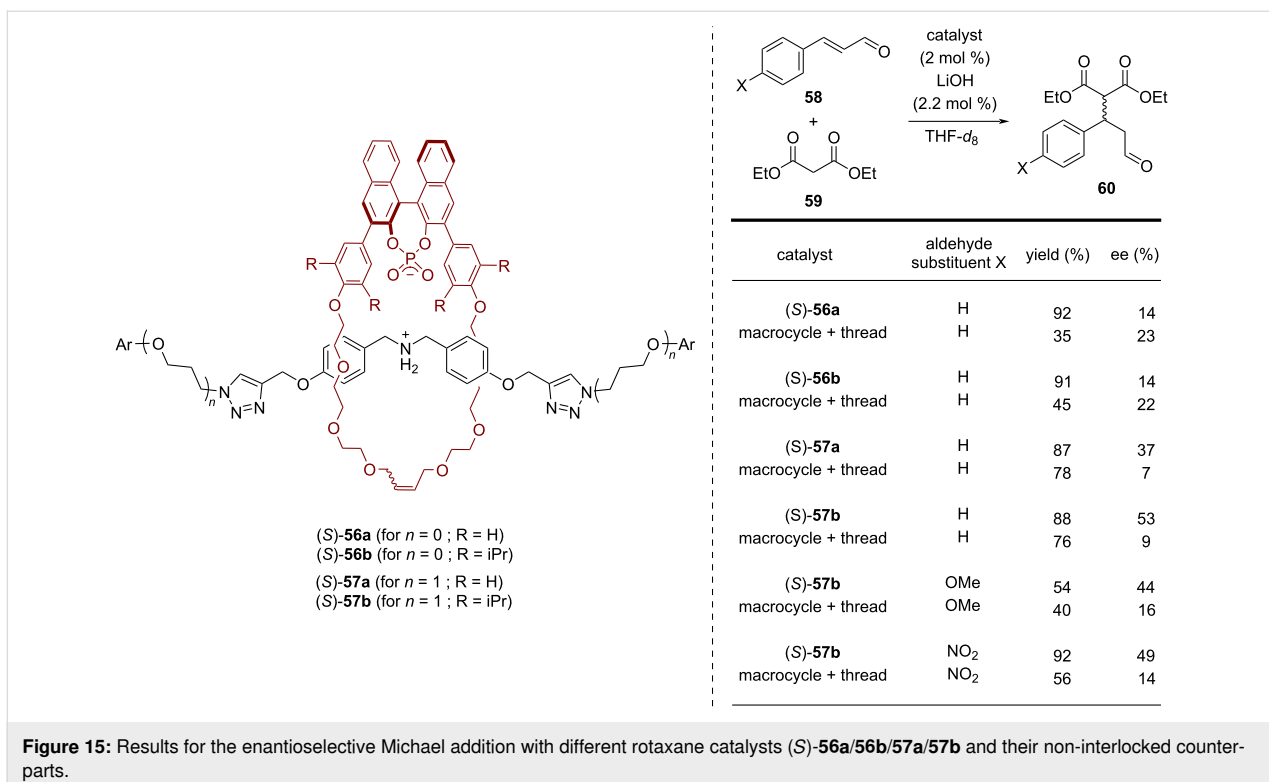


Figure 15: Results for the enantioselective Michael addition with different rotaxane catalysts (S)-56a/56b/57a/57b and their non-interlocked counterparts.

rotaxanes **64a/b** in 23/37% overall yield, both of which feature four iodotriazoles as XB donors. While rotaxane (S)-**64a** only possesses the BINOL unit as a stereogenic element, the system (S,S,S)-**64b** features two additional chiral centers on the thread (see Figure 16).

The stereoselective binding of chiral anions by rotaxanes **64a/b** was studied by ¹H NMR titration experiments, using the dicar-

tion macrocycle (S)-**61-Me₂²⁺** (obtained by methylation of the triazole units in (S)-**61**) as a reference system. As guest molecules, the Boc-protected amino acids *N*-Boc-leucine, *N*-Boc-proline, and *N*-Boc-tryptophane were used. Overall, rotaxane **64a** shows lower association constants ($K = 138$ – 2589 M^{-1}) with preference for the (*R*)-isomers of the guest molecules ($K_{(S)}/K_{(R)} = 0.29$ – 0.66). In contrast, rotaxane **64b** preferentially binds the (*S*)-isomers ($K_{(S)}/K_{(R)} = 1.62$ – 2.93) and shows higher

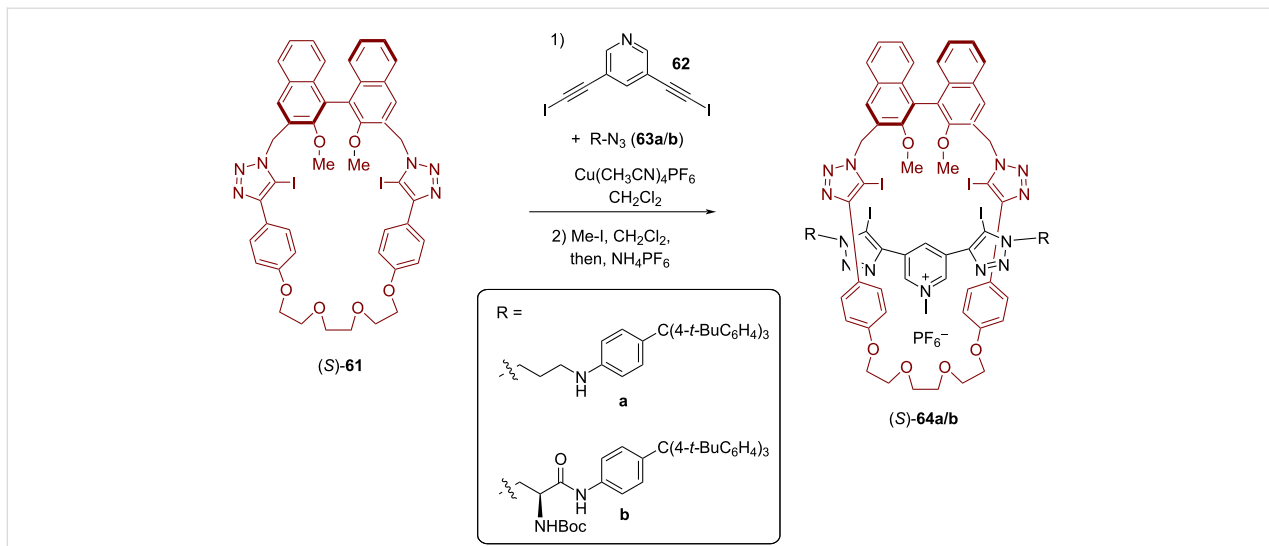


Figure 16: Synthesis of Beer's [2]rotaxanes **64a/b** for anion recognition.

association constants ($K = 1465$ – 4990 M^{-1}), probably due to additional interactions with the functionalized thread. Comparison with the macrocycle (S)-**61** \cdot Me_2^{2+} ($K = 423$ – 4961 M^{-1} , $K_{(S)}/K_{(R)} = 0.66$ – 0.70) shows that the interlocked nature of the rotaxane hosts gives rise to slightly better stereodiscrimination of the guest molecules (see Figure 17).

Subsequently, Beer and co-workers reported the first example of a chiral halogen-bonding [3]rotaxane for the recognition and sensing of dicarboxylate anions [64]. The [3]rotaxane (S)-**68** was prepared in a two-fold clipping reaction, namely reaction of bis-amine **66** and bis-acid chloride **67** in the presence of the

dicationic axle (S)-**65**. The resulting rotaxane (S)-**68** (37% yield, see Figure 18) features a central chiral BINOL unit with two adjacent binding sites for anions, each made of two iodotriazole-XB donors (on the thread) and two NH donors (on the macrocycle).

For the anion-recognition experiments, the binding of selected dicarboxylate anions ((*S/R*)-glutamate, fumarate, and maleate) was investigated by fluorescence titrations. This revealed an impressive chiral discrimination towards (S)-Glu $^{2-}$ with a selectivity of $K_{(S)}/K_{(R)} = 5.7$. In comparison, the free chiral axle alone displayed no significant enantioselectivity ($K_{(S)}/K_{(R)} =$

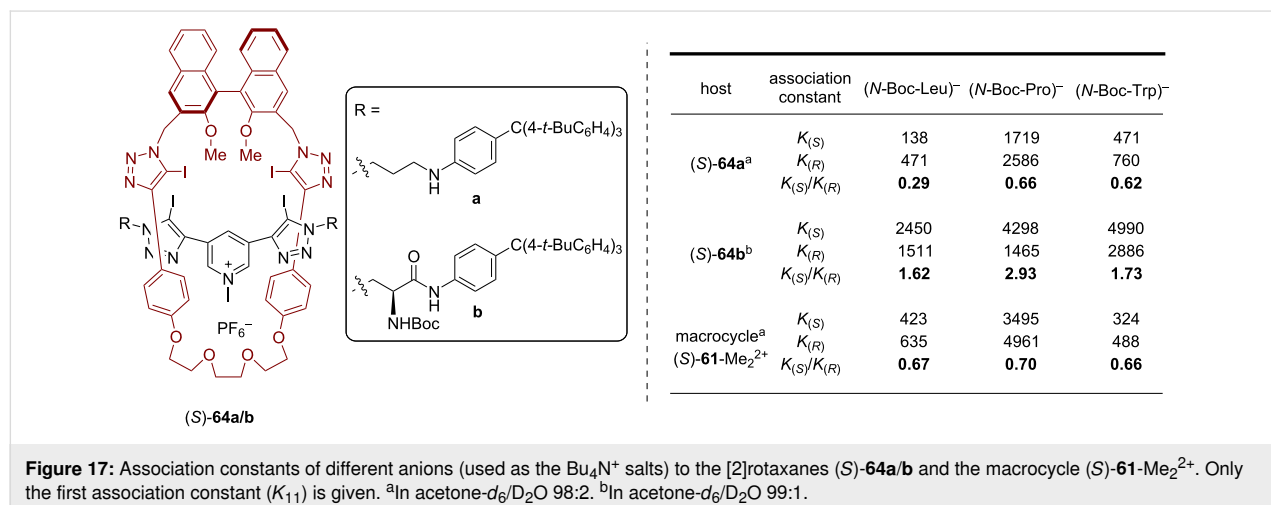
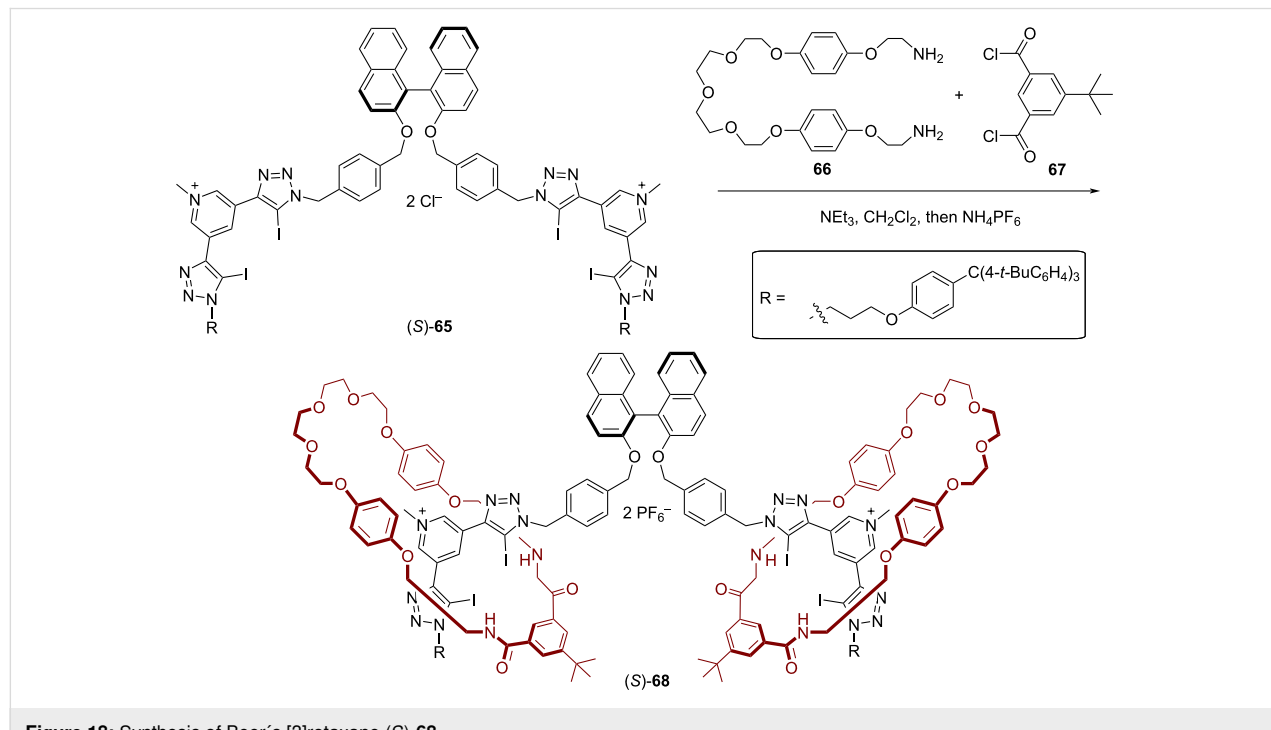


Figure 17: Association constants of different anions (used as the Bu_4N^+ salts) to the [2]rotaxanes (S)-**64a/b** and the macrocycle (S)-**61** \cdot Me_2^{2+} . Only the first association constant (K_{11}) is given. ^aIn acetone- d_6 /D₂O 98:2. ^bIn acetone- d_6 /D₂O 99:1.



0.96). With the rotaxane host, it was also possible to discriminate between the double-bond isomers fumarate and maleate, with strong preference for fumarate ($K_{\text{fum}}/K_{\text{mal}} = 4.4$, see Figure 19).

Conclusion

By the introduction of an axially chiral BINOL unit into a MIM, it is possible to combine the unique applicability of the chiral BINOL unit with the special possibilities offered by interlocked molecules. The synthesis of BINOL-based interlocked compounds can be achieved by different types of supramolecular template strategies that have been developed in the past decades, including passive metal templates, active metal templates, anion templates, ammonium crown ether templates, and templates based on π – π interactions. This has opened the way for the application of the resulting chiral MIMs.

The mechanical bond allows a chirality transfer from a chiral, BINOL-based macrocycle to an achiral thread, leading to applications in (mechano)intramolecular chirality transfer. Furthermore, placing a catalytically active group into a BINOL-based MIM generates chiral catalysts for asymmetric catalysis. Finally, chiral MIMs based on the BINOL framework can also be applied for stereoselective chemosensing.

While the introduction of BINOL as a chiral element in mechanically interlocked molecules has already delivered many insights and first useful applications, we believe that this research area will continue to grow in the future. Especially the combination of the BINOL unit with other stereogenic elements might further increase the chiral induction in catalysis and/or chemosensing. This can be achieved by placing a second

stereogenic element (e.g., an axially chiral, a planar chiral unit or a point chiral unit) on one of the subunits. However, interlocked molecules also offer the exciting possibility to introduce mechanical or topological chirality, which might be especially useful when combined with BINOL as an additional chiral element.

Funding

Funding from the DFG (Sachbeihilfe NI1273/2-2 and Heisenberg-Professorship to J.N., NI1273/4-1) is gratefully acknowledged.

ORCID® iDs

Matthias Krajnc - <https://orcid.org/0000-0002-4354-0950>
Jochen Niemeyer - <https://orcid.org/0000-0002-9295-4260>

References

1. Bruns, C. J.; Stoddart, J. F. *The Nature of the Mechanical Bond: From Molecules to Machines*; John Wiley & Sons: Hoboken, NJ, USA, 2016. doi:10.1002/9781119044123
2. Gil-Ramírez, G.; Leigh, D. A.; Stephens, A. J. *Angew. Chem., Int. Ed.* **2015**, *54*, 6110–6150. doi:10.1002/anie.201411619
3. Xue, M.; Yang, Y.; Chi, X.; Yan, X.; Huang, F. *Chem. Rev.* **2015**, *115*, 7398–7501. doi:10.1021/cr5005869
4. Evans, N. H.; Beer, P. D. *Chem. Soc. Rev.* **2014**, *43*, 4658–4683. doi:10.1039/c4cs00029c
5. Feng, Y.; Ovalle, M.; Seale, J. S. W.; Lee, C. K.; Kim, D. J.; Astumian, R. D.; Stoddart, J. F. *J. Am. Chem. Soc.* **2021**, *143*, 5569–5591. doi:10.1021/jacs.0c13388
6. Erbas-Cakmak, S.; Leigh, D. A.; McTernan, C. T.; Nussbaumer, A. L. *Chem. Rev.* **2015**, *115*, 10081–10206. doi:10.1021/acs.chemrev.5b00146
7. Bruns, C. J.; Stoddart, J. F. *Acc. Chem. Res.* **2014**, *47*, 2186–2199. doi:10.1021/ar500138u

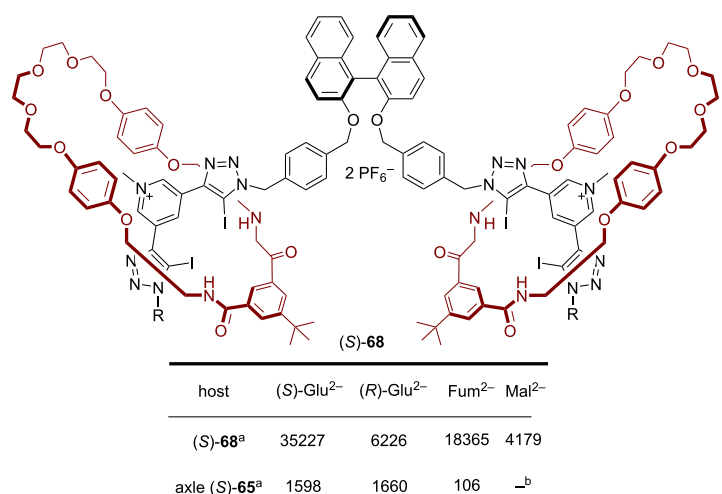


Figure 19: Association constants of different anions (used as the Bu_4N^+ -salts) to the [2]rotaxane (S)-68 and axle (S)-65. Only the first association constant (K_{11}) is given. ^aIn $\text{CHCl}_3/\text{CH}_3\text{OH}/\text{H}_2\text{O}$ 60:39:1. ^bComplex equilibria, no association constant determined.

8. Yang, W.; Li, Y.; Liu, H.; Chi, L.; Li, Y. *Small* **2012**, *8*, 504–516. doi:10.1002/smll.201101738
9. Kay, E. R.; Leigh, D. A. *Pure Appl. Chem.* **2008**, *80*, 17–29. doi:10.1351/pac200880010017
10. Kay, E. R.; Leigh, D. A.; Zerbetto, F. *Angew. Chem., Int. Ed.* **2007**, *46*, 72–191. doi:10.1002/anie.200504313
11. Kay, E. R.; Leigh, D. A. Hydrogen Bond-Assembled Synthetic Molecular Motors and Machines. In *Molecular Machines*; Kelly, T. R., Ed.; Top. Curr. Chem., Vol. 262; Springer: Berlin, Heidelberg, 2005; pp 133–177. doi:10.1007/128_011
12. Mena-Hernando, S.; Pérez, E. M. *Chem. Soc. Rev.* **2019**, *48*, 5016–5032. doi:10.1039/c8cs00888d
13. Pairault, N.; Barat, R.; Tranoy-Opalinski, I.; Renoux, B.; Thomas, M.; Papot, S. *C. R. Chim.* **2016**, *19*, 103–112. doi:10.1016/j.crci.2015.05.012
14. Riebe, J.; Niemeyer, J. *Eur. J. Org. Chem.* **2021**, 5106–5116. doi:10.1002/ejoc.202100749
15. Leigh, D. A.; Marcos, V.; Wilson, M. R. *ACS Catal.* **2014**, *4*, 4490–4497. doi:10.1021/cs5013415
16. Blanco, V.; Leigh, D. A.; Marcos, V. *Chem. Soc. Rev.* **2015**, *44*, 5341–5370. doi:10.1039/c5cs00096c
17. Kwamen, C.; Niemeyer, J. *Chem. – Eur. J.* **2021**, *27*, 175–186. doi:10.1002/chem.202002876
18. Kauerhof, D.; Niemeyer, J. *ChemPlusChem* **2020**, *85*, 889–899. doi:10.1002/cplu.202000152
19. Heard, A. W.; Suárez, J. M.; Goldup, S. M. *Nat. Rev. Chem.* **2022**, *6*, 182–196. doi:10.1038/s41570-021-00348-4
20. Langton, M. J.; Beer, P. D. *Acc. Chem. Res.* **2014**, *47*, 1935–1949. doi:10.1021/ar500012a
21. Langton, M. J.; Serpell, C. J.; Beer, P. D. *Angew. Chem., Int. Ed.* **2016**, *55*, 1974–1987. doi:10.1002/anie.201506589
22. McConnell, A. J.; Docker, A.; Beer, P. D. *ChemPlusChem* **2020**, *85*, 1824–1841. doi:10.1002/cplu.202000484
23. Pancholi, J.; Beer, P. D. *Coord. Chem. Rev.* **2020**, *416*, 213281. doi:10.1016/j.ccr.2020.213281
24. Chmielewski, M. J.; Davis, J. J.; Beer, P. D. *Org. Biomol. Chem.* **2009**, *7*, 415–424. doi:10.1039/b818351a
25. Sluysmans, D.; Stoddart, J. F. *Trends Chem.* **2019**, *1*, 185–197. doi:10.1016/j.trechm.2019.02.013
26. Maynard, J. R. J.; Goldup, S. M. *Chem* **2020**, *6*, 1914–1932. doi:10.1016/j.chempr.2020.07.012
27. Jamieson, E. M. G.; Modicom, F.; Goldup, S. M. *Chem. Soc. Rev.* **2018**, *47*, 5266–5311. doi:10.1039/c8cs00097b
28. Bruns, C. J. *Symmetry* **2019**, *11*, 1249. doi:10.3390/sym11101249
29. Brunel, J. M. *Chem. Rev.* **2005**, *105*, 857–898. doi:10.1021/cr040079g
30. Parmar, D.; Sugiono, E.; Raja, S.; Rueping, M. *Chem. Rev.* **2014**, *114*, 9047–9153. doi:10.1021/cr5001496
31. Yu, S.; Pu, L. *Tetrahedron* **2015**, *71*, 745–772. doi:10.1016/j.tet.2014.11.007
32. Pu, L. *Acc. Chem. Res.* **2012**, *45*, 150–163. doi:10.1021/ar200048d
33. Lewis, J. E. M.; Beer, P. D.; Loeb, S. J.; Goldup, S. M. *Chem. Soc. Rev.* **2017**, *46*, 2577–2591. doi:10.1039/c7cs00199a
34. Beves, J. E.; Blight, B. A.; Campbell, C. J.; Leigh, D. A.; McBurney, R. T. *Angew. Chem., Int. Ed.* **2011**, *50*, 9260–9327. doi:10.1002/anie.201007963
35. Denis, M.; Goldup, S. M. *Nat. Rev. Chem.* **2017**, *1*, 0061. doi:10.1038/s41570-017-0061
36. Qu, D.-H.; Tian, H. *Chem. Sci.* **2011**, *2*, 1011–1015. doi:10.1039/c0sc00653j
37. Hänni, K. D.; Leigh, D. A. *Chem. Soc. Rev.* **2010**, *39*, 1240–1251. doi:10.1039/b901974j
38. Crowley, J. D.; Goldup, S. M.; Lee, A.-L.; Leigh, D. A.; McBurney, R. T. *Chem. Soc. Rev.* **2009**, *38*, 1530–1541. doi:10.1039/b804243h
39. Spence, G. T.; Beer, P. D. *Acc. Chem. Res.* **2013**, *46*, 571–586. doi:10.1021/ar300264n
40. Beer, P. D.; Sambrook, M. R.; Curiel, D. *Chem. Commun.* **2006**, 2105–2117. doi:10.1039/b516435b
41. Schalley, C. A.; Weilandt, T.; Brüggemann, J.; Vögtle, F. Hydrogen-Bond-Mediated Template Synthesis of Rotaxanes, Catenanes, and Knotanes. In *Templates in Chemistry I*; Schalley, C. A.; Vögtle, F.; Dötz, K. H., Eds.; Topics in Current Chemistry, Vol. 248; Springer: Berlin, Heidelberg, 2005; pp 141–200. doi:10.1007/b99913
42. Barin, G.; Coskun, A.; Fouda, M. M. G.; Stoddart, J. F. *ChemPlusChem* **2012**, *77*, 159–185. doi:10.1002/cplu.201100075
43. Koizumi, M.; Dietrich-Buchecker, C.; Sauvage, J.-P. *Eur. J. Org. Chem.* **2004**, 770–775. doi:10.1002/ejoc.200300572
44. Saito, S.; Hirano, Y.; Mutoh, Y.; Kasama, T. *Chem. Lett.* **2015**, *44*, 1509–1511. doi:10.1246/cl.150693
45. Saito, S.; Takahashi, E.; Nakazono, K. *Org. Lett.* **2006**, *8*, 5133–5136. doi:10.1021/o1062247s
46. Cantrill, S. J.; Fyfe, M. C. T.; Heiss, A. M.; Stoddart, J. F.; White, A. J. P.; Williams, D. J. *Chem. Commun.* **1999**, 1251–1252. doi:10.1039/a902096i
47. Kang, S.; Aprahamian, I.; Stoddart, J. F. *Isr. J. Chem.* **2007**, *47*, 253–262. doi:10.1560/ijc.47.2.253
48. Ashton, P. R.; Heiss, A. M.; Pasini, D.; Raymo, F. M.; Shipway, A. N.; Stoddart, J. F.; Spencer, N. *Eur. J. Org. Chem.* **1999**, 995–1004. doi:10.1002/(sici)1099-0690(199905)1999:5<995::aid-ejoc995>3.0.co;2-k
49. Li, Y.; Feng, Y.; He, Y.-M.; Chen, F.; Pan, J.; Fan, Q.-H. *Tetrahedron Lett.* **2008**, *49*, 2878–2881. doi:10.1016/j.tetlet.2008.03.039
50. Hattori, G.; Hori, T.; Miyake, Y.; Nishibayashi, Y. *J. Am. Chem. Soc.* **2007**, *129*, 12930–12931. doi:10.1021/ja0752311
51. Zhu, X.-Z.; Chen, C.-F. *Chem. – Eur. J.* **2006**, *12*, 5603–5609. doi:10.1002/chem.200600195
52. Tachibana, Y.; Kihara, N.; Ohga, Y.; Takata, T. *Chem. Lett.* **2000**, *29*, 806–807. doi:10.1246/cl.2000.806
53. Xu, K.; Nakazono, K.; Takata, T. *Tetrahedron Lett.* **2016**, *57*, 4356–4359. doi:10.1016/j.tetlet.2016.08.046
54. Ishiwari, F.; Fukasawa, K.-i.; Sato, T.; Nakazono, K.; Koyama, Y.; Takata, T. *Chem. – Eur. J.* **2011**, *17*, 12067–12075. doi:10.1002/chem.201101727
55. Ishiwari, F.; Nakazono, K.; Koyama, Y.; Takata, T. *Chem. Commun.* **2011**, *47*, 11739–11741. doi:10.1039/c1cc14404a
56. Tachibana, Y.; Kihara, N.; Nakazono, K.; Takata, T. *Phosphorus, Sulfur Silicon Relat. Elem.* **2010**, *185*, 1182–1205. doi:10.1080/10426501003773589
57. Tachibana, Y.; Kihara, N.; Takata, T. *J. Am. Chem. Soc.* **2004**, *126*, 3438–3439. doi:10.1021/ja0394611
58. Xu, K.; Nakazono, K.; Takata, T. *Chem. Lett.* **2016**, *45*, 1274–1276. doi:10.1246/cl.160649
59. Mitra, R.; Thiele, M.; Octa-Smolin, F.; Letzel, M. C.; Niemeyer, J. *Chem. Commun.* **2016**, *52*, 5977–5980. doi:10.1039/c6cc01980c
60. Mitra, R.; Zhu, H.; Grimme, S.; Niemeyer, J. *Angew. Chem., Int. Ed.* **2017**, *56*, 11456–11459. doi:10.1002/anie.201704647

61. Jansen, D.; Gramüller, J.; Niemeyer, F.; Schaller, T.; Letzel, M. C.;
Grimme, S.; Zhu, H.; Gschwind, R. M.; Niemeyer, J. *Chem. Sci.* **2020**,
11, 4381–4390. doi:10.1039/d0sc01026j
62. Pairault, N.; Zhu, H.; Jansen, D.; Huber, A.; Daniliuc, C. G.;
Grimme, S.; Niemeyer, J. *Angew. Chem., Int. Ed.* **2020**, *59*,
5102–5107. doi:10.1002/anie.201913781
63. Lim, J. Y. C.; Marques, I.; Félix, V.; Beer, P. D. *J. Am. Chem. Soc.*
2017, *139*, 12228–12239. doi:10.1021/jacs.7b06144
64. Lim, J. Y. C.; Marques, I.; Félix, V.; Beer, P. D. *Angew. Chem., Int. Ed.*
2018, *57*, 584–588. doi:10.1002/anie.201711176

License and Terms

This is an open access article licensed under the terms of the Beilstein-Institut Open Access License Agreement (<https://www.beilstein-journals.org/bjoc/terms>), which is identical to the Creative Commons Attribution 4.0 International License (<https://creativecommons.org/licenses/by/4.0>). The reuse of material under this license requires that the author(s), source and license are credited. Third-party material in this article could be subject to other licenses (typically indicated in the credit line), and in this case, users are required to obtain permission from the license holder to reuse the material.

The definitive version of this article is the electronic one which can be found at:

<https://doi.org/10.3762/bjoc.18.53>



Heteroleptic metallosupramolecular aggregates/complexation for supramolecular catalysis

Prodip Howlader and Michael Schmittel*

Review

Open Access

Address:

Center of Micro- and Nanochemistry and (Bio)Technology, Universität Siegen, Organische Chemie I, Adolf-Reichwein-Str. 2, D-57068 Siegen, Germany

Email:

Michael Schmittel* - schmittel@chemie.uni-siegen.de

* Corresponding author

Keywords:

heteroleptic complexation; information science; supramolecular catalysis; switching catalysis; systems chemistry

Beilstein J. Org. Chem. **2022**, *18*, 597–630.

<https://doi.org/10.3762/bjoc.18.62>

Received: 31 January 2022

Accepted: 11 May 2022

Published: 27 May 2022

This article is part of the thematic issue "Supramolecular approaches to mediate chemical reactivity".

Guest Editor: C. Gaeta

© 2022 Howlader and Schmittel; licensee Beilstein-Institut.

License and terms: see end of document.

Abstract

Supramolecular catalysis is reviewed with an eye on heteroleptic aggregates/complexation. Since most of the current metallosupramolecular catalytic systems are homoleptic in nature, the idea of breaking/reducing symmetry has ignited a vivid search for heteroleptic aggregates that are made up by different components. Their higher degree of functional diversity and structural heterogeneity allows, as demonstrated by Nature by the multicomponent ATP synthase motor, a more detailed and refined configuration of purposeful machinery. Furthermore, (metallo)supramolecular catalysis is shown to extend beyond the single "supramolecular unit" and to reach far into the field and concepts of systems chemistry and information science.

Introduction

Supramolecular catalysis [1–3] for most chemists is associated with a catalytically active capsule providing either activating groups or surface/volume properties for catalytic activation [4–12]. In the present short review, limited to discrete heteroleptic metallo-supramolecular ensembles [13,14], we will show that, in addition to the above-mentioned way, there are other diverse possibilities to profit from supramolecular protocols in catalysis [9].

Metal–ligand-based 2D and 3D self-assembled architectures have been extensively studied over the past decades [15–21].

While in the early years, the focus has been on the exploration of structural features, more recent advancements have led to a multitude of extremely useful functional applications (molecular recognition, ion sensing, catalysis, etc.) [9,22]. Since most of these structures are homoleptic in nature, i.e., they are constructed from a single type of ligand [4–22], the idea of breaking/reducing symmetry has ignited a vivid search for heteroleptic aggregates that are made up by different components. Their higher degree of functional diversity and structural heterogeneity should allow, as amply demonstrated by Nature, for instance, by the multicomponent ATP synthase motor [23],

a more detailed and refined configuration of purposeful machinery [24].

For the preparation of heteroleptic aggregates, one must differentiate between dynamic (rapidly exchanging) and kinetically inert heteroleptic metal–ligand interactions. While the inert heteroleptic metal–ligand motifs often center about iridium, ruthenium, rhodium etc. [25], the dynamic ones are constructed using copper(I), zinc(II), cadmium(II), iron(II), palladium(II), etc. as metal ions due to their more rapid ligand exchange rates [24–26].

The strategies to prepare inert vs dynamic heteroleptic aggregates are quite different. While in the former often a step-by-step attachment of the different ligands to the metal centers under kinetic control is dominating, the formation of dynamic aggregates relies on effective self-sorting protocols under thermodynamic control [24].

In its initial definition, self-sorting describes the capability to distinguish "self" from "non-self" in a mixture of constituents [27–30], i.e., the formation of well-defined homomeric aggregates [31] instead of a random combination of constituents in the product. This definition was later extended to heteromeric complexes by Issacs' classification [32] of two main categories: (a) social self-sorting, which involves the assembly of different species, and (b) narcissistic self-sorting, which only involves aggregation of the same component. Over the past few years, a variety of social self-sorting protocols has led to a significant number of self-sorted cages/assemblies that have demonstrated their potential to act as functional materials [30].

Various self-sorting protocols leading to quantitative formation of heteroaggregates under thermodynamic control have recently proven their capacity. A prominent procedure developed by Sauvage on the basis of topological control [33] has found ample use in the preparation of rotaxane-based machines and devices [34]. A key element is a macrocyclic phenanthroline with an endotopic binding site as it precludes homoleptic complex formation. A further principle, introduced by Lehn, uses maximum site occupancy to afford heteroleptic aggregates [35]. While this principle is limited, the charge-separation approach by Stang is of much wider use [36]. Probably, most contributions in the literature, though, are based on using steric constraints in heteroleptic aggregation, since a variety of heteroleptic aggregation protocols have been developed by Schmittel [37] (for copper(I), zinc(II), cadmium(II), mercury(II) ions) and Yoshizawa/Fujita [38] (for palladium(II) ion) that involve pyridine-derived ligands. Highly innovative are the approaches for terpyridine-based complexes by Chan using complementary ligand binding [39], sometimes combined with con-

formational regulation [40], and of Newkome/Li [41] applying mainly geometric complementarity [42]. Clever utilized shape complementarity [21] for building heteroleptic palladium(II) cages whereas Crowley developed a procedure to kinetically metastable cages using naked Pd^{2+} [43,44].

The following selected structures (Figure 1) shall give a flavor of recent achievements in making fascinating heteroleptic structures using dynamic binding motifs.

The availability of powerful tools for building heteroleptic aggregates has led to a multitude of fascinating structures, accompanied by bright and confident prospects for interesting future applications. Concentrating on the topic of catalysis, however, one must confess that despite ample promises, so far, the number of established cases is rather small. For this brief account, we have identified four different categories under which the current examples describing supramolecular catalysis profiting from heteroleptic binding motifs may be summarized:

- Catalysis using heteroleptic discrete supramolecular architectures
- Catalytic effects due to nanomechanical motion
- Switchable catalysis due to reversible assembly/disassembly
- Toggling between intra- and intermolecular complexation in nanoswitches

Review

Catalysis using heteroleptic discrete supramolecular architectures

In its early years, supramolecular chemistry mainly focused on host–guest interactions, primarily on the electrostatic interaction of crown ethers and alkali metals [4]. While, in the beginning, crown ethers were an excellent choice for metal ion complexation, they later received ample recognition as supramolecular catalysts [49].

The majority of host capsules, however, has been constructed using aromatic walls that offer van-der-Waals and π – π stacking interactions in order to compensate for the absence of a strong electrostatic interaction. These non-covalent/ionic interactions play an important role in encapsulating aromatic organic molecules, especially in aqueous medium. Along this rationale, organic host molecules such as cyclodextrin [50], pillararenes, and cucurbiturils [51] have been developed in the last decades. Although, these exhibit excellent host–guest encapsulation properties with a variety of organic molecules, there are major drawbacks associated with them: variation of the

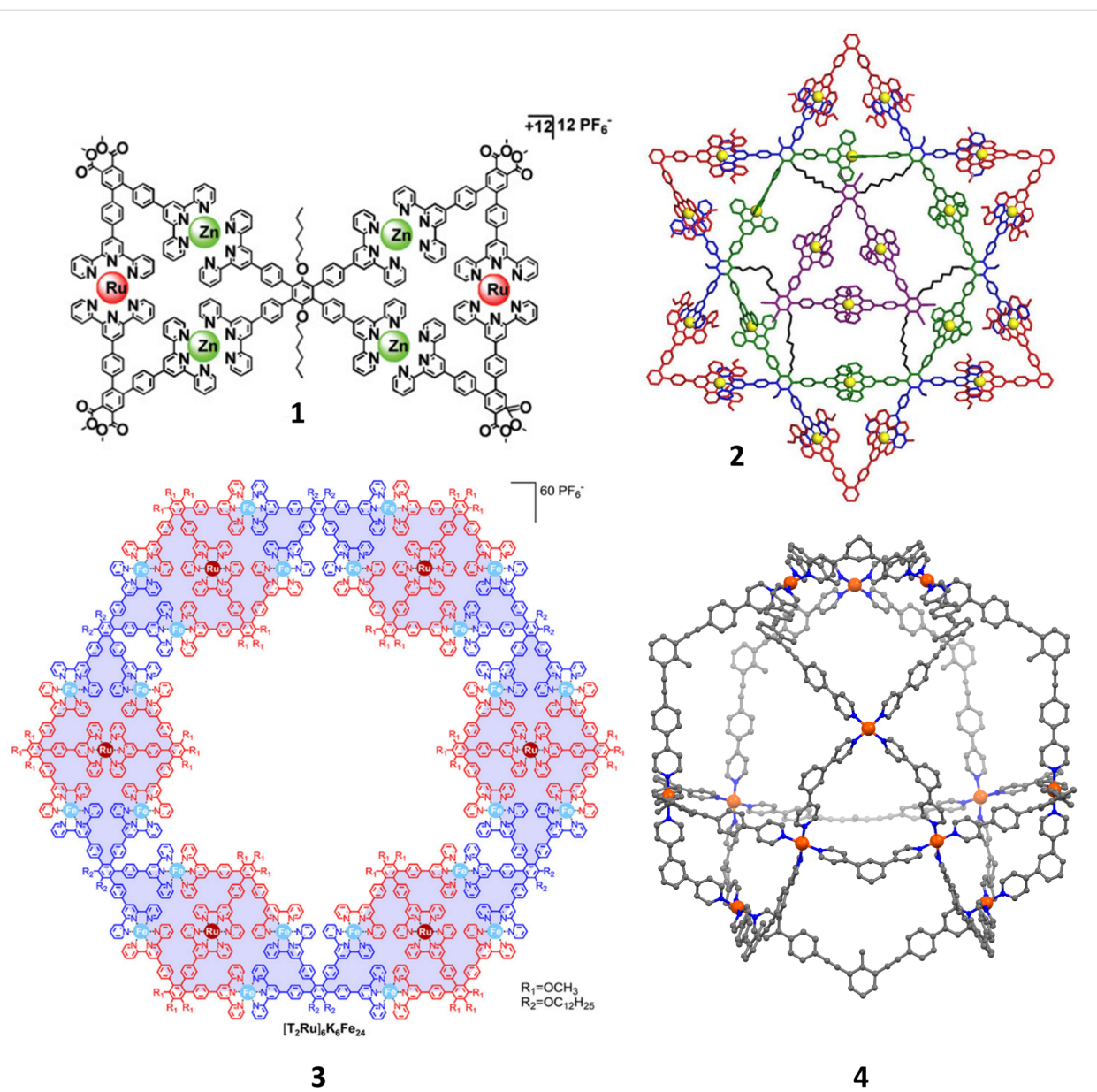


Figure 1: Butterfly **1** (Figure was reprinted with permission from [45]. Copyright 2012 American Chemical Society. This content is not subject to CC BY 4.0.). Six-pointed star **2** = $[\text{Cd}_{21}\text{L}_{33}\text{L}'_6]$ (Figure was reprinted with permission from [46]. Copyright 2019 American Chemical Society. This content is not subject to CC BY 4.0.). Hexagonal supramolecular nut **3** (Figure was reprinted with permission from [47]. Copyright 2016 American Chemical Society. This content is not subject to CC BY 4.0.). Cantellated tetrahedron **4** = $\text{Pd}_{12}\text{L}_{12}\text{L}'_{12}$ (Fujita 2014 [48]).

shape and size of their cavity requires often tedious de-novo synthesis.

Eventually, these drawbacks have been tackled by synthesizing discrete supramolecular hosts based on metal–ligand coordination-driven self-assembly [15–22,52]. This approach not only solved the issue with low overall yields, but it also provided chemists with a superior control over the shape and size of the host’s cavity. Since the coordination bonds which define the host structure are labile in nature, they allow the formation of

thermodynamically controlled architectures using a self-correcting mechanism [15,53]. Generally, the construction is spontaneous and highly selective with quantitative conversion.

In search of supramolecular cavity-induced catalysis, chemists have become fascinated toward the design of large and sophisticated molecular vessels. In this context, Stang [54], Nitschke [55], Fujita [56], and others [57] have reported several template-free assemblies giving access to novel structures. The primary objective of these nanovessels as supramolecular cata-

lysts is to encapsulate organic reactant/s to lower the activation barrier, thereby mimicking the functions of enzymes (without replicating their structures). The structural dissimilarity between the reactants and the subsequent product often contributes to the successful release of the product from the reaction vessel, thus, reducing product inhibition. Hence, it can be envisioned that the introduction of functionality within the building blocks to decorate the inner cavity of the host would produce efficient types of catalyst, where the substrates get activated for a particular reaction upon interaction with the functional group inside the cavity.

Mukherjee et al. have demonstrated the construction of 3D nanocages employing imidazole-based multidentate donors [58]. The conformational asymmetry of the imidazole units opened the venue to nanocages of different shapes and sizes with ease. To take the directional self-assembly to the next level, a three-component self-assembly of the tetra- and tri-imidazole donors **6** and **7**, respectively, was carried out with **5** via social self-sorting to form the Pd₇ molecular cage **8** (Figure 2) as driven by the directionality of the donor nitrogen of the building ligands. The unique three-component Pd₇ molecular boat has a proper internal nanocavity showing preferential affinity towards aromatic molecules through π - π stacking with the hydrophobic aromatic wall of the host. Finally, the boat was investigated as a catalyst for the Knoevenagel condensation reaction (Figure 2) of a series of aromatic aldehydes with

1,3-dimethylbarbituric acid and Meldrum's acid in aqueous media.

One of the primary advantages of utilizing self-assembly to construct discrete nanocages with predetermined geometry and function is the use of a one-pot reaction employing complementary organic linkers with inorganic metal ions. Although the one-pot synthesis of homoleptic metallacages has been thoroughly investigated over the years [15–22] a more accurate understanding of the self-assembly of diverse components and the development of functionally integrated smart architectures for catalysis as “artificial enzymes” certainly demands further attention. Enticed by this idea, Mukherjee and co-worker have demonstrated the design and synthesis of urea-functionalized 2D/3D architectures and their catalytic activity. The urea moieties were incorporated within the building blocks and were meant to serve as binding sites for appropriate substrates, therefore, promoting selectivity and reactivity. For this purpose, they have chosen the ditopic bisurea “strut” **12** (Figure 3), which generated a 2D discrete molecular triangle **14** in the presence of an equimolar amount of the *cis*-(tmen)Pd(NO₃)₂ acceptor **5** [59].

In order to prevent the urea moieties on the triangle to get engaged in intermolecular H-bonding, which would lead to catalytic quenching, a unique design strategy was applied. Instead of using a *cis*-blocked palladium(II) unit for self-assembly,

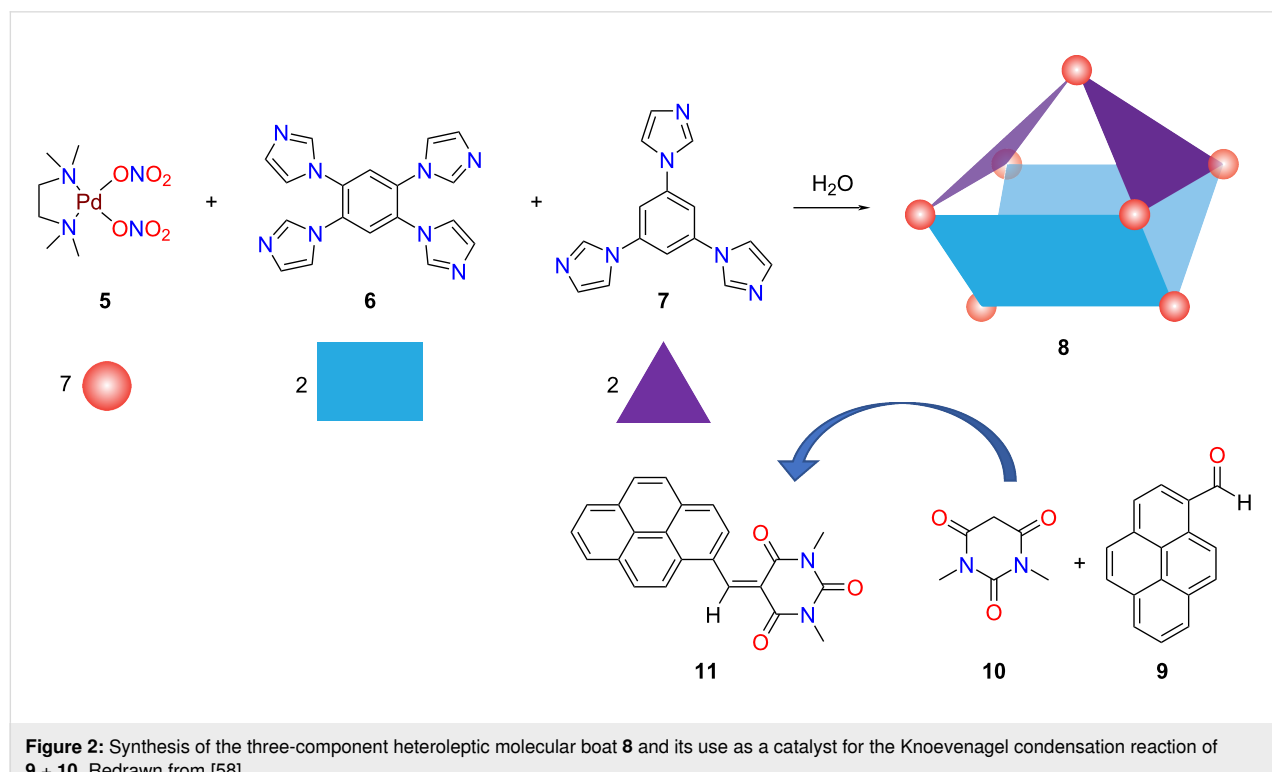


Figure 2: Synthesis of the three-component heteroleptic molecular boat **8** and its use as a catalyst for the Knoevenagel condensation reaction of **9** + **10**. Redrawn from [58].

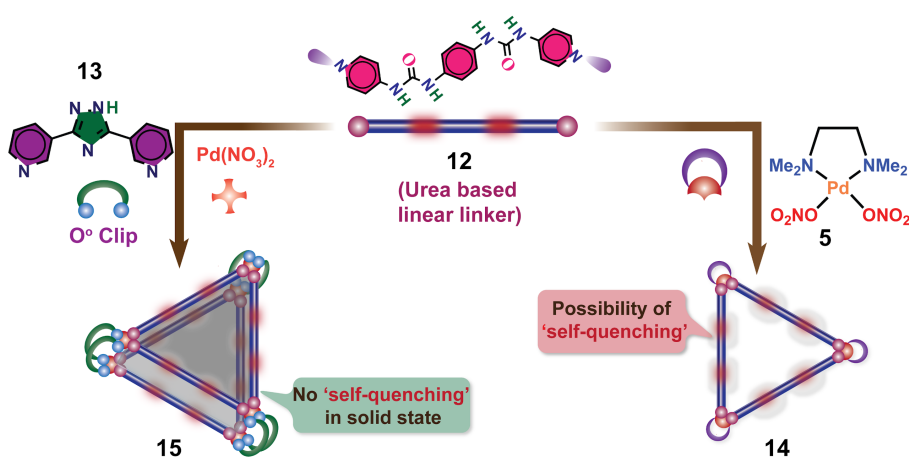


Figure 3: Synthesis of the two-component triangle **14** and three-component heteroleptic prism **15** [59]. Figure was adapted with permission from [59]. Copyright 2016 American Chemical Society. This content is not subject to CC BY 4.0.

$\text{Pd}(\text{NO}_3)_2$ was employed along with the triazole-based 0° clip **13**. In a one-pot reaction, **12** and **13** in DMSO were treated with $\text{Pd}(\text{NO}_3)_2$ in a 1:1:1 ratio, which entailed the quantitative formation of the edge-directed molecular prism **15** (Figure 3). The adequate length of the ditopic clip **13** constrained the urea triangle from intersupramolecular H-bonding. Thus, the urea moieties in this newly assembled 3D architecture were freely available for interactions with appropriate guest molecules through H-bonding. Different organic molecules, such as nitroolefins, capable of forming H-bonding with the urea moieties inside the cavity were investigated in water for their ability to encapsulate in the cavity under heterogeneous conditions. Successful binding of the guest molecule was proven by UV-vis and IR spectroscopy. The multicomponent prism (Figure 3) was finally utilized as a heterogeneous catalyst for Michael and Diels–Alder (DA) reactions in water, representing an uncommon hydrogen-bond donating heterogeneous catalyst [59]. Intrigued by the successful guest-inclusion, Michael reactions were performed with prism **15** (Figure 4). Generally, most

of the organocatalysts get destroyed during the work-up procedure, so that recovery is often difficult. However, in the present case the catalyst could be easily recovered, and multiple catalytic cycles could be performed.

Supramolecular systems based on non-covalent interactions have drawn considerable attention in assembling efficient light harvesting systems (LHSs) in the last decade [60,61]. Significant attention has been centered to construct artificial LHSs via FRET (fluorescence resonance energy transfer) that include organic materials and supramolecular assemblies. Recently, FRET phenomena have been successfully demonstrated in supramolecular architectures based on metal organic frameworks and covalent organic frameworks [62–64]. However, poor solubility of such polymeric systems in common solvents restricts their use in potential applications. In this aspect, coordination-driven discrete architectures provide a promising future due to their facile one-pot synthesis and high solubility in common solvents.

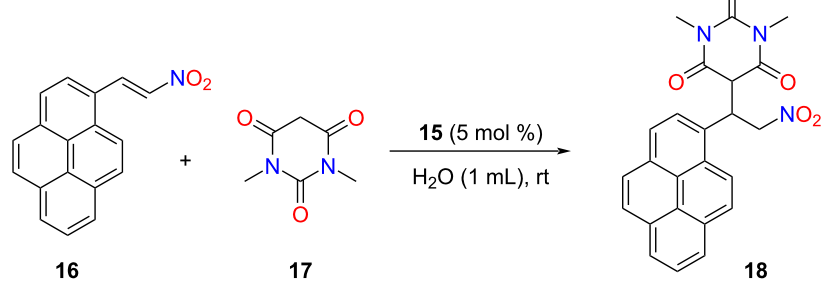


Figure 4: Catalytic Michael addition reaction using the urea-decorated molecular prism **15** [59].

Mukherjee and co-workers have developed supramolecular architectures containing tetraphenylethene (TPE) units which act as an aggregation-induced emissive (AIE) fluorophore [65]. The newly designed TPE-based tetraimidazole donor **19** has been treated with 180°/120° *trans*-Pt(II) acceptors which led to the coordination-driven self-assembly of 3D discrete molecular cages in aqueous medium (Figure 5). The 180° acceptor without an organic spacer, *trans*-[Pt(PEt₃)₂(ONO₂)₂] **20**, provided the cage **23a** with the molecular composition (20)₄(19)₂(NO₃)₈, whereas **21** (with a spacer unit) led to the formation of the Pt₈ cage **24a** = (21)₄(19)₂(NO₃)₈. In a similar fashion the bent 120° acceptor **22** also assembled into the Pt₈ cage **25a** = (22)₄(19)₂(NO₃)₈ [65]. Counter anion exchange from NO₃[−] to PF₆[−] made the cages soluble in acetonitrile. All three cages formed spherical supramolecular nano-aggregates in a water/acetonitrile (9:1) mixture and showed increased emission in the aggregated state [66]. Rhodamine B (**26**) was chosen as a FRET acceptor as there is a considerable overlap in energy of the donor emission and acceptor absorption. Then, artificial LHSs were constructed with aggregates from **24b** or **25b** at a donor/acceptor ratio of 5:1 (Figure 6). Finally, the light harvesting ma-

terials (**24b** + **26**) and (**25b** + **26**), respectively, were successfully employed as visible-light photocatalysts for a cross-coupling cyclization of *N,N*-dimethylaniline (**27**) and *N*-alkyl/aryl maleimides **28** (Figure 6). Notably, the systems showed much higher catalytic activity compared to similar reactions with the dye or cages alone.

Transition-metal catalysts play an important role for the development of intricate pharmaceutical drugs. Although transition-metal catalysts based on rhodium, cobalt, and palladium have been intensively studied, gold catalysis has received encouraging attention only recently [67,68]. Since selectivity of gold-catalyzed reactions is still a concern, the catalytic transformation is often controlled by introducing a ligand as a first coordination sphere of the active gold species. In a supramolecular approach, introduction of the ligated gold complex inside a hollow cage may significantly improve the reactivity and selectivity because the cage provides a second coordination sphere around the catalyst thus controlling the catalytic reaction. This idea has been impressively demonstrated by Reek [69], Ballester [70], and Raymond [71], where a single gold-based catalytic unit

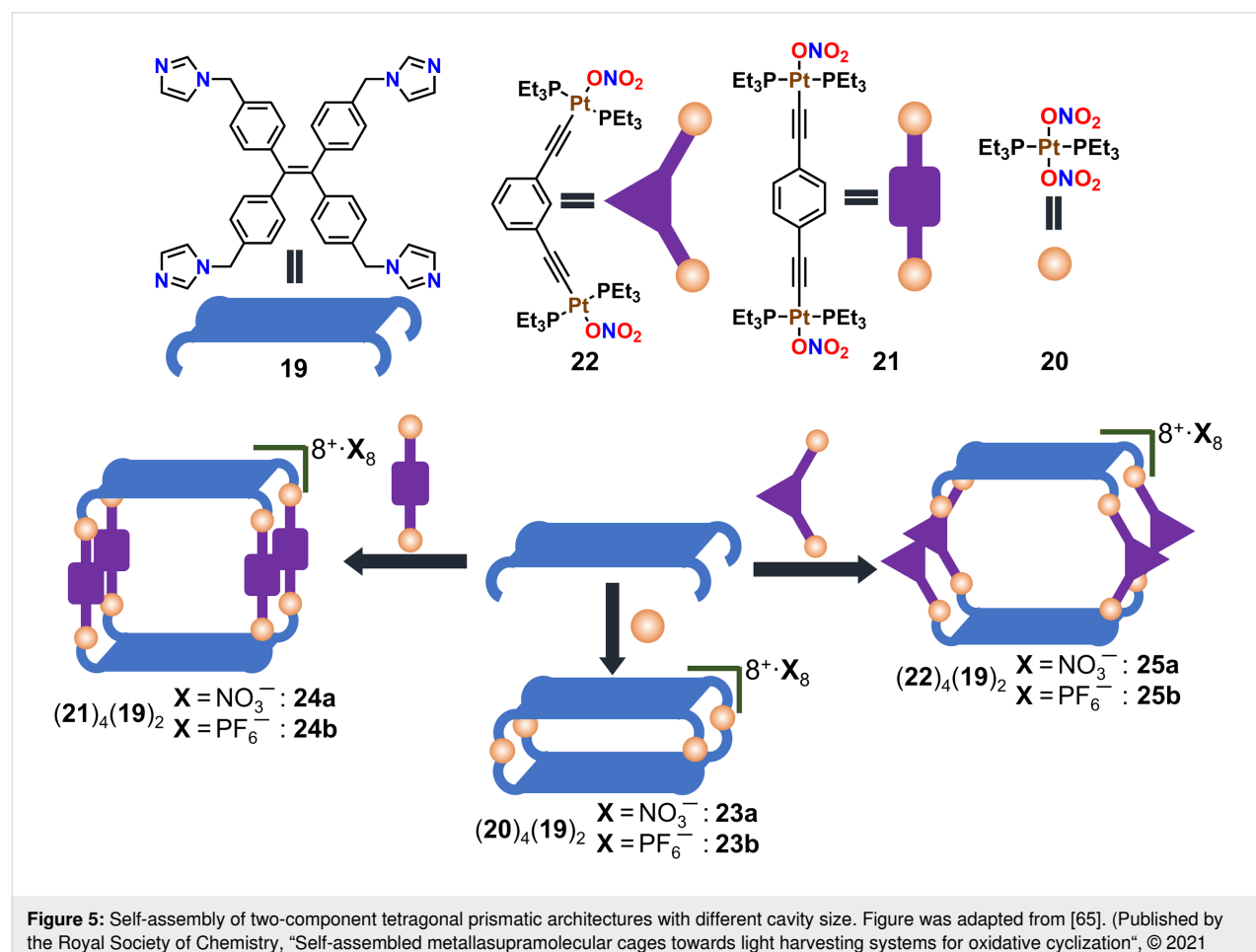


Figure 5: Self-assembly of two-component tetragonal prismatic architectures with different cavity size. Figure was adapted from [65]. (Published by the Royal Society of Chemistry, “Self-assembled metallasupramolecular cages towards light harvesting systems for oxidative cyclization”, © 2021 A. Kumar et al., distributed under the terms of the Creative Commons Attribution 3.0 Unported License, <https://creativecommons.org/licenses/by/3.0/>).

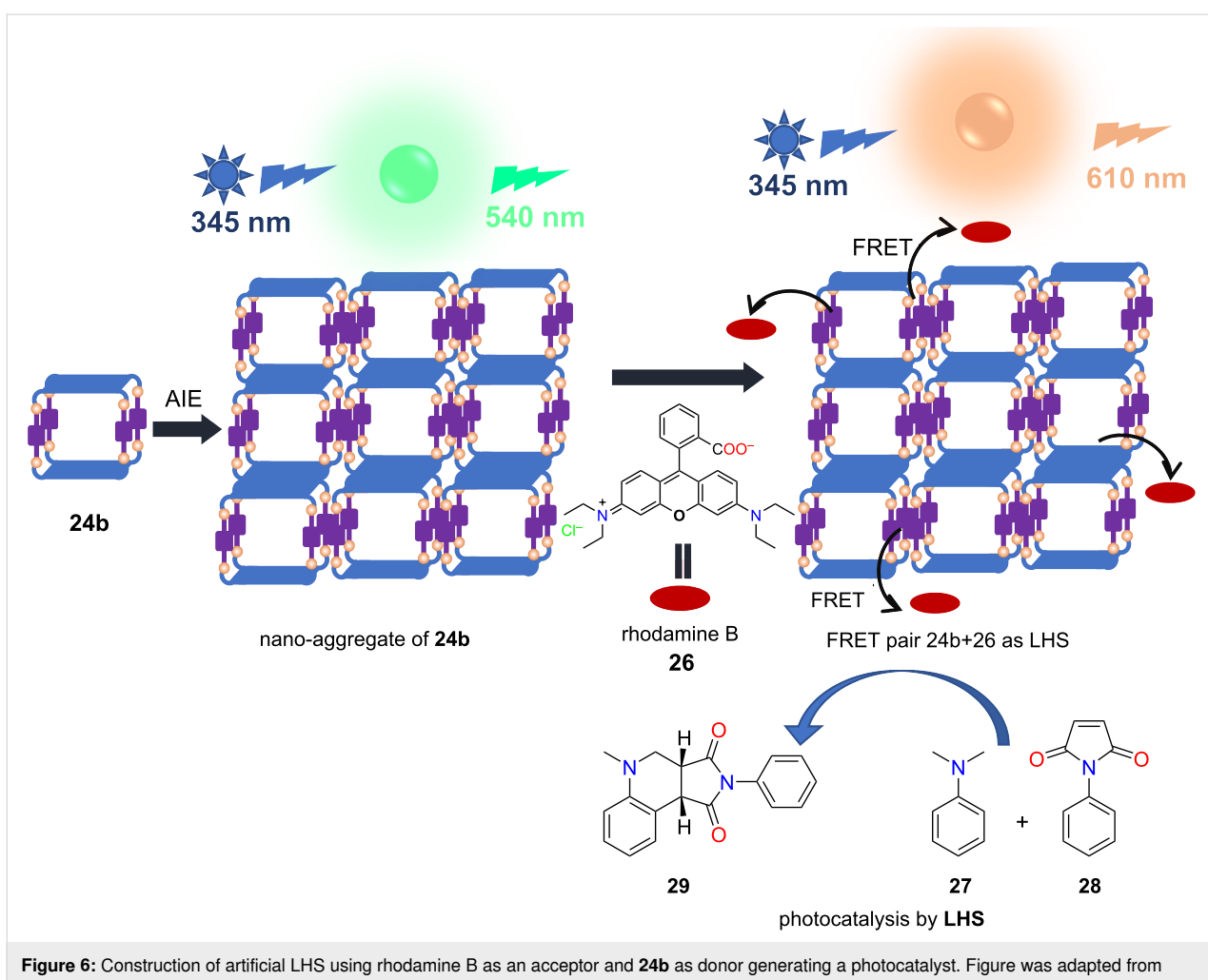


Figure 6: Construction of artificial LHS using rhodamine B as an acceptor and **24b** as donor generating a photocatalyst. Figure was adapted from [65]. (Published by the Royal Society of Chemistry, “Self-assembled metallasupramolecular cages towards light harvesting systems for oxidative cyclization”, © 2021 A. Kumar et al., distributed under the terms of the Creative Commons Attribution 3.0 Unported License, <https://creativecommons.org/licenses/by/3.0/>).

is encapsulated inside a molecular host to modulate the reactivity.

Recently, Reek and co-workers have constructed an $M_{12}L_{24}$ nanosphere by treating the bispyridyl 120° ligand **30** with a Pd(II) precursor [72]. Here, the ligand **30** is optimally functionalized with a phosphine gold(I) chloride moiety so that the metal catalyst will reside inside the sphere (Figure 7). In order to vary the local gold concentration inside the cavity, heteroleptic cages were assembled from a multicomponent one-pot reaction of Pd(II) with **30** and the analogous non-functionalized ligand **31**. By controlling the ratio of **30** and **31**, spheres with varying concentrations of AuCl could be constructed. Finally, the various spheres were investigated regarding the catalytic effect of the local gold concentration on the hydroalkoxylation of γ -allenol **34** (Figure 8). Since all catalytic tests were carried out at the same overall gold concentration of 5 mM, it was very interesting to observe that nanospheres with a very

low local gold concentration could not catalyze the reaction at all. Actually, product formation was observed only with nanospheres having a higher **30/31** ratio (>6:18). Surprisingly, only the formation of the five-membered ring product **35** was observed, with a maximum yield of 88% at the highest **30/31** ratio of 24:0. The system was benchmarked with the building unit **30** itself and Ph_3PAuCl where they observed a negligible conversion, which points toward the importance of local catalyst concentration.

A wide range of cavity-based artificial supramolecular catalysts has been successfully developed employing dynamic metal–ligand coordination bonds. While only a small fraction of these 3D architectures was useful for chiral catalysis, an even smaller fraction was able to provide a high stereoselectivity during asymmetric catalysis [5]. For instance, an enantiopure tetrahedral Pt_{12} cage has been previously studied for catalytic Michael addition reactions, but no enantioselectivity was

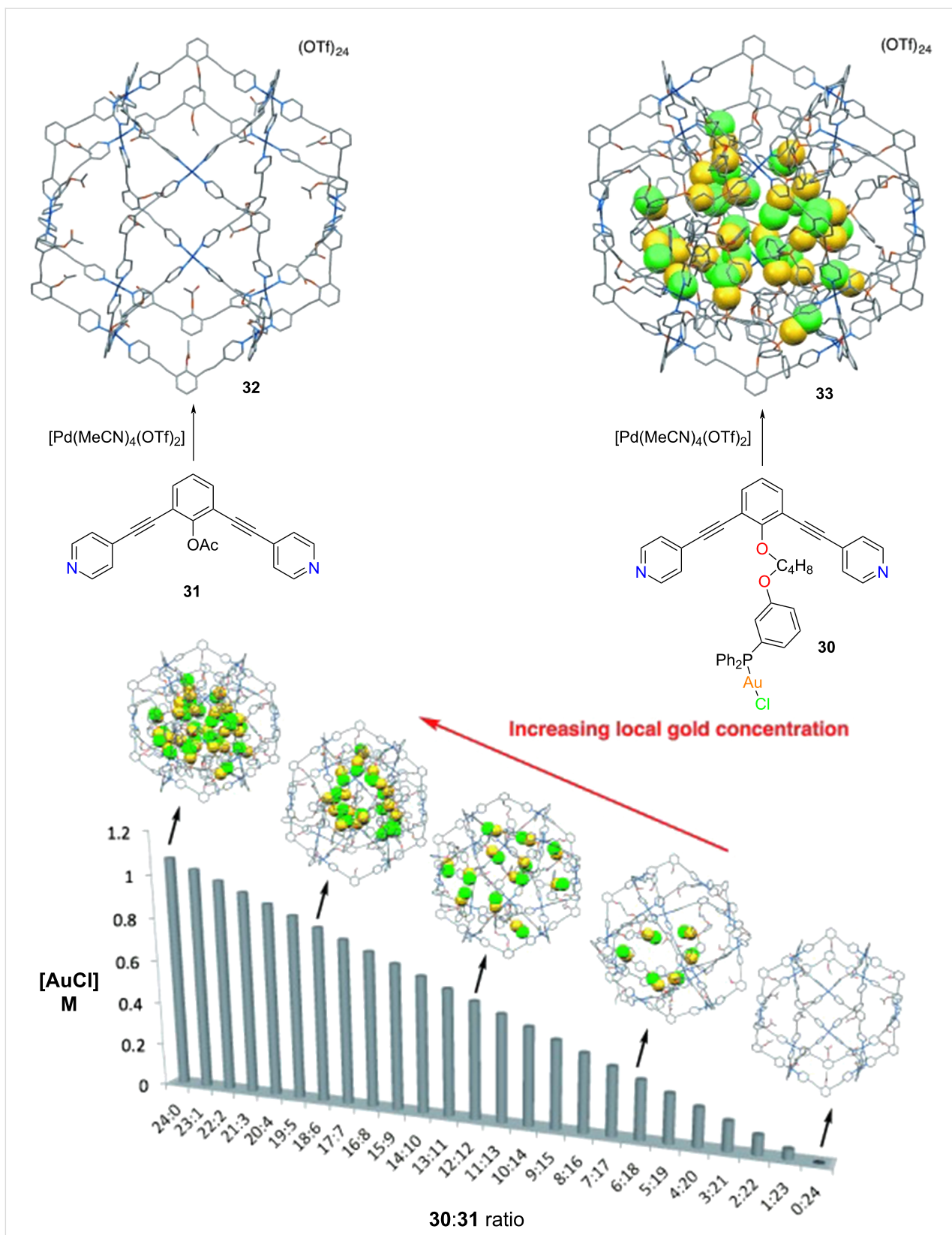


Figure 7: Synthesis of supramolecular spheres with varying $[\text{AuCl}]$ concentration inside the cavity. Figure was adapted from [72], R. Gramage-Doria et al., "Gold(I) Catalysis at Extreme Concentrations Inside Self-Assembled Nanospheres", *Angewandte Chemie, International Edition*, with permission from John Wiley and Sons. Copyright © 2014 Wiley-VCH Verlag GmbH & Co. KGaA, Weinheim. This content is not subject to CC BY 4.0.

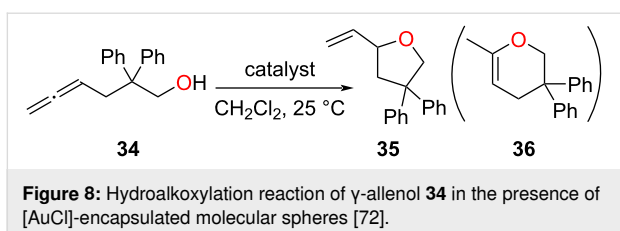


Figure 8: Hydroalkylation reaction of γ -allenol **34** in the presence of $[\text{AuCl}]$ -encapsulated molecular spheres [72].

detected because the chiral building blocks were located at peripheral positions thus not sufficiently breaking symmetry within the cavity [73]. Therefore, it was envisioned that the chiral moiety should be incorporated in the ligand unit in order to provide an enantiopure assembly with an asymmetric cavity. 1,1'-Binaphthol (BINOL) is one such chiral building block, which has been successfully utilized to carry out numerous asymmetric catalytic reactions [74]. Keeping this in mind, Stang

and co-workers constructed heteroleptic triangles via the assembly of a BINOL-based ditopic ligand and 180° *trans*-Pt(II) acceptors. The 3,3'-dipyridyl-substituted chiral BINOL donor (*S*)-**37** has a bite angle of 60° and when treated with linear 180° acceptors **38** and **39**, it produced the differently sized triangles (*S*)-**40** and (*S*)-**41** depending on the length of the organic spacer in the acceptor unit (Figure 9) [75].

Since the interior cavity of the homochiral macrocycles was equipped with BINOL units, they were utilized as catalysts for the asymmetric conjugate addition of chalcone **42** with *trans*-styrylboronic acid (**43**, Figure 10). The catalytic reaction inside the chiral cavity of (*S*)-**40** provided a yield up to 91% with a very high enantioselectivity (94% ee). In contrast, the larger chiral macrocycle (*S*)-**41** afforded a slightly lower catalytic activity (87%), however, at a similar enantioselectivity (94% ee).

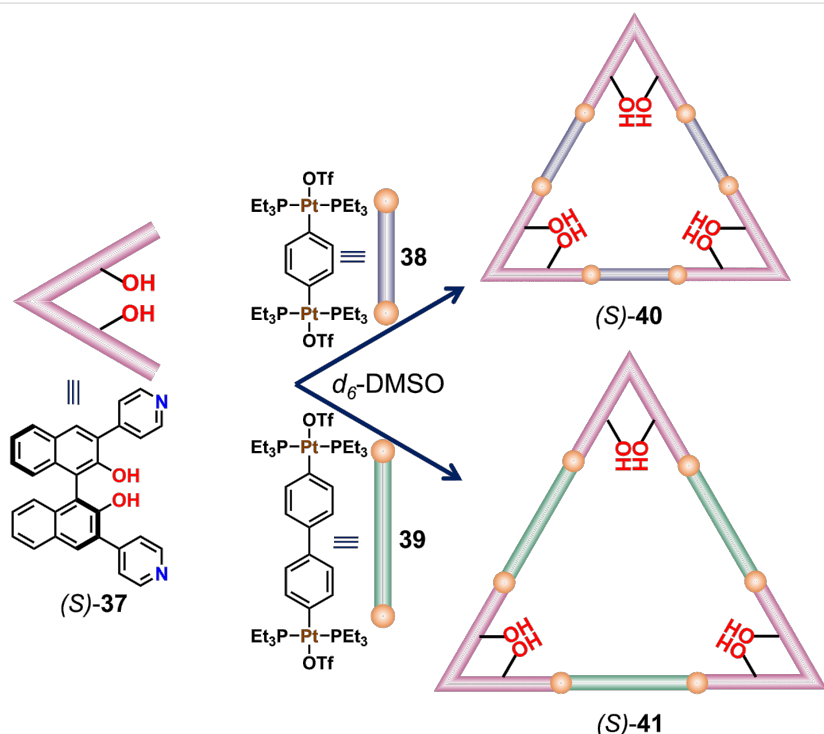


Figure 9: Two-component heteroleptic triangles of different size containing a BINOL functionality. Figure was adapted with permission from [75]. Copyright 2020 American Chemical Society. This content is not subject to CC BY 4.0.

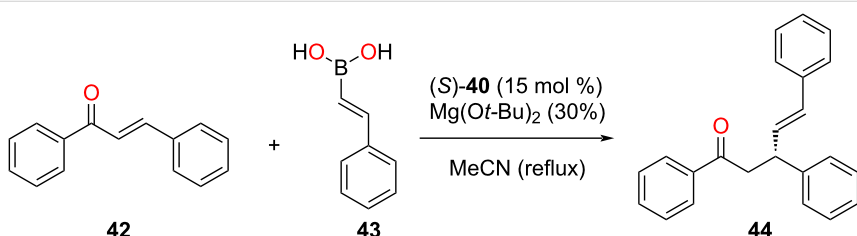


Figure 10: Asymmetric conjugate addition of chalcone **42** with *trans*-styrylboronic acid (**43**) catalyzed by BINOL-functionalized triangle (*S*)-**40** [75].

Using similar reaction conditions, the non-assembled BINOL derivative (*S*)-3,3'-dibromo-[1,1'-binaphthyl]-2,2'-diol acted as a superior catalyst (99% yield) but achieved a lower enantioselectivity (84% ee). Therefore, this result indicates that the incorporation of multiple catalytic sites and an appropriate asymmetric cavity is the key for the enhancement of catalytic activity and stereoselectivity [75].

Strictly speaking, the above example does not contain fully dynamic heteroleptic metal fragments, as the aryl–Pt bond is not kinetically labile. Nevertheless, the example illustrates the opportunities in running enantioselective catalysis in mixed-ligand frameworks.

Instead of constructing supramolecular catalysts by functionalization of the linker units, a different approach can be adopted where a catalytically active molecule is encapsulated inside a confined space, as demonstrated by Reek and co-workers by using a previously reported heteroleptic bisporphyrin cage [76]. The tetragonal prismatic nanocage **47** consisted of two zinc-porphyrin units along the two tetragonal faces (Figure 11), which allowed encapsulation of the chiral phosphoramidite **48** as a precursor for the final catalyst. In the next step, a transition-metal-ion based catalyst was prepared *in situ* by addition of one

equiv of $[\text{Rh}(\text{acac})(\text{CO})_2]$, which generated the monoligated rhodium complex. Finally, catalysis was carried out at 5 bar of H_2/CO (1:1) that converted the $[\text{Rh}(\text{acac})(\text{CO})_2]$ complex into the active hydride species **49** that is well known for hydroformylation reactions [77]. Incorporation of the monoligated catalyst into the confined cavity of the capsule showed very good catalytic activity towards the hydroformylation of styrene (**50**, Figure 11) with a high stereoselectivity (65% ee) at 32% conversion compared to the non-encapsulated catalyst, which only managed to yield 8% ee at 4% of conversion. Thus, the molecular capsule **47** can be viewed as a second coordination sphere of the catalyst, reminiscent of enzymatic active sites.

In summary, the above discrete molecular architectures containing cavity and sometimes smart functionality describe a new class of supramolecular catalysts that are effective tools to control the activity and selectivity of organic transformations. Clearly, building heteroleptic assemblies provides an unprecedented flexibility towards controlling the dimension as well as functionality. For instance, a particular catalytic reaction can be efficiently carried out by choosing a specific functionality. The functional entity responsible for catalysis can either be incorporated with the building blocks, or the catalyst itself may be

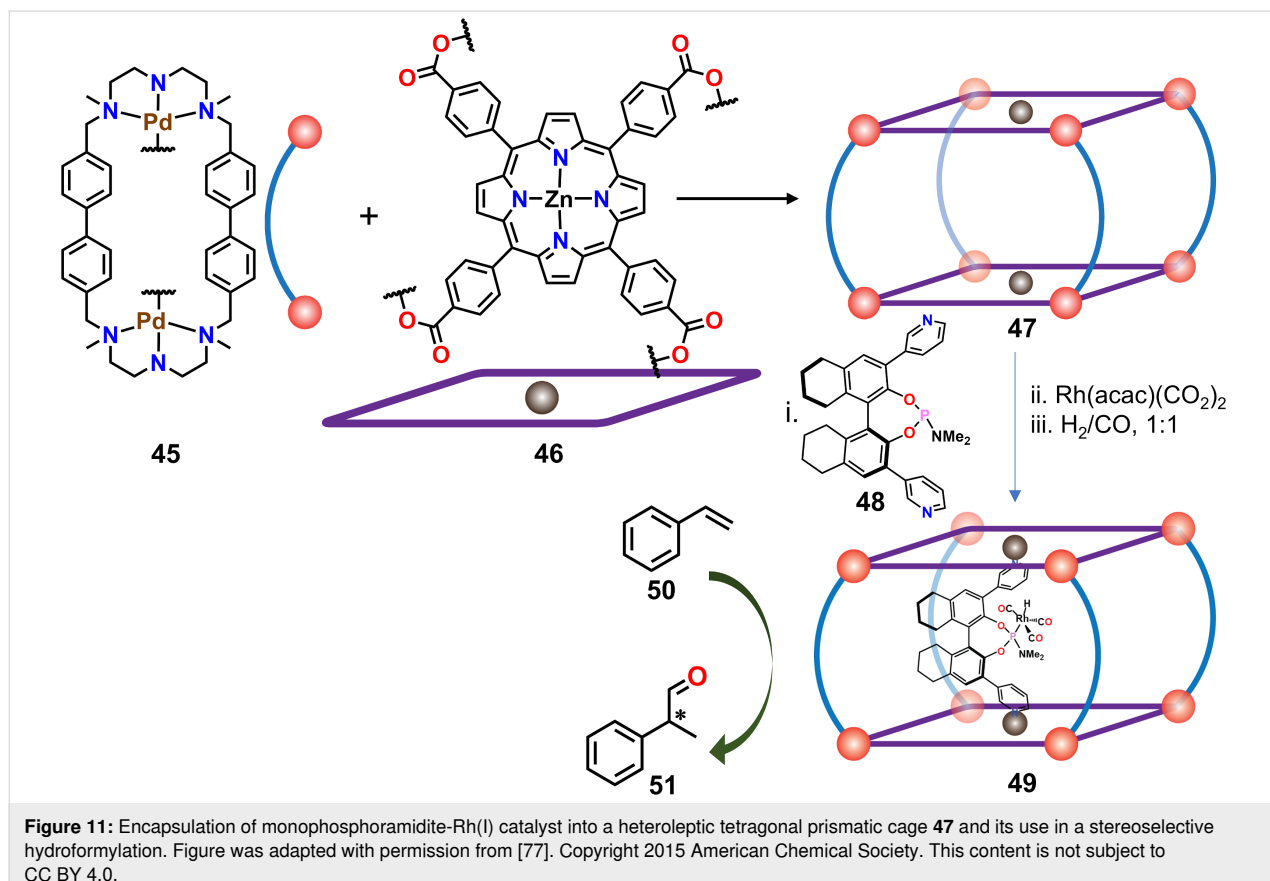


Figure 11: Encapsulation of monophosphoramidite-Rh(I) catalyst into a heteroleptic tetragonal prismatic cage **47** and its use in a stereoselective hydroformylation. Figure was adapted with permission from [77]. Copyright 2015 American Chemical Society. This content is not subject to CC BY 4.0.

encapsulated into the cavity. Unfortunately, the examples of heteroleptic cages acting as catalysts are limited so that further development is urgently needed.

Catalytic effects due to nanomechanical motion

The above examples have demonstrated the potential of heteroleptic cages to enable catalysis under various conditions. In this subchapter, the role of the cage/architecture depends on its dynamics: the catalytic activity will correlate with the rate of thermal motion. As illustrated below, there are presently two phenomena known where continuous nanomechanical motion influences the catalytic activity: a) Increasing nanomechanical speed reduces product inhibition, and b) higher nanomechanical speed enlarges catalyst liberation.

While the development of multicomponent rotors has started almost 20 years ago with seminal works by Shionoya [78–80] and Kume [81,82], the fascinating prospects of discrete nanomechanical motion was impressively demonstrated by Aida with the development of multicomponent tweezers [83,84]. Using a variety of orthogonal complexation motifs, the Schmittel group has developed over the past five years a general approach to multicomponent rotors that relies on the binding difference found in the HETPYP (HETeroleptic PYridine and Phenanthroline complexes [85,86]), HETPHEN (HETeroleptic bisPHENanthroline complexes [87]) and HETTAP (HETeroleptic Terpyridine And Phenanthroline complexes

[88]) interactions (Figure 12). Due to the different amount of donor atoms about the metal ion, the binding strength will decrease in the series of HETTAP > HETPHEN > HETPYP [37]. In any dynamic system designed for exchange motion predictably the weakest interaction will be the most dynamic one. This protocol is quite generally applicable and is readily illustrated by the ensuing example. The three-component rotor **52** = $[\text{Zn}(\mathbf{53})(\mathbf{54})]^{2+}$ was developed on the basis of two complexation events, i.e., the zinc(II) HETTAP ($\log \beta = 14$, $\log K_1 \geq 6$) and $N_{\text{py}} \rightarrow \text{ZnPor}$ ($\log K = 4.45$) binding motifs (Figure 12) [89]. Due to the design of **52**, the pyridine terminal oscillates between the two degenerate zinc porphyrin (ZnPor) stations of **53** at $k_{298} = 24$ kHz (at 298 K).

A similar exchange process was observed in the four-component rotors [90] developed along two orthogonal self-sorting motifs ($\text{HETPYP} = N_{\text{py}} \rightarrow [\text{Cu}(\text{phenAr}_2)]^+$ and $N_{\text{DABCO}} \rightarrow \text{ZnPor}$ interactions). Again, the synthetic approach is a straightforward multicomponent self-sorting assembly. Accordingly, the distinct zinc porphyrins **55** and **57** were positioned at a defined distance through two $N_{\text{DABCO}} \rightarrow \text{ZnPor}$ interactions. Clearly, without additional measures, homo- and heteromeric assemblies would form. However, due to the additional HETPYP interaction(s) in the presence of copper(I) ions, thermodynamic stabilization quantitatively drives the reaction to the hetero-assembly **59**, simply by mixing the components in the correct stoichiometric ratio (Figure 13). Various nanorotor assemblies are possible by this approach.

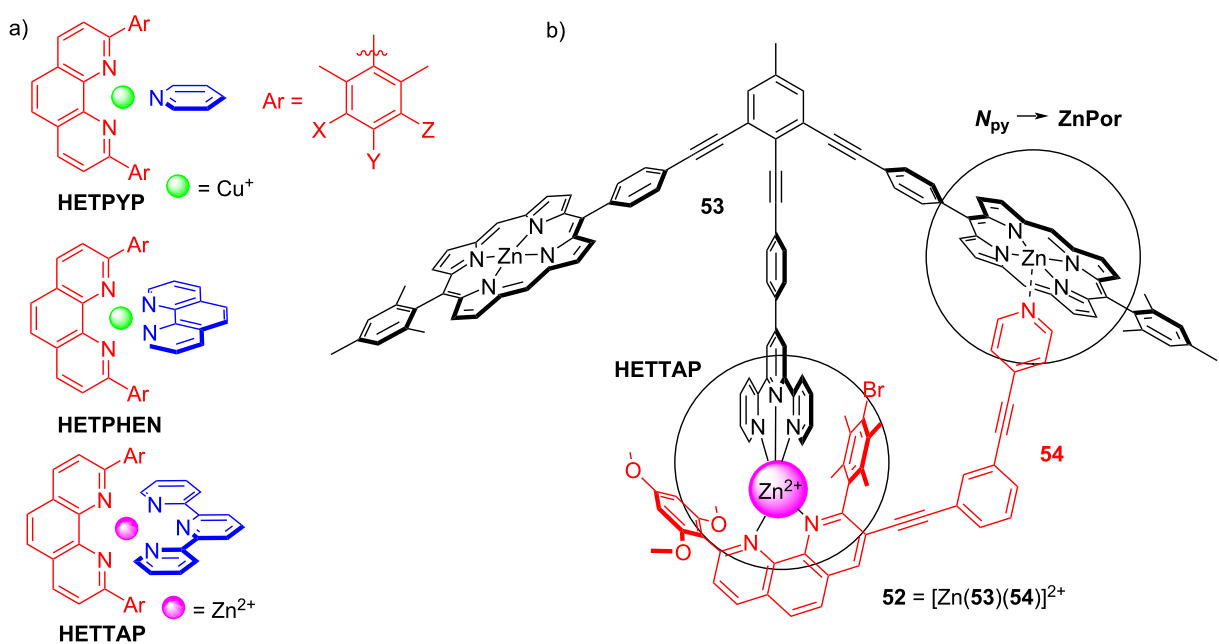


Figure 12: (a) Representations of the basic HETPYP, HETPHEN, and HETTAP complex motifs. (b) The three-component rotor **52** built on zinc(II) HETTAP and $N_{\text{py}} \rightarrow \text{ZnPor}$ coordination motifs [89].

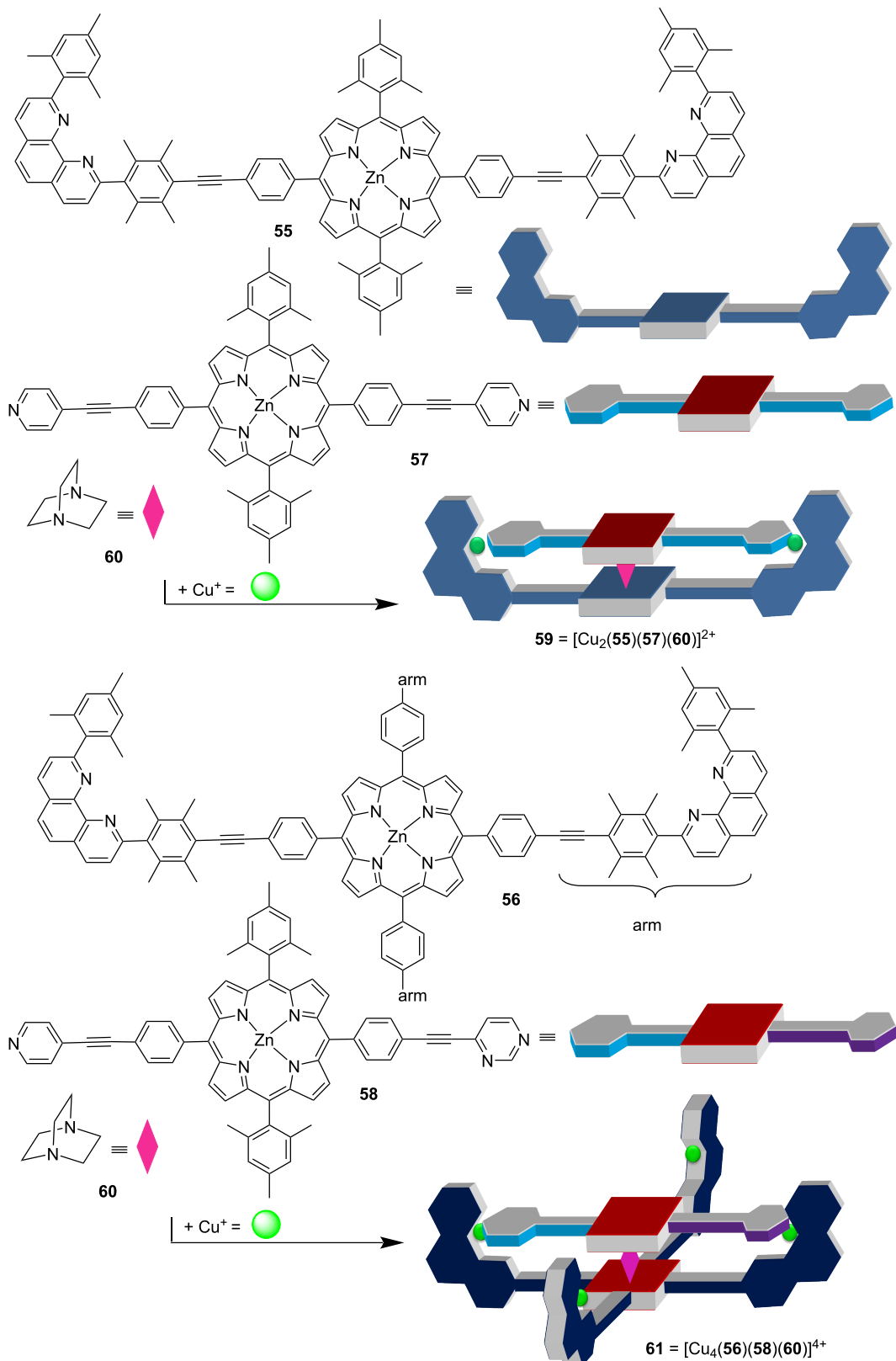


Figure 13: Two representative four-component rotors, with a (top) two-arm stator and (bottom) a four-arm stator. Figure was adapted with permission from [90]. Copyright 2013 American Chemical Society. This content is not subject to CC BY 4.0.

The dynamics of the four-component rotor **59** = $[\text{Cu}_2(\text{55})(\text{57})(\text{60})]^{2+}$ cannot be resolved due to the high symmetry in both the rotator and stator [91]. However, when rotator **58** with two different terminals was used then the rotational speed could be measured using VT ^1H NMR [90]. Over the years, both the stator and the rotators were varied over a wide range, i.e., see **61**, changing the geometrical or constitutional situation at the binding sites [92]. In a detailed recent study, the finding of a Hammett correlation in such nanorotors corroborated that a rate-determining dissociation at the rotator–metal binding interaction dictated the rotational speed [93].

Reducing Product Inhibition (RPI) through nanomechanical motion. Recently, the suitability of the four-component rotors to act as catalysts in various click reactions was investigated having a look at nanorotors $[\text{Cu}_2(\text{55})(\text{60})(\text{X})]^{2+}$ (with $\text{X} = \text{62, 63 or 64}$), revealing an unexpected correlation between their rotational speed and catalytic activity [94] (Figure 14). Because in any moment of the rotation there should at least one copper(I) phenanthroline be freed from contact with the monodentate rotator X , one would expect that the temporarily exposed copper(I) ions are catalytically active. It is important to

note that this copper ion due to steric impediments at the phenanthroline site will not engage in complexation with a second phenanthroline (see HETPYP concept [85,86]).

The concept was probed by using nanorotors $[\text{Cu}_2(\text{55})(\text{60})(\text{X})]^{2+}$ as catalyst (10 mol %) for the click reaction of 9-(azidomethyl)anthracene (**65**) and (prop-2-yn-1-yloxy)benzene (**66**) at 55 °C (4 h) [94]. Notably, the fastest nanorotor $[\text{Cu}_2(\text{55})(\text{60})(\text{64})]^{2+}$ afforded the highest yield of the click product **67** (62%) followed by nanorotors $[\text{Cu}_2(\text{55})(\text{60})(\text{63})]^{2+}$ (44%) and $[\text{Cu}_2(\text{55})(\text{60})(\text{62})]^{2+}$ (20%) (Figure 15). The analogous tendency was recognized in a second click reaction, using now reactants **68** and **69** furnishing **70**. Markedly, the yield of both click reactions was linearly correlated with the exchange speed of the catalytic nanorotors (Figure 15, right). With faster rotational exchange of the nanorotor both the measured rate of catalysis at time = zero, v_0 , and the catalytic yield increased in a linear fashion. Such a clear correlation asks for a convincing theory. A straightforward explanation is that higher rotational speed should lead to a reduction of product inhibition by kicking out the product bound at the catalytic copper center. As shown experimentally, only the copper(I) phenanthroline unit which is temporarily not occu-

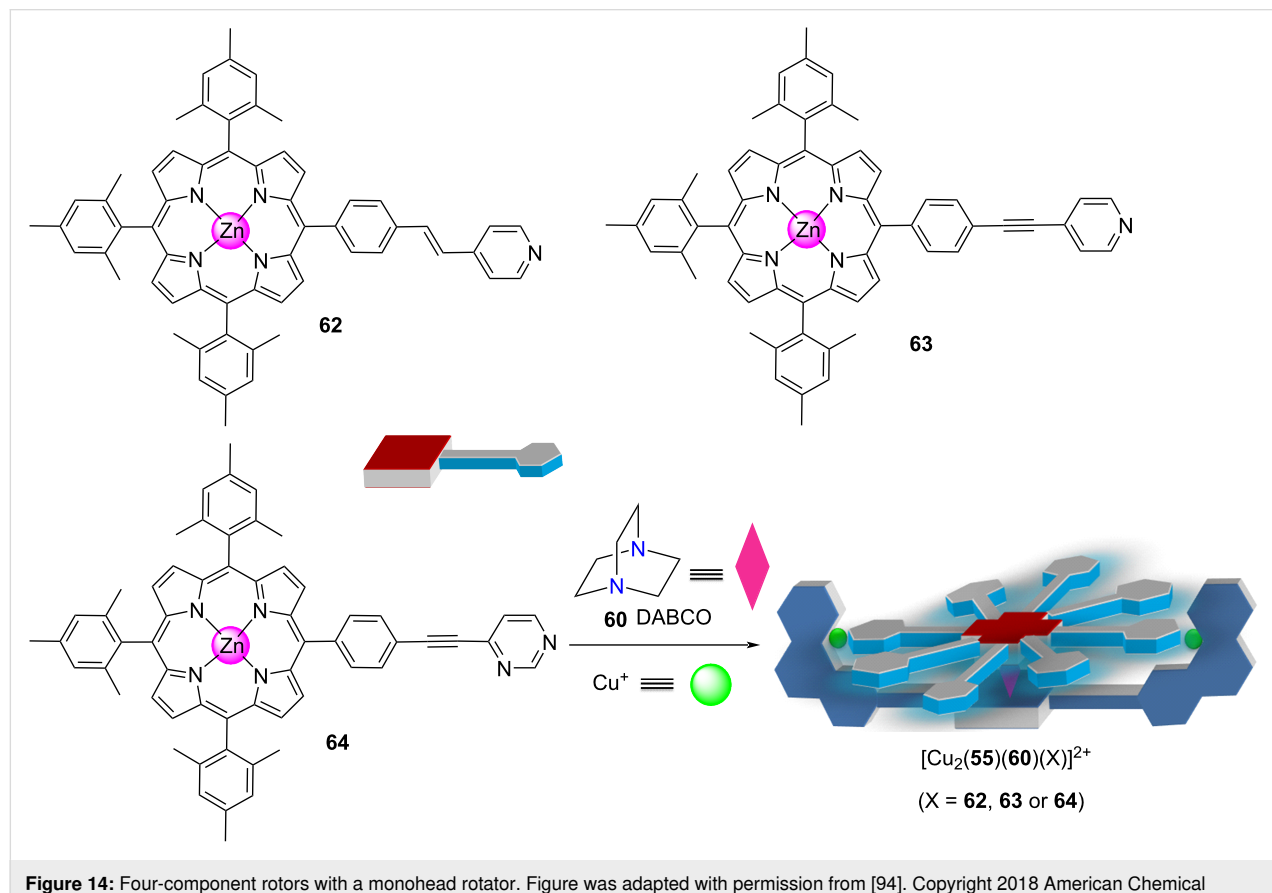


Figure 14: Four-component rotors with a monohead rotator. Figure was adapted with permission from [94]. Copyright 2018 American Chemical Society. This content is not subject to CC BY 4.0.

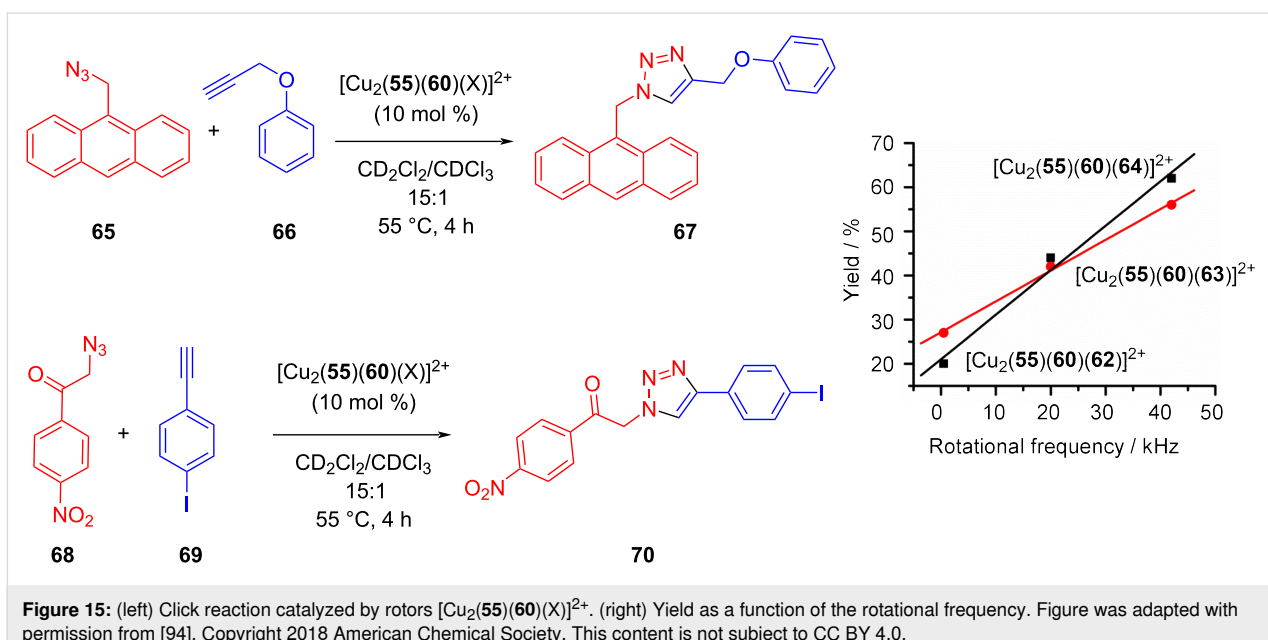


Figure 15: (left) Click reaction catalyzed by rotors $[\text{Cu}_2(55)(60)(X)]^{2+}$. (right) Yield as a function of the rotational frequency. Figure was adapted with permission from [94]. Copyright 2018 American Chemical Society. This content is not subject to CC BY 4.0.

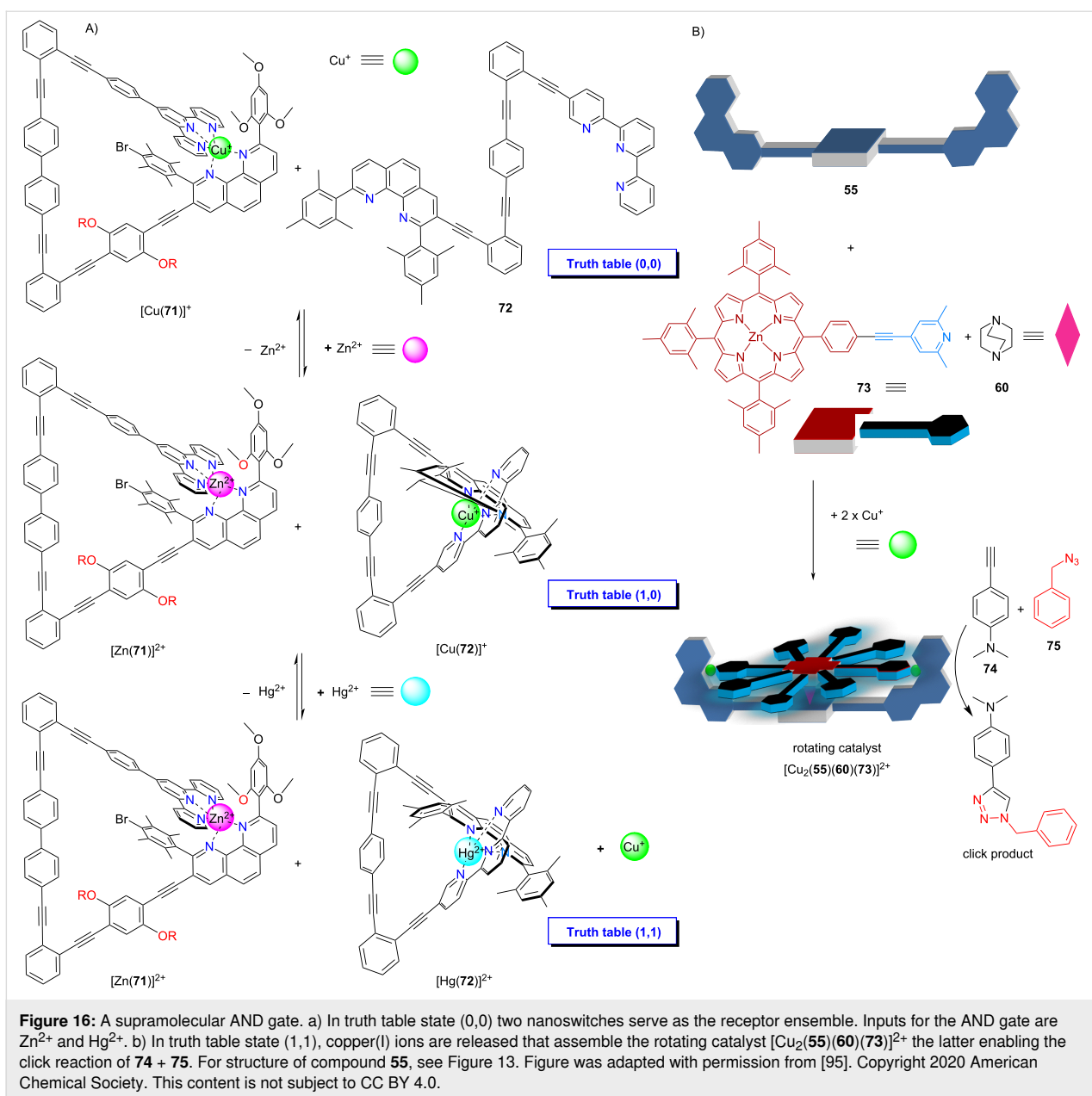
pied by the rotator head is catalytically active. Thus, when the rotator dissociates from the copper(I) phenanthroline and moves to the product-filled site it should liberate the product into solution. The increased liberation of product with increasing speed of the nanorotor was proven by independent experiments, and additionally it was demonstrated that a “static” reference catalyst showed only a turnover of 1 due to product inhibition.

The capacity of the four-component nanorotors to act as catalyst in click reactions was more recently utilized for setting up a multicomponent logic AND gate that required the networking of altogether twelve components (Figure 16) [95]. At the heart of the logic operation, the ensemble of the copper(I)-loaded nanoswitch $[\text{Cu}(71)]^+$ and ligand **72** was actuated by two metal-ion inputs (Zn^{2+} and Hg^{2+}) and generated a stoichiometric Cu^+ output according to the AND gate logic only in truth table state (1,1). The released copper(I) ions self-assembled the four-component rotor $[\text{Cu}_2(55)(60)(73)]^{2+}$ which enabled catalysis of a click reaction. In summary, copper(I) ions as stoichiometric output of the AND gate finally generated a catalytic output due to the assembly of a rotating four-component catalyst. Moreover, the AND gate could reversibly be reset into truth table state (0,0).

Like the nanorotors above, domino nanorotors with two exchanging rotational axes showed catalytic action that depended on the rotational speed [96]. Ligands **53** and **76** were conceived based on geometric complementarity at their coordination sites using the HETPYP interaction in both aggregates $[\text{Cu}_4(76)_2]^{4+}$ and **77** = $[\text{Cu}_2(53)(76)]^{2+}$ (Figure 17). The structure of **76** suggested that the dimeric parallelogram-type double

rotor $[\text{Cu}_4(76)_2]^{4+}$ with two antiparallel pyridyl head groups operating as axles would form. Again, it is important to stress that the coordinatively frustrated terminal $[\text{Cu}(\text{phenAr}_2)]^+$ units will not engage in complexation with a second phenanthroline due to steric control in the HETPYP concept [85,86]. Since at a given time, only one of both HETPYP-bound pyridines in $[\text{Cu}_4(76)_2]^{4+}$ can serve as axle, the rotor undergoes a domino rotation that was measured to occur at $k_{298} = 142$ kHz. For the heteromeric rotor $[\text{Cu}_2(53)(76)]^{2+}$, two orthogonal dynamic interactions are relevant, i.e., the weak $N_{\text{py}} \rightarrow \text{ZnPor}$ binding ($\log K = 4.3$) and the stronger copper(I) HETTAP linkage ($\log \beta = 9.3$). Ligand **53** with its terpyridine (tpy) and two ZnPor sites was designed in the way that the tpy should connect with **76** via a HETTAP binding motif while simultaneously allowing binding of the pyridine terminus of **76** to one of both ZnPor units of **53**. Now there are two motions possible that can only occur in a domino fashion. When the strong HETTAP complexation is intact, the exchange of the pyridine head of **76** between both ZnPor sites of **53** occurs at 64 kHz at rt. When the much stronger HETTAP complex dissociates, the much weaker $N_{\text{py}} \rightarrow \text{ZnPor}$ interaction remains intact and serves as a rotational axle, but now the exchange is slower by several orders of magnitude ($k_{298} = 0.55$ Hz).

The two rotors and reference complex $[\text{Cu}(78)]^+$ (Figure 17) were compared for their catalytic activity in the click reaction of **79** + **80** (Table 1), after normalizing for their different content of copper [96]. Reactants **79** and **80** were chosen, because their click product **81** should be a rather good chelate ligand leading to product inhibition. The data given in Table 1 indicate that the rotor $[\text{Cu}_2(53)(76)]^{2+}$ has basically the same catalytic activity as



a non-dynamic reference catalyst (turnover close to 1), because the exchange at the copper(I) sites preventing product inhibition is extremely slow ($k_{298} = 0.55$ Hz). The much faster rotation leading to an exchange of the $N_{py} \rightarrow ZnPor$ interaction is irrelevant for the catalysis. In contrast, the faster domino rotor $[Cu_4(76)_2]^{4+}$ produced far superior yields (Table 1). The different yields correlate with the distinct v_0 of the catalytic reaction. In conclusion, we see a clear trend in several rotating catalysts that with higher speed product inhibition is reduced (RPI).

Increased Liberation of Catalyst (ILC) through nanomechanical motion. While the previous and related examples [97] are based on a reduction of product inhibition (RPI) with

increasing speed of the rotating catalyst, there is a second general concept, i.e., ILC, for linking catalytic activity with the speed of a nanomechanical device. It is based on the increasing liberation of a bound organocatalyst with rising speed of the catalytic machinery. This concept was first realized in the slider-on-deck systems (**82**•X) (X = **83**, **84**, or **85**) (Figure 18) that were simply generated by mixing the tris-ZnPor deck **82** with one of the bipeds **83**–**85** (1:1) [98]. The thermal sliding speed of the biped across the deck **82** depends on the thermodynamic strength of the pyridine (or pyrimidine, methylpyridine) \rightarrow ZnPor interactions of the biped's feet with the ZnPor units. Obviously, weaker binding to ZnPor should lead to faster sliding [17].

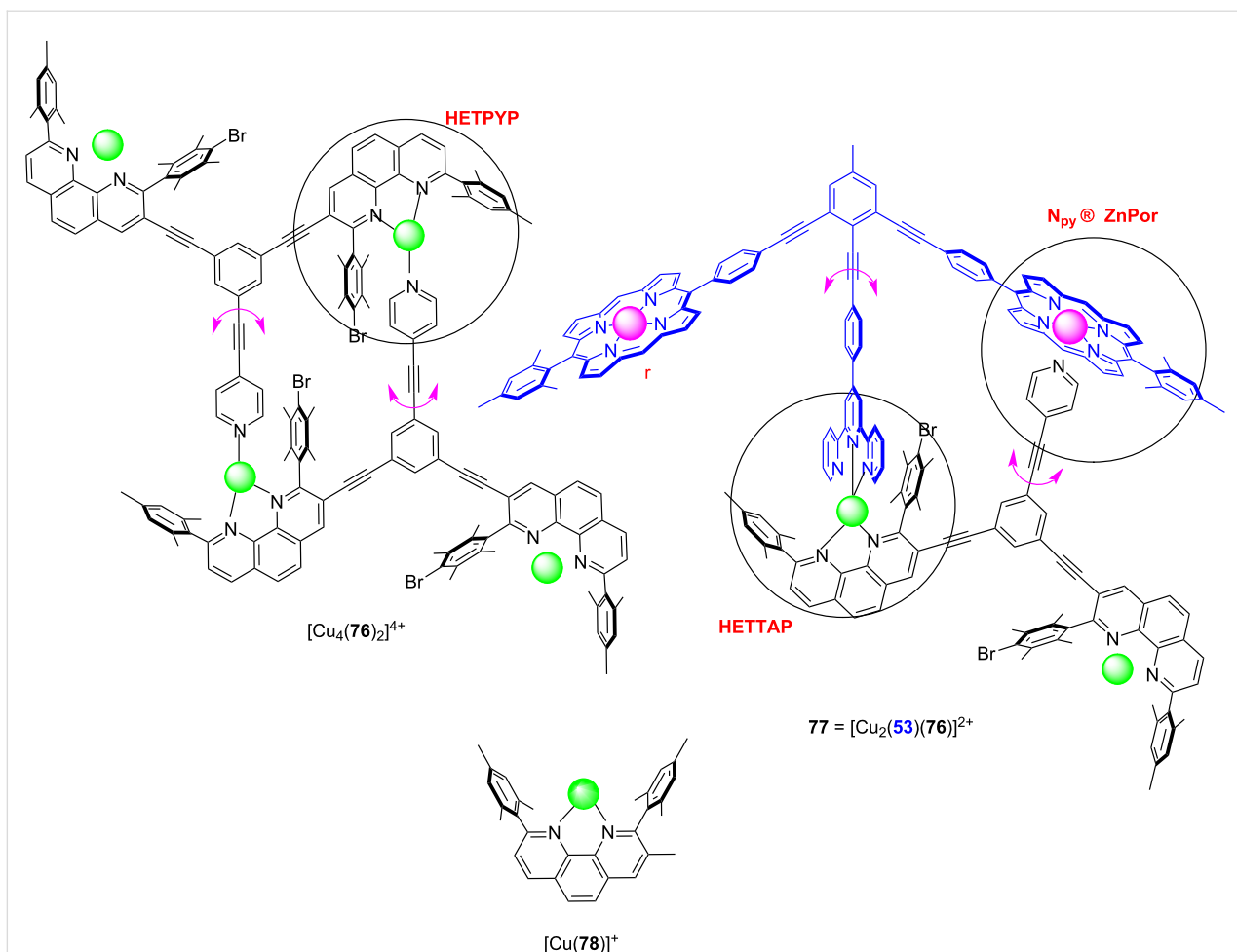


Figure 17: Two supramolecular double rotors (each has two rotational axes) and reference complex $[\text{Cu}(78)]^+$ for catalysis. Figure is a derivative work from [96]. (Published by Wiley-VCH Verlag GmbH & Co. KGaA, Weinheim, © 2020 Goswami, A.; Schmittel, M. distributed under the terms of the Creative Commons Attribution 4.0 International License, <https://creativecommons.org/licenses/by/4.0/>).

Table 1: Yield of click product **81** using different catalysts [96]. Fast rotation leads to high yield.

$\text{O}_2\text{N}-\text{C}_6\text{H}_3(\text{NO}_2)-\text{C}(=\text{O})-\text{CH}_2-\text{N}_3$ 79		$+\text{C}_6\text{H}_5\text{C}\equiv\text{C}-\text{C}_6\text{H}_5$ 80	$\xrightarrow[\text{50 } ^\circ\text{C}]{\text{cat.}}$	$\text{O}_2\text{N}-\text{C}_6\text{H}_3(\text{NO}_2)-\text{C}(=\text{O})-\text{CH}_2-\text{N}=\text{N}-\text{C}_6\text{H}_5$ 81
catalyst	speed [Hz]		yield of 81 ^a	$v_0 [\text{mol L}^{-1} \text{s}^{-1}]$
$[\text{Cu}_4(76)_2]^{4+}$	142×10^3		63%	4.2×10^6
$[\text{Cu}_2(76)(77)]^{2+}$	0.55		28%	1.8×10^6
$[\text{Cu}(78)]^+$ (static ref.)	0		26%	1.4×10^6

^aYields determined from 3 independent runs.

With one of the three ZnPor units being available for the attachment (immobilization) of an organocatalyst, we wondered about the catalytic activity of the dynamic three-component ensembles **89**•(**82**•X) using *N*-methylpyrrolidine (**89**) as organocata-

lyst. For assessment, the conjugate addition of **86** and **87** was studied at different temperatures for 4 h (Figure 19). In comparison with the static reference system **89**•**90** (no yield at 50 °C), there was a clear trend for higher yields (Table 2) the faster the

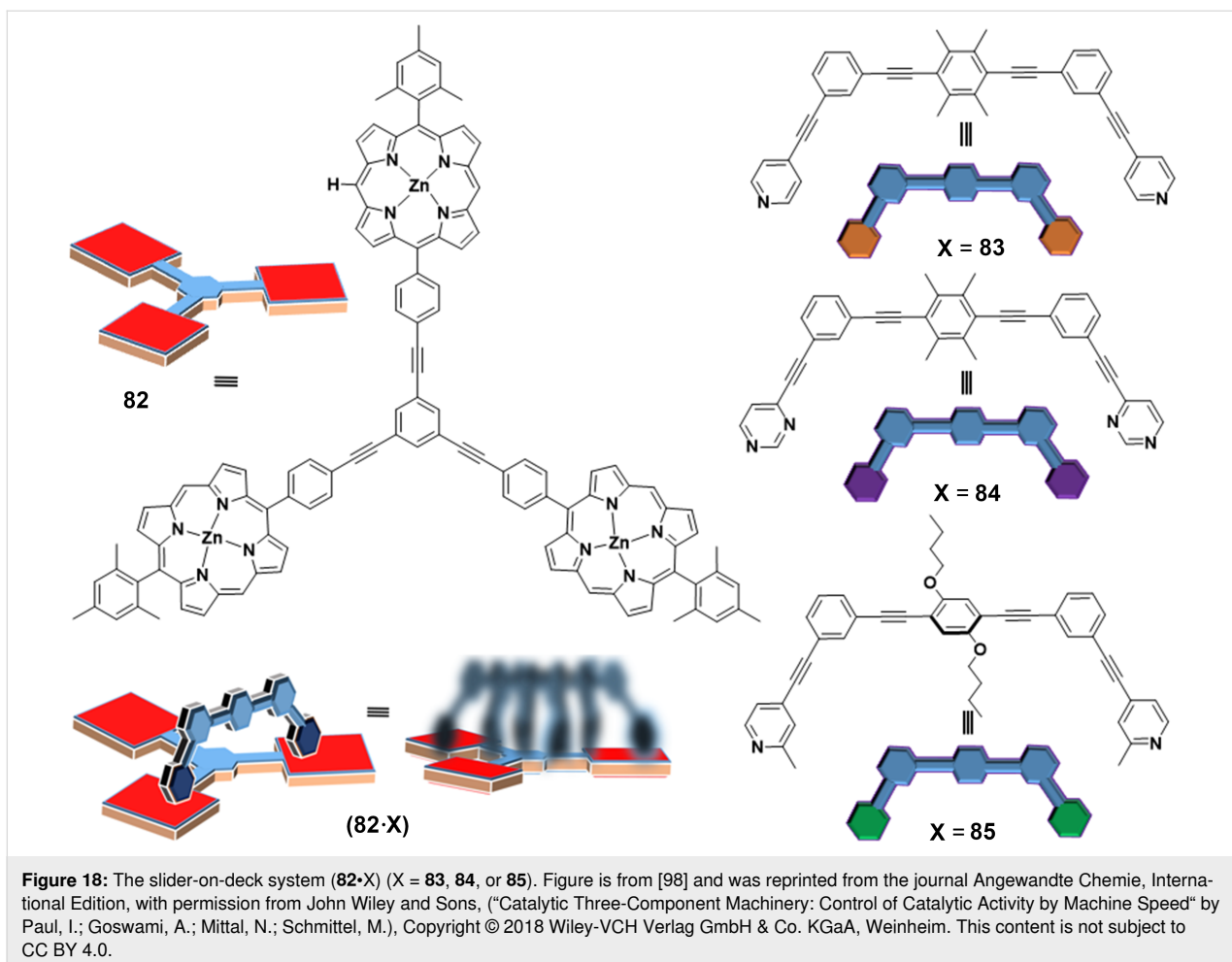


Figure 18: The slider-on-deck system ($82 \cdot X$) ($X = 83, 84$, or 85). Figure is from [98] and was reprinted from the journal Angewandte Chemie, International Edition, with permission from John Wiley and Sons, (“Catalytic Three-Component Machinery: Control of Catalytic Activity by Machine Speed” by Paul, I.; Goswami, A.; Mittal, N.; Schmittel, M.), Copyright © 2018 Wiley-VCH Verlag GmbH & Co. KGaA, Weinheim. This content is not subject to CC BY 4.0.

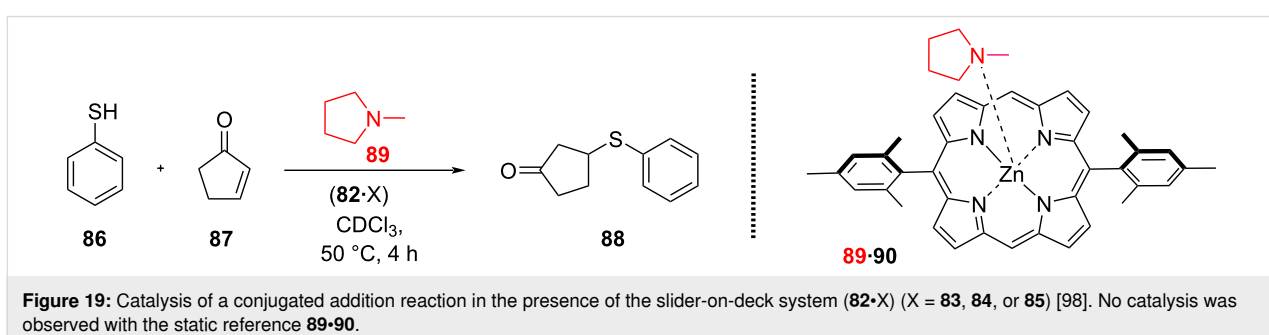


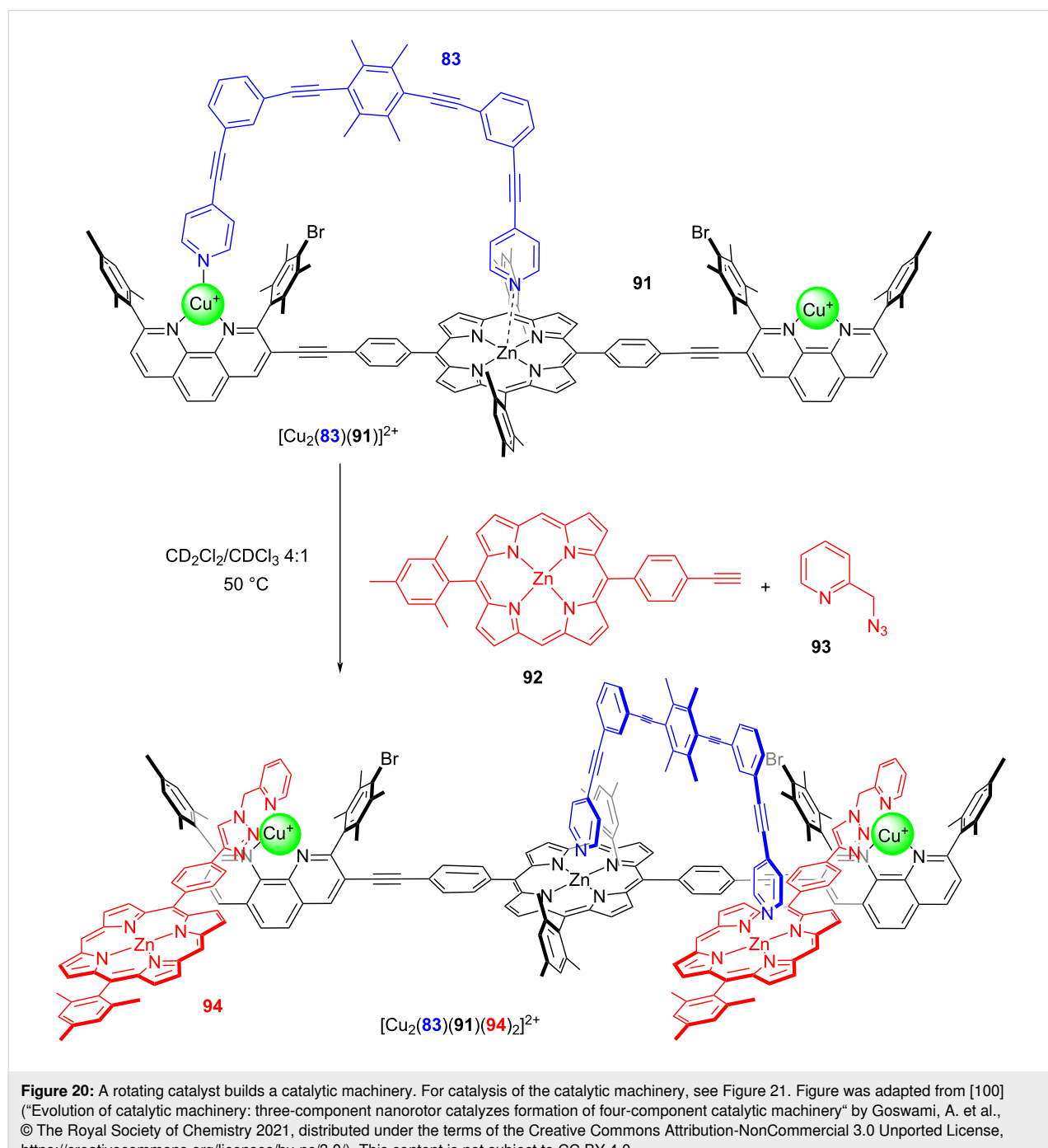
Figure 19: Catalysis of a conjugated addition reaction in the presence of the slider-on-deck system ($82 \cdot X$) ($X = 83, 84$, or 85) [98]. No catalysis was observed with the static reference $89 \cdot 90$.

Table 2: Activation data (sliding motion) of the slider-on-deck systems ($82 \cdot X$) ($X = 83, 84$, or 85) [98] and their performance in catalyzing the formation of 88 in presence of catalyst 89 (see Figure 19).

Slider-on-deck	($82 \cdot 83$)	($82 \cdot 84$)	($82 \cdot 85$)
ΔH^\ddagger [kJ mol $^{-1}$]	54.7 ± 0.5	45.5 ± 0.6	42.9 ± 0.6
ΔS^\ddagger [J mol $^{-1}$ K $^{-1}$]	24.8 ± 2.2	10.1 ± 2.5	7.5 ± 2.5
ΔG^\ddagger_{298} [kJ mol $^{-1}$]	47.3	42.5	40.7
k_{298} [s $^{-1}$]	32.2×10^3	220×10^3	440×10^3
yield of 88 [%]	18 ± 2	32 ± 2	50 ± 2
liberated cat. 89	29%	48%	76%

exchange process in the slider-on-deck is: system **89**•(**82**•**83**) furnished (18 ± 2)%, **89**•(**82**•**84**) afforded (32 ± 2)%, and **89**•(**82**•**85**) provided (50 ± 2) of **88** at 50 °C after 4 h. Control experiments uncovered that product formation was kinetically controlled and that the slider-on-deck systems on their own were catalytically silent. With various controls one could demonstrate that the effect on catalysis in the catalytic machinery was due to kinetic and not thermodynamic reasons (Figure 19).

While the concept of increased liberation of an organocatalyst (ILC) has been demonstrated in other dynamic nanomechanical systems as well [99], a particular highlight was recently realized with a catalytic nanorotor that was able to build a new catalytic machinery [100]. Hereunto, the two concepts RPI and ILC were combined in a synergistic manner, starting with rotor $[\text{Cu}_2(\mathbf{83})(\mathbf{91})]^{2+}$ ($k_{298} = 46.0$ kHz) that catalyzed the click reaction between the zinc porphyrin ligand **92** and the azide **93** furnishing triazole **94** (Figure 20). As it was possible to drive



this reaction to completion and as the click product **94** proved to be a good chelate ligand for the two copper(I) phenanthroline sites of $[\text{Cu}_2(\mathbf{83})(\mathbf{91})]^{2+}$, the formation of the dynamic four-component slider-on-deck $[\text{Cu}_2(\mathbf{83})(\mathbf{91})(\mathbf{94})_2]^{2+}$ was warranted. The exchange of the biped **83** across the newly generated deck $[\text{Cu}_2(\mathbf{83})(\mathbf{91})(\mathbf{94})_2]^{2+}$ occurred at a rate of $k_{298} = 65.0$ kHz.

As known from earlier ILC work (vide supra ref. [98]), a carefully chosen organocatalyst can be immobilized at a ZnPor unit in a way that no catalysis will result (at a specific temperature and in a defined time). We thus started with the rotor $[\text{Cu}_2(\mathbf{83})(\mathbf{91})]^{2+}$ in the presence of ligand **92** as well as organocatalyst *N*-methylpyrrolidine (**89**) and the substrates **95** and **96**

for a Michael addition (Figure 21). No formation of product **97** was observed, because the complex between the catalyst **89** and the zinc porphyrin **92** is catalytically inactive.

However, upon addition of azide **93**, the formation of $[\text{Cu}_2(\mathbf{83})(\mathbf{91})(\mathbf{94})_2]^{2+}$ was detected. Since the organocatalyst originally firmly bound at the ZnPor of ligand **92** is now part of the dynamic slider-on-deck $[\text{Cu}_2(\mathbf{83})(\mathbf{91})(\mathbf{94})_2]^{2+}$, the motion of biped **83** will dynamically release **89** into solution. Indeed, now the catalysis of addition product **97** was turned ON. While supramolecular transformations are widely recognized [101–103], the present example illustrates how a supramolecular catalyst (three-component rotor) transforms itself into a new catalyt-

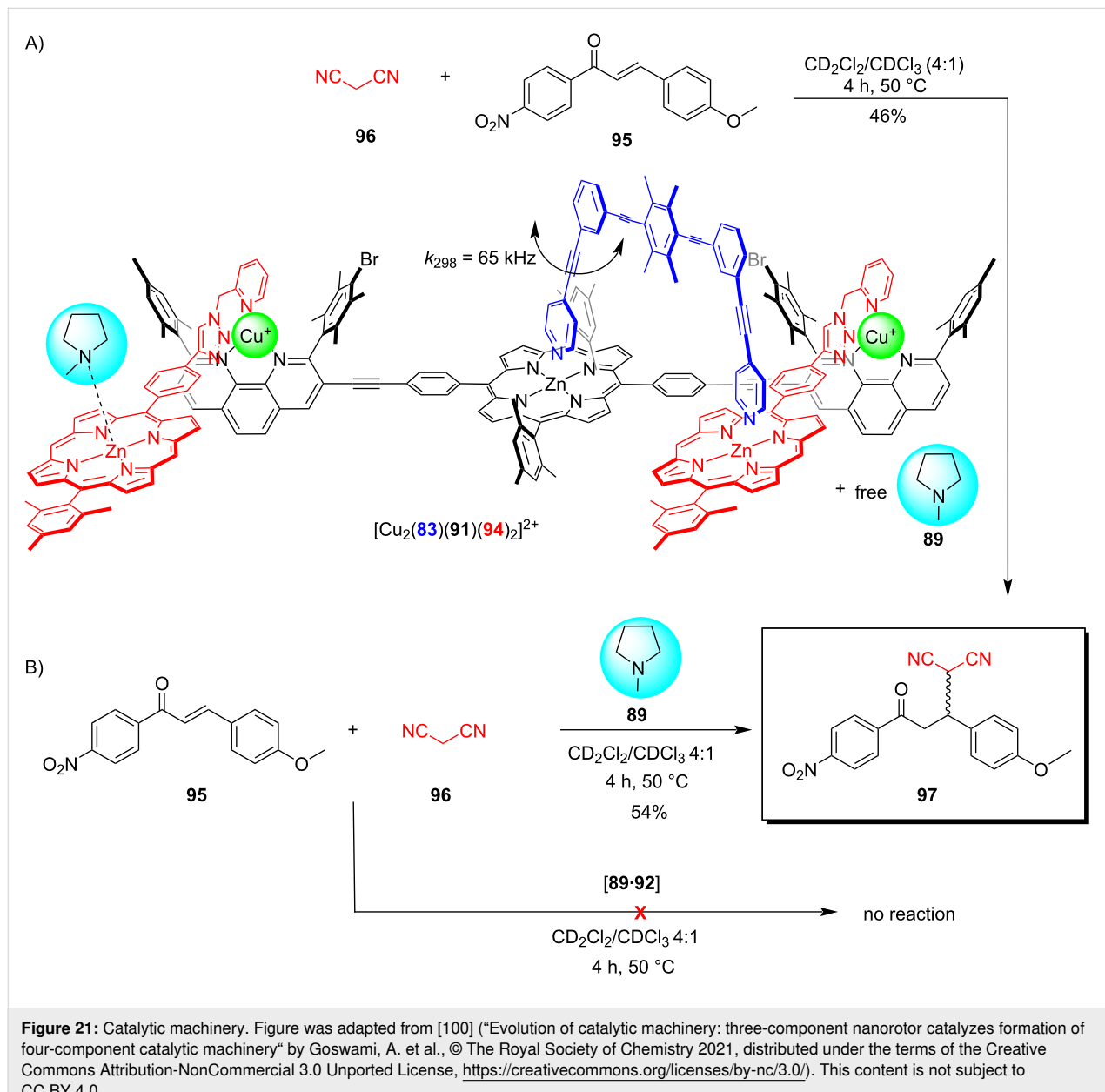


Figure 21: Catalytic machinery. Figure was adapted from [100] (“Evolution of catalytic machinery: three-component nanorotor catalyzes formation of four-component catalytic machinery” by Goswami, A. et al., © The Royal Society of Chemistry 2021, distributed under the terms of the Creative Commons Attribution-NonCommercial 3.0 Unported License, <https://creativecommons.org/licenses/by-nc/3.0/>). This content is not subject to CC BY 4.0.

ic machinery and turns on the respective catalytic process. All in all, this protocol is remotely reminiscent of gradual evolutionary processes [100].

In summary, both the RPI and ILC concepts using variable speed of nanomechanical machinery for catalytic effects are novel and innovative not only for supramolecular, but certainly also for common catalysis. In particular, product inhibition in catalysis is a frequently encountered challenge during catalyst development. Moreover, the RPI concept may point the way towards the development of endergonic catalytic transformations, because in many of those the product needs to be stabilized within the catalytic cavity. Release from the active site then requires destruction of the stabilizing interactions. For instance, Nature has chosen in the ATP-synthase to use “fueled” nanomechanical motion to release ATP from the active site [23].

Switchable catalysis due to reversible assembly/disassembly

The common modus operandi to set up switchable catalysis usually relies on systems that can be toggled between two (or more) distinct switching states within a molecule [104–107]. In contrast, supramolecular approaches allow the shuffling and reshuffling of components to switch ON/OFF catalytic processes, a topic that has not yet found adequate attention, but links supramolecular catalysis to systems chemistry [108,109].

The following information system utilizes a seven-component mixture that is reversibly reconfigured through fully reversible assembly and disassembly thereby tuning ON/OFF two diverse catalytic reactions [99]. Addition and removal of zinc(II) ions triggered altogether three diverse processes: i) mutual re-shuffling of components leading to two different nanorotors, ii) catalysis depending on decisively different exchange rates in the nanorotors, and iii) two different catalytic processes (Figure 22).

The key challenge in the toggling process was to interconvert two nanorotors by exchange of two components but with a single-input trigger from outside. Eventually, the two-component reshuffling was solved by providing zinc as trigger (component 1) and by using a ligand (component 2) from a ligand reservoir. In the initial self-sorted State-I, the rotor $[\text{Cu}(\mathbf{53})(\mathbf{98})]^+$ was paired with $[\text{Cu}_2(\mathbf{100})_2]^{2+}$, the latter representing a reservoir for the rotator arm **100**. Addition of zinc(II) ions induced a second self-sorting that encompassed transfer of two components along the following equation: $2 \times [\text{Cu}(\mathbf{53})(\mathbf{98})]^+ + [\text{Cu}_2(\mathbf{100})_2]^{2+} + 2 \times \text{Zn}^{2+} \rightarrow 2 \times [\text{Zn}(\mathbf{53})(\mathbf{100})]^{2+} + [\text{Cu}_2(\mathbf{98})_2]^{2+} + 2 \times \text{Cu}^+$. Accordingly, the added zinc(II) ions and ligand **100** from the reservoir

$[\text{Cu}_2(\mathbf{100})_2]^{2+}$ enabled the formation of the zinc(II)-based rotor $[\text{Zn}(\mathbf{53})(\mathbf{100})]^{2+}$ (Figure 22a). The liberated ligand **98** reacted with the copper(I) ions to afford $[\text{Cu}_2(\mathbf{98})_2]^{2+}$ representing again a reservoir for a rotator. Based on the stoichiometry of the above equation, two equiv of copper(I) ions were liberated. Since the released free copper(I) ions generated problems with reversibility of the transformation, 1-aza-18-crown-6 (**99**) (2.0 equiv) had to be added as a receptor for Cu^+ .

As State-I contains the azacrown ether **99**, a potential organocatalyst, and State-II harbors the copper complex $[\text{Cu}(\mathbf{99})]^+$ a likely click catalyst, both networked states were expected to be catalytically active, possibly even in an ON/OFF manner [99]. To test for dual catalysis (Figure 22b), State-I was reacted at 50 °C with 1.0 equiv of catalyst **99** (with respect to rotor) and 10.0 equiv (with respect to rotor) of substrates **75**, **86**, **95**, and **102** in $\text{CD}_2\text{Cl}_2/\text{CD}_3\text{CN}$ 5:1 for 2 h. Analysis demonstrated that 30% of product **101** but no click product **103** had formed. State-II was furnished by addition of 1.0 equiv of zinc(II) ions (with respect to the rotor) and heated under identical conditions. Finally, 55% of the click product **103** was revealed, but without further conversion of product **101**. A notable reproducibility of the yields was identified in two consecutive catalytic cycles. As a result, an astounding switchable catalytic system could be based on information processing (Figure 22).

The following example of switchable catalysis involves the interconversion of the closed dimeric parallelogram $[\text{Cu}_2(\mathbf{104})_2]^{2+}$ and the bishomoleptic complex $[\text{FeCu}_2(\mathbf{104})_2]^{4+}$ (Figure 23), the latter controlling a double-click catalytic access to rotaxanes **109**, by addition/removal of iron(II) ions [110]. Although $[\text{FeCu}_2(\mathbf{104})_2]^{4+}$ is an open and flexible structure, the availability of two catalytic copper(I) centers positioned at 34 Å in the transition state of the second click reaction, leads to an astounding synthetic efficiency, although there is a major distance mismatch between the copper(I) ions in $[\text{FeCu}_2(\mathbf{104})_2]^{4+}$ and two triazole units of the rotaxane.

For instance, the system $[\text{FeCu}_2(\mathbf{104})_2]^{4+}$ ($d_{\text{Cu}-\text{Cu}} = 34$ Å) afforded the formation of both **109a** (73%) and **109b** (82%) in high yield (Figure 23b) [110], although the relevant distances in the pseudo-rotaxane **110a,b** (prior to the second click reaction) are 14.3 and 21.1 Å. Actually, the yield with $[\text{FeCu}_2(\mathbf{104})_2]^{4+}$ was far better than with a dicopper reference catalyst, where the separation of the copper(I) ions was optimal ($d_{\text{Cu}-\text{Cu}} = 14.6$ Å) for the formation of **109a**. The findings were explained based on a model in which the monotriazoles **110a,b** were bound to both copper centers prior to the second click reaction. Aside of one copper(I)-triazole interaction, the model suggested a chelate cooperative effect resulting from an additional η^2 -binding of the second copper(I) at the acetylene unit at

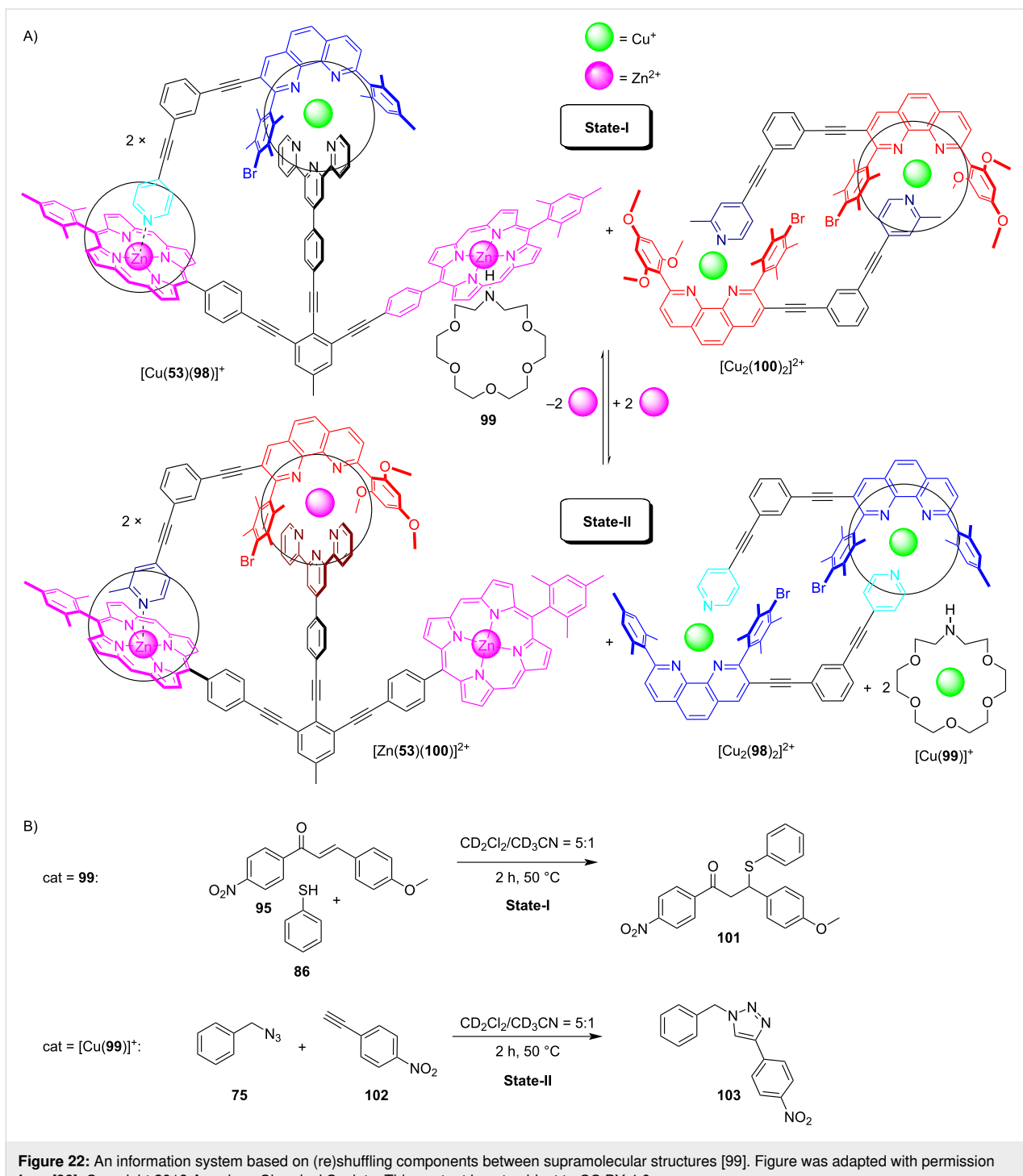


Figure 22: An information system based on (re)shuffling components between supramolecular structures [99]. Figure was adapted with permission from [99]. Copyright 2019 American Chemical Society. This content is not subject to CC BY 4.0.

which the second click reaction would take place. In case of distance mismatch, it is the formation of this copper–alkyne η^2 -complex that compensates for the build-up of strain as demonstrated by DFT computations [110]. Once the second click reaction has occurred, the rotaxane is liberated under release of strain in the catalyst if there was a distance mismatch. For cases with a close match of distances, product inhibition

reduced the yield. Due to the high relevance of the CuAAC approach [111] for the preparation of rotaxanes, the exploitation of cooperative and strain effects in double-click strategies is a promising strategy.

A completely different approach to switchable supramolecular catalysis made use of a supramolecular cage-to-device transfor-

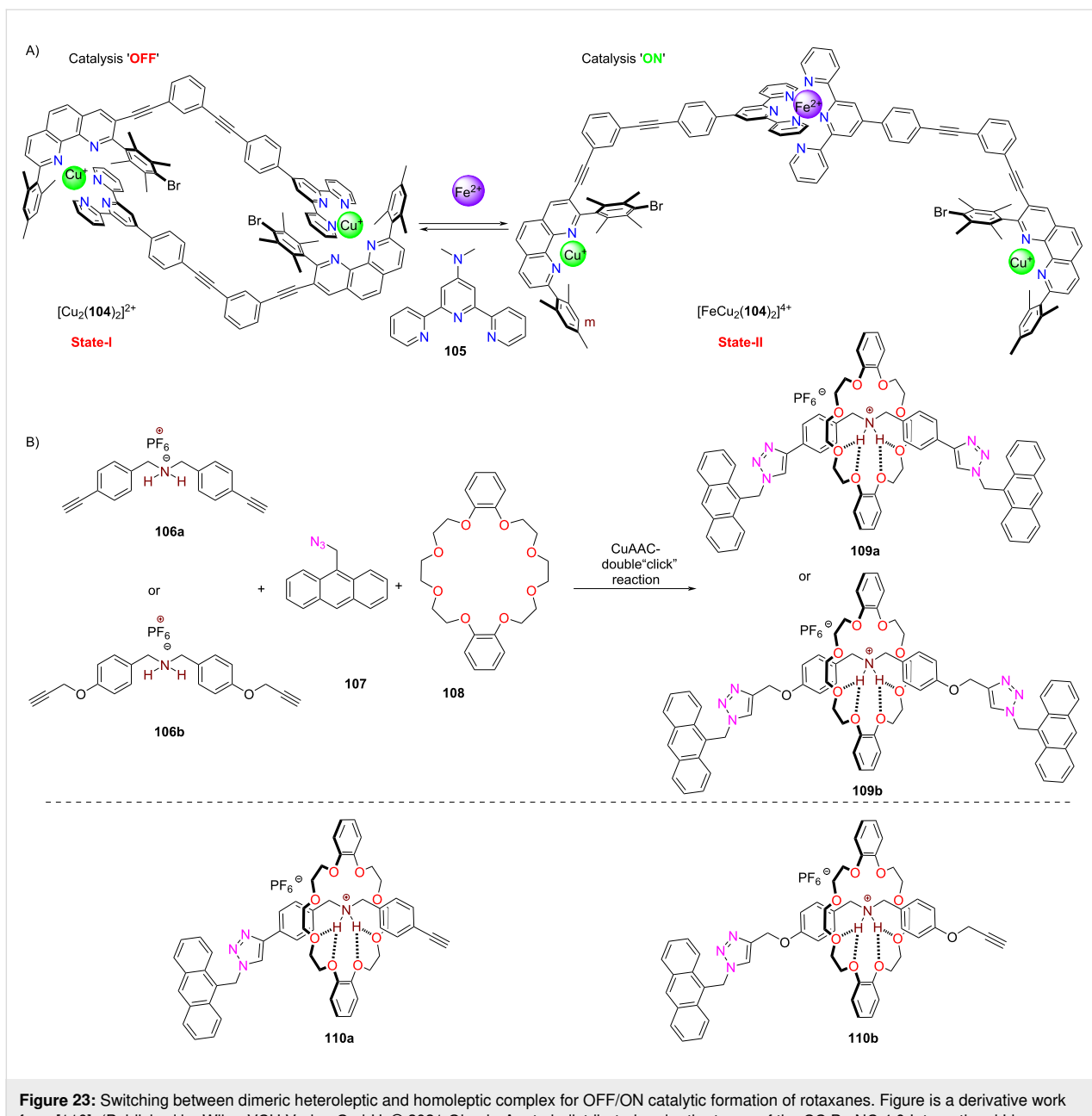
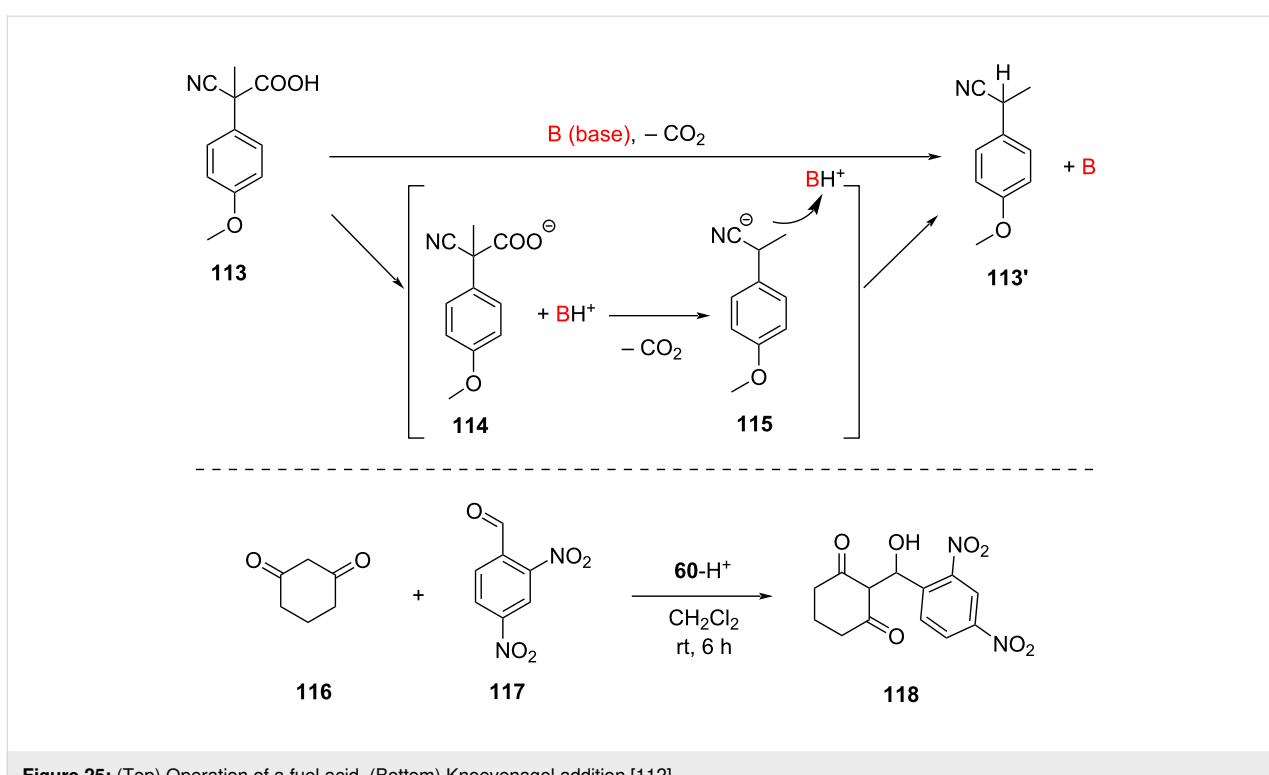
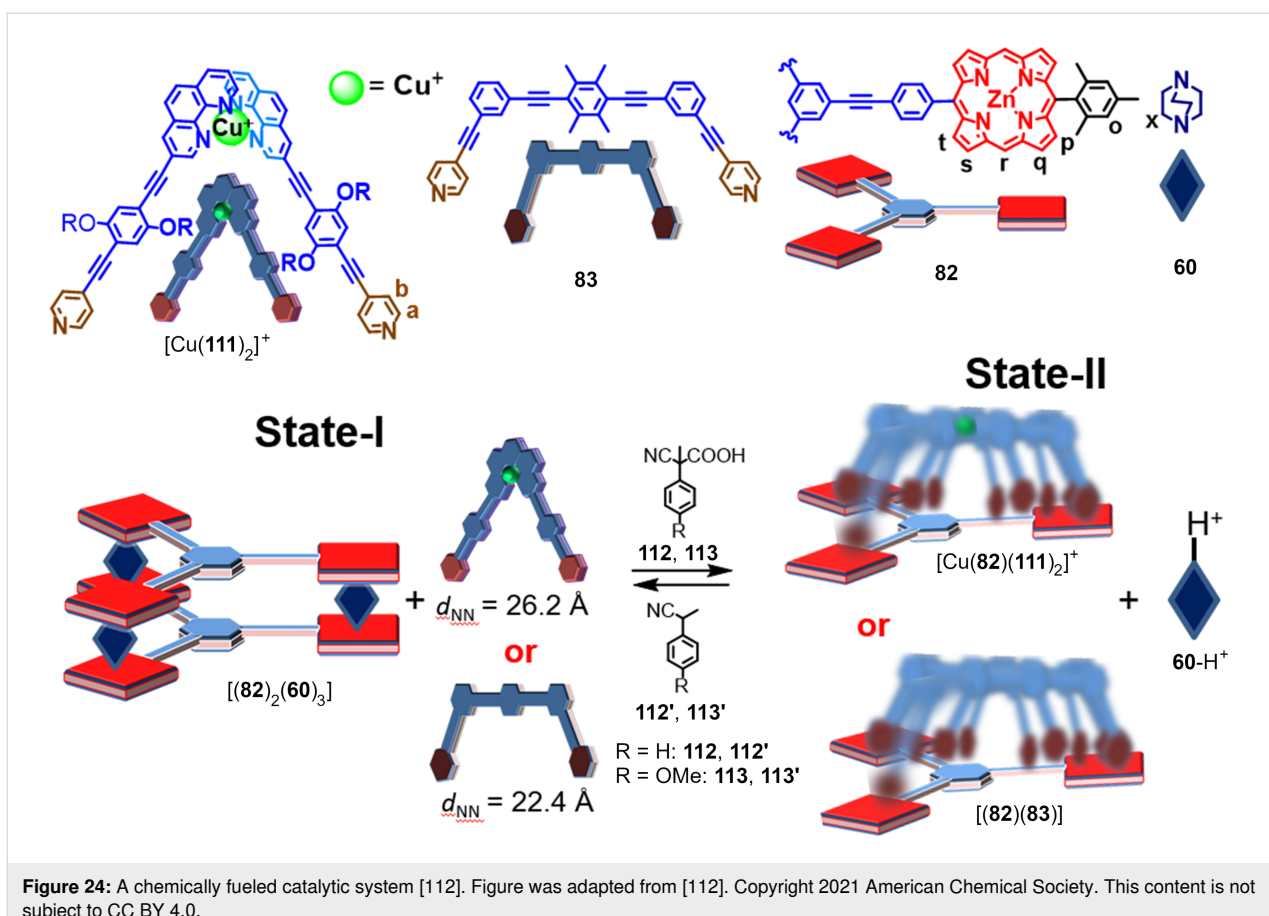


Figure 23: Switching between dimeric heteroleptic and homoleptic complex for OFF/ON catalytic formation of rotaxanes. Figure is a derivative work from [110]. (Published by Wiley-VCH Verlag GmbH, © 2021 Ghosh, A. et al. distributed under the terms of the CC By-NC 4.0 International License, <https://creativecommons.org/licenses/by-nc/4.0/>). This content is not subject to CC BY 4.0.

mation under dissipative conditions (Figure 24) [112]. Notably, the dissipative conditions were realized by addition of a fuel acid [113,114] that surprisingly ignited a base-catalyzed Knoevenagel addition reaction (Figure 25).

As DABCO is a stronger binding ligand ($\log \beta = 7.20$) [115] towards zinc porphyrin (ZnPor) than pyridine ($\log K = 4.45$) [90] the reaction of ligand **111**, deck **82**, DABCO (**60**), and $[\text{Cu}(\text{CH}_3\text{CN})_4](\text{PF}_6^-)$ (4:2:3:2) furnished the supramolecular cage $[(\mathbf{82})_2(\mathbf{60})_3]$ with **60** = DABCO acting as pillars whereas biped $[\text{Cu}(\mathbf{111})_2]^+$ remained uncoordinated [112]. In an analo-

gous self-assembly with **83** instead of $[\text{Cu}(\mathbf{111})_2]^+$, ligand **83** was left uncoordinated. When State-I was treated with TFA, then the reshuffling of the components afforded the slider-on-deck $[\text{Cu}(\mathbf{82})(\mathbf{111})_2]^+$ (or $[(\mathbf{82})(\mathbf{83})]$) and the monoprotonated DABCO (**60**– H^+). Addition of DBU reversed the process. The bipeds in the slider-on-deck systems $[\text{Cu}(\mathbf{82})(\mathbf{111})_2]^+$ ($k_{298} = 42.2$ kHz) and $[(\mathbf{82})(\mathbf{83})]$ ($k_{298} = 32.2$ kHz) move across the deck **82** and prevent binding of the protonated DABCO at the ZnPor binding sites. Use of the fuel acid **112** or **113** instead of applying the TFA/DBU acid/base combination leads initially to protonation of DABCO but due to the decarboxylation of **114**



the resulting strong base **115** reclaims the proton back (Figure 25, top). As a result, State-II may be afforded under dissipative conditions.

A surprising facet of this State-I/State-II interconversion (Figure 24) [112] was the finding that the protonated DABCO (**60-H⁺**) was a rather efficient base catalyst for a Knoevenagel addition (Figure 25, bottom). Several control experiments excluded the possibility that the reaction was triggered by acid or by alternative pathways. The remaining unprotonated nitrogen in monoprotonated DABCO (**60-H⁺**) hence is a sufficiently strong base for the reaction of **116** and **117**. Finally, the State-I/State-II interconversion in the presence of **116** and **117** was triggered by addition of the fuel acid. The traces in Figure 26 show the amount of Knoevenagel addition product **118** within two subsequent pulses of the fuel.

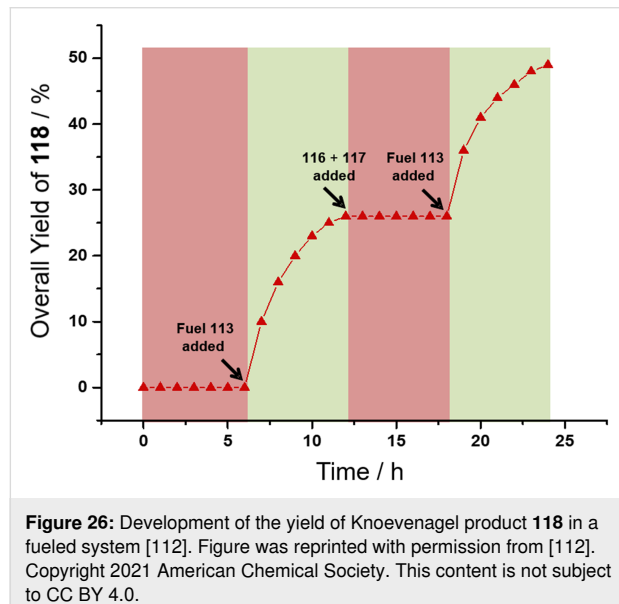


Figure 26: Development of the yield of Knoevenagel product **118** in a fueled system [112]. Figure was reprinted with permission from [112]. Copyright 2021 American Chemical Society. This content is not subject to CC BY 4.0.

In summary, the examples listed in this subchapter shed some light on the manifold opportunities for switchable ON/OFF catalysis controlled by supramolecular interconversions. Switchable catalysis decided by an ensemble of communicating molecules, which act as an information system and control the switching states, remodels somehow the situation in a living cell, where a desired event is only ignited when several signaling parameters agree. Explicitly, the subchapter demonstrates three distinct examples, in which metal–ligand coordination was shuffled by addition/removal of either metal ions or acid. To (re)shuffle metal–ligand coordination by acid/base generates a number of further options. In particular, the protocol of acid addition and removal (upon base addition) may be elegantly replaced by using a suitable fuel acid thus opening the field of supramolecular catalysis for out-of-equilibrium processing.

Toggling between intra- and intermolecular complexation in nanoswitches

Heteroleptic complexation does not only open the way to multi-component assembly but also to switchable catalysis in coordination-based toggles. An important and widely applicable protocol is the weak-link approach (WLA) that was developed and exploited by Mirkin [116]. It is based on the association/dissociation of hemilabile ligands bound to a metal center. Through the addition of secondary ligands, the weakly coordinated donor sites are substituted which allows an opening of the switch from a rigid-closed to a flexible semi-open form [117]. A common protocol used addition/removal of strongly binding monodentate ligands (CO or Cl⁻) at rhodium centers to dissociate/reassociate the weakly coordinated donor, for instance in tweezer-type structures [118].

An early contribution by Mirkin (Figure 27) described the opening of the closed structure **119²⁺** to the open form

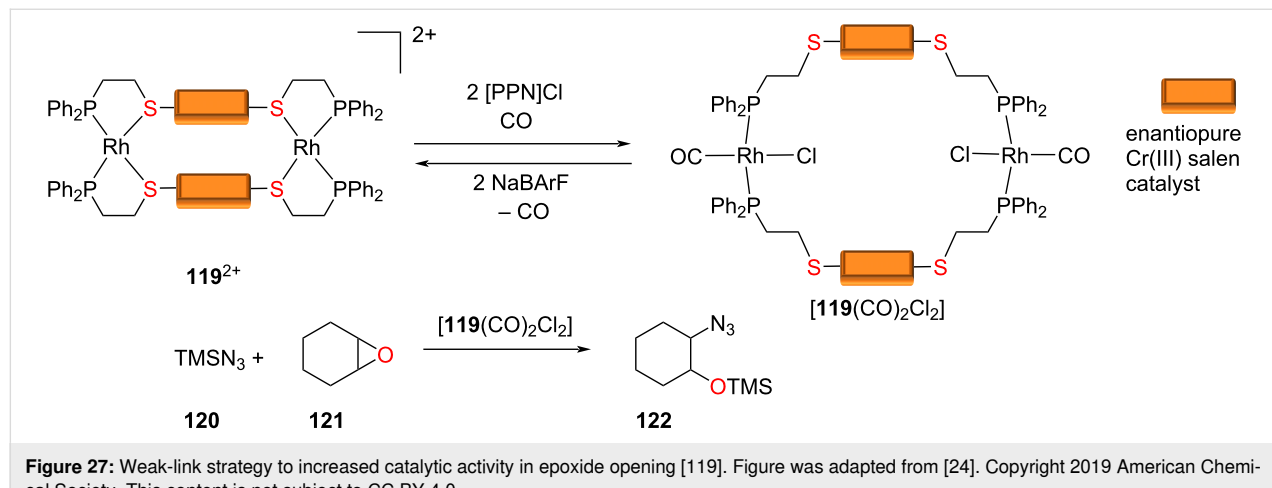


Figure 27: Weak-link strategy to increased catalytic activity in epoxide opening [119]. Figure was adapted from [24]. Copyright 2019 American Chemical Society. This content is not subject to CC BY 4.0.

[119(CO)₂Cl₂] that showed a two-fold activity in the catalytic opening of epoxide **121** to **122** [119].

In another example by Mirkin, a well-known aluminum(III) salen catalyst was hidden in switch **125²⁺** [118] between steri-

cally demanding biphenyl rings preventing ϵ -caprolactone from accessing the catalytic site (Figure 28). As a result, the polymerization of ϵ -caprolactone (**123**) was switched OFF. Addition of chloride anions from *n*-Bu₄NCl led to the substitution of the tertiary amine ligand at both rhodium centers generating the

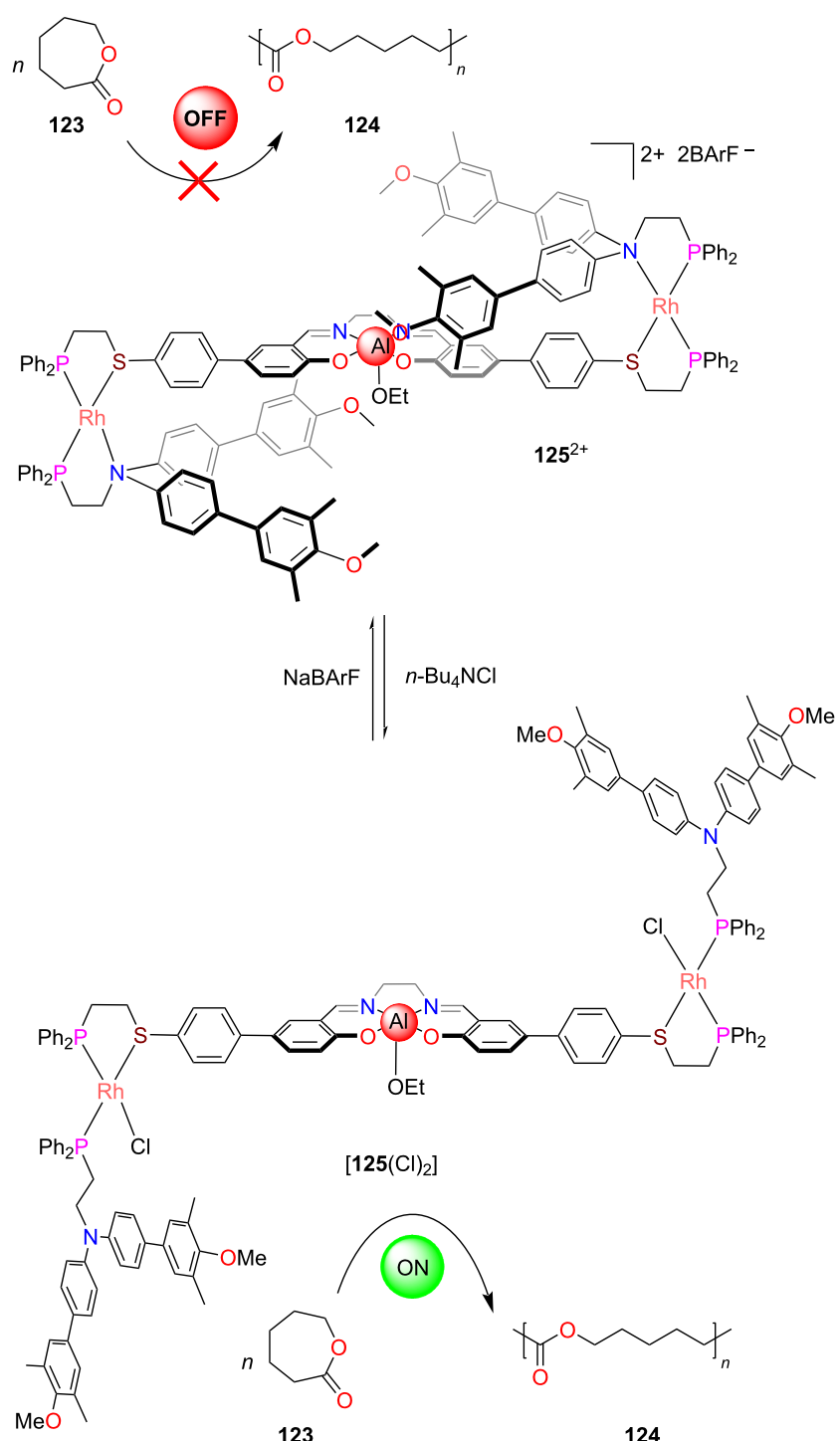


Figure 28: A ON/OFF polymerization switch based on the weak-link approach [118]. Figure was reprinted with permission from [24]. Copyright 2019 American Chemical Society. This content is not subject to CC BY 4.0.

semi-open form $[125(\text{Cl})_2]$. Since the aluminum(III) salen center became now exposed, the catalytic polymerization of ϵ -caprolactone (**123**) was turned ON. The chloride was readily removed by adding sodium tetrakis[(3,5-trifluoromethyl)phenyl]borate (NaBArF) and as result catalysis was turned OFF again.

Along this protocol, Mirkin et al. have developed a variety of allosterically modulated catalysts that allow ON/OFF reaction control in photoredox catalysis [120], phosphate diester transesterification [121], Friedel–Crafts reaction, ring opening of epoxides, oligomerization [116], and acyl-transfer reactions [122,123].

While there are further examples by Mirkin [124–126], Schmittel [127,128], and others [129,130] that operate at the borderline of dynamic heteroleptic complexation events, the supramolecular cases selected in the following are characterized by the reshuffling of inter- and intramolecular coordination events to realize different toggling states for catalysis [131].

Using addition and removal of chloride, the Mirkin group reversibly and quantitatively toggled the platinum(II)-based

switch **126**²⁺ between a homo- and heteroligated form (Figure 29) [132]. In the closed platinum(II) complex **126**²⁺, the urea units were available for activation of butenone (**127**) by hydrogen bonding. As a result, the Diels–Alder reaction of cyclopentadiene (**128**) and **127** was catalyzed. Upon addition of $n\text{-Bu}_4\text{NCl}$, the open form was afforded that aggregated to oligomers $[(126\bullet\text{Cl})_n]^{n+}$ through intermolecular hydrogen bonding at the urea moieties. Now, activation of **127** stopped and catalysis was turned OFF. Catalysis was turned back ON after trapping of the chloride ions with NaBArF .

The next example bridges in some way the gap between the preceding (Figure 23) and the present chapter because it addresses again catalysis with two catalytically active copper(I) centers held at a defined distance, now though for proximity catalysis using acyl transfer. The utility of this approach was demonstrated when a duo of catalysts was used for achieving substrate selectivity [133].

In detail, nanoswitch $[\text{Cu}(\mathbf{130})]^+$ was transformed into the slow rotor $[\text{Cu}_2(\mathbf{130})]^{2+}$ ($k_{298} = 1.34 \text{ s}^{-1}$) upon the addition of a second equiv of copper(I) ions (Figure 30). When 0.5 equiv of iron(II) was added, the rotator arm got involved in iron(II) bis(terpyridine) complexation affording $[\text{Fe}(\text{Cu}_2(\mathbf{130}))_2]^{6+}$. An

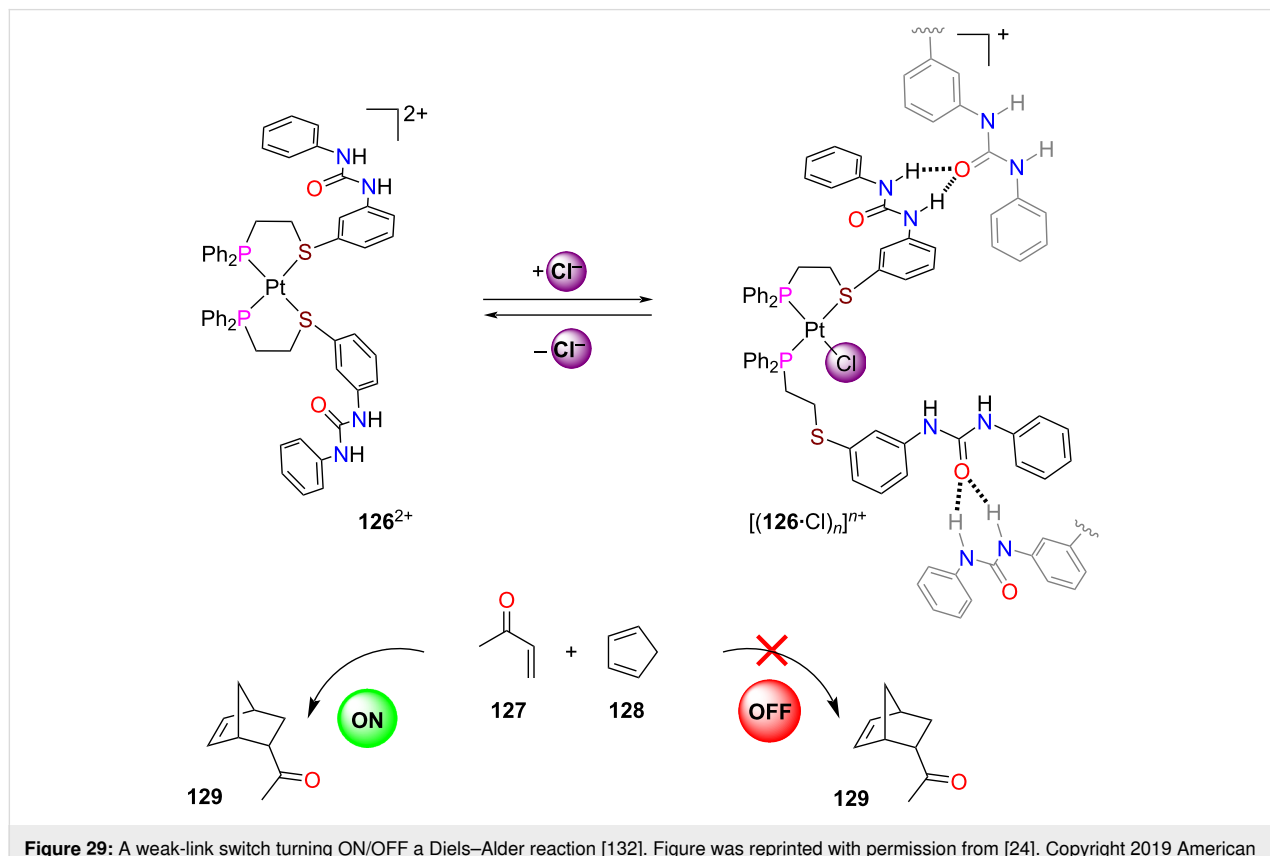


Figure 29: A weak-link switch turning ON/OFF a Diels–Alder reaction [132]. Figure was reprinted with permission from [24]. Copyright 2019 American Chemical Society. This content is not subject to CC BY 4.0.

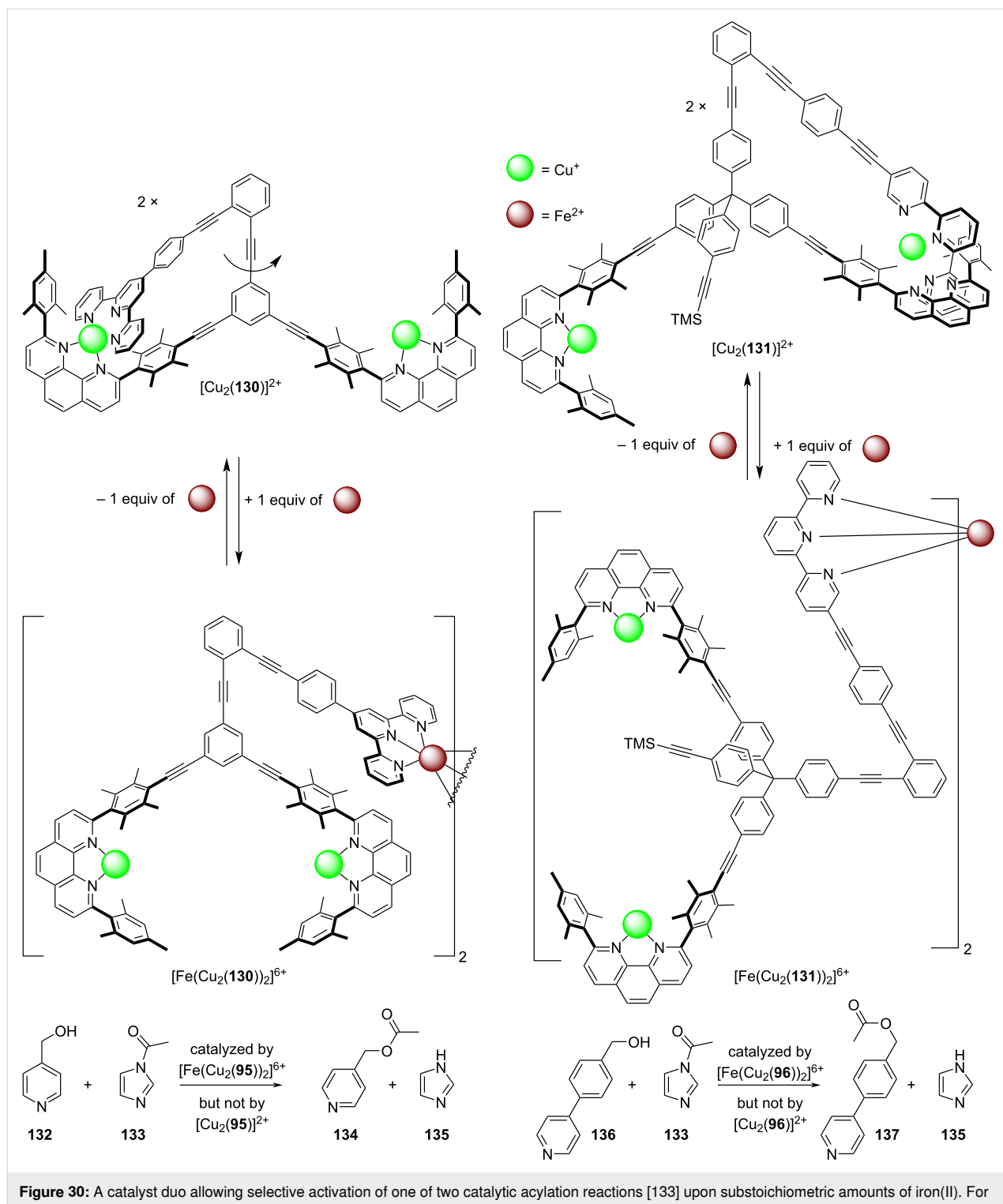


Figure 30: A catalyst duo allowing selective activation of one of two catalytic acylation reactions [133] upon substoichiometric amounts of iron(II). For explanations, see text. Redrawn from reference [133].

analogous transformation was seen for $[\text{Cu}(131)]^+ \rightarrow [\text{Cu}_2(131)]^{2+} \rightarrow [\text{Fe}(\text{Cu}_2(131))_2]^{6+}$.

When hydroxymethylpyridine **132** and the acetylation agent **133** (Figure 30) were reacted in the presence of the copper(I)-

loaded rotor $[\text{Cu}_2(130)]^{2+}$ no reaction was detected. In contrast, the dimeric complex $[\text{Fe}(\text{Cu}_2(130))_2]^{6+}$, formed after addition of iron(II) ions, offers two cavities each with two copper(I) ions to pre-bind both **132** and **133** at an optimal reaction distance. It was no surprise, that due to the increased local concentration,

the acetylation $\mathbf{132} + \mathbf{133} \rightarrow \mathbf{134}$ did rapidly take place. Similarly, the bigger dimeric nanoswitch $[\text{Fe}(\text{Cu}_2(\mathbf{131}))_2]^{6+}$ catalyzed the acetylation of the larger substrate $\mathbf{136}$ due to size-matching [133]. In order to test the reversibility, both switches were toggled by adding and removing the iron(II) ions over 2.5 cycles demonstrating that ON/OFF catalysis was reversible and reproducible.

Interestingly, the nanoswitches $[\text{Cu}_2(\mathbf{130})]^{2+}$ and $[\text{Cu}_2(\mathbf{131})]^{2+}$ (1:1) could be selectively addressed in the presence of all substrates and reagents (**132**, **133**, and **136**). Upon addition of stoichiometric amounts of iron(II), predominantly nanoswitch $[\text{Cu}_2(\mathbf{131})]^{2+}$ reacted to afford $[\text{Fe}(\text{Cu}_2(\mathbf{131}))_2]^{6+}$ which selectively turned on the reaction affording **137**. As a result, this example highlights a sophisticated case of a multicatalyst system

that can select between substrates of essentially identical reactivity but different size.

A spectacular and unique example of toggling catalysis was demonstrated in nanoswitch **138** (Figure 31) with its four distinct switching states [134]. In State-I, i.e. $[\text{Cu}(\mathbf{138})]^+$, an intramolecular HETTAP complex between a copper(I) phenanthroline and a terpyridine site was realized. Upon addition of 0.5 equiv of iron(II) ions the HETTAP interaction opened up and the “dimeric” bishomoleptic nanoswitch $[\text{Fe}(\text{Cu}(\mathbf{138}))_2]^{4+}$ was furnished in State-II held together by a bis(tpy) iron(II) complexation. Due to the eradication of the HETTAP binding, the copper(I) ions were left coordinatively frustrated, which made them potentially available for catalysis of a click reaction. In the next switching step, the removal of copper(I) ion led to

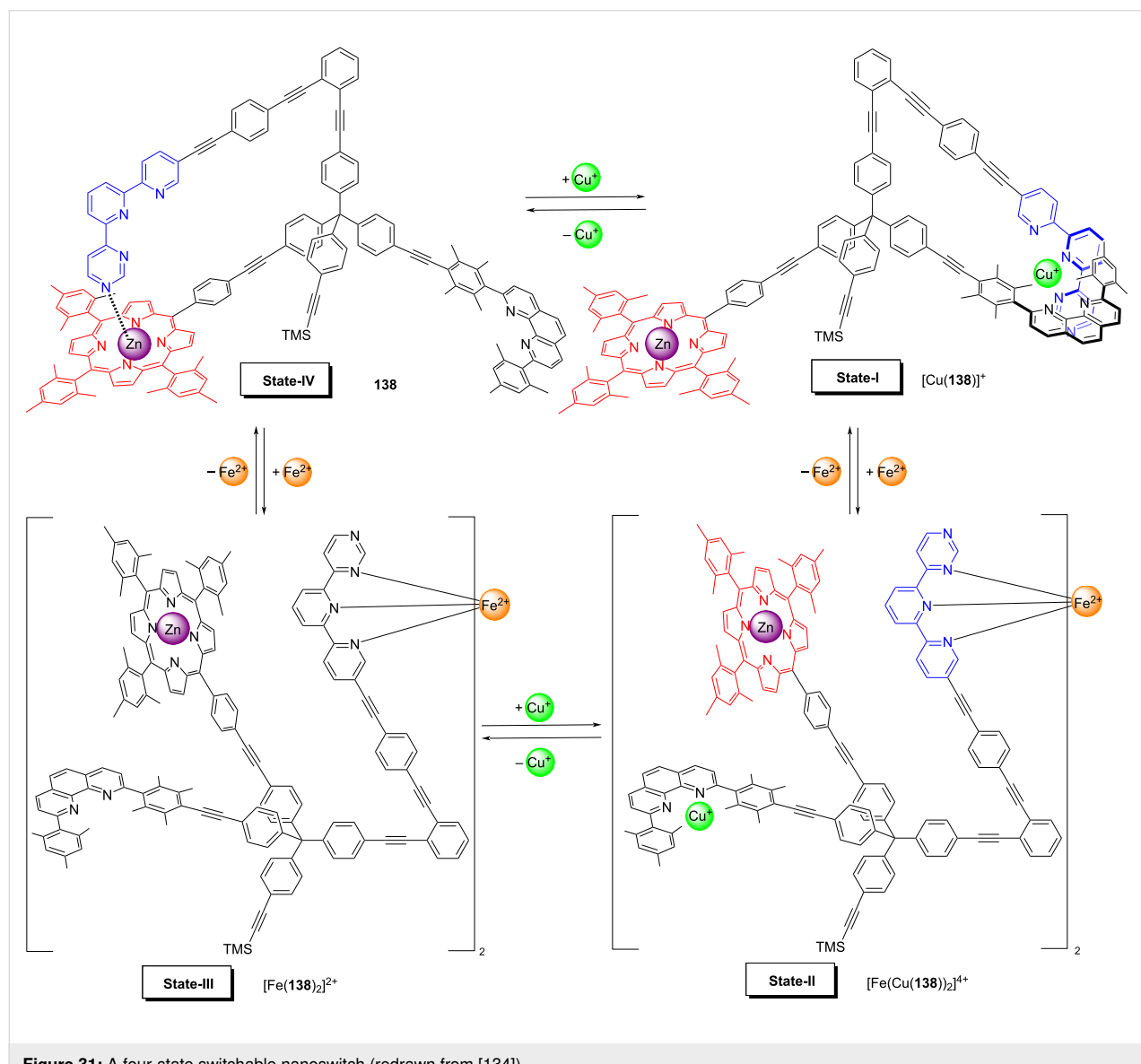


Figure 31: A four-state switchable nanoswitch (redrawn from [134]).

State-III, i.e. $[\text{Fe}(138)_2]^{2+}$. The ensuing removal of iron(II) ions broke down the bis(tpy) complex $[\text{Fe}(138)_2]^{2+}$ and afforded State-IV. The latter state was characterized by a closed structure of the nanoswitch 138 due to the intramolecular N_{pym} \rightarrow ZnPor binding (pym = pyrimidine). The full switching cycle using addition/removal of ions was repeated without fatigue.

The above sequence of four switching states has been demonstrated to activate sequential catalysis (Figure 32), once the protocol is executed in the presence of piperidine (139) as a catalyst and the reactants 79, 80, and 95 [134]. Due to the “free” ZnPor unit in State I, catalyst 139 was strongly bound at the ZnPor unit of $[\text{Cu}(138)]^+$, while the copper(I) ion was firmly encapsulated in a HETTAP binding site. Thus, State-I should be catalytically inactive. Upon addition of iron(II), the tpy unit of the HETTAP unit became involved in the bishomoleptic iron(II) terpyridine complex $[\text{Fe}(\text{Cu}(138))_2]^{4+}$, while the copper(I) ions were exposed for catalysis in State-II. Indeed, in this state 50% of the click product 81 was formed. Removal of copper(I) and formation of State-III stopped the click catalysis. The ensuing removal of iron(II) ions finally afforded nanoswitch 138 (= State-IV). Due to the intramolecular linkage of the azater-

pyridine to the ZnPor unit, the piperidine that was firmly bound in States I \rightarrow III, was now released from the ZnPor unit. Remarkably, product 81 formed in State-II now underwent a catalyzed Michael addition to provide 140 in 28% yield. When the catalytic cycle was repeated, it fully reproduced the yields of the first cycle, thus demonstrating that a catalytic eleven-component machinery may work without destructive interference despite the large number of functional groups in the switches, reagents, and products [134].

The following example (Figure 33) does not reach the complexity of the above nanoswitch system, but it is remarkable as it involves a remote control of catalysis [135]. Here, the complex $[\text{Cu}(141)]^+$ with its heteroleptic HETTAP binding site controlled the switching state of nanoswitch 142 by using fully reversible communication via ion signaling. State-I was characterized by a clean self-sorting of the copper(I) ions resulting in $[\text{Cu}(141)]^+$ + switch 142. In the presence of *N*-methylpyrrolidine (89), a conjugate addition was observed in State-I. However, upon addition of iron(II) (0.5 equiv) ligand 141 became involved in the bishomoleptic iron(II) terpyridine complex $[\text{Fe}(141)_2]^{2+}$ with the effect that now weakly bound copper(I)

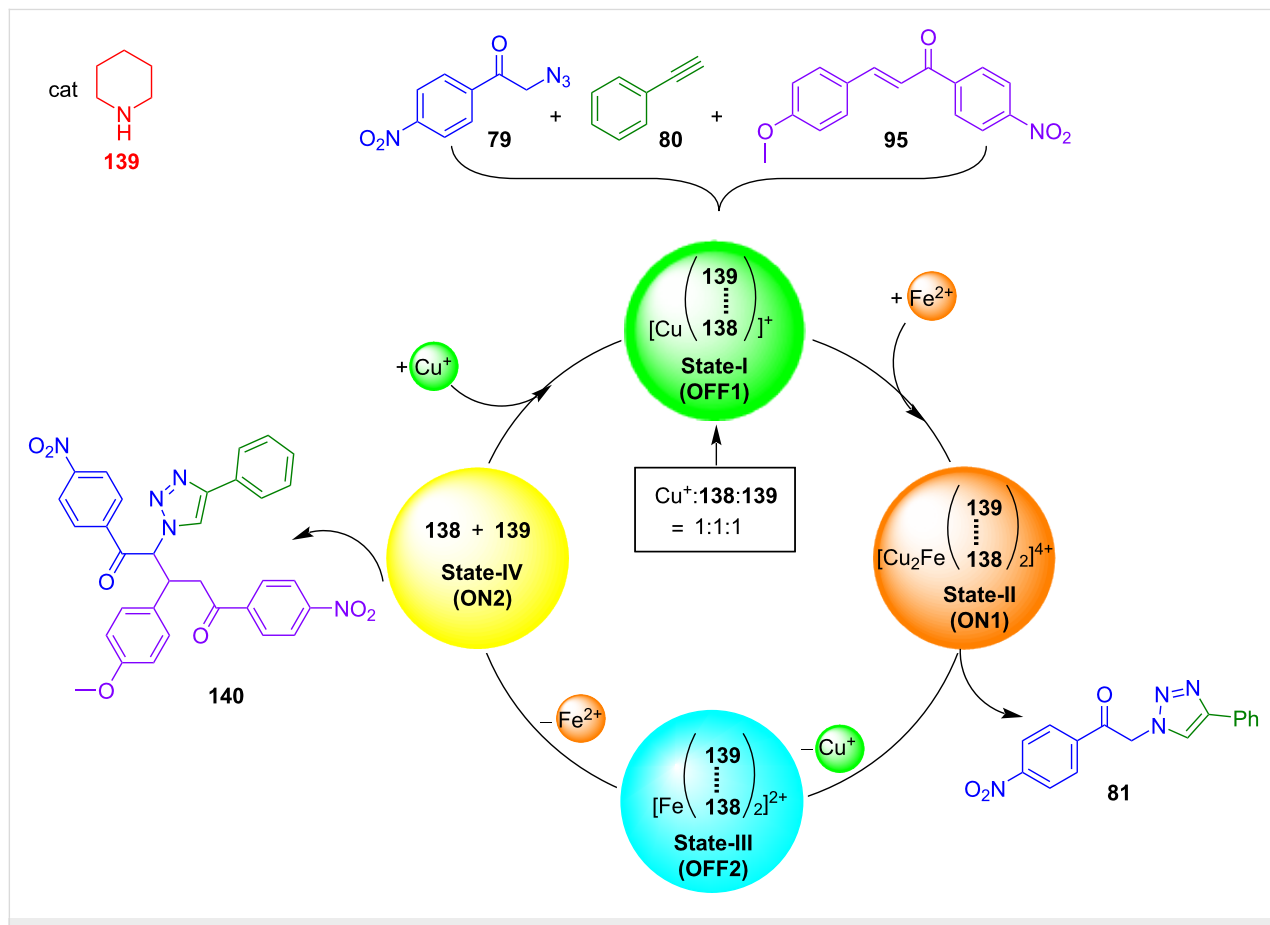


Figure 32: Sequential catalysis as regulated by nanoswitch 138 and catalyst 139 in the presence of metal ions (redrawn from [134]).

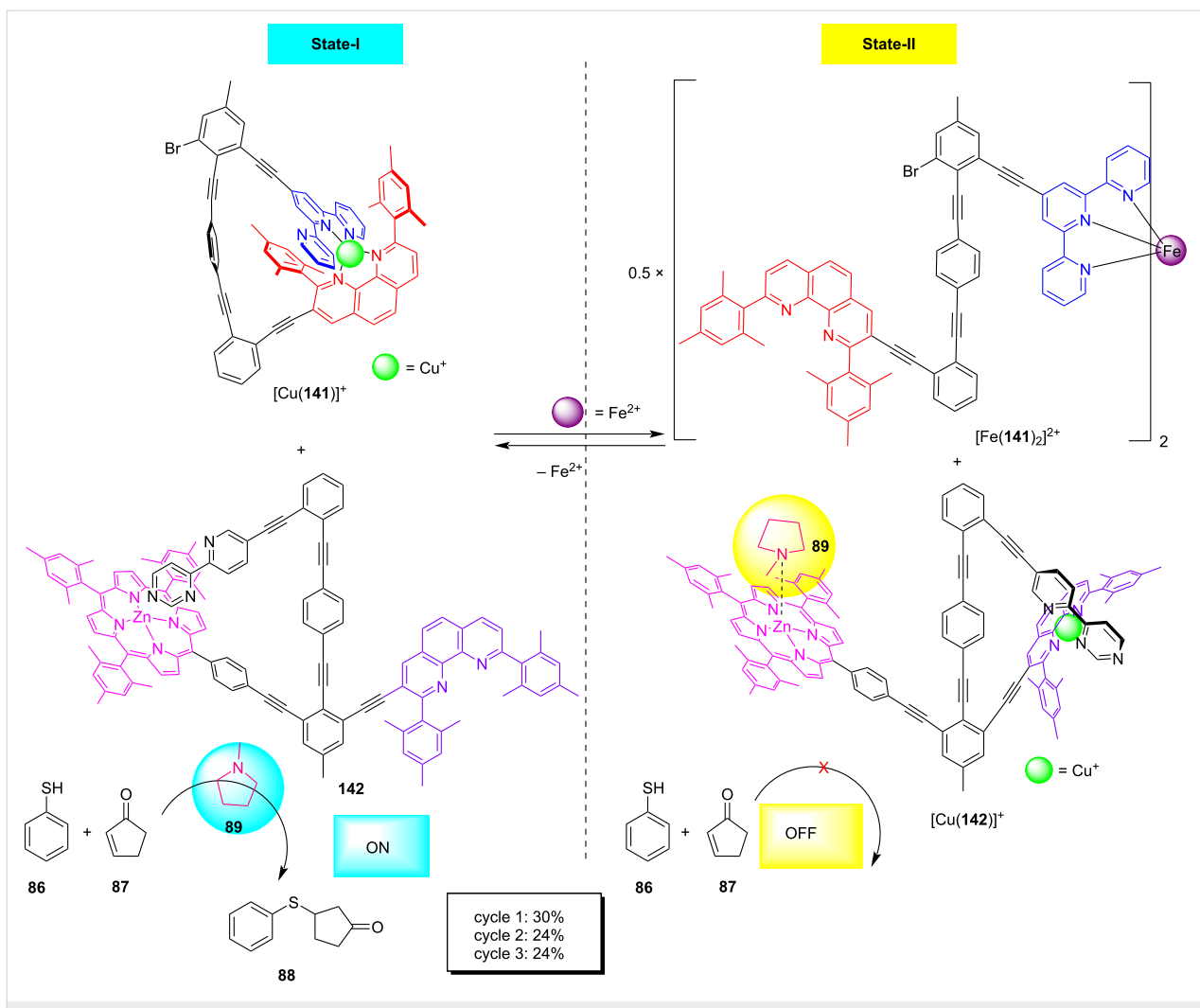


Figure 33: Remote control of ON/OFF catalysis administrated by two nanoswitches through ion signaling (redrawn from [135]).

ions travelled to nanoswitch **142**. In the thus formed complex $[\text{Cu(142)}]^+$ the azabipyridine dissociated from the ZnPor binding site to generate a HETPHEN complexation site for copper(I). With the ZnPor unit being freed from intramolecular binding, it now served as coordination site for the *N*-methylpyrrolidine (**89**), preventing the latter from catalyzing the conjugate addition [135]. As a result, catalysis was stopped in State-II. The cycle could be repeated two more times, however, generating a lower yield (Figure 33). The reduction of the yield in cycles two and three was traced to the slow switching of State-II to State-I.

In summary, this subchapter highlighted switching systems that were built using dynamic heteroleptic complexation together with supramolecular dissociation/association events for regulating catalysis. It is noteworthy that switching in all cases went along with a major nanomechanical reorganization of one (or all) constituents.

Conclusion

Supramolecular catalysis is an emerging field that has attracted a lot of attention recently. Its comprehensive coverage encompasses several fields [3], however, still with a main focus on catalysis that is promoted by discrete cages, capsules, and in a variety of confined environments. The present short account with a focus on dynamic heteroleptic metal complexation seeks to demonstrate that (metallo)supramolecular catalysis has many more opportunities to offer. While the examples in the first subchapter illustrate the much higher diversity of heteroleptic over homoleptic cages, the following subchapters above all exemplify that supramolecular chemistry extends beyond the single "supramolecular structure", as complex it may be, thus reaching far into the field and concepts of systems chemistry [30,136] and information science [137,138]. For instance, toggling between and dynamic exchange within supramolecular structures add features to catalysis as ON/OFF or UP/DOWN regulation of catalytic activity. If these factors will

be consequently developed, they should eventually open opportunities to autonomous catalytic systems.

A look at systems biology, where enzymatic catalysis is tightly regulated by various chemical messengers to enable life, can serve as a guide. In this regard, we expect that upcoming endeavors will increasingly focus on the development of artificial systems that can make autonomous decisions and that energetically operate out-of-equilibrium.

Funding

The authors thank the DFG (Schm 647/20-2 and 647/22-1; No 491092614) and the AvH foundation (personal stipend to P.H.) for generous support.

ORCID® iDs

Prodip Howlader - <https://orcid.org/0000-0001-6762-529X>

Michael Schmittel - <https://orcid.org/0000-0001-8622-2883>

References

1. Raynal, M.; Ballester, P.; Vidal-Ferran, A.; van Leeuwen, P. W. N. M. *Chem. Soc. Rev.* **2014**, *43*, 1660–1733. doi:10.1039/c3cs60027k
2. Raynal, M.; Ballester, P.; Vidal-Ferran, A.; van Leeuwen, P. W. N. M. *Chem. Soc. Rev.* **2014**, *43*, 1734–1787. doi:10.1039/c3cs60037h
3. van Leeuwen, P. W. N. M.; Raynal, M., Eds. *Supramolecular Catalysis: New Directions and Developments*; Wiley-VCH: Weinheim, Germany, 2022. doi:10.1002/9783527832033
4. Zhao, L.; Jing, X.; Li, X.; Guo, X.; Zeng, L.; He, C.; Duan, C. *Coord. Chem. Rev.* **2019**, *378*, 151–187. doi:10.1016/j.ccr.2017.11.005
5. Tan, C.; Chu, D.; Tang, X.; Liu, Y.; Xuan, W.; Cui, Y. *Chem. – Eur. J.* **2019**, *25*, 662–672. doi:10.1002/chem.201802817
6. Fang, Y.; Powell, J. A.; Li, E.; Wang, Q.; Perry, Z.; Kirchon, A.; Yang, X.; Xiao, Z.; Zhu, C.; Zhang, L.; Huang, F.; Zhou, H.-C. *Chem. Soc. Rev.* **2019**, *48*, 4707–4730. doi:10.1039/c9cs00091g
7. Grommet, A. B.; Feller, M.; Klajn, R. *Nat. Nanotechnol.* **2020**, *15*, 256–271. doi:10.1038/s41565-020-0652-2
8. Morimoto, M.; Bierschenk, S. M.; Xia, K. T.; Bergman, R. G.; Raymond, K. N.; Toste, F. D. *Nat. Catal.* **2020**, *3*, 969–984. doi:10.1038/s41929-020-00528-3
9. Antipin, I. S.; Alifimov, M. V.; Arslanov, V. V.; Burilov, V. A.; Vatsadze, S. Z.; Voloshin, Y. Z.; Volcho, K. P.; Gorbatchuk, V. V.; Gorbunova, Y. G.; Gromov, S. P.; Dudkin, S. V.; Zaitsev, S. Y.; Zakharchova, L. Y.; Ziganshin, M. A.; Zolotukhina, A. V.; Kalinina, M. A.; Karakhanov, E. A.; Kashapov, R. R.; Koifman, O. I.; Konovalov, A. I.; Korenev, V. S.; Maksimov, A. L.; Mamardashvili, N. Z.; Mamardashvili, G. M.; Martynov, A. G.; Mustafina, A. R.; Nugmanov, R. I.; Ovsyannikov, A. S.; Padnya, P. L.; Potapov, A. S.; Selektor, S. L.; Sokolov, M. N.; Solovieva, S. E.; Stoikov, I. I.; Stuzhin, P. A.; Suslov, E. V.; Ushakov, E. N.; Fedin, V. P.; Fedorenko, S. V.; Fedorova, O. A.; Fedorov, Y. V.; Chvalun, S. N.; Tsivadze, A. Y.; Shtykov, S. N.; Shurpik, D. N.; Shcherbina, M. A.; Yakimova, L. S. *Russ. Chem. Rev.* **2021**, *90*, 895–1107. doi:10.1070/rccr5011
10. Sun, Y.; Stang, P. J. *Aggregate* **2021**, *2*, e94. doi:10.1002/agt2.94
11. Olivo, G.; Capocasa, G.; Del Giudice, D.; Lanzalunga, O.; Di Stefano, S. *Chem. Soc. Rev.* **2021**, *50*, 7681–7724. doi:10.1039/d1cs00175b
12. Gaeta, C.; La Manna, P.; De Rosa, M.; Soriente, A.; Talotta, C.; Neri, P. *ChemCatChem* **2021**, *13*, 1638–1658. doi:10.1002/cctc.202001570
13. Pullen, S.; Clever, G. H. *Acc. Chem. Res.* **2018**, *51*, 3052–3064. doi:10.1021/acs.accounts.8b00415
14. Gao, W.-X.; Zhang, H.-N.; Jin, G.-X. *Coord. Chem. Rev.* **2019**, *386*, 69–84. doi:10.1016/j.ccr.2019.01.023
15. Chakrabarty, R.; Mukherjee, P. S.; Stang, P. J. *Chem. Rev.* **2011**, *111*, 6810–6918. doi:10.1021/cr200077m
16. Cook, T. R.; Stang, P. J. *Chem. Rev.* **2015**, *115*, 7001–7045. doi:10.1021/cr500566k
17. Liu, S.; Kondratuk, D. V.; Rousseaux, S. A. L.; Gil-Ramírez, G.; O'Sullivan, M. C.; Cremers, J.; Claridge, T. D. W.; Anderson, H. L. *Angew. Chem., Int. Ed.* **2015**, *54*, 5355–5359. doi:10.1002/anie.201412293
18. Chakraborty, S.; Newkome, G. R. *Chem. Soc. Rev.* **2018**, *47*, 3991–4016. doi:10.1039/c8cs00030a
19. Zhang, D.; Ronson, T. K.; Nitschke, J. R. *Acc. Chem. Res.* **2018**, *51*, 2423–2436. doi:10.1021/acs.accounts.8b00303
20. Sun, Y.; Chen, C.; Liu, J.; Stang, P. J. *Chem. Soc. Rev.* **2020**, *49*, 3889–3919. doi:10.1039/d0cs00038h
21. Pullen, S.; Tessarolo, J.; Clever, G. H. *Chem. Sci.* **2021**, *12*, 7269–7293. doi:10.1039/d1sc01226f
22. McConnell, A. J.; Wood, C. S.; Neelakandan, P. P.; Nitschke, J. R. *Chem. Rev.* **2015**, *115*, 7729–7793. doi:10.1021/cr500632f
23. Noji, H.; Yasuda, R.; Yoshida, M.; Kinoshita, K., Jr. *Nature* **1997**, *386*, 299–302. doi:10.1038/386299a0
24. Goswami, A.; Saha, S.; Biswas, P. K.; Schmittel, M. *Chem. Rev.* **2020**, *120*, 125–199. doi:10.1021/acs.chemrev.9b00159
25. Helm, L.; Merbach, A. E. *Coord. Chem. Rev.* **1999**, *187*, 151–181. doi:10.1016/s0010-8545(99)90232-1
26. Goswami, A.; Schmittel, M. *Coord. Chem. Rev.* **2018**, *376*, 478–505. doi:10.1016/j.ccr.2018.08.011
27. Safont-Sempere, M. M.; Fernández, G.; Würthner, F. *Chem. Rev.* **2011**, *111*, 5784–5814. doi:10.1021/cr100357h
28. Saha, M. L.; Schmittel, M. *Org. Biomol. Chem.* **2012**, *10*, 4651–4684. doi:10.1039/c2ob25098e
29. He, Z.; Jiang, W.; Schalley, C. A. *Chem. Soc. Rev.* **2015**, *44*, 779–789. doi:10.1039/c4cs00305e
30. Ghosh, A.; Schmittel, M. *Beilstein J. Org. Chem.* **2020**, *16*, 2831–2853. doi:10.3762/bjoc.16.233
31. Smith, V. C. M.; Lehn, J.-M. *Chem. Commun.* **1996**, 2733–2734. doi:10.1039/cc9960002733
32. Wu, A.; Isaacs, L. J. *Am. Chem. Soc.* **2003**, *125*, 4831–4835. doi:10.1021/ja028913b
33. Chambron, J.-C.; Heitz, V.; Sauvage, J.-P. *J. Chem. Soc., Chem. Commun.* **1992**, 1131–1133. doi:10.1039/c39920001131
34. Sauvage, J.-P. *Angew. Chem., Int. Ed.* **2017**, *56*, 11080–11093. doi:10.1002/anie.201702992
35. Krämer, R.; Lehn, J.-M.; Marquis-Rigault, A. *Proc. Natl. Acad. Sci. U. S. A.* **1993**, *90*, 5394–5398. doi:10.1073/pnas.90.12.5394
36. Zhang, M.; Saha, M. L.; Stang, P. J. *Struct. Chem.* **2017**, *28*, 453–459. doi:10.1007/s11224-016-0859-x
37. Schmittel, M. *Chem. Commun.* **2015**, *51*, 14956–14968. doi:10.1039/c5cc06605k

38. Yoshizawa, M.; Nagao, M.; Kumazawa, K.; Fujita, M. *J. Organomet. Chem.* **2005**, *690*, 5383–5388. doi:10.1016/j.jorganchem.2005.06.022
39. Prusty, S.; Chan, Y.-T. *Chem. Lett.* **2021**, *50*, 1202–1212. doi:10.1246/cl.210048
40. Wang, S.-C.; Cheng, K.-Y.; Fu, J.-H.; Cheng, Y.-C.; Chan, Y.-T. *J. Am. Chem. Soc.* **2020**, *142*, 16661–16667. doi:10.1021/jacs.0c06618
41. Lu, X.; Li, X.; Wang, J.-L.; Moorefield, C. N.; Wesdemiotis, C.; Newkome, G. R. *Chem. Commun.* **2012**, *48*, 9873–9875. doi:10.1039/c2cc35510h
42. Wang, H.; Li, Y.; Li, N.; Filosa, A.; Li, X. *Nat. Rev. Mater.* **2021**, *6*, 145–167. doi:10.1038/s41578-020-00257-w
43. Preston, D.; Barnsley, J. E.; Gordon, K. C.; Crowley, J. D. *J. Am. Chem. Soc.* **2016**, *138*, 10578–10585. doi:10.1021/jacs.6b05629
44. Lewis, J. E. M.; Crowley, J. D. *ChemPlusChem* **2020**, *85*, 815–827. doi:10.1002/cplu.202000153
45. Schultz, A.; Li, X.; Barkakaty, B.; Moorefield, C. N.; Wesdemiotis, C.; Newkome, G. R. *J. Am. Chem. Soc.* **2012**, *134*, 7672–7675. doi:10.1021/ja303177v
46. Fu, J.-H.; Wang, S.-Y.; Chen, Y.-S.; Prusty, S.; Chan, Y.-T. *J. Am. Chem. Soc.* **2019**, *141*, 16217–16221. doi:10.1021/jacs.9b08731
47. Li, Y.; Jiang, Z.; Wang, M.; Yuan, J.; Liu, D.; Yang, X.; Chen, M.; Yan, J.; Li, X.; Wang, P. *J. Am. Chem. Soc.* **2016**, *138*, 10041–10046. doi:10.1021/jacs.6b06021
48. Sun, Q.-F.; Sato, S.; Fujita, M. *Angew. Chem., Int. Ed.* **2014**, *53*, 13510–13513. doi:10.1002/anie.201408652
49. Di Stefano, S.; Capocasa, G.; Mandolini, L. *Eur. J. Org. Chem.* **2020**, 3340–3350. doi:10.1002/ejoc.201901914
50. Connors, K. A. *Chem. Rev.* **1997**, *97*, 1325–1358. doi:10.1021/cr960371r
51. Schneider, H.-J. *Acc. Chem. Res.* **2015**, *48*, 1815–1822. doi:10.1021/acs.accounts.5b00111
52. Percástegui, E. G.; Ronson, T. K.; Nitschke, J. R. *Chem. Rev.* **2020**, *120*, 13480–13544. doi:10.1021/acs.chemrev.0c00672
53. Bardhan, D.; Chand, D. K. *Chem. – Eur. J.* **2019**, *25*, 12241–12269. doi:10.1002/chem.201900831
54. Zhu, H.; Li, Q.; Shi, B.; Xing, H.; Sun, Y.; Lu, S.; Shangguan, L.; Li, X.; Huang, F.; Stang, P. J. *J. Am. Chem. Soc.* **2020**, *142*, 17340–17345. doi:10.1021/jacs.0c09598
55. Zou, Y.-Q.; Zhang, D.; Ronson, T. K.; Tarzia, A.; Lu, Z.; Jelfs, K. E.; Nitschke, J. R. *J. Am. Chem. Soc.* **2021**, *143*, 9009–9015. doi:10.1021/jacs.1c05172
56. Domoto, Y.; Abe, M.; Fujita, M. *J. Am. Chem. Soc.* **2021**, *143*, 8578–8582. doi:10.1021/jacs.1c03208
57. Purba, P. C.; Maity, M.; Bhattacharyya, S.; Mukherjee, P. S. *Angew. Chem., Int. Ed.* **2021**, *60*, 14109–14116. doi:10.1002/anie.202103822
58. Samanta, D.; Mukherjee, P. S. *Chem. Commun.* **2013**, *49*, 4307–4309. doi:10.1039/c2cc37377g
59. Howlader, P.; Das, P.; Zangrandi, E.; Mukherjee, P. S. *J. Am. Chem. Soc.* **2016**, *138*, 1668–1676. doi:10.1021/jacs.5b12237
60. Acharyya, K.; Bhattacharyya, S.; Sepehrpour, H.; Chakraborty, S.; Lu, S.; Shi, B.; Li, X.; Mukherjee, P. S.; Stang, P. J. *J. Am. Chem. Soc.* **2019**, *141*, 14565–14569. doi:10.1021/jacs.9b08403
61. Li, Y.; Rajasree, S. S.; Lee, G. Y.; Yu, J.; Tang, J.-H.; Ni, R.; Li, G.; Houk, K. N.; Deria, P.; Stang, P. J. *J. Am. Chem. Soc.* **2021**, *143*, 2908–2919. doi:10.1021/jacs.0c12853
62. Meng, G.; Zhen, L.; Sun, S.; Hai, J.; Zhang, Z.; Sun, D.; Liu, Q.; Wang, B. *J. Mater. Chem. A* **2021**, *9*, 24365–24373. doi:10.1039/d1ta07733c
63. Li, X.; Yu, J.; Gosztola, D. J.; Fry, H. C.; Deria, P. *J. Am. Chem. Soc.* **2019**, *141*, 16849–16857. doi:10.1021/jacs.9b08078
64. Jiang, Z. W.; Zhao, T. T.; Zhen, S. J.; Li, C. M.; Li, Y. F.; Huang, C. Z. *J. Mater. Chem. A* **2021**, *9*, 9301–9306. doi:10.1039/d1ta01278a
65. Kumar, A.; Saha, R.; Mukherjee, P. S. *Chem. Sci.* **2021**, *12*, 5319–5329. doi:10.1039/d1sc00097g
66. Yan, X.; Cook, T. R.; Wang, P.; Huang, F.; Stang, P. *J. Nat. Chem.* **2015**, *7*, 342–348. doi:10.1038/nchem.2201
67. Nolan, S. P. *Acc. Chem. Res.* **2011**, *44*, 91–100. doi:10.1021/ar1000764
68. Hashmi, A. S. K. *Chem. Rev.* **2007**, *107*, 3180–3211. doi:10.1021/cr000436x
69. Cavarzan, A.; Scarso, A.; Sgarbossa, P.; Strukul, G.; Reek, J. N. H. *J. Am. Chem. Soc.* **2011**, *133*, 2848–2851. doi:10.1021/ja111106x
70. Adriaenssens, L.; Escribano-Cuesta, A.; Homs, A.; Echavarren, A. M.; Ballester, P. *Eur. J. Org. Chem.* **2013**, 1494–1500. doi:10.1002/ejoc.201201592
71. Wang, Z. J.; Brown, C. J.; Bergman, R. G.; Raymond, K. N.; Toste, F. D. *J. Am. Chem. Soc.* **2011**, *133*, 7358–7360. doi:10.1021/ja202055v
72. Gramage-Doria, R.; Hessels, J.; Leenders, S. H. A. M.; Tröppner, O.; Dürr, M.; Ivanović-Burmazović, I.; Reek, J. N. H. *Angew. Chem., Int. Ed.* **2014**, *53*, 13380–13384. doi:10.1002/anie.201406415
73. Das, P.; Kumar, A.; Howlader, P.; Mukherjee, P. S. *Chem. – Eur. J.* **2017**, *23*, 12565–12574. doi:10.1002/chem.201702263
74. Brunel, J. M. *Chem. Rev.* **2005**, *105*, 857–897. doi:10.1021/cr040079g
75. Hong, T.; Zhang, Z.; Sun, Y.; Tao, J.-J.; Tang, J.-D.; Xie, C.; Wang, M.; Chen, F.; Xie, S.-S.; Li, S.; Stang, P. *J. J. Am. Chem. Soc.* **2020**, *142*, 10244–10249. doi:10.1021/jacs.0c01563
76. García-Simón, C.; García-Borràs, M.; Gómez, L.; Parella, T.; Osuna, S.; Juanhuix, J.; Imaz, I.; Maspoch, D.; Costas, M.; Ribas, X. *Nat. Commun.* **2014**, *5*, 5557. doi:10.1038/ncomms6557
77. García-Simón, C.; Gramage-Doria, R.; Raouf moghaddam, S.; Parella, T.; Costas, M.; Ribas, X.; Reek, J. N. H. *J. Am. Chem. Soc.* **2015**, *137*, 2680–2687. doi:10.1021/ja512637k
78. Hiraoka, S.; Hirata, K.; Shionoya, M. *Angew. Chem., Int. Ed.* **2004**, *43*, 3814–3818. doi:10.1002/anie.200453753
79. Hiraoka, S.; Shiro, M.; Shionoya, M. *J. Am. Chem. Soc.* **2004**, *126*, 1214–1218. doi:10.1021/ja036388q
80. Hiraoka, S.; Okuno, E.; Tanaka, T.; Shiro, M.; Shionoya, M. *J. Am. Chem. Soc.* **2008**, *130*, 9089–9098. doi:10.1021/ja8014583
81. Kume, S.; Nomoto, K.; Kusamoto, T.; Nishihara, H. *J. Am. Chem. Soc.* **2009**, *131*, 14198–14199. doi:10.1021/ja906684g
82. Kume, S.; Nishihara, H. *Chem. Commun.* **2011**, *47*, 415–417. doi:10.1039/c0cc02193h
83. Muraoka, T.; Kinbara, K.; Aida, T. *Nature* **2006**, *440*, 512–515. doi:10.1038/nature04635
84. Kai, H.; Nara, S.; Kinbara, K.; Aida, T. *J. Am. Chem. Soc.* **2008**, *130*, 6725–6727. doi:10.1021/ja801646b
85. Schmittel, M.; He, B.; Fan, J.; Bats, J. W.; Engeser, M.; Schlosser, M.; Deiseroth, H.-J. *Inorg. Chem.* **2009**, *48*, 8192–8200. doi:10.1021/ic900657w

86. Neogi, S.; Lorenz, Y.; Engeser, M.; Samanta, D.; Schmittel, M. *Inorg. Chem.* **2013**, *52*, 6975–6984. doi:10.1021/ic400328d
87. Schmittel, M.; Ammon, H.; Kalsani, V.; Wiegrefe, A.; Michel, C. *Chem. Commun.* **2002**, 2566–2567. doi:10.1039/b207801e
88. Schmittel, M.; Kalsani, V.; Mal, P.; Bats, J. W. *Inorg. Chem.* **2006**, *45*, 6370–6377. doi:10.1021/ic060403i
89. Goswami, A.; Paul, I.; Schmittel, M. *Chem. Commun.* **2017**, *53*, 5186–5189. doi:10.1039/c7cc01977g
90. Samanta, S. K.; Schmittel, M. *J. Am. Chem. Soc.* **2013**, *135*, 18794–18797. doi:10.1021/ja411011a
91. Samanta, S. K.; Samanta, D.; Bats, J. W.; Schmittel, M. *J. Org. Chem.* **2011**, *76*, 7466–7473. doi:10.1021/jo201252q
92. Biswas, P. K.; Saha, S.; Nanaji, Y.; Rana, A.; Schmittel, M. *Inorg. Chem.* **2017**, *56*, 6662–6670. doi:10.1021/acs.inorgchem.7b00740
93. Li, Y.-F.; Ghosh, A.; Biswas, P. K.; Saha, S.; Schmittel, M. *Chemistry* **2021**, *3*, 116–125. doi:10.3390/chemistry3010009
94. Biswas, P. K.; Saha, S.; Paululat, T.; Schmittel, M. *J. Am. Chem. Soc.* **2018**, *140*, 9038–9041. doi:10.1021/jacs.8b04437
95. Biswas, P. K.; Saha, S.; Gaikwad, S.; Schmittel, M. *J. Am. Chem. Soc.* **2020**, *142*, 7889–7897. doi:10.1021/jacs.0c01315
96. Goswami, A.; Schmittel, M. *Angew. Chem., Int. Ed.* **2020**, *59*, 12362–12366. doi:10.1002/anie.202002739
97. Goswami, A.; Pramanik, S.; Schmittel, M. *Chem. Commun.* **2018**, *54*, 3955–3958. doi:10.1039/c8cc01496e
98. Paul, I.; Goswami, A.; Mittal, N.; Schmittel, M. *Angew. Chem., Int. Ed.* **2018**, *57*, 354–358. doi:10.1002/anie.201709644
99. Goswami, A.; Paululat, T.; Schmittel, M. *J. Am. Chem. Soc.* **2019**, *141*, 15656–15663. doi:10.1021/jacs.9b07737
100. Goswami, A.; Özer, M. S.; Paul, I.; Schmittel, M. *Chem. Commun.* **2021**, *57*, 7180–7183. doi:10.1039/d1cc02805g
101. Wang, W.; Wang, Y.-X.; Yang, H.-B. *Chem. Soc. Rev.* **2016**, *45*, 2656–2693. doi:10.1039/c5cs00301f
102. Bloch, W. M.; Holstein, J. J.; Hiller, W.; Clever, G. H. *Angew. Chem., Int. Ed.* **2017**, *56*, 8285–8289. doi:10.1002/anie.201702573
103. Li, G.; Zhou, Z.; Yuan, C.; Guo, Z.; Liu, Y.; Zhao, D.; Liu, K.; Zhao, J.; Tan, H.; Yan, X. *Angew. Chem., Int. Ed.* **2020**, *59*, 10013–10017. doi:10.1002/anie.202000078
104. Leigh, D. A.; Marcos, V.; Wilson, M. R. *ACS Catal.* **2014**, *4*, 4490–4497. doi:10.1021/cs5013415
105. Choudhury, J. *Tetrahedron Lett.* **2018**, *59*, 487–495. doi:10.1016/j.tetlet.2017.12.070
106. van Dijk, L.; Tilby, M. J.; Szpera, R.; Smith, O. A.; Bunce, H. A. P.; Fletcher, S. P. *Nat. Rev. Chem.* **2018**, *2*, 117. doi:10.1038/s41570-018-0117
107. Tang, Y.; He, Y.; Fan, Q. *Chin. J. Org. Chem.* **2020**, *40*, 3672. doi:10.6023/cjoc202006076
108. Mattia, E.; Otto, S. *Nat. Nanotechnol.* **2015**, *10*, 111–119. doi:10.1038/nnano.2014.337
109. Ashkenasy, G.; Hermans, T. M.; Otto, S.; Taylor, A. F. *Chem. Soc. Rev.* **2017**, *46*, 2543–2554. doi:10.1039/c7cs00117g
110. Ghosh, A.; Paul, I.; Schmittel, M. *Angew. Chem., Int. Ed.* **2021**, *60*, 20558–20562. doi:10.1002/anie.202108269
111. Meldal, M.; Diness, F. *Trends Chem.* **2020**, *2*, 569–584. doi:10.1016/j.trechm.2020.03.007
112. Mondal, D.; Ghosh, A.; Paul, I.; Schmittel, M. *Org. Lett.* **2022**, *24*, 69–73. doi:10.1021/acs.orglett.1c03654
113. Biagini, C.; Albano, S.; Caruso, R.; Mandolini, L.; Berrocal, J. A.; Di Stefano, S. *Chem. Sci.* **2018**, *9*, 181–188. doi:10.1039/c7sc04123c
114. Biagini, C.; Di Stefano, S. *Angew. Chem., Int. Ed.* **2020**, *59*, 8344–8354. doi:10.1002/anie.201912659
115. Paul, I.; Samanta, D.; Gaikwad, S.; Schmittel, M. *Beilstein J. Org. Chem.* **2019**, *15*, 1371–1378. doi:10.3762/bjoc.15.137
116. Lifschitz, A. M.; Rosen, M. S.; McGuirk, C. M.; Mirkin, C. A. *J. Am. Chem. Soc.* **2015**, *137*, 7252–7261. doi:10.1021/jacs.5b01054
117. Yoon, H. J.; Mirkin, C. A. *J. Am. Chem. Soc.* **2008**, *130*, 11590–11591. doi:10.1021/ja804076q
118. Yoon, H. J.; Kuwabara, J.; Kim, J.-H.; Mirkin, C. A. *Science* **2010**, *330*, 66–69. doi:10.1126/science.1193928
119. Gianneschi, N. C.; Bertin, P. A.; Nguyen, S. T.; Mirkin, C. A.; Zakharov, L. N.; Rheingold, A. L. *J. Am. Chem. Soc.* **2003**, *125*, 10508–10509. doi:10.1021/ja035621h
120. Lifschitz, A. M.; Young, R. M.; Mendez-Arroyo, J.; Stern, C. L.; McGuirk, C. M.; Wasielewski, M. R.; Mirkin, C. A. *Nat. Commun.* **2015**, *6*, 6541. doi:10.1038/ncomms7541
121. Yoon, H. J.; Heo, J.; Mirkin, C. A. *J. Am. Chem. Soc.* **2007**, *129*, 14182–14183. doi:10.1021/ja077467v
122. Oliveri, C. G.; Gianneschi, N. C.; Nguyen, S. T.; Mirkin, C. A.; Stern, C. L.; Wawrzak, Z.; Pink, M. J. *Am. Chem. Soc.* **2006**, *128*, 16286–16296. doi:10.1021/ja0661010
123. Masar, M. S.; Gianneschi, N. C.; Oliveri, C. G.; Stern, C. L.; Nguyen, S. T.; Mirkin, C. A. *J. Am. Chem. Soc.* **2007**, *129*, 10149–10158. doi:10.1021/ja0711516
124. Gianneschi, N. C.; Cho, S.-H.; Nguyen, S. T.; Mirkin, C. A. *Angew. Chem., Int. Ed.* **2004**, *43*, 5503–5507. doi:10.1002/anie.200460932
125. Gianneschi, N. C.; Nguyen, S. T.; Mirkin, C. A. *J. Am. Chem. Soc.* **2005**, *127*, 1644–1645. doi:10.1021/ja0437306
126. Oliveri, C. G.; Ullmann, P. A.; Wiester, M. J.; Mirkin, C. A. *Acc. Chem. Res.* **2008**, *41*, 1618–1629. doi:10.1021/ar800025w
127. Schmittel, M.; De, S.; Pramanik, S. *Angew. Chem., Int. Ed.* **2012**, *51*, 3832–3836. doi:10.1002/anie.201108089
128. De, S.; Pramanik, S.; Schmittel, M. *Angew. Chem., Int. Ed.* **2014**, *53*, 14255–14259. doi:10.1002/anie.201408457
129. Waloch, C.; Wieland, J.; Keller, M.; Breit, B. *Angew. Chem., Int. Ed.* **2007**, *46*, 3037–3039. doi:10.1002/anie.200605202
130. Teator, A. J.; Lastovickova, D. N.; Bielawski, C. W. *Chem. Rev.* **2016**, *116*, 1969–1992. doi:10.1021/acs.chemrev.5b00426
131. De, S.; Pramanik, S.; Schmittel, M. *Dalton Trans.* **2014**, *43*, 10977–10982. doi:10.1039/c4dt01508h
132. McGuirk, C. M.; Stern, C. L.; Mirkin, C. A. *J. Am. Chem. Soc.* **2014**, *136*, 4689–4696. doi:10.1021/ja500214r
133. Goswami, A.; Gaikwad, S.; Schmittel, M. *Chem. – Eur. J.* **2021**, *27*, 2997–3001. doi:10.1002/chem.202004416
134. Gaikwad, S.; Goswami, A.; De, S.; Schmittel, M. *Angew. Chem., Int. Ed.* **2016**, *55*, 10512–10517. doi:10.1002/anie.201604658
135. Mittal, N.; Pramanik, S.; Paul, I.; De, S.; Schmittel, M. *J. Am. Chem. Soc.* **2017**, *139*, 4270–4273. doi:10.1021/jacs.6b12951
136. Lehn, J.-M. *Angew. Chem., Int. Ed.* **2013**, *52*, 2836–2850. doi:10.1002/anie.201208397
137. Remón, P.; Pischel, U. *ChemPhysChem* **2017**, *18*, 1667–1677. doi:10.1002/cphc.201700387
138. Andréasson, J.; Pischel, U. *Coord. Chem. Rev.* **2021**, *429*, 213695. doi:10.1016/j.ccr.2020.213695

License and Terms

This is an open access article licensed under the terms of the Beilstein-Institut Open Access License Agreement (<https://www.beilstein-journals.org/bjoc/terms>), which is identical to the Creative Commons Attribution 4.0 International License (<https://creativecommons.org/licenses/by/4.0>). The reuse of material under this license requires that the author(s), source and license are credited. Third-party material in this article could be subject to other licenses (typically indicated in the credit line), and in this case, users are required to obtain permission from the license holder to reuse the material.

The definitive version of this article is the electronic one which can be found at:

<https://doi.org/10.3762/bjoc.18.62>